THE SYNTHESIS, SPECTROSCOPIC AND ELECTROCHEMICAL CHARACTERISATION OF RUTHENIUM(II) POLYPYRIDYL COMPLEXES CONTAINING A CATECHOL MOIETY.

by

Luke O'Brien, Bsc.

A Thesis presented to Dublin City University for the degree of Doctor of Philosophy.

Supervisor Prof. J.G. Vos

School of Chemical Sciences

Dublin City University

February 2001

To my family and friends past and present.

I hereby certify that this material which I now submit for assessment on the programme of Study leading to award of Doctor of Philosophy by research and thesis is entirely my own work and has not been taken from the work of others save and to the extent that such work has been cited and acknowledged within the text of my work.

Signed: Luke O'Brien

Luke O'Brien

I.D. No. : 95970703

Date: 20/2/01

"They say in Kerry that being born
in Kerry is the greatest gift that God
can bestow on any man, that when
you belong to Kerry you know you
have a head start on the other fellow"

John B. Keane, Poet, Playwright, Novelist, Kerryman.

Acknowledgements

There are so many people to thank in some way for their help with this thesis. Firstly I would like to sincerely thank and acknowledge my supervisor Han, for the faith, persistence, encouragement and help that he has given through the years including the few kicks in the rear!

Next I would like to thank the members of the Vos research group. The story began in the old lab, AG 12, which looked so impressive from the outside, but quite different from the inside. Back then the oddessy began with Luke and the women. What a bunch they were! Christy (Moore), Rachel (do ya want a pint) Keirse, Frances (Up the Royal, not!) Weldon, Bronagh (Woody's) Myers, Una (Deuterated) O 'Dwyer, Miriam (Decathlete) Walshe, Karen (redhead, no hair) Mongey and Tia. Then the balance began to swing, I got a few lads in to restore the sanity and sway the conversations from dresses and make-up to Football and well other things!! Stefano was the first recruit and though not a kerryman or even an Irishman, his impressive knowledge of Gaelic Sports went a long way towards acceptance into the team. The girlies too got a new recruit in Anthea (dicarboxy) Lees. Then there was the outside members of the group who deserve a mention, such as Tim and Nick (or is it Nick and Tim?), Sven and Astrid (I will visit Jena someday!!), Egbert and Johan (lets go for one). Then the newer recruits came and remain today in the new X2 46, Helen, Scott, Marco (Blackbook Pantani), Adrian (did you score yet?), Declan (of Barcelona fame), Wesley, Moss and The Fionas.

Thanks also to all the postgrads new and old, you've made life good fun and we've had some good laughs through the years, too many to recount here. The names that spring to mind are Fayner (Mr. Social animal), Mike (How're ya doin') Sheehy,

Teresa (Mayo will win some day!), Brendan (Mr. HPLC), Cormac, Ollie, Shane, Jimmy, Colm, Peter, Ciaran, Davnat, Siobhan, Orla, Ben, Paddy (Dub) Kane, Joe, Conor, , Aoife, Dominic, Andrea, Frank, Richard and Jenny and Mary (for the use of the printer), Cathal, Carol and Mairead.

Life in the DCU Chemistry department wouldn't be possible without the help of the technicians and their light-hearted, helpful and some-time crazy (I'm not talking about you Damian!!) behaviour has been a tonic on days when things weren't going so well. I learned a lot from ye and thanks for all the help to Maurice, Mick, Ambrose, Veronica, Damien, Ann, Niall, Shane, Vinny and John.

So to the infamous 106 Iveragh road, although it often felt like a hostel or a refuge for wayward postgrads lost in the nite, it was home for many years. The all-star postgrad line-up was evenly split between Munster and Leinster for a few years with Conor (Cat) Hogan and Joe (Wannabe-Cat) Kelly while Munster was represented by myself and Ben (chilli) Costello. Thanks for all the memories lads and remember I will find out some day who burned my Kerry flag. In between times Sharon, Pepe, Quique, Dave, Hendrik and Bernard have resided in that mad auld house.

I must thank all my friends through the years for taking my mind off the chemistry and giving me some great memories; Pat (R), Trev, Nocky (your memory lives on), Derek, John (F), Fin, Sophie, Michelle, Holly, Declan, Sean and Pat (H).

Finally, but most importantly, I must thank the people who have supported me through thick and thin and without whose help and encouragement I could not have done without. My greatest appreciation and love goes to all my family but especially Ma and John and to my beautiful girlfriend Brigid. Thank ye all for always listening and now in answer to that persistant question: "Yes I am Finished".

Abstract.

The synthesis, spectroscopic and electrochemical characterisation of ruthenium (II) polypyridyl mononuclear and dinuclear complexes of a 5-(2-pyridyl)-1,2,4-triazole ligand containing a catechol moiety are described. Chapter one is an introduction relevant to the work described in the thesis. The methods of characterisation, which are described in chapter two, include High Performance Liquid Chromatography, ^{1}H-NMR, UV/Visible spectroscopy, fluorimetry, electrochemistry, spectroelectrochemistry, mass spectrometry, X-Ray crystallography and lifetime emission measurements. Chapter three, describes the synthesis of the mononuclear ruthenium (II) complexes of the protected catechol ligand 3-(1′,2′-dimethoxyphenyl)-5-(pyridin-2-yl)-1,2,4-triazole. The protected catechol moiety results in coordination of the $Ru(L_x)_2$ (where L_x is bpy, d_8-bpy, phen, d_8-phen or dcbpy) via N1 of the triazole and N1 of the pyridyl ring, which is confirmed by X-Ray crystallography. The synthesis of deuteriated complexes, is of significant benefit for the purposes of structural elucidation. Examination of the acid-base chemistry of the complexes by UV/Visible spectroscopy reveals information about the location of the excited state. The excited state of all the complexes is located on L_x. Electrochemical studies show a reversible metal centred Ru^{II}/Ru^{III} couple. Evidence of irreversible oxidation of the dimethoxy moieties is observed at more anodic potentials.

Chapter four describes the deprotection of the $Ru(L_x)_2$ complexes of 3-(1′,2′-dimethoxyphenyl)-5-(pyridin-2-yl)-1,2,4-triazole forming complexes with a peripheral catechol binding site. These catechol complexes are precursors for the synthesis of dinuclear ruthenium complexes bound through the catechol binding site, the subject of chapter five, and for complexation of various other transition metals such as Fe(II), Fe(III) and Cu(II), the subject of chapter six. The electrochemical studies of the complexes in chapter four are complicated in comparison to their protected analogues. The oxidation of the catechol ligand precedes that of the metal centre and is quasi-reversible. Pretreatment of the glassy carbon electrode was necessary to resolve the processes due to adsorption of oxidised species onto the surface of the electrode. Attachment of the catechol complexes to nanocrystalline TiO_2 films indicates incident photon-to-current efficiency (IPCE) of greater than 30%.

Chapter five describes the synthesis of the dinuclear complexes of 3-(1′,2′-dihydroxyphenyl)-5-(pyridin-2-yl)-1,2,4-triazole from the mononuclear complexes discussed in chapter four. Semipreparative HPLC was required for purification and the dinuclear complexes were isolated in the semiquinone form. The complexes were characterised by mass spectrometry, HPLC and elemental analysis. Electrochemical analysis shows a reversible one-electron process for the hq/sq process and quasi reversible one electron processes for the sq/q and for the metal centre bound via the triazole. The second metal centre is not accessible with the conditions used. The complexes exhibit weak emission at neutral conditions.

Finally chapter six explores the complexation of the mononuclear catechol complexes with various transition metals by titration of the catechol complexes with known molar equilavents of the metal. The stability constants and stoichiometry were estimated by attention to changes in the UV/VIS and emission spectra. The most interesting results were achieved with Fe(II), Fe(III) and Cu(II).

Table of Contents

Chapter One

Introduction

1.1 Photosynthesis.

1.1.1 General aspects of photosynthesis.

In green plants energy can be provided by respiration and photosynthesis. The conversion of the electromagnetic energy of light into chemical energy in photosynthesis is a process unique to green plants and certain bacteria. Virtually all life on earth depends on the products of the reactions of photosynthesis which fix CO_2 into organic compounds and free O_2 from H_2O. The basic principle of photosynthesis and overall equation is summarised below in equation 1.

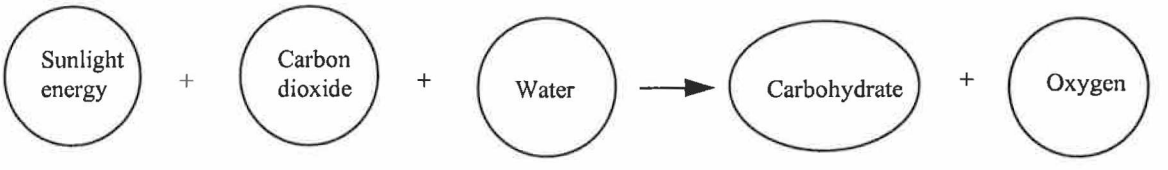

Overall equation for photosynthesis: $6CO_2 + 6H_2O$ --------> $C_6H_{12}O_6 + 6O_2$ (1.1)

Chlorophylls, carotenoids and phycobilin pigments actively participate in photosynthesis. Only organisms containing these organic pigments perform photosynthesis and they must be built into bigger structures and associated with many other cofactors in order to participate in photosynthesis[1]. Efficient photosynthetic transformation of sunlight energy in the visible region (380 - 750 nm) requires the absorption of as many photons as possible. This condition is fulfilled through the presence of the above mentioned organic pigments.

Light is absorbed by these photosynthetic pigments with the absorbed energy ultimately being utilised for the assimilation of CO_2. Photosynthesis consists of two sets

of reactions, the degradative reactions and the synthetic ones. The degradative reactions produce the ATP and NADPH needed for the synthetic reactions, during which reduction occurs. The degradative part of photosynthesis consists of the splitting of water with the release of oxygen, and the synthetic portion consists of the reduction of carbon dioxide to carbohydrate. These set of reactions are often referred to as the *light-dependent reactions* - because they require solar energy - and the *light independent reactions* - because light is not required.

In the light-dependent reactions, after absorbing solar energy, chlorophyll sends energised electrons to an electron transport system that pumps hydrogen ions (H^+). This allows ATP to be produced while at the same time the flow of electrons is used to reduce $NADP^+$ to NADPH. A fresh supply of electrons is derived from water, which splits to release oxygen (O_2)[2].

In the light independent reactions, the ATP and NADPH made during the light-dependent reactions are used as a source of energy and reducing power, respectively, to drive the synthetic conversion of CO_2 to carbohydrate $(CH_2O)_n$[3].

The light-dependent reactions require the participation of two *photosystems*, called *Photosystem I* and *Photosystem II*[4]. The proposed arrangement of these photosystems and associated electron transport systems is shown in Figure 1.1. Each photosystem consists of a pigment complex containing several hundred pigment molecules, including chlorophyll and carotenoids, and electron acceptors. These pigment complexes have been termed *light-harvesting antennae*. Photosynthesis begins when the pigment molecules absorb light energy and funnel it to their respective reaction centres, that are located within the antenna of both Photosystem I and Photosystem II.

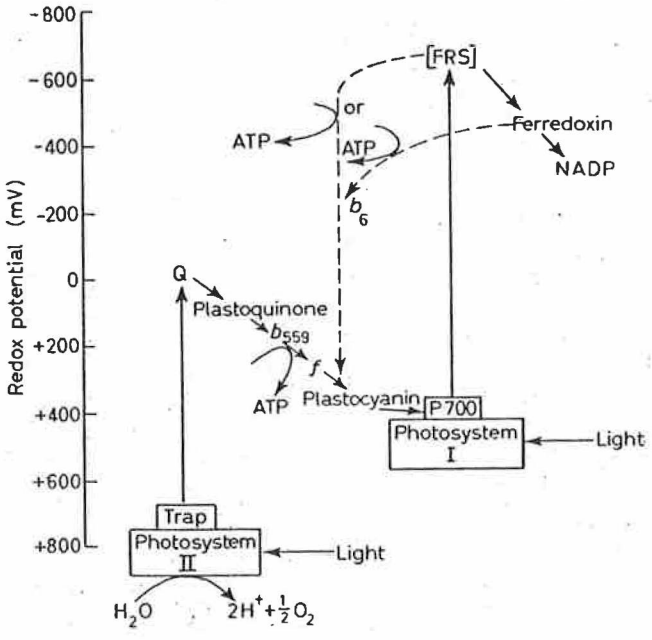

Figure 1.1 *Electron transfer between photosystems I and II. FRS (ferredoxin-reducing substance) may serve as a reductant to ferredoxin*[4].

The antenna of Photosystem I has a reaction- centre chlorphyll *a* whose absorption spectrum peaks at a wavelength of around 700 nm and is therefore called *P700*[5] The antenna of Photosystem II has a reaction-centre chlorophyll *a* whose absorption spectrum peaks at a slightly shorter wavelength and is called *P680.* Each reaction-centre chlorophyll *a* molecule is associated with an electron acceptor and these two molecules form the essential part of the photosystem. The solar energy received by a reaction centre energises electrons within the chlorophyll molecule so that the electrons can pass from it to an acceptor molecule.

These two different kinds of photochemical systems act in concert. In Photosystem I a primary reductant is strong enough to reduce pyridine nucleotides and the primary oxidant is relatively weak. Photosystem I functions as a method of

oxidising reduced plastocyanin and transferring the electrons as a soluble form of the Fe-S protein called ferredoxin. PS II generates a weak reductant and a strong oxidant, capable of taking electrons from water. The electron holes remaining in PS II represent a very positive potential which is used to oxidise two water molecules to dioxygen in an overall four-electron process. It is known that in this four-electron oxidation of water to O_2 a polymanganese system acts as an electron reservoir, accumulating charge in an exactly controlled fashion.

The overall reaction in photosystem II can be summed up as follows (see Figure 1.2) employing quinonoid proton and electron carriers (PQ : plastoquinone, PQH_2 : plastohydroquinone):

$$2\,H_2O + 2\,PQ + 4\,H^+(\text{out}) \xrightarrow[[Mn]x\ (\text{catalysing})]{4h\nu} O_2 + 2\,PQH_2 + 4H^+(\text{in})$$

Figure 1.2 Overall reaction in PS II.

The overall function of Photosystem II is to use light energy to reduce oxidised plastoquinone (PQ) to its fully reduced form (PQH_2) using electrons from water. The required four oxidation equivalents for O_2 production are available only after excitation of Photosystem II with at least four photons[6].

1.1.2 Artificial photosynthesis - trends.

The harvesting of light energy by plants and its conversion to chemically useful forms is not only a fascinating scientific phenomenon, but also of the utmost importance to mankind. Photosynthesis, ancient or modern, is responsible for our oxygenic atmosphere and fills most of our food and energy requirements and many of our raw material needs. These facts led to the notion of constructing a synthetic device that derives energy from sunlight by using the basic principles of photosynthesis[7,8]. In terms of primary energy conversion, the secrets of the molecular electronics of photoreaction centres is now available to us at atomic resolution, and such data is becoming available for a number of different light-harvesting proteins[9]. The challenge is now to devise an artificial system based on this knowledge. The theoretical approach towards artificial photosynthesis is to mimic the unit functions of photosynthesis while the ultimate practical aim for artificial photosynthetic devices is to develop molecular devices capable of photosensitisation leading to efficient charge separation and ultimately the photochemical induced splitting of water into O_2 and energy rich H_2. Solar radiation must be trapped in the wavelength region where it is most intense by employing an appropriate antenna molecule and transmit this energy to the splitting of water[10]. Much of the study into simple artificial photosynthetic systems has focussed on systems that use the types of small organic molecules found in the natural system (chorophylls, quinones, and such) but that do so without the protein component of the reaction centre[7]. With regard to synthetic polymanganese complexes, the emphasis has mainly been on spectroscopic and structural model compounds such as the dimer-of-dimers complex reported by M.L. Kirk et al[11]. This complex possesses structural features which are similar to those observed for the S_1 state of the photosystem II water oxidation catalyst[12].

The active site for water oxidation in photosystem II consists of a polynuclear manganese aggregate. The water oxidation catalyst (WOC) undergoes four sequential one-electron oxidations before the liberation of molecular oxygen and regeneration of the catalyst. These five oxidation levels are known as the KoK states and are labeled S_0-S_4. The synthesis of various manganese complexes is of particular interest at present in the area of photosynthetic water oxidation[13-16]

Following nature's principles, light impinging on the photochemical system must be absorbed, and it's energy then used to start a chain of electron transfer reactions. Eventually, an electron may be harvested at one end of the system, and be used to produce fuels like hydrogen. At the other end, there must be a supply of electrons, so that the system can continue it's function. In nature, the endless supply of electrons consists of water that is oxidised to oxygen using solar energy. This is catalysed by the key enzyme photosystem II that carries out this function using a cluster of manganese ions.

One approach towards artificial photosynthesis is to mimic principles from photosystem II by the construction of a ruthenium-manganese complex that is able to take up electrons from water using light energy. The future of such projects require the development of several components; a synthetic antenna that captures light efficiently, a molecular array to transport electrons, and some means to separate the electron-side of the transport chain from the water-splitting complex. For ruthenium there are some functional models available. The $Ru(bpy)_2$ unit itself has provided the basis for a myriad of diverse photoactive complexes[17].

Two approaches have been followed for the creation of an antenna device capable of fulfilling the same role as the chorophyll photosensitisers: the *biomimetic* and

the *abiotic* approach. The *biomimetic* approach ultimately attempts to create antenna devices which utilise moieties that are present in the green leaf i.e. porphyrins, carotenoids and quinones[18,19,20]. The *Abiotic* approach integrates chemical representations which possess similar properties to the naturally occurring compounds. Alsfasser et al are interested in creating novel building blocks for biomimetic assemblies[21]. Their aim is to develop strategies for tuning the reactivity of metal complexes in order to optimise their properties with respect to fundamental chemical reactions such as electron transfer and the activation of small molecules. The goal is to construct polyfunctional assemblies from versatile modules well suited for different tasks in biomimetic processes like the photoreduction of CO_2 or the activation of oxygen. An ideal candidate for this purpose should be small peptides, since they permit the control of physical and chemical properties such as dielectric constants, charge, and hydrophobicity or the tendency to form hydrogen bonds, as well as the distance between two reaction centres, over a wide range by variation of their amino acid sequence. These factors are essential for the highly specific function of metalloproteins, and their controlled utilisation is vital for the development of efficient biomimetic coordination compounds[22].

1.1.2.1. Photochemical molecular devices (PMD's) .

Photochemical molecular devices (PMD's) and supramolecular assemblies have led the way in the field of creating light harvesting devices for energy production and the cleavage of water[23]. PMD's are defined as an assembly of molecular components capable of performing light induced functions, such as vectorial electron transfer, migration of electronic energy and switching on/off of receptor ability. Single

molecules cannot perform these functions thus requiring the cooperation of several components. To convert solar energy into fuel it is not necessary to design an artificial chloroplast that mimics the natural photosynthetic process; rather it would be sufficient to construct a PMD, presumably much simpler than a chloroplast, capable of performing, for example, the photoinduced splitting of water into hydrogen and oxygen[6]. PMD's comprise of a microstructure of the photosynthetic membrane generating vectorial electron transfer along an organised chain of relays that rapidly transfer the photoexcited electron to the ultimate acceptor and a charge separated state.

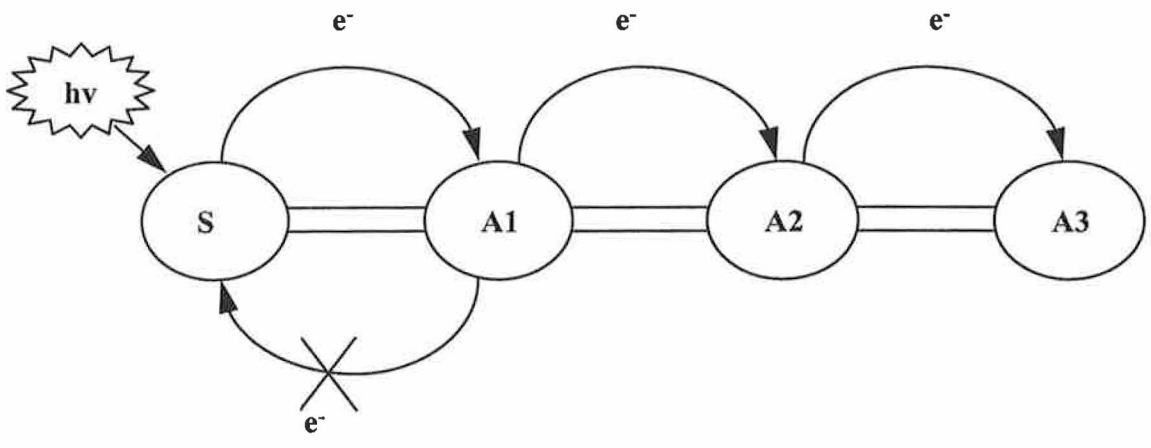

Figure 1.3 A typical PMD configuration exhibiting vectorial electron transfer.

A typical PMD system (see Figure 1.3) contains a sensitiser species S, possessing suitable redox, ground and excited properties. This is linked to a series of relay species, i.e. a series of electron acceptors Ax along a redox gradient. Following sensitisation, via light absorption, an electron is transferred from the excited sensitiser to

the relays until charge separation has been accomplished via oxidation of the sensitiser and reduction of the final acceptor.

The design of photoactive PMD's based on transition metal complexes is based on the linking of a photoactive centre to a donor and acceptor group via a spacer. Often the photoactive species plays the dual role of chromophore and terminal donor or acceptor. The choice of donor and acceptor will be dictated by the redox potentials of these species. Such assemblies involving the $Ru(bpy)_2$ chromophore have shown encouraging performances in the regions of vectorial electron and energy transfer. Redox charge separation is also a fundamental process in the utilisation of absorbed light energy in PMD's[23]. All natural and artificial systems share a common principle: a chromophore (C) with associated redox-active quenchers which may accept (A) or donate (D) electrons.

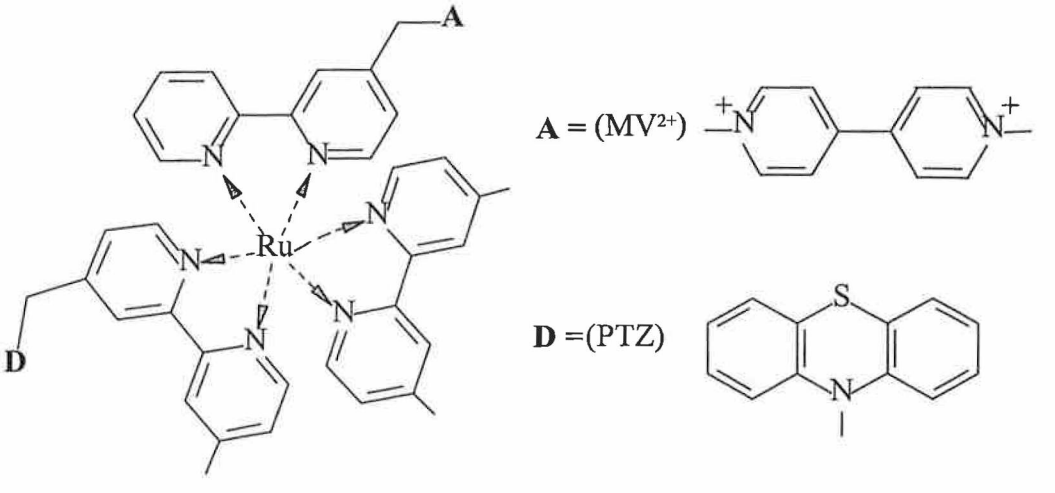

Figure 1.4 Structure of the chromophore-quencher complex $[Ru(Me_2bpy)(bpy\text{-}MV^{2+})(bpy\text{-}PTZ)]^{4+}$ (cis-2 isomer).

In the model, the initial D-C-A species absorbs light energy and forms an excited state D-*C-A, which produces the charge separated species D^+-C-A^- by a series of electron transfer steps. Rutherford et al have investigated a monomeric chromophore-quencher

complex of Ru(II), $[Ru(Me_2bpy)(bpy\text{-}MV^{2+})(bpy\text{-}PTZ)]^{4+}$, containing one donor (phenothiazine, PTZ) and one acceptor (methyl viologen, MV^{2+}) functionality (See Figure 1.4)[24]. In this study the isolation of the stereoisomers of the aforementioned mononuclear chromophore-quencher (D-C-A) species was presented with the aim of probing the influence that the spatial relationship of the donor and acceptor groups have on intramolecular electron transfer processes.

1.1.2.1. Dye-sensitised titanium dioxide solar cells.

A solar cell harnesses light from the sun and converts it into electrical energy. The light energy can be thought to boost the electrons within certain regions of the solar cell to more energetic regions and these electrons which will be high in energy can be subsequently withdrawn as electricity. One of the most interesting schemes for chemistry-based solar energy conversion (light-to-electrical energy conversion) is the dye-sensitised wide bandgap semiconductors. The development of dye-sensitised titanium dioxide cells incorporating ruthenium (II) complexes has received quite a degree of recent attention[25,26,27,28]. In the "Grätzel-cell" type system, the photophysical properties of the Ru(II) complex is united with the semi-conducting titanium dioxide material, and the conduction band potential is adjusted, by a phenomenon of solid state physics called "band-bending", to the redox potential of the Ru(II) complex. This results in the light absorption of the "dyed" TiO_2 being shifted into the visible light range, thus (sun-)light can be absorbed at more convenient wavelengths than without the "dye". Figure 1.5 shows a schematic representation of a regenerative dye-sensitised photovoltaic cell where D represents the surface-bound dye and the specific solution redox species is the I^-/I_3^- couple. Excitation of an absorbed dye molecule (D^*) is

followed by electron injection to the semiconductor conduction band (CB). The oxidised dye molecule is reduced by an electron donor, which is present in the electrolyte. Reduction of the oxidised dye molecule (D^+) takes place via the sacrificial donor I^-, which is regenerative at the Pt counter electrode. Losses in efficiency can occur by radiative and nonradiative decay of the excited state (D^*), by recombination of electrons in TiO_2 with oxidised dye molecules and by electrons in TiO_2 which react with oxidants in solution.

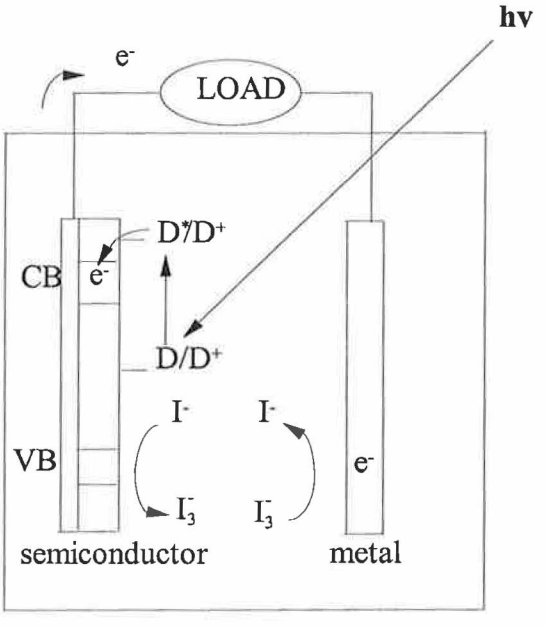

Figure 1.5 General mechanism of sensitisation in a regenerative dye solar cell.

The monochromatic incident photon-to-current efficiency, IPCE, gives the overall efficiency of the processes involved in the photovoltaic cell. The IPCE is directly linked to the absorption characteristics of the dye, the surface coverage of the TiO_2 electrode (LHE), the quantum yield for charge injection to the semiconductor (ϕ), and the efficiency of collecting electrons in the external circuit (η).

$$IPCE = (LHE)(\phi)(\eta) \qquad (1.2)$$

The performance of ruthenium based polypyridyl moieties incorporating negative monodentate ligands such as NCS^- have demonstrated the most promising characteristics to date[27,29]. The performance of the Ru(II) complex of *cis*-di(thiocyanoato)bis(2,2'-bipyridyl-4,4'-dicarboxylate) is so far found to be unmatched by any other known sensitiser. A solar-to-electric energy conversion efficiency of 10% was attained with this system.

1.2 Origins and occurrence of ruthenium.

The nine elements Fe, Ru, Os, Co, Rh, Ir, Ni, Pd and Pt together form group VIII of Mendeleev's periodic table. The horizontal similarities between Fe, Co and Ni has led the remaining six to be known collectively as the "platinum metals". Ruthenium and osmium are relative newcomers in comparison to iron and are distinctly different. They were discovered independently in the residues remaining when crude platinum had been dissolved in aqua regia; ruthenium in 1884 from ores in the Urals by K.Klaus who named it after ruthenia, the Latin name for Russia ; and osmium in 1803 by S.Tennant who named it from the Greek word for odour (osme) because of the characteristic and pungent smell of the volatile oxide OsO_4[17,30].

Ruthenium and Osmium are generally found in the metallic state along with the other "platinum" metals and the "coinage" metals. Ruthenium is particularly rare with an estimated abundance in the earth's crust of 0.0001 ppm. It has up to nine known oxidation states, the most common being Ru(III). Some of the uses of ruthenium include catalysis (reduction of NO in car exhaust applications), antitumour agents, alloys and solar cells. The principal use of ruthenium is for hardening alloys with

palladium and platinum. Such alloys find applications as electrical contacts, jewellery and fountain pen nibs. Ruthenium has also been known to electrodeposit, an example being RuO_2 thick-film resistors[17]. Ruthenium has a rich coordination chemistry, and oxidation states from VIII (d^0 valence electron configuration) to II (d^6 valence configuration) are represented in complexes with nitrogen-, phosphorous- and some oxygen-containing ligands. The scope of this thesis is confined to coordination compounds of Ru(II) with nitrogen and oxygen donor ligands. These are intensely red-coloured complexes which display interesting photophysical and photochemical behaviour.

1.3 Photophysical properties of $[Ru(bpy)_3]^{2+}$.

$[Ru(bpy)_3]^{2+}$ is one of the most studied of Ru(II) metal complexes with the first report of light emission from the complex in 1959 (see Figure 1.6)[31]. Since then the interest in the photochemistry of $[Ru(bpy)_3]^{2+}$ has flourished and as a result much is known about the photophysical and photochemical properties of the complex[32-36]. The chemical stability and redox properties together with its excited state reactivity, luminescence and excited state lifetime are many of the reasons for the extent of interest in $[Ru(bpy)_3]^{2+}$.

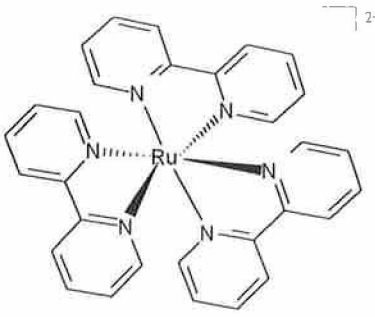

Figure 1.6 Structure of $[Ru(bpy)_3]^{2+}$.

Ruthenium(II) is a stable low-spin d^6 species and forms octahedral coordination complexes with a diamagnetic t_{2g}^6 electronic configuration. Ru(II) compounds can be oxidised (removal of a metal-localised electron) or reduced (addition of an electron in a ligand π^* orbital). The absorption spectrum of $[Ru(bpy)_3]^{2+}$ exhibits an intense absorption band at 452 nm. This band has been assigned to a metal-to-ligand charge-transfer (MLCT) transition.

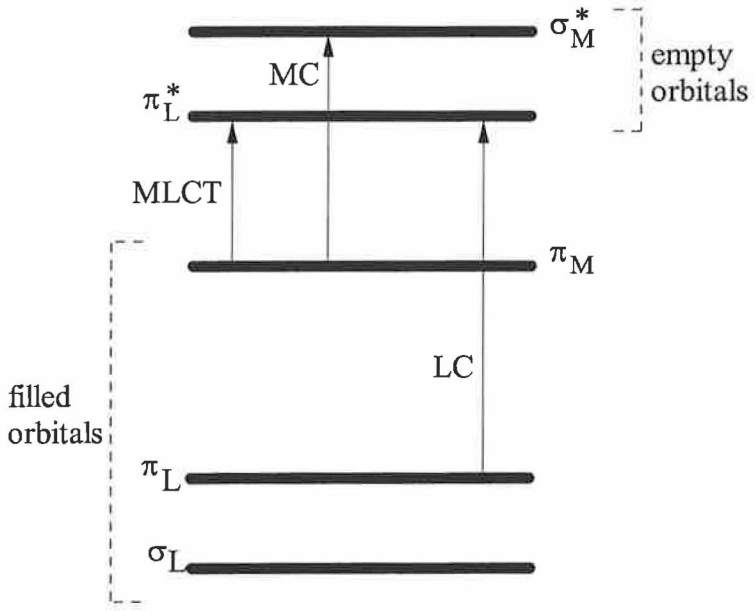

Figure 1.7 *The molecular orbitals of $[Ru(bpy)_3]^{2+}$ showing their relative energies and the possible electronic transitions of which the MLCT is lowest energy.*

In $[Ru(bpy)_3]^{2+}$, the three bipyridyl ligands contain σ-donor orbitals localised on the nitrogen atoms and π-donor and π^* acceptor orbitals delocalised on the aromatic rings. The ligand- centred π^* orbitals are low-lying and are lower in energy than the metal-centred $\sigma^*(e_g)$ orbitals. When $[Ru(bpy)_3]^{2+}$ absorbs the energy of an incident light beam an electron from the ground state orbital (π_M) of ruthenium is promoted to a ligand orbital (π_L^*) localised on one of the bipyridyl rings, resulting in a MLCT excited state (see Figure 1.7). The excited state can be represented as follows:

$$[Ru^{II}(bpy)_3]^{2+} + h\nu \rightarrow [Ru^{III}(bpy)_2(bpy^{-\bullet})]^{2+*}$$

The other important excited states that can arise following the other transitions shown in Figure 1.7 are metal centred (MC) excited state, between π_M and σ_M^* orbitals, and ligand-centred excited state (LC), between π_L and π_L^* orbitals. The relative ordering of these excited states, together with the possible radiative, non-radiative and deactivation pathways are shown in Figure 1.8.

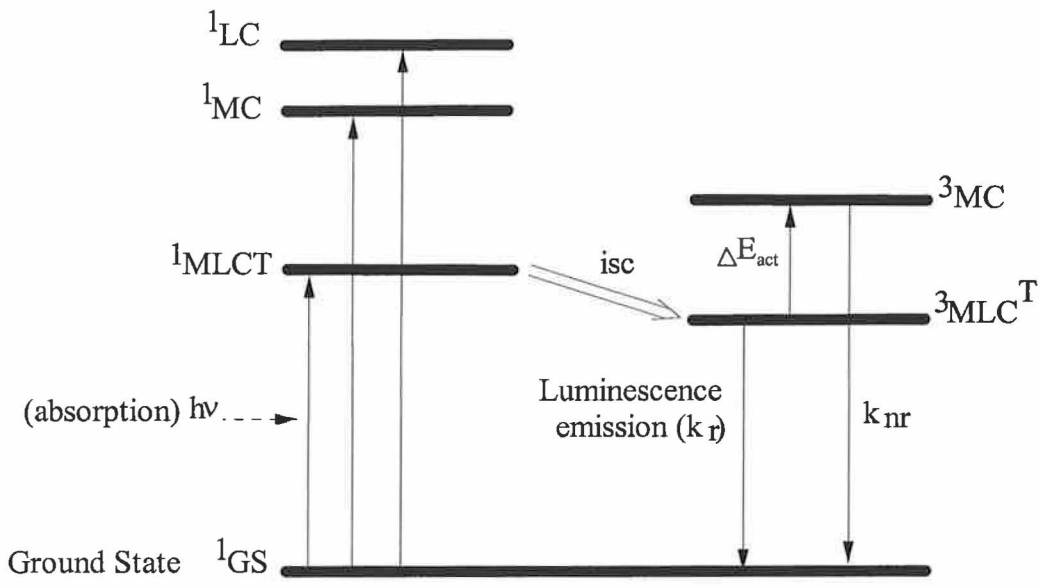

Figure 1.8 *Scheme of the photophysical properties of $[Ru(bpy)_3]^{2+}$ showing the relative order of the excited states.*

The singlet state ^{1}MLCT has a very short lifetime and converts into a triplet excited state (^{3}MLCT) by fast intersystem crossing. This is a spin forbidden transition but is made possible by spin orbit coupling. This is a process whereby an electron flips spin. The interaction of the orbital momentum and the spin momentum allows the spin momentum to be pulled around by the orbit moment. Intersystem crossing is dependent on spin

reversal and the energy gap between the first singlet state and the ground state of the molecule[34,35,36].

Emission from the triplet state to the ground state (k_r) or radiationless deactivation to the ground state (k_{nr}) can take place. Radiative decay can occur as fluorescence or phosphorescence. Fluorescence is radiative decay in which there is no change in multiplicity between the excited state and the ground state i.e. fast, spontaneous and spin allowed emission from the first singlet state to the ground state. The most common type of radiative decay for our compounds is phosphorescence whereby the spin multiplicity of the excited state differs from that of the ground state. The spin-orbit coupling results in mixing of the singlet and triplet states in phosphorescence for the spin forbidden transition T_1 --> S_o i.e. emission from a triplet state to singlet ground state[37,38,39].

Another deactivating pathway is population of the metal centred (^{3}MC) excited state, giving rise to either radiationless deactivation (k_{nr}') or photodecomposition of the complex. Population of the ^{3}MC is dependent on ΔE_{act}, the energy separation between the ^{3}MLCT and ^{3}MC states, and is thermally activated leading to decomposition of the complex or non-radiative decay (k_{nr}).

1.4 Ruthenium(II) polypyridyl complexes containing pyridyltriazole ligands.

The properties of ruthenium(II) compounds are governed by the σ-donor and π-acceptor properties of the ligands. The σ-donor capacities of the ligands can be

estimated by measuring the pKa of the free ligand whilst the π-acceptor properties are related to the reduction potential of the ligands[40,41]. The first report of 1,2,4-triazole ligands and their ruthenium complexes was by Vos and co-workers in 1983[42]. It is noted in these reports that triazoles possess weak π-acceptor properties, compared to 2,2′-bipyridine, which increase on protonation of the triazole ligand. Ligands of this nature are referred to as 'class b type ligands'(strong σ-donors, weak π-acceptors). Ruthenium(II) complexes possessing 'class b type ligands' donate much electron density into the d orbitals, causing lower oxidation potentials and more negative reduction potentials[41]. Other ligands with these characteristics (strong σ-donor capacity) are 2-(pyridin-2-yl)imidazole[43] and 2-(pyridin-2-yl)pyrazole[44]. Their strong σ-donor capacaties may result in larger ligand-field splitting, thus preventing photodecomposition. Due to their strong σ-donor capabilities, the ligands possess π^* levels of much higher energy than bpy and as a result the excited state is always bpy based in mixed chelate complexes containing both bpy and class b type ligands. If a ligand is a weaker σ-donor but stronger π-acceptor than bipyridine it is referred to as a 'class a type ligand'. Apart from bpy, several ruthenium(II) complexes containing strong π-accepting ligands such as 2,2′-bipyrazine (bpz), 2,2′-bipyrimidine (bpm) and 2,2′-biquinoline (biq) have been reported in the literature[45,46,47]. These complexes are more susceptible to photodecomposition due to the easier population of the ^{3}MC state after excitation, causing a reduction in the emission yield. This is a result of the reduction in the ligand-field splitting of Ru(II). However more recently, with the combination of class a and b type ligands i.e biquinolines and triazoles, photostability has been achieved[48].

Pyridyltriazole ligands (see Figure 1.9) possess an acid-base chemistry that can be utilised to manipulate the properties of their ruthenium(II) complexes[49]. Protonation/deprotonation of the uncoordinated nitrogen of the triazole leads to important changes in the properties of the complexes. Protonation reduces the σ-donor capacity of the ligand that results in marked effects on the ground and excited state properties of the complex[40,50]. In the deprotonated state the pyridyltriazole complexes are in general photostable, while in the protonated state they exhibit a marked photochemical reactivity due to their decreased σ-donating ability.

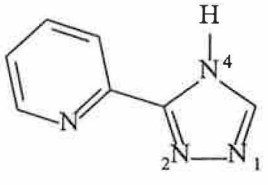

Figure 1.9 3-(pyridin-2-yl)-1,2,4-triazole.

Another important feature of pyridyltriazole type complexes is the asymmetry of the coordination sites of the triazole whereby the specific sites chosen affects the magnitude of σ-donation experienced by the metal[51]. In the thesis of R. Hage[40] an extensive study of the syntheses and structures of ruthenium(II) complexes with six substituted 3-(pyridin-2-yl)-1,2,4-triazole ligands are presented. It was deduced from ^{1}H-NMR and X-ray analysis that the metal ion can bind via N2 or N4 of the triazole ring with the most favourable coordination mode depending on the position of the substituent. The pyridyltriazole without substituents exhibits both coordination modes whereby column chromatography or HPLC was required for separation.

1.5 Applications of catechol chemistry.

1.5.1 Occurrence and properties of catechols and hydroquinones.

Hydroquinones and quinones play an essential role as electron mediators in the charge separation processes in photosynthesis. Linked porphyrin-quinones, carotenoid-quinone triads and chorophyll-porphyrin-quinone triads have been prepared and studied in detail and are active examples of biomimetic chemistry [18,19,20]. Quinonoid species as a result of their redox properties have found frequent use as acceptors and donors in charge transfer complexes or as excited state quenching agents, free in solution. The involvement of quinones in electron donor-acceptor complex formation is a consequence of the fact that such molecules possess low-lying unoccupied electronic energy levels and are therefore ready acceptors of electrons[52].

Catechol is a very powerful bidentate chelating agent, having a great affinity for metal ions in high oxidation states e.g. Fe(III), Mn(IV), V(V), Cr(III), Ti(IV), Co(III), Ac(IV), Mb(VI), Rh(VI). They are also very important in biological systems because structures with functional groups like catechol are found in certain siderophores forming very stable species with Fe(III), Mn(III) and Mn(IV)[53].

There has been a growing interest in catechol and its oxidation products (semiquinone and quinone) as ligands. Interest centres mainly on the generation of redox chains, structural characterisation, magnetic effects, the identification of effective oxidation levels, relationships with some natural biological catechol systems and the

quite complex electrochemistry that can arise through internal electron transfers and disproportionation.

Coordinated catechols show two characteristic intense bands near 1480 cm^{-1} (ring stretching C-C bond between the two oxygen atoms) and 1250 cm^{-1} (C-O stretching) . These features gain intensity in the coordinated species compared to the free ligand. Visible and near IR spectra are dominated by charge-transfer transitions[54].

More than 200 different siderophores are currently known as isolated from bacteria, yeast and fungi. All are naturally occurring chelate ligands with low molecular masses between 500 and 1000 Da and a high affinity for iron(III). The majority of effective siderophores can be divided into two groups of which the catecholate group is the one of most interest to us. The ligand is able to form unstrained and unsaturated five membered ring chelate systems with negatively charged oxygen atoms as coordination centres. This results in a high stability of corresponding complexes with the highly charged Fe^{3+}.

1.5.2 Catechols - Uses and applications.

Catechol's affinity for metal ions, mentioned earlier, leads to a wide scope for its applications. Metal-catechol complexes often exhibit unusual electronic effects due to the ability of both the ligand and metal ion to undergo electron-transfer and are of major interest since such systems represent models for the biological transport of iron, for some enzymes, and for the primary photoelectron donor-acceptor centre in bacterial photosynthesis[55].

In excess, iron(III) is very toxic in the body. Indeed, acute iron overload (e.g. from ingestion of iron supplement preparations by infants) was one of the most common

forms of poisoning in the US in the early eighties. Long-term overload can result in a blood disorder[56].

Iron (III) chelators are essential as therapeutic tools for the treatment of iron overload and as analytical tools for the precise monitoring of dietary iron intake and excretion in body fluids. Whether in vivo these agents have membrane permeation properties or not is still under investigation.

The design of organic ligands to selectively remove and recover metal ions from aqueous solution is a new and important area of environmental inorganic chemistry[57]. An example of this is the polymer-supported, sulfonated catechol ligand that is chemically bonded to modified 6% cross-linked macroporous polystyrene-divinylbenzene beads for selective removal and recovery of environmentally and economically important metal ions from aqueous solution. This can be performed as a function of pH and the metal ion selectivity could be changed by varying pH. Since diffusion of the metal ions into the hydrophobic polymer macropore/gel phases is so important, it is highly desirable to modify the catechol ligands with a hydrophilic group, such as a sulphonic acid substituent, to increase the kinetics and capacities of metal binding in aqueous solution, while also preventing the catechol ligand from being oxidised to the weaker metal binding *o*-quinone ligand.

Iron (III) removal from biological sources using a fluorescent siderophore has also been a topic of investigation[58]. The claimed sensitivity of the method and the iron specificity indicate its potential for monitoring iron under conditions of iron-mediated cell damage, iron overload, and diseases causing iron imbalance such as malaria. New iron sequestering compounds intended to be potential therapeutic agents in the treatment

of iron overload are analogues of the catechol-containing siderophore, enterobactin, shown below (see Figure 1.10)[57].

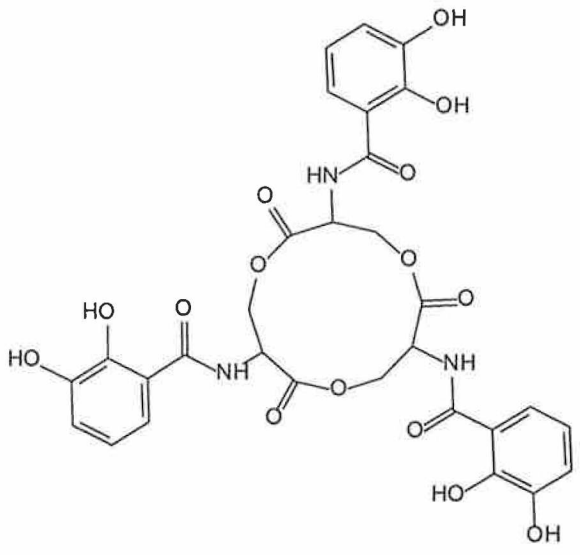

Fig. 1.10 *Structural diagram of enterobactin, the siderophore for enteric bacteria.*

Despite its extremely high affinity for iron ($K_f \approx 10^{49}$) which may even result in the 'extraction' of Fe^{III} from glass, enterobactin is not suitable as a therapy against iron poisoning. One reason is that enterobactin contains a hydrolytically labile triester ring and catecholate moieties which are sensitive toward oxidation, being transformed to *o*-semiquinones and further to *o*-quinones. In addition, the free ligand is quite insoluble in aqueous solution. Finally, the iron complex of enterobactin supports the growth of higher bacteria and may thus lead to their propagation in the human body inducing the risk of infection. It has been known to cause toxic bacteremia in iron-overloaded mice. Nevertheless, chemical derivatives of enterobactin are continuing to be tested as promising chelating agents for iron therapy.

Much of the bioinorganic chemistry of catechols has concerned complexes of iron. Much of the characterisation of biological iron(III) catecholate complexes has relied upon spectroscopic data obtained on well characterised synthetic complexes[59]. Structural studies have been carried out on complexes containing one, two or three catecholate ligands per iron. The structural features of the simple $Fe(Cat)Cl_2^-$ anion reveal that it exists as the five-coordinate $[Fe_2(cat)_2Cl_4]^{2-}$ dimer. The ligand is able to form unstrained and unsaturated five membered ring chelate systems with negatively charged oxygen atoms as coordination centres. This results in a high stability of corresponding complexes with the hard, highly charged Fe^{3+}.

1.5.3 Occurrence of ruthenium-catecholate complexes.

The ability of polypyridyl complexes of ruthenium(II) to act as photosensitisers is well established. Recently attention has turned to the incorporation of 'light-harvesting' ruthenium centres into large molecular assemblies. Such assemblies contain covalently attached quenching groups, so that energy or electron transfer from the chromophore to the accepting group is intramolecular and not dependent on collision of the two species in solution. The aim of Howard, Ward and coworkers[60] is to synthesise large molecular assemblies, *photochemical devices*, which mimic biological photosynthesis by efficient intramolecular transfer of energy from the excited state 'antenna' to a reaction centre. The reaction centre then uses the energy in a catalytic process. The successful synthesis of multicomponent supramolecular assemblies of this type may be achieved by the stepwise synthesis of heteropolynuclear complexes with a 'complexes as ligands' approach, in which a metal complex is prepared which contains a vacant, externally directed binding site. A second complex may then be attached to the

vacant site, allowing the stepwise build-up of polynuclear species from individual building blocks whose properties are known.

The ligand 4′-(3,4-dimethoxyphenyl)-2,2′:6′,2″-terpyridine (L^2), containing a terpyridyl binding site and a masked catechol binding site was prepared by Howard, Ward and coworkers and is shown in Figure 1.11 (a)[60] along with some of its related complexes in Figure 1.11 (b).

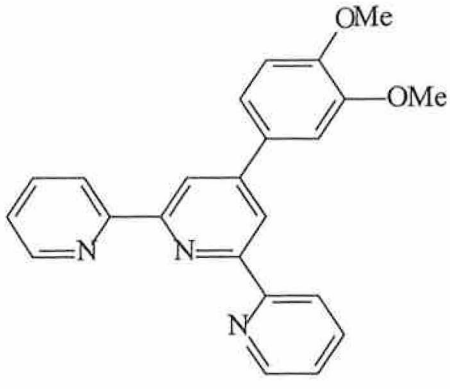

(a)

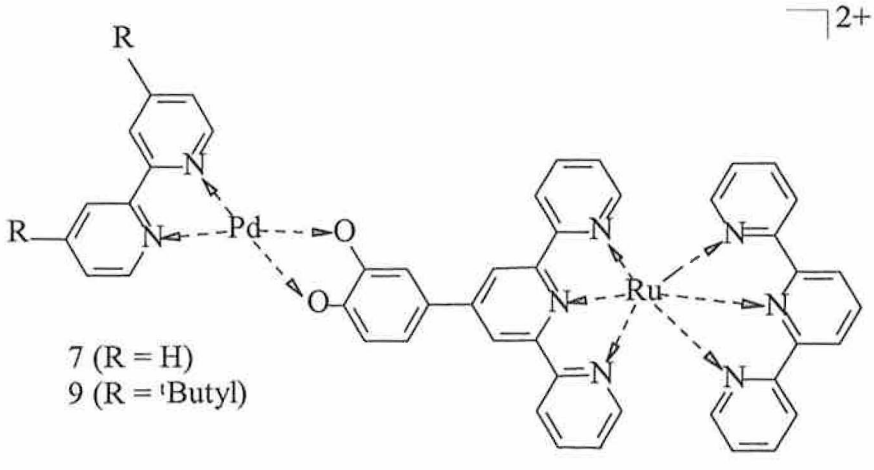

(b)

Figure 1.11 Structure of (a) L^2 ligand and (b) some of its related complexes (7), (9)[60].

From the ligand L^2 the complexes $[Ru(terpy)\text{-}(L^2)][PF_6]_2$ (1)and $[Ru(L^2)_2][PF_6]_2$ (2) containing one and two dimethoxyphenyl subunits were prepared using standard

methods and demethylation with BBr_3 afforded $[Ru(terpy)(H_2L^1)][PF_6]_2$ (3) and $[Ru(H_2L^1)_2][PF_6]_2$ (4), respectively, which have one or two free catechol binding sites pendant from the $[Ru(terpy)_2]^{2+}$ core. Binuclear complexes (based on (3)) and trinuclear complexes (based on (4)) were then prepared by attachment of other metal fragments at the catechol sites. In $[Ru(terpy)(\mu\text{-}L^1)Ru(bpy)_2][PF_6]_3$ (5) and $[Ru(\mu\text{-}L^1)_2\{Ru(bpy)_2\}_2][PF_6]_4$ (6) the pendent $\{Ru(bpy)_2(O\text{-}O)\}^{n+}$ sites (O-O = catecholate, n = 0; *o*-benzosemiquinone, n = 1; *o*-benzoquinone, n = 2) are redox active and may be reversibly interconverted between the three oxidation levels. The pendent {Pd(bpy)(catecholate)} fragments in $[Ru(terpy)(\mu\text{-}L^1)Pd(bpy)][PF_6]_2$ (7), $[Ru(\mu\text{-}L^1)_2\{Pd(bpy)_2\}_2][PF_6]_2$ (8), $[Ru(terpy)(\mu\text{-}L^1)Pd(4,4'\text{-}{}^t\!Bu_2\text{-}bpy)][PF_6]_2$ (9), and $[Ru(\mu\text{-}L^1)_2\{Pd(4,4'\text{-}{}^t\!Bu_2\text{-}bpy)\}_2][PF_6]_2$ (10), are known to be photocatalysts for the production of $^1O_2$ in their own right. The compounds (1) - (10), excluding (5) and (6) were characterised by ^1H NMR. (5) and (6) are paramagnetic due to the presence of coordinated semiquinone groups and had to be examined by ESR. The more complex ^1H NMR spectra of (7) - (10) were assigned with the aid of COSY spectra. Preparative layer chromatography on silica and alumina was used for purification in some cases. The yields of the dimers (5) and (7) were no higher than 40 %. The trimer (6) had only a reported yield of 20 % while (8) was 40% and (10) gave a yield of between 50 -70 %. Reaction of (3) and (4) with 1 or 2 equivalents, respectively, of $[Pd(bpy)Cl_2]$ gave (7) or (9), in which the $\{Ru(terpy)_2\}^{2+}$ core is attached to one or two {Pd(bpy)(cat)} substituents. These complexes are reportedly quite insoluble, so (8) and (10) using $[Pd(4,4'\text{-}{}^t\!Bu_2\text{-}bpy)_2Cl_2]$ as starting material, in which the ^{t}Bu substituents make the complexes much more soluble in organic solvents. All of the complexes were also characterised by FAB mass spectrometry and elemental analysis. Electrochemical and

UV/Vis studies were performed on all complexes and consistently indicated the presence of interactions between the components in (5)-(10).

The major disadvantage of a $[Ru(terpy)_2]^{2+}$ core compared to $[Ru(bpy)_3]^{2+}$ is that its photochemical characteristics are not so desirable as it has a much shorter excited-state lifetime and does not luminesce in fluid solution. However recent work has shown that with appropriate substituents on the ligands, derivatives of $[Ru(terpy)_2]^{2+}$ may be luminescent in fluid solution[61].

The catechol is an appealing peripheral binding site for several reasons. First, it forms stable, well characterised complexes with many transition and main-group metals. Second, by using the templating effects of complexes such as $[M(cat)_3]^{3-}$ (M = Fe, Cr ; cat = dianion of catechol)[62-65] it should be possible to assemble several photoactive polypyridyl-ruthenium chromophores around a single central metal ion for examination of the antenna effect. Third, catechol is redox active and undergoes reversible catecholate/semiquinone/quinone (cat/sq/q) interconversions in many metal complexes, allowing the possibility of the energy or electron transfer characteristics of polynuclear complexes being switchable according to the redox level of the peripheral fragments[66-68].

1.6 Scope of this thesis

In chapter 2 the experimental methodology used to characterise the complexes synthesised in the course of the work will be described. Chapter 3 will describe the synthesis, purification and characterisation of the mononuclear ruthenium complexes of the bridging ligand 3-(1′,2′-methoxyphenyl)-5-(pyridin-2-yl)-1,2,4-triazole ligand (**HL1**). The mononuclear complexes discussed will include $Ru(bpy)_2$, $Ru(phen)_2$ and $Ru(dcbpy)_2$ adducts of **HL1**. Deuteriated complexes, whereby the phenanthroline and bipyridine

rings are deuteriated will also be examined to enable clearer elucidation of the complexes in ^{1}H NMR spectra. Chapter 4 will discuss the deprotection of two mononuclear complexes of **HL1**. Synthesis and characterisation of the catechol complexes (**ML2** where M = bpy or phen) will be discussed with attention paid to the attachment of the complexes to TiO_2 . The efficiency of the catechol complexes to behave as sensitisers will be assessed along with that of the $Ru(dcbpy)_2$ complex of **HL1** (**dcbpyL1**). In chapter 5 the synthesis of the ruthenium dinuclear complexes from the catechol complexes **ML2** will be discussed. The complex electrochemistry of the semiquinone bound complexes will be examined and communication between the metal centres will be examined. The purification and characterisation of the dinuclear complexes will also be examined. Investigation of the complexation of transition metals by a ruthenium mononuclear complex containing a catechol binding site (**bpyL2**) will be examined in chapter 6. Some final remarks on the work and suggestions for future work will be considered in chapter 7.

Finally three appendices are supplemented to the thesis. The first consists of ^{1}H NMR spectra for the ligands **HL1** and **HL2** and the complex **dcbpyL1**. The second includes the X-Ray crystal data for the mononuclear complexes of **HL1** (**d_8-bpyL1** and **phenL1**). The third appendix refers to the poster presentations made during the course of the research.

1.7 References.

1 R.K. Clayton, Photosynthesis; Physical methods and chemical patterns, 1st ed., Cambridge University Press, 1980.

2 D.A. Baker, Transport phenomena in plants, Halsted Press, 1978.

3 J.F. Sutcliffe and D.A. Baker, Plants and mineral salts, Camelot Press, 1974.

4 D.B. Knaff, D.I. Arnon, *Biochemistry*, 1969, 64, 715.

5 B. Lagoutte, P. Mathis, *Photochem. Photobiol.*, 1989, 49, 833.

6 J.D. Coyle, R.R. Hill and D.R. Roberts, Light, chemical change and Life; a source book in photochemistry, The Open University Press1982.

7 D.A. Gust, T.A. Moore, *Science*, 1989, 244, 35.

8 J.R. Norris, P. Gast, *J. Photochem.*, 1985, 29, 185.

9 J. Barber, B. Andersson, *Nature*, 1994, 370, 31.

10 T.E. Keyes, Ph.D. Thesis, Dublin City University, 1995.

11 M.L. Kirk, M.K. Chan, W.H. Armstrong, E.I. Solomon, *J. Am. Chem. Soc.*, 1992, 114, 10432.

12 G.N. George, R.C. Prince, S.P. Cramer, *Science*, 1989, 243, 789.

13 W.F. Ruettinger, D.M. Ho, G.C. Dismukes, *Inorg. Chem.*, 1999, 38, 1036.

14 D. Chin, D.T. Sawyer, W.P. Schaefer, C.J. Simmons, *Inorg. Chem.*, 1983, 22, 752.

15 M.W. Lynch, D.N. Hendrickson, B.J. Fitzgerald, C.G. Pierpont, *J. Am. Chem. Soc.*, 1984, 106, 2041.

16 J.E. McGrady, R. Stranger, *J. Am. Chem. Soc.*, 1997, 119, 8512.

17 K.R. Seddon, E. Seddon, The Chemistry of Ruthenium, Elsevier, Amsterdam,

1984.

[18] Y. Aoyama, M. Asakawa, Y. Matsui, H. Ogoshi, *J. Am. Chem. Soc.*, 1991, 113, 6233.

[19] D.G. Johnson, M.P. Niemczyk, D.W. Minsek, G.P. Wiederrecht, G.L. Svec, G.L. Gaines III, M.R. Wasielewski, *J. Am. Chem. Soc.*, 1993, 115, 5692.

[20] D. Gust, T.A. Moore, P.A. Liddell, G.A Nemeth, L.R. Makings, A.L. Moore, D. Barrett, P.J. Pessiki, R.V. Benasson, M. Rougee, C. Chachaty, F.C. De Schryver, M. Van der Auweraep, A.R. Hotzwarth, J.S. Connolly, *J. Am. Chem. Soc.*, 1987, 109, 846.

[21] R. Alsfasser, R. van Eldik, *Inorg. Chem.*, 1996, 35, 628.

[22] Lippard, S.J., *Science*, 1993, 261, 699.

[23] V. Balzani and F. Scandola, *SupramolecularPhotochemistry*; Horwood: Chichester,UK 1991.

[24] T.J. Rutherford, F.R. Keene, *Inorg. Chem.*, 1997, 36, 2872.

[25] P. Liska, N. Vlachopoulos, M.K. Nazeeruddin, P. Comte, M. Grätzel, *J. Am. Chem. Soc.*, 1988, 110, 3686.

[26] S.G. Yan, L.A. Lyon, B.I. Lemon, J.S. Preiskorn, J.T. Hupp, *J. Chem. Ed.*, 1997, 74, 657.

[27] R. Argazzi, C.A. Bignozzi, T.A. Heimer, F.N. Castellano, G.J. Meyer, *Inorg. Chem.*, 1994, 33, 5741.

[28] A.C. Lees, B. Evrard, T.E. Keyes, J.G. Vos, C.J. Kleverlaan, M. Alebbi, C.A. Bignozzi, *Eur. J. Inorg. Chem.*, 1999, 2309.

[29] M.K. Nazeeruddin, A. Kay, I. Rodicio, R. Humphry-Baker, E. Müller, P. Liska,

N. Vlachopoulos, M. Grätzel, *J. Am. Chem. Soc.*, 1993, 115, 6382.

30 F.A. Cotton, G. Wilkinson, Advanced Inorganic Chemistry, Wiley, Chichester, 5th ed., 1988.

31 J.P. Paris, W.W. Brandt, *J. Am. Chem. Soc.*, 1959, 81, 5001.

32 B. Durham, J.V. Casper, J.K. Nagle, T.J. Meyer, *J. Am. Chem. Soc.*, 1982, 104, 4803.

33 R.J. Watts, *J. Chem. Ed.*, 1983, 60, 834.

34 J.V. Casper, T.J. Meyer, *J. Am. Chem. Soc.*, 1983, 105, 5583.

35 N.H. Damrauer, G. Cerullo, A. Yeh, T. R. Boussie, C.V. Shank, J.K. McCusker, *Science*, 1997, 275, 54.

36 C. Li, M.Z. Hoffman, *Inorg. Chem.*, 1998, 37, 830.

37 E.M. Kober, T.J. Meyer, *Inorg. Chem.*, 1982, 21, 3967.

38 E.M. Kober, T.J. Meyer, *Inorg. Chem.*, 1983, 22, 1614.

39 E.M. Kober, T.J. Meyer, *Inorg. Chem.*, 1984, 23, 3877.

40 R. Hage, Ph.D Thesis, Leiden University, 1991.

41 S.D. Ernst, W. Kaim, *Inorg. Chem.*, 1989, 28, 1520.

42 J.G. Vos, J.G. Haasnoot, G.Vos, *Inorg. Chim. Acta.*, 1983, 162, 155.

43 M.Haga, T. Matsumura-Inoue, K. Shimizu, G.P. Sato, *J.Chem. Soc., Dalton Trans.*, 1989, 371.

44 P.J. Steel, E.C. Constable, *J. Chem. Soc, Dalton. Trans.*, 1990, 1389.

45 G.D. Danzer, K.R. Kincaid, *J. Phys. Chem.*, 1990, 94, 3976.

46 E.V. Dose, L.J. Wilson, *Inorg. Chem.*, 1978, 17, 2660.

47 R.P. Thummel, F. Lefoulon, S. Chirayil, *Inorg. Chem.*, 1987, 26, 3072.

[48] T.E. Keyes, J.G. Vos, J.A. Kolnaar, J.G. Haasnoot, J. Reedijk, R. Hage, *Inorg. Chim. Acta*, 1996, 245, 237.

[49] B.E. Buchanan, J.G. Vos, M. Kaneko, W.J.M van der Putten, J.M. Kelly, R. Hage, R.A.G. de Graaff, R. Prins, J.G. Haasnoot, J. Reedijk, *J. Chem Soc.,Dalton Trans.*, 1990, 2425.

[50] R.Hage, J.G. Haasnoot, H.A. Niewenhuis, J. Reedijk, D.H. de Ridder, J.G. Vos, R. Wang, *J. Am. Chem. Soc*, 1990, 112, 9245.

[51] R.Hage, J.G. Haasnoot, H.A. Nieuwenhuis, J. Reedijk, R. Wang, J.G. Vos, *J. Chem. Soc., Dalton Trans.*, 1991, 3271.

[52] The Chemistry of Quinone compounds, Ed. Spatai, Chapter 6; R. Foster and M. I. Foreman, Wiley and Sons, 1988.

[53] M.E. Bodini, V. Arancibia, *Transition Met. Chem.*, 1997, 22, 150.

[54] J. Balla, T. Kiss, R.F. Jameson, *Inorg. Chem.*, 1992, 31, 58.

[55] R.B. Salmonson, A. Abelleiron, I.M.J. Clarke, *Inorg. Chem.*, 1984, 23, 385.

[56] V.L Pecoraro, F.L Weitl, K.N. Raymond, *J. Am. Chem. Soc.*, 1981, 103, 5133.

[57] S-P. Huang, W. Li, K.J. Franz, R.L. Albright, R.H. Fish, *Inorg. Chem*, 1995, 34, 2813.

[58] S.D. Lytton, B. Mester, J. Libman, A. Shanzer, Z.I. Cabantchik, *Anal. Biochem.*, 1992, 205, 326.

[59] D. Zirong, R.C. Haltiwanger, S. Bhattacharya, C.G. Pierpont, *Inorg. Chem.*, 1991, 30, 4288.

[60] B. Whittle, N.S. Everest, C. Howard, M.D. Ward, *Inorg. Chem.*, 1995, 2025.

[61] J.R. Kirchhoff, D.R. McMillan, P.A. Marnot, J.P. Sauvage, *J. Am. Chem. Soc.*, 1985, 107, 1138.

[62] R.M. Buchanan, S.L. Kessel, H.H. Downs, C.G. Pierpont, D.N. Hendrickson, *J. Am. Chem. Soc.*, 1978, 100, 7894.

[63] S.R. Sofen, D.C. Ware, S.R. Cooper, K.N. Raymond, *Inorg. Chem.*, 1979, 18, 234.

[64] R.M. Buchanan, J. Claflin, C.G. Pierpont, *Inorg. Chem.*, 1983, 22, 2552.

[65] S.R. Boone, G.H. Purser, H.R. Chang, M.D. Lowery, D.N. Hendrickson, C.G. Pierpont, *J. Am. Chem. Soc.*, 1989, 111, 2292.

[66] W.P. Griffith, *Trans. Met. Chem.*, 1993, 18, 250.

[67] L.F. Joulié, E. Schatz, M.D. Ward, F. Weber, L.J. Yellowlees, *J. Chem. Soc., Dalton Trans.*, 1994, 799.

[68] A.M. Barthram, R.L. Cleary, J.C. Jeffery, S.M. Couchman, M.D. Ward, *Inorg. Chim. Acta*, 1998, 267, 1.

Chapter Two

Experimental Procedures

2.0 Introduction.

This section is intended to present the experimental procedures used in the characterisation of the ruthenium complexes and the methods used for obtaining the physical measurements. The synthesis and purification of the compounds are described in subsequent chapters.

2.1 Materials and reagents.

All synthetic reagents were of commercial grade and no other purification was employed. The solvents used in spectroscopic measurements, with the exception of ethanol, were HPLC grade. Cis-$[Ru(bpy)_2Cl_2].2H_2O$, cis-$[Ru(d_8\text{-}bpy)_2Cl_2].2H_2O$ and per deuteriated 1,10-phenanthroline (d_8-phen) were obtained from earlier studies[1]. Cis-$[Ru(dcbpy)_2Cl_2].2H_2O$ was also obtained from earlier studies[2]. Cis-$[Ru(phen)_2Cl_2].2H_2O$ and $[Ru(d_8\text{-}phen)_2Cl_2]$ were synthesised according to the method published by Sullivan[3].

2.2 Nuclear Magnetic Resonance Spectroscopy.

^{1}H-NMR spectra were recorded on a Bruker AC400 (400 MHz) instrument. The solvent used for the complexes was mainly deuteriated acetonitrile. Deuterium oxide was used in some of the spectra but this is clearly stated. Deuteriated dimethyl sulphoxide was used for the ligands. The chemical shifts were recorded relative to the standard tetramethylsilane (TMS). The spectra were converted from their Free Induction Decay (FID) profiles using a Bruker WINNMR software package.

The 2-D COSY (correlated spectroscopy) experiments involved the accumulation of 128 FIDs of 16 scans. Digital filtering was sine-bell squared and the

FID was zero filled in the F1 dimension. Acquisition parameters were F1 = ± 500 Hz, F2 = 1000 Hz and $t_{1/2}$ = 0.001 s. The cycle time delay was 2 s.

2.3 Absorption and Emission Measurements.

UV/Visible spectra were obtained using a Shimadzu UV3100 UV-Vis-NIR spectrophotometer interfaced to an Elonex PC433 personal computer. The extinction coefficients are accurate up to 5 %.

Emission spectra were obtained on a Perkin-Elmer LS50B luminescence spectrometer equipped with a red sensitive Hamamatsu R928 detector, interfaced to an Elonex PC466 personal computer employing Perkin-Elmer FL WinLab custom built software. Excitation and emission slit widths of 10 nm respectively were used for all the measurements. The spectra were not corrected for the photomultiplier response.

HPLC grade acetonitrile was used for the pH dependent absorption and emission studies of the complexes with the exception of the dicarboxy complex where distilled water was used. To ensure protonation/deprotonation, a few drops of perchloric acid or diethyl amine solution were added to the sample.

The ground state pKas were measured by manipulating the observed changes in the UV/Vis absorption intensity as a function of pH. The excited state acid-base equilibria were measured by manipulating the changes in the emission intensity as a function of pH. The excitation wavelength for the emission titration was chosen from a suitable isobestic point determined from the absorption acid/base titration spectra. The samples were dissolved in a few drops of acetonitrile ($\approx 10^{-5}$ M) and diluted with 100 cm^3 of Britton-Robinson buffer (0.04 M boric acid, 0.04 M acetic acid, 0.04 M phosphoric acid). The pH was adjusted by adding conc. NaOH or conc. H_2SO_4 and was

measured using a Corning 240 digital pH meter. The pKas were determined from the point of inflection of a plot of percentage change in absorbance versus pH.

2.4 Complexation titrations.

Investigation of the stability constants (complexation) of the ruthenium catechol complexes with various transition metals was followed by UV/Vis (absorption titrations) and emission (spectrofluorimetric titrations). The latter require excitation at an appropriately selected isobestic point from the absorption titrations. The solvent used was HPLC grade methanol. The stability constants were evaluated using a DOS based program, SIRKO, V2 1994 designed by A.V. Bogatsky Physico-Chemical Institute, Odessa, Ukraine[4,5].

2.5 Luminescent lifetime measurements.

These measurements were carried out with the assistance of Marco Duati. The instrument, that we used, is a Single Photon Counter of Edinburgh Analytical Instrument in a T setting. The lamp is a nF900, in a Nitrogen setting, the monochromators are J-yA models, the detector is a Single Photon Photomultiplier Detection System, model S 300, with a MCA card type Norland N5000 and a PC interface Cd900 serial. The program used for the data correlation and manipulation is F900 Program, Version 5.13.

The measurements were performed in spectroscopic grade acetonitrile, basified with diiethylamine and acidified with perchloric acid. The samples were excited using 337 nm as excitation wavelength and the lifetimes were collected in the maxima of the emission.

2.6 Electrochemistry.

The electrochemistry of the compounds was performed in dry acetonitrile (dried over molecular sieve) with tetraethylammonium perchlorate (TEAP) as electrolyte except where stated. The electrolyte was prepared by dissolving tetraethylammonium bromide (1 M) in water. Perchloric acid (1 M) was added dropwise until precipitation of the white perchlorate salt ceased. The product was collected by filtration and redissolved in hot water, neutralised and then recrystalised several times from hot water.

The standard three electrode method was used. The reference electrode used was a Ag/AgCl reference electrode. The working electrode was a 3 mm diameter teflon shrouded glassy carbon electrode and a platinum gauze was used as the counter electrode. The electrochemistry was run in a small beaker making sure there was no contact between the respective electrodes. Prior to looking at the ligand based reduction, the solutions were degassed for 15 minutes with nitrogen and during runs a gentle flow of nitrogen was maintained above the solvent surface. Cyclic voltammetry and square wave voltammetry were carried out using a CH instrument Model 660 potentiostat electrochemical workstation interfaced to an Elonex 486 PC.

2.7 Spectroelectrochemistry.

Spectroelectrochemistry was carried out as using a home-made pyrex glass thin layer cell (1 mm), a platinum gauze as working electrode , a Ag/AgCl quasi-reference electrode and a platinum wire as counter electrode. The electrolyte used was 0.1 M TEAP in acetonitrile and the UV/Visible/NIR spectra were recorded using the Shimadzu 3100 UV/NIR spectrometer interfaced to an Elonex PC433 computer. The working

electrode was held at the required potential during the spectral scan using a CH instrument Model 660 potentiostat electrochemical workstation interfaced to an Elonex 486 PC. Scans at anodic potentials required degassing of the samples.

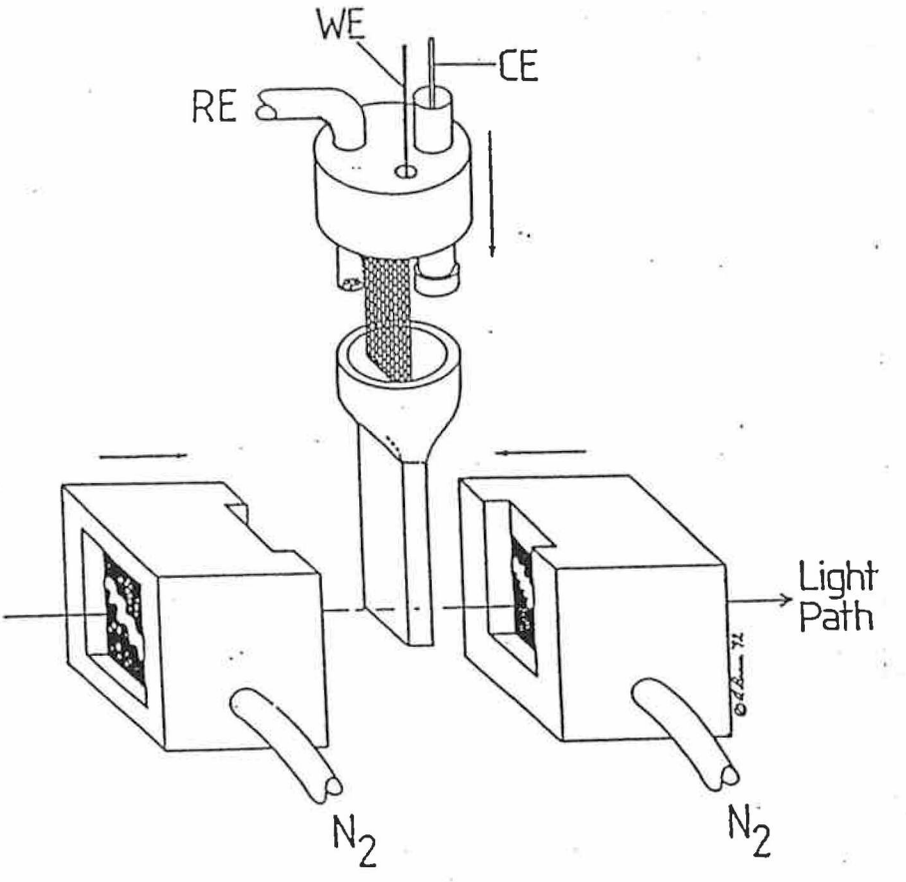

Figure 2.1 Diagram of the OTTLE cell used for spectroelectrochemistry.

2.8 High Performance Liquid Chromatography (HPLC).

Analytical cation exchange chromatography was used for analysis of the possitively charged complexes. The analytical HPLC experiments were carried out using a Waters HPLC system, consisting of a model 501 pump, a 20 µl injector loop, a Partisil SCX steel column and a 990 photodiode array detector. The system was controlled by an NEC APCIII computer. The detection wavelength was 280 nm where the most intense band in the absorption spectra (π-π^*), for the ruthenium complexes

studied, occurs. The mobile phase used in all the analyses was 0.08 M $LiClO_4$ in 80/20 acetonitrile/water. The flow rate was 1.8 cm^3/min.

Analysis of the dicarboxy compound required an anion exchange column, Partisil SAX radial PAK cartridge mounted in a radial compression Z module. This was linked to the same system described earlier by simply replacing the Partisil SCX column (stored in methanol). The mobile phase used in this case was 0.025 M Na_2HPO_4 ; 0.025 M NaH_2PO_4 in 50/50 acetonitrile/water. The flow rate was 2.0 cm^3\min.

Semi-preparative HPLC was performed using an ACS pump, a 1 cm^3 injection loop and a Waters Partisil SCX 10 μm cation exchange column (25 x 100 mm). The mobile phase used 0.12 M KNO_3 in 80/20 acetonitrile/water. The flow rate used 2.0 cm^3/min.

2.9 Elemental analysis.

C,H,N elemental analyses were carried out by the Microanalytical laboratories at University College Dublin.

2.10 X-Ray Analysis.

X-Ray data collection and analysis were obtained from the University of Jena, Germany with the co-operation of Sven Rau (see appendix 2).

2.11 Titanium dioxide solar cells.

Solar energy conversion studies were performed in Bologna by Monica Alebbi from the group of Prof. Carlo Bignozzi.

2.12 Mass Spectra.

The Mass Spectra data were obtained from the University of Jena, Germany by Sven Rau. Electrospray ionization mass spectrometry (ESI-MS) was used for the samples investigated.

2.13 References.

[1] C. O' Connor, Ph.D. Thesis, Dublin City University, 2000.

[2] A.C. Lees, Unpublished results.

[3] B.P. Sullivan, D.J. Salmon, T.J. Meyer, *Inorg. Chem.*, 1978, 17, 3334.

[4] A.V. Bogatsky, Physico-Chemical Institute, Odessa. Laboratoire de Chemie Physique, ECPM, Strasbourg.
http://www.geocities.com/capecanaveral/Lab/9065.

[5] V.I. Vetrogon, N.G. Lukyanenko, M.-J. Schwing-Weill, F. Arnaud-Neu, *Talanta*, 1994, 41, 2105.

Chapter Three

Synthesis and Characterisation of Mononuclear Ruthenium Complexes Containing a Pyridyl-1,2,4-Triazole Ligand with a Protected Catechol Ring

3.0. Introduction.

An introduction to ruthenium(II) polypyridyl complexes containing pyridyltriazole ligands was presented earlier in chapter one in section 1.4. In the following chapter the synthesis of a pyridyltriazole based ligand with a protected catechol ring and the ruthenium(II) complexes of the ligand, prepared in the course of the work, are described. The purpose of protecting the catechol ring was to simplify the synthesis of the ruthenium complexes ensuring that binding is solely through the pyridyltriazole and inhibiting O,O bound complexes and dimer formation. The characterisation of the complexes is also described and discussed in detail. The complexes prepared and investigated in this chapter provide the precursors to the remaining work presented in chapters four, five and six. An important aspect of the work involving ruthenium(II) complexes with various ligands, and in our case pyridyltriazole ligands, is the location of excited states. A method described in the work of Hage is the manipualation of the acid/base properties of the complexes[1]. Measuring the ground state and excited state pKa values can indeed reveal information concerning the nature of the lowest unoccupied molecular orbital of the complexes. Mixed-ligand complexes of the type $[Ru(LL)_2(LL')]^{2+}$ may have the excited state emission located on the LL ligand (like bpy) or on the LL′ ligand and evaluation of the pKa and pKa^* can help ascertain its location. When excited if the complex is more basic than in the ground state, emission occurs from the ligand that can be protonated/deprotonated. After excitation, more electron density is present on the ligand and it is easier to bind a proton. On the other hand if the excited state is more acidic than the ground state, this is due to the non participation of the ligand that can be protonated/deprotonated. After

excitation the metal ion becomes formally 3+ and more charge is donated from the ligand to the metal ion.

Another important tool in the location of excited states, in mixed-ligand ruthenium (II) polypyridyl complexes, is the application of deuteriation. The deuteriation of ligands as a tool for the study of excited states is a relatively under-exploited method and was reported upon by T.E. Keyes et al in 1995[2]. It was previously reported upon as an important tool in the simplification of ^{1}H-NMR spectra[3] and is also used, as such, in the work presented in this chapter. According to Siebrand's theory of the non-radiative transition[45], high energy, anharmonic C-H stretching vibrations are important promotional modes in non-radiative decay. This implies that excited-state lifetimes should increase upon deuteriation. The results presented by T.E. Keyes et al show a strong correlation with this theory. It was suggested that the emission lifetimes of the heteroleptic compounds will only increase upon deuteriation of a particular ligand when the excited state is located on that ligand. This type of selective deuteriation of particular ligands can be employed in larger supramolecular systems like those described by Balzani and Scandola[6] lending to much more information about the relative excited-state energies of these components relative to the whole system.

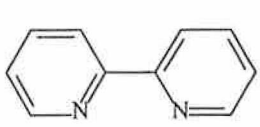

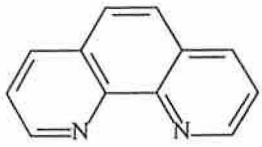

2,2′-bipyridine (bpy) 1,10-phenanthroline (phen)

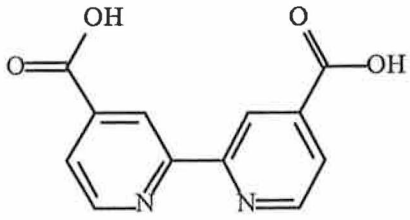

4,4′-dicarboxylicacid-2,2-bipyridine (dcbpy)

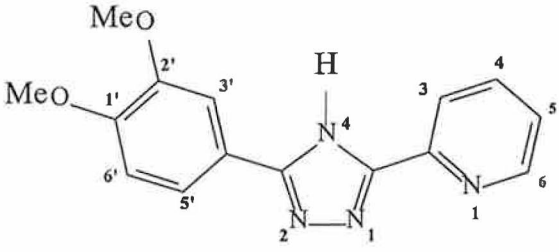

3-(1′,2′-dimethoxyphenyl)-5-(pyridin-2-yl)-1,2,4-triazole (HL1)

Figure 3.1 Structures of the polypyridyl ligands cited in the text.

3.1. Experimental

3.1.1. Synthesis of the Metal Complexes.

The synthesis of the mononuclear complexes of the ligand 3-(1′,2′-dimethoxyphenyl)-5-(pyridin-2-yl)-1,2,4-triazole (HL1) are presented in this section. The synthetic difficulties and purification of the complexes will be discussed in section 3.2.1. The ligand 3-(1′,2′-dimethoxyphenyl)-5-(pyridin-2-yl)-1,2,4-triazole (HL1) was obtained from earlier studies by Sven Rau[7,8] and the ruthenium dichlorides are referred to in section 2.1 of Chapter two.

$[Ru(bpy)_2(L1)]PF_6.H_2O$ **(bpyL1)**

0.395 g (1.41 mmol) of HL1 ligand was dissolved in 50 cm^3 ethanol:water (1:1 v/v). This was heated to reflux until the ligand was fully dissolved. 0.520g (1 mmol) cis-$[Ru(bpy)_2Cl_2].2H_2O$ (see section 2.0) was added and the reaction allowed to reflux for 5-8 hours. Periodically, samples were removed and monitored by analytical HPLC to assess completion of the reaction. After the solution was allowed to cool the reaction was filtered and the volume reduced to ca 15 cm^3. The complex was precipitated by addition of a concentrated aqueous solution of ammonium hexafluorophosphate. The precipitate was filtered and washed with a small volume of water (10-15 cm^3). The product was dried by washing with diethylether and left under vacuum for a few hours. The dry complex was recrystallised from acetone/water (2:1 v/v) to which a few drops of aqueous NH_3 was added. Purity was determined by HPLC (see Sect. 2.8) and ^{1}H-NMR spectroscopy. The complex was generally between 90-95 % pure and column chromatography on neutral alumina using acetonitrile as eleunt was used to remove any

final impurities. Yield = 0.53 g (60 %). Calcd. for : $Ru_1C_{35}H_{31}N_8O_3P_1F_6$ C: 49.00; H: 3.60; N: 13.10 %. Anal. Found: C: 48.58; H: 3.34; N: 12.66 %.

[Ru(phen)$_2$(L1)]PF$_6$.H$_2$O **(phenL1)**

This complex was prepared similarly to [Ru(bpy)$_2$(L1)]PF$_6$.H$_2$O. O.395 g (1.41 mmol) of ligand HL1 and 0.568 g (1 mmol) of cis-[Ru(phen)$_2$Cl$_2$].2H$_2$O (see section 2.1) were refluxed for 5-8 hours. The progress of the reaction was followed by analytical HPLC (Sect 2.8). The complex was recrystallised from acetone/water (2:1 v/v) to which a few drops of aqueous NH_3 was added. Further purification was performed using column chromatography on neutral alumina with acetonitrile as eluent. Yield = 0.45 g (50%). Calcd. for : $Ru_1C_{39}H_{31}N_8O_3P_1F_6$ C: 51.72; H: 3.45; N: 12.37 %. Anal. Found: C: 52.12; H: 3.54; N: 12.17 %.

[Ru(d$_8$-bpy)$_2$(L1)]PF$_6$.H$_2$O **(d$_8$-bpyL1)**

This complex was prepared in a similar manner to [Ru(bpy)$_2$(L1)]PF$_6$.H$_2$O. O.395 g (1.41 mmol) of ligand HL1 and 0.520 g (0.97 mmol) of cis-[Ru(d$_8$-bpy)$_2$Cl$_2$].2H$_2$O (see section 2.1) were refluxed for 5-8 hours. The complex was recrystallised from acetone/water (2:1 v/v), to which a few drops of aqueous NH_3 was added, and purified as before using neutral alumina with acetonitrile as eluent. Yield = 0.46 g (54 %). Calcd. for : $Ru_1C_{35}H_{15}D_{16}N_8O_3P_1F_6$ C: 48.11; H: 3.55; N: 12.82 %. Anal. Found: C: 47.90; H: 3.48; N: 12.49 %.

$[Ru(d_8\text{-phen})_2(L1)]PF_6.H_2O$ **(d_8-phenL1)**

This complex was prepared in a similar manner to that described for $[Ru(bpy)_2(L1)]PF_6.H_2O$. 0.395 g (1.41 mmol) of ligand and 0.584 g (1 mmol) of cis-$[Ru(d_8\text{-phen})_2Cl_2].2H_2O$ (see section 2.1) were refluxed for 5-8 hours. The complex was recrystallised from acetone/water (2:1 v/v), to which a few drops of aqueous NH_3 was added. Further purification was performed using column chromatography on neutral alumina with acetonitrile as eluent. Yield = 0.52 g (56 %). Calcd. for : $Ru_1C_{39}H_{15}D_{16}N_8O_3P_1F_6$ C: 50.80; H: 3.39; N: 12.16 %. Anal. Found: C: 50.75; H: 3.42; N: 11.91 %.

$[Ru(H_4dcbpy)_2(HL1)]Cl_2.5H_2O$ **(dcbpyL1)**

0.555 g (0.8 mmol) $[Ru(dcbpy)_2Cl_2].2H_2O$ (see section 2.1) was dissolved in 30 cm^3 ethanol/water(2:1 v/v) using one pellet of NaOH. This was slowly added, over a period of 30 minutes, to 0.236 g (0.84 mmol) HL1 ligand refluxing in 20 cm^3 ethanol/water (2:1 v/v). The reaction was allowed to reflux for 5-8 hours and was monitored periodically using analytical anion exchange HPLC. After cooling the volume was reduced to ca 10 cm^3 under vacuum. This was then poured into a beaker and the pH adjusted to approximately pH 2.7 with 0.2 M HCl at which stage the complex precipitates. It was then filtered under gravity using a very fine pore filter paper due to the very fine nature of the product. Purification of the complex was performed by column chromatography on a size exclusion separating agent, sephadex LH20. Water was used as the eluent and it was necessary to swell the LH20 in water for 3-4 hours before packing. The complex was adjusted to around pH 7 prior to application. Three main bands were observed with the second band being the main fraction. It was

necessary to repeat this step with LH20 to fully remove all impurities. Isolation of the product after chromatography was achieved by adjusting the pH with HCl as before. The yield is quite low Yield = 0.21 g (30 %). Calcd. for : $Ru_1C_{39}H_{39}N_8O_{15}Cl_2$ C: 45.40; H: 3.81; N: 10.86 %. Anal. Found: C: 45.83; H: 3.74; N: 10.96 %.

3.2. Results and Discussion.

3.2.1 Synthetic Procedure.

The syntheses of the ruthenium(II) complexes of the ligand 3-(1′,2′-dimethoxyphenyl)-5-(pyridin-2-yl)-1,2,4-triazole (HL1) were straight forward and all performed similarly with the exception of $[Ru(H_4dcbpy)_2HL1]Cl_2.5H_2O$ which will be discussed at the end of this section. An important feature of the complex synthesis was the use of an ethanol/water mixture. This was necessary to remove both chlorides from the respective ruthenium dichloride precursors as the presence of ethanol alone only removes one chloride[9]. The ruthenium dichloride ($[Ru(L)_2Cl_2].2H_2O$) (see chapter 2, section 2.1) was added to a slight excess of the ligand which was at reflux temperature in ethanol/water. It was important to ensure that the ligand was completely dissolved before the addition of the dichloride. An important precaution taken with all the reactions was to avoid longterm exposure to light due to the possibility of photodecomposition of the complexes via population of the ^3MC state[10,11,12]. The reactions were covered from direct light using tin foil.

As has been observed with other pyridyltriazole complexes the ligand HL**1** deprotonates upon coordination of the metal centre[1]. The complexes were isolated as PF_6^- salts of the monocations and the presence of any excess PF_6^- can be removed by washing the complexes with copius amounts of water. However to ensure that in all cases the deprotonated complexes were isolated all the complexes were recrystalised with a few drops of aqueous ammonia.

A feature of many pyridyltriazole ligands is the possibility of coordination via N1 and N4 of the triazole. The influence of this coordination geometry on the electronic

properties was examined by Hage[1] who established that the acid base properties and pKa values are different for the two coordination modes. Due to steric hindrance, coordination is expected through N1 of the triazole though a small percentage of N4 could be expected. In a study carried out by E. Ryan on the complexes $[Ru(phen)_2(1M3ptr)]^{2+}$ and $[Ru(dmbpy)_2(1M3ptr)]^{2+}$ (dmbpy = 4,4′-dimethyl-2,2′-bipyridine), it was found that coordination occured via both N4 and N2 (comparable with N1 in HL1 see Fig 3.1) in a ratio of approximately 90:10[13]

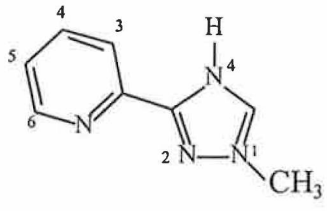

Figure 3.2 1-Methyl-3-(2-pyridyl)-1,2,4-triazole (1M3ptr)

From HPLC analysis of the recrystallised complexes three main impurities were usually present. The nature of the first two can be assigned to unreacted ligand and some unreacted dichloride. However the third impurity which was generally only 5-10 % and eluted at a slightly longer retention time (30-60 seconds longer) had a similar UV-Vis spectrum to that of the main product. Although it was not isolated there is a strong possibility that this may be the N4 bound complex. Recrystallisation alone did not successfully purify the complexes and column chromatography on neutral alumina was necessary. Excellent separation was achieved with acetontrile as eluent. Three main bands were visible with the pure complex eluting first from the column. The second band eluted more slowly and streaked down the column. The final band remained on top of the column and required methanol to move through the alumina. HPLC analysis

of the fractions confirmed the purity of the main product. However the identity of the two other major bands proved inconclusive due to the fact that an overlap between the first and second bands was observed from HPLC analysis. They were not isolated and characterised due to the small amounts involved (5-10 %).

The synthesis and purification of the ruthenium(II) dicarboxy complex $[Ru(H_4dcbpy)_2HL1]Cl_2.5H_2O$ was slightly different from the others. $[Ru(dcbpy)_2Cl_2]$ required a basic pH, adjusted with NaOH, to enable solubility in the ethanol/water solvent mixture. The reaction then proceeds similarly to those described previously and was monitored using anionic HPLC as opposed to the cationic HPLC used for the other complexes. Anion exchange chromatography was required due to the lack of separation on the cation exchange system and failure to elute from the column. This may be due to negative charges associated with the dicarboxy units on $[Ru(H_4dcbpy)_2HL1]Cl_2.5H_2O$. Purification of the dicarboxy complex was performed using size exclusion chromatography on a Sephadex material called LH20. The pH of the complex in a minimum of the eluent, water, is adjusted to pH 7 prior to application on the column. After collection of the pure fractions the water was reduced in volume under vacuum and the complex isolated by adjusting the pH to approximately pH 2.7. After analysis by HPLC and ^{1}H-NMR it proved necessary to repeat the purification step with LH20 in the same manner as described above. This lowered the yield considerably. The elemental analysis confirms that the triazole and dicarboxy moieties are protonated at the pH at which the complex was isolated (pH 2.7).

3.2.2 ^{1}H-NMR Spectroscopy.

Representative ^{1}H-NMR spectra and 2D COSY spectra of some of the ruthenium(II) complexes of the ligand HL1 are shown in the following section in Figures 3.3 - 3.8. The ^{1}H-NMR spectra of the ligand HL1 and the complex [Ru(H_4 dcbpy)$_2$HL1]Cl_2.5H_2O are included in appendix 1. Table 3.1 presents the ^{1}H-NMR data for the complexes with the assignment of the HL1 ligand protons. It has only been possible to assign ranges of proton resonances for the bpy, phen and dcbpy ligands due to their coincidental shifts. These fall within the ranges normally observed for analogous compounds[8,14]. The ^{1}H-NMR spectra are quite complicated and assignment of the HL1 ligand protons in the complexes was performed by combining information from a number of sources and techniques. The assignment of the ligand is known from previous studies[8] and by use of this information in conjunction with the ^{1}H-NMR, 2D-COSY NMR and spectra of the deuteriated complexes a complete assignment of the bridging ligand protons was possible.

One of the most significant shifts observed in all the complexes when compared to the free ligand is that of the pyridyl H^6 proton of the ligand L1. Coordination of Ru(L)$_2$ unit induces an upfield shift of over 1 ppm which is observed in all of the complexes. This is typical of coordinated pyridine rings and is due to the diamagnetic anisotropic interaction of the H^6 proton with an adjacent bpy, phen or dcbpy ligand[15,16]. The upfield shift of the H^6 proton also confirms that the ligand L1 is bound via N1 of the triazole. If this were not the case the H^6 proton would be free from anisotropic interaction. The N1 coordination is also confirmed in the X-ray data for the **d_8-bpyL1** and **phenL1** complexes. Identification of this H^6 proton is also made possible by taking into account the chemical shift of the H^3 proton.

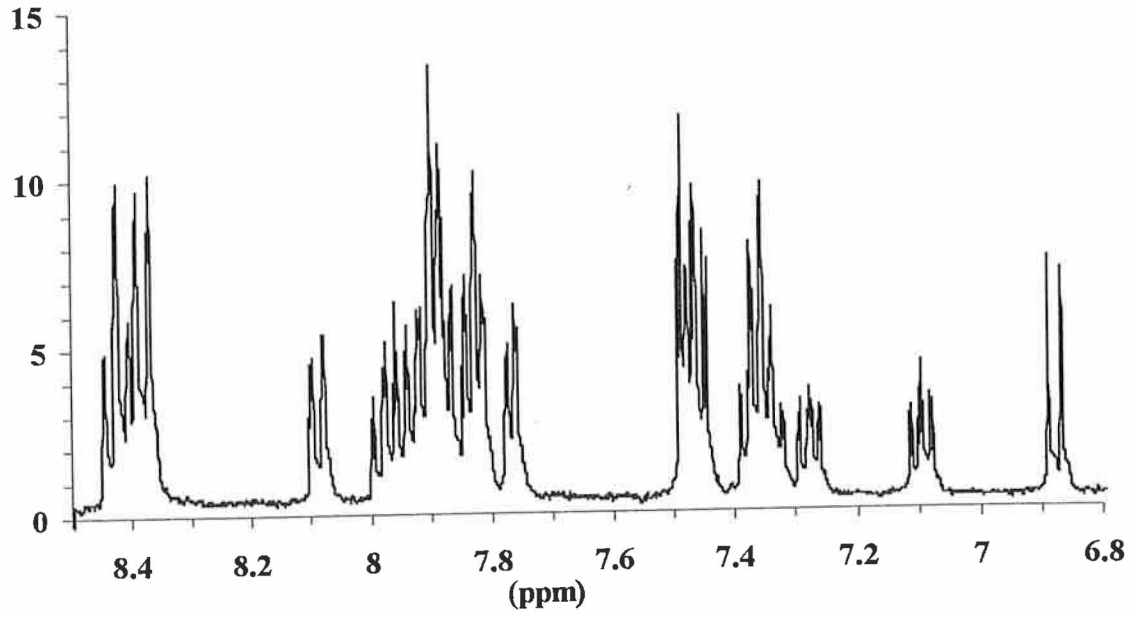

Figure 3.3 *^{1}H-NMR spectrum of $[Ru(bpy)_2(L1)]PF_6.H_2O$ in d_3 -acetonitrile.*

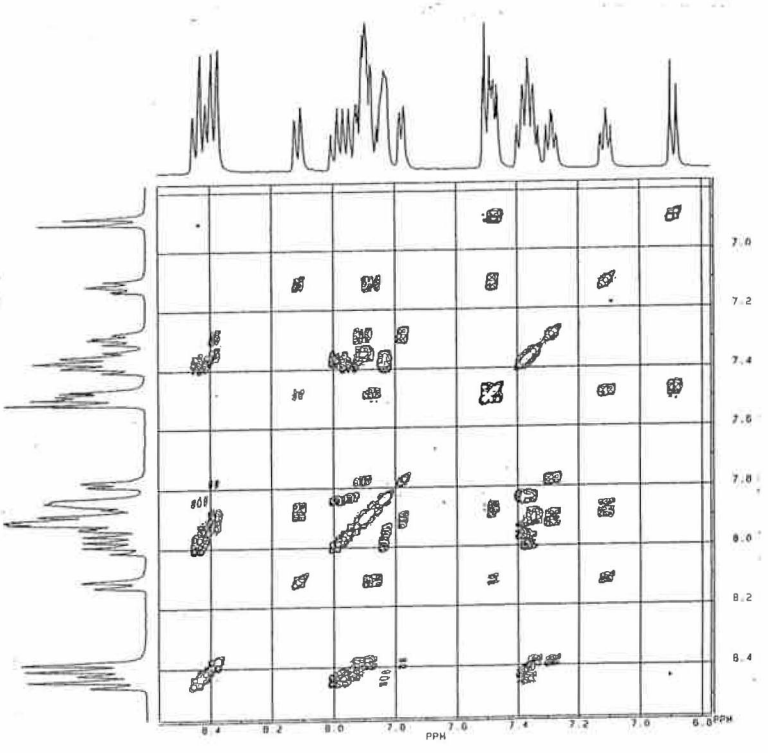

Figure 3.4 *COSY NMR spectrum of $[Ru(bpy)_2(L1)]PF_6.H_2O$ in d_3-acetonitrile.*

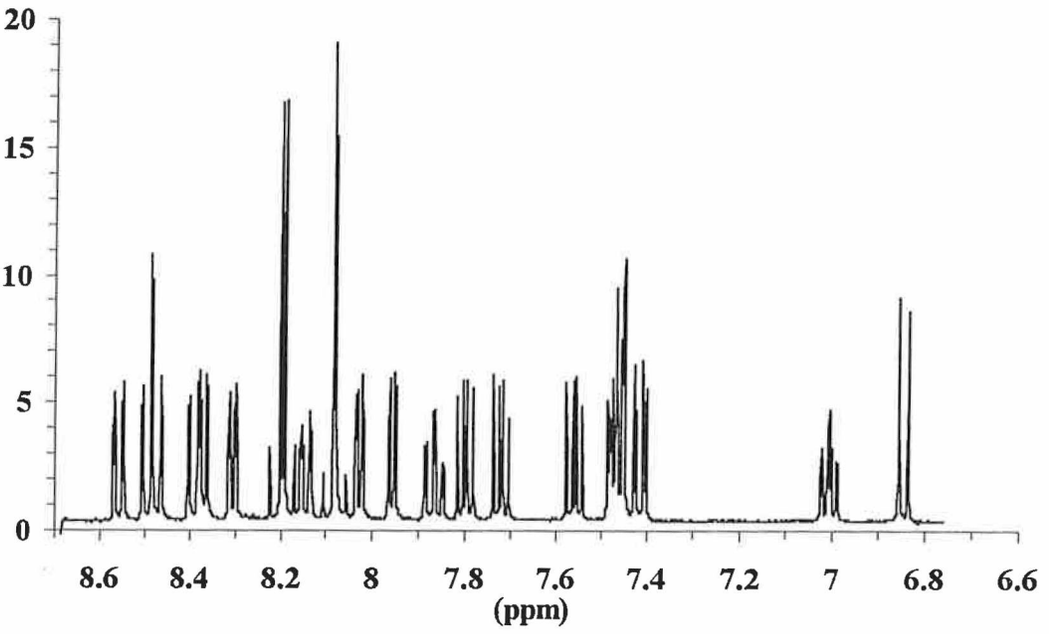

Figure 3.5 *^{1}H-NMR spectrum of $[Ru(phen)_2(L1)]PF_6.H_2O$ in d_3 -acetonitrile.*

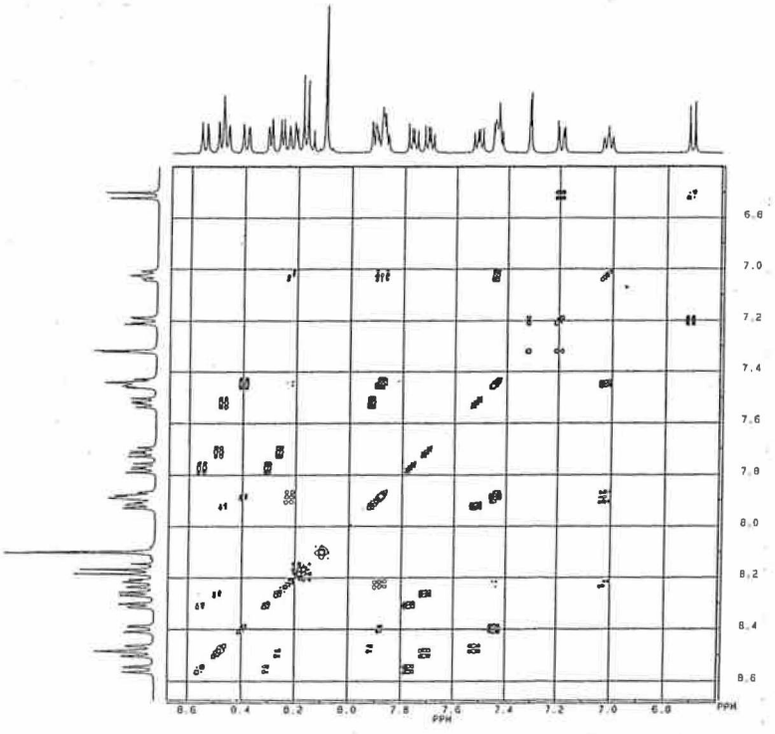

Figure 3.6 *COSY NMR spectrum of $[Ru(phen)_2(L1)]PF_6.H_2O$ in d_3 -acetonitrile.*

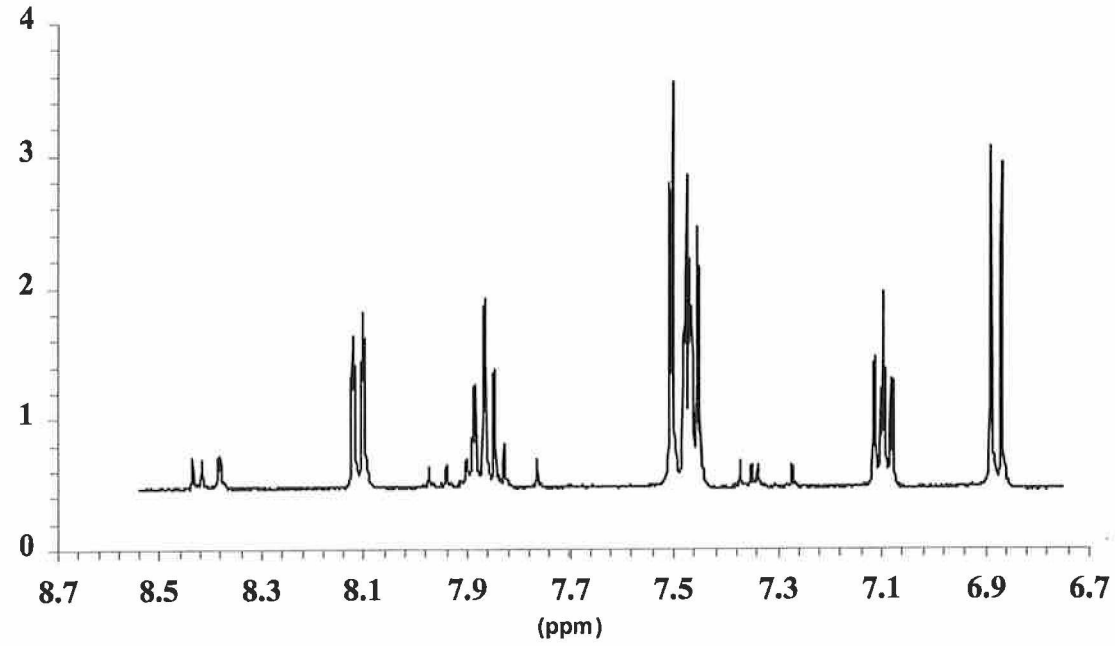

Figure 3.7 *^{1}H-NMR spectrum of [Ru(d_8-bpy)$_2$(L1)]PF_6.H_2O in d_3-acetonitrile.*

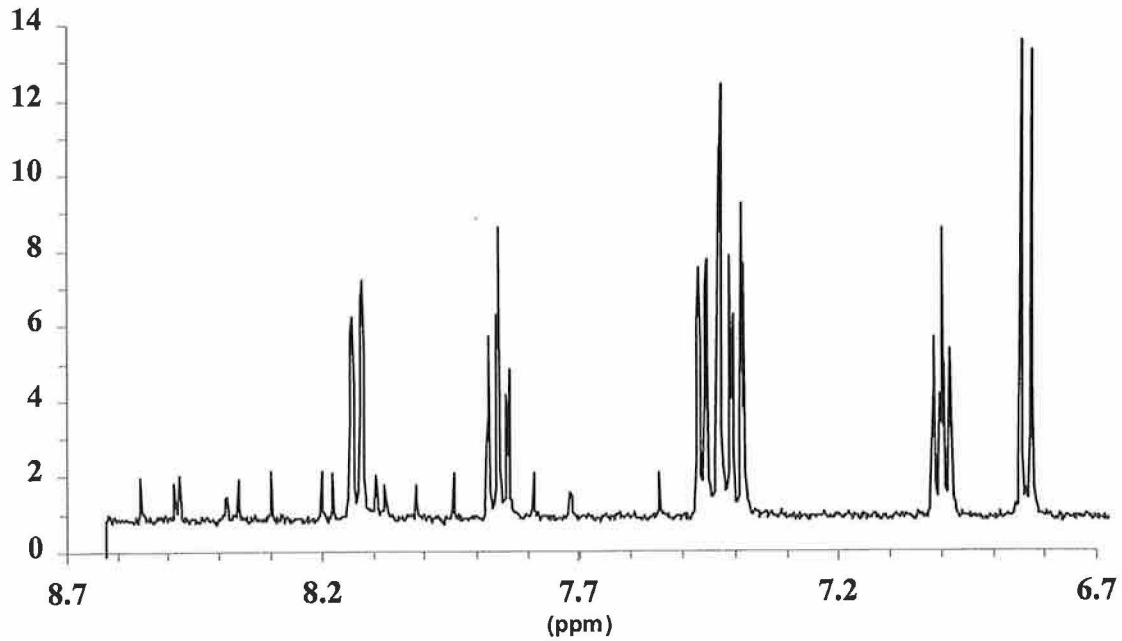

Figure 3.8 *^{1}H-NMR spectrum of [Ru(d_8-phen)$_2$(L1)]PF_6.H_2O in d_3-acetonitrile.*

Table 3.1 *^{1}H-NMR data for the ruthenium(II) complexes of HL1 measured in d_3-acetonitrile and for ligand HL1 in d_6-dimethyl sulphoxide[A,B].*

	L1 Resonances (Chemical Shifts / ppm vs Me_4Si)						
Complex	**H^3**	**H^4**	**H^5**	**H^6**	**$H^{3'}$**	**$H^{5'}$**	**$H^{6'}$**
bpyL1	8.08(d)	7.89(dd)	7.10(dd)	7.46(d)	7.49(s)	7.48(d)	6.88(d)
phenL1	8.14(d)	7.87(dd)	7.01(dd)	7.49(d)	7.47(s)	7.40(d)	6.86(d)
d_8-bpyL1	8.13(d)	7.88(dd)	7.14(dd)	7.47(d)	7.52(s)	7.49(d)	6.90(d)
d_8-phenL1	8.12(d)	7.84(dd)	6.99(dd)	7.45(d)	7.42(s)	7.39(d)	6.83(d)
dcbpyL1	8.17(d)	7.93(dd)	7.22(dd)	7.41(d)	7.51(s)	7.43(d)	6.89(d)
HL1	8.15(d)	7.98(dd)	7.51(dd)	8.70(d)	7.63(s)	7.66(d)	7.09(d)

A: bpy, phen, dcbpy and resonances respectively were observed to occur in the following regions: **bpy**- 8.36-8.45 (H^3); 7.80-7.90 (H^4); 7.20-7.40 (H^5); 7.70-8.00 (H^6) **phen-** 8.35-8.60; 7.95-8.25; 7.50-7.85; 7.40-7.50; **dcbpy-** 8.74-8.80 (H^6); 7.60-7.80 (H^3 and H^5)

B: -OMe Resonances occur as two singlets between 3.70 and 3.90 for all the complexes.

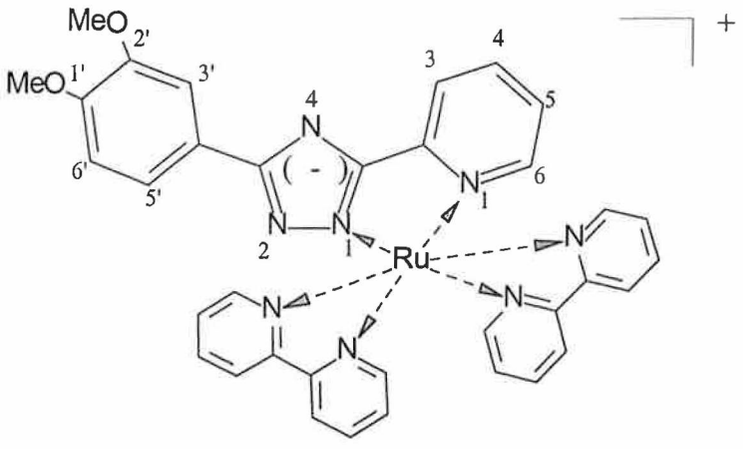

*Figure 3.9 Structure of $[Ru(bpy)_2(L1)]^{1+}$ (**bpyL1**).*

It remains more or less unshifted in the coordinated ligand when compared to the free ligand. Assignment of the complexes was also made possible by finding cross-peaks in the 2D COSY NMR spectra. The spectra of the undeuteriated complexes were quite complicated (see Figure 3.3 - 3.6), however the pyridyl ring protons H^3, H^4, H^5 and H^6 appear in a distinctive coupled line while the phenyl ring protons $H^{3'}$, $H^{5'}$and $H^{6'}$ are more difficult to assign as they coincide with some of the other proton signals from the ligands L of the $Ru(L)_2$ unit (see Figure 3.9 for numbering scheme). Comparison of the ^{1}H-NMR spectra of the complexes, whereby the ligand L is deuteriated, with those of the undeuteriated complexes enables full structural elucidation of the more complicated spectra. In the ^{1}H-NMR spectra of the deuteriated complexes the proton signals for the ligand L are almost silent thus simplifying the spectra enormously. Thus we have spectra of the coordinated ligand where only the signals for the bridging ligand L1 are dominant. As can be seen from the ^{1}H-NMR spectra of **d_8-bpyL1** and **d_8-phenL1** (see Figure 3.7 and 3.8) there is evidence of trace amounts of undeuteriated **bpyL1** and **phenL1** respectively in the complexes. It was estimated from study of the integration values in the ^{1}H-NMR spectra of the complexes that the bpy was 94.06% deuteriated

and the phen was 98.86% deuteriated. This does not present any difficulties for structural elucidation but does cause difficulties in the photophysical studies.

3.2.3 X-Ray Data for $[Ru(d_8\text{-bpy})_2(L1)]PF_6.H_2O$ and $[Ru(phen)_2(L1)]PF_6.H_2O$

The crystals of the two complexes presented here were obtained after purification on a neutral alumina column using acetonitrile as eluent and subsequent recrystallisation from acetone/water (2:1 v/v). Projections of the structures of the complexes $[Ru(d_8\text{-bpy})_2(L1)]PF_6.H_2O$ (**d_8-bpyL1**) and $[Ru(phen)_2(L1)]PF_6.H_2O$ (**phenL1**) are presented in Figures 3.10 and 3.11 respectively. Selected bond lengths and angles are listed in Table 3.5. A complete list of bond angles and distances can be found in appendix 2. The data for the complexes $[Ru(bpy)_2(3Mptr)]PF_6.4H_2O$ (3Mptr) and $[Ru(bpy)_2(pt)]PF_6.CH_3COCH_3$ (pt) (see Figure 3.14) are used for comparison purposes due to the similarity of the ligands and modes of coordination[1]. In the case of the complex **d_8-bpyL1** the ruthenium atom is coordinated by one pyridyltriazole ligand and two deuteriated bipyridine molecules. As expected there is evidence of only one PF_6 counterion in the structure. Similarly with the complex **phenL1** the ruthenium atom is coordinated by one pyridyltriazole ligand and two phenanthroline molecules. There is also evidence of only one PF_6 counterion. The 'bite angles' (N4 - Ru - N3, N1B - Ru - N2B and N2A - Ru - N1A) of all ligands are 77-79^o , comparable to chelating angles observed normally for similar structures[17,18,19]. All the complexes are bound via N3 and N4 (i.e. bound through N1 of the triazole using numbering in Figure 3.1).

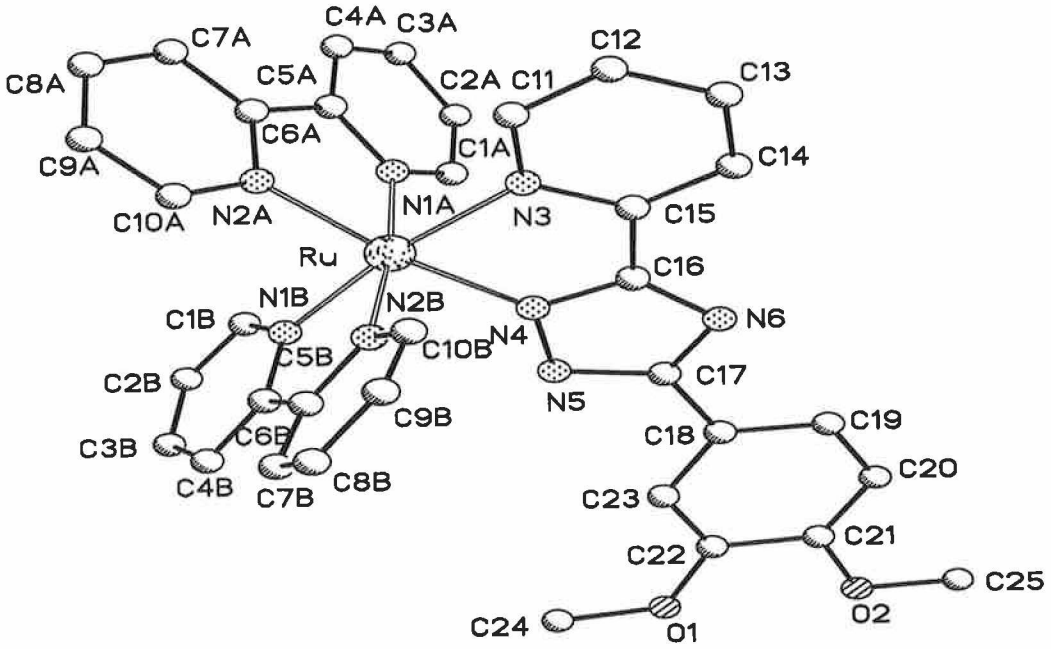

Figure 3.10 *X-Ray Crystal structure of* ***d_8-bpyL1*** *obtained showing atomic numbering used.*

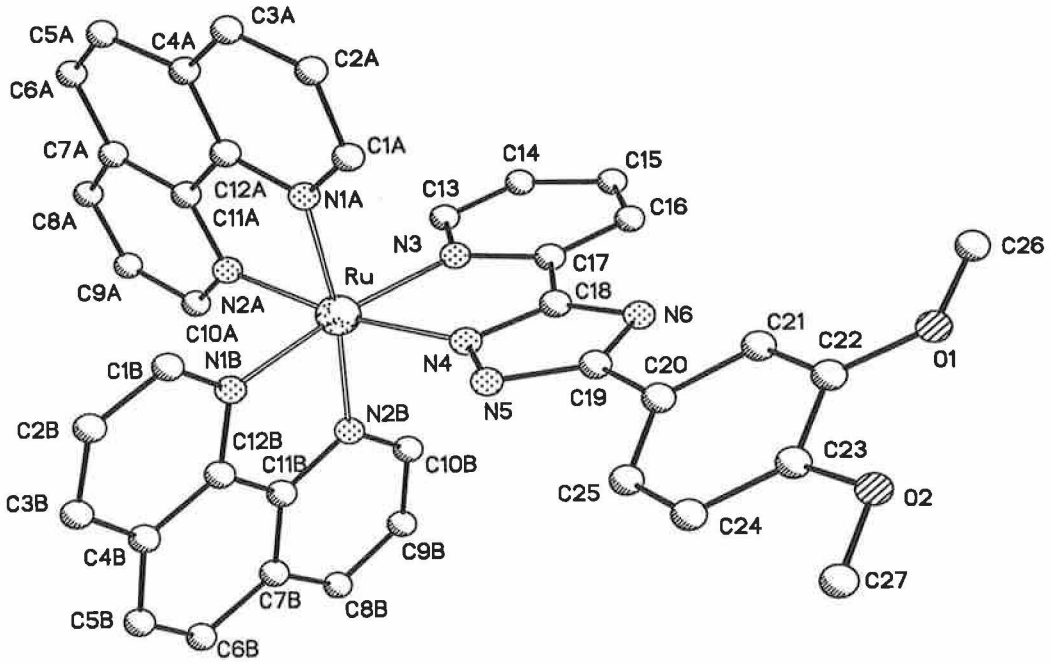

Figure 3.11 *X-Ray Crystal structure of* ***phenL1*** *obtained showing atomic numbering used.*

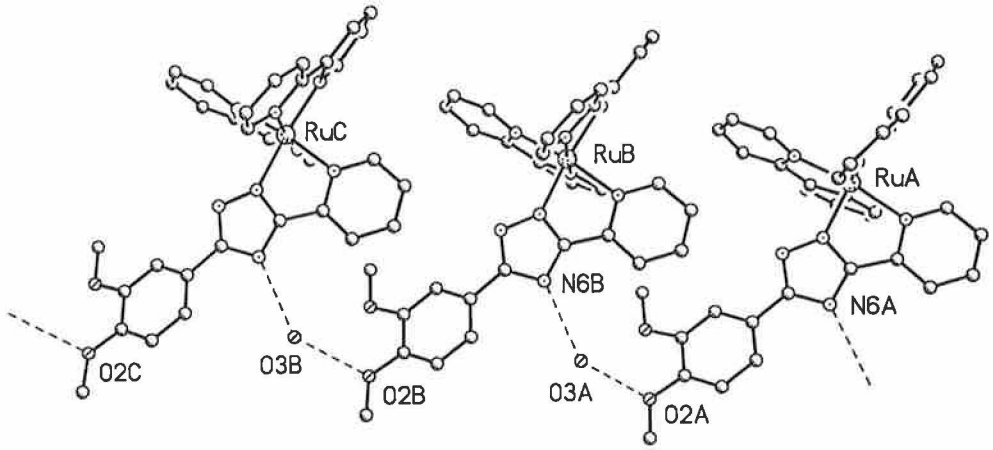

Figure 3.12 *Schematic representation of the inter-molecular interaction in a crystal of* ***d_8-bpy***.

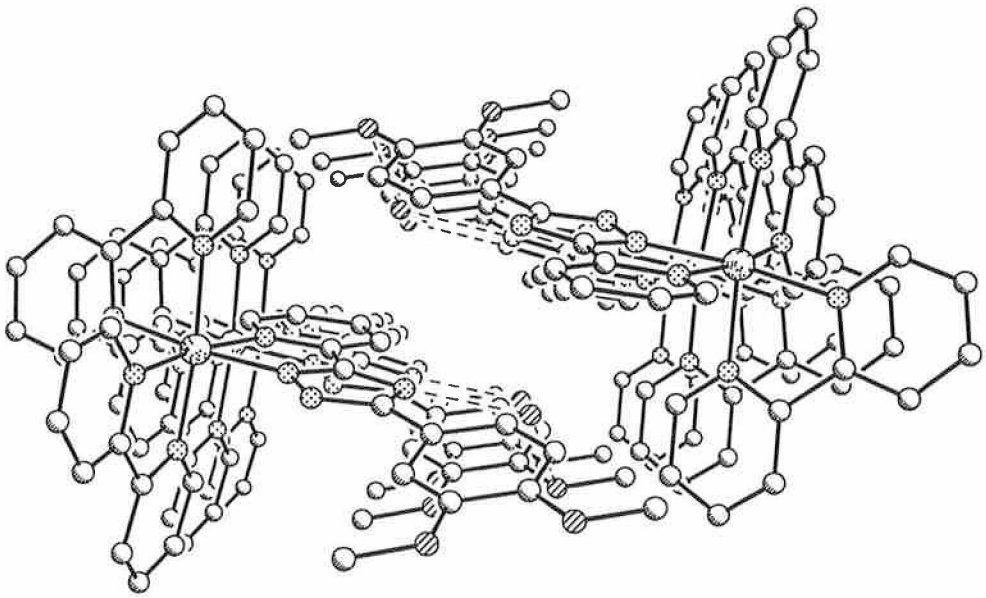

Figure 3.13 *X-Ray crystal structure showing the organised packing in a crystal of* ***d_8-bpy***.

Table 3.2 *Selected bond distances (Å) and angles (°) of* ***d_8-bpyL1*** *and* ***phenL1***^{A,B,C}.

Bond distances (Å)				
	d_8-bpyL1	**phenL1**	**3Mptr**	**pt**
Ru - N4	2.038(4)	2.036(4)	2.050(5)	2.051(3)
Ru - N3	2.109(4)	2.089(4)	2.086(4)	2.085(3)
Ru - N1B	2.044(4)	2.057(4)	2.055(4)	2.056(3)
Ru - N2B	2.044(4)	2.054(4)	2.042(5)	2.056(3)
Ru - N2A	2.043(4)	2.071(4)	2.060(4)	2.063(3)
Ru - N1A	2.062(4)	2.054(4)	2.056(4)	2.049(3)

Bond angles (°)				
	d_8-bpyL1	**phenL1**	**3Mptr**	**pt**
N4 - Ru - N3	77.86(15)	78.16(15)	78.0(2)	77.9(1)
N4 - Ru - N1B	94.29(15)	96.42(15)	96.1(2)	92.3(1)
N4 - Ru - N1A	96.11(15)	93.73(16)	96.5(5)	91.8(1)
N4 - Ru - N2B	89.88(15)	92.47(15)	87.4(2)	97.6(1)
N3 - Ru - N2B	96.25(17)	95.88(17)	95.0(2)	94.3(1)
N3 - Ru - N2A	94.88(15)	94.66(15)	95.9(2)	90.7(1)
N3 - Ru - N1A	86.28(15)	90.17(16)	90.9(2)	96.3(1)
N1B - Ru - N2B	79.00(17)	79.86(17)	79.4(2)	79.9(1)
N1B - Ru - N2A	93.29(15)	91.19(15)	90.5(2)	97.8(1)
N2B - Ru - N2A	95.48(16)	94.59(16)	98.0(2)	90.9(1)
N2A - Ru - N1A	78.73(16)	79.83(15)	78.7(2)	78.7(1)

A: **3Mptr** = $[Ru(bpy)_2(3Mptr)]PF_6.4H_2O$ and **pt** = $[Ru(bpy)_2(pt)]PF_6.CH_3COCH_3$.

B: Data for 3Mptr and pt taken from reference[1] (see Fig 3.14).

C: Note atom numbering in reference[1] is different to that used in Figures 3.10 and 3.11 however they correspond to the same bonds quoted here in Table 3.2.

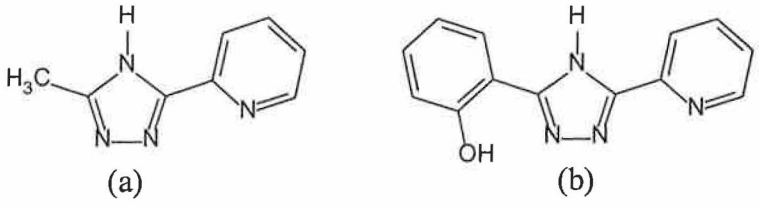

Figure 3.14 Structures of ligands (a) 3Mptr and (b) pt

The Ru-N distances of 2.038-2.109 Å observed in the complexes compare with those found in Mptr and pt and other ruthenium complexes[1,8,20]. One significant difference between the two complexes $[Ru(d_8\text{-bpy})_2(L1)]PF_6.H_2O$ and $[Ru(phen)_2(L1)]PF_6.H_2O$ appears to be the position and orientation of the phenyl ring. In the **phenL1** complex the OMe unit appears closer to the N6 of the trialoze than with the **d_8-bpyL1** complex. Here the phenyl ring is twisted approximately 180 ^{O} in comparison with **phenL1**. This may be due to increased steric hindrance caused by the phenanthroline units in comparison with the bipyridyl units and might also be as a result of the more hydrophobic nature of the phenanthroline rings. In Figure 3.12 and 3.13 the stacking of individual molecules of **d_8-bpyL1** is shown. There is evidence of intermolecular interactions between the oxygen of the protected catechol ring (labelled O2) and the N4 of the triazole ring of the neighbouring molecule via a water molecule (see Figure 3.12). Figure 3.13 shows an X-Ray crystal structure of the packed molecules of **d_8-bpyL1** which are held together by the interactions shown in Figure 3.12

3.2.4 Electronic and Photophysical properties.

The electronic spectra of all the complexes are consistent with those of similar ruthenium(II) complexes. The spectra are characterised in the visible region (300-500 nm) by $d\pi$-π^* metal-to-ligand charge transfer (MLCT) transitions typical of complexes of this type[21]. On absorption of a photon an electron is removed from the $d(t_{2g})$ orbitals of Ru(II) to the lowest π^* level of the ligand which is located between the filled $d(t_{2g})$ (π_M) and the empty $d(e_g)$ (σ^*_M) orbitals of the metal ion (see Figure 3.15). The relative energies of the orbitals involved in the ^{1}MLCT transitions are influenced by the properties of the coordinated ligands. The absorption spectra of the complexes are characterised in the UV region (250-300 nm) by intense π-π^* transitions associated with the pyridyltriazole ligand and the ligands L from the $Ru(L)_2$ unit.

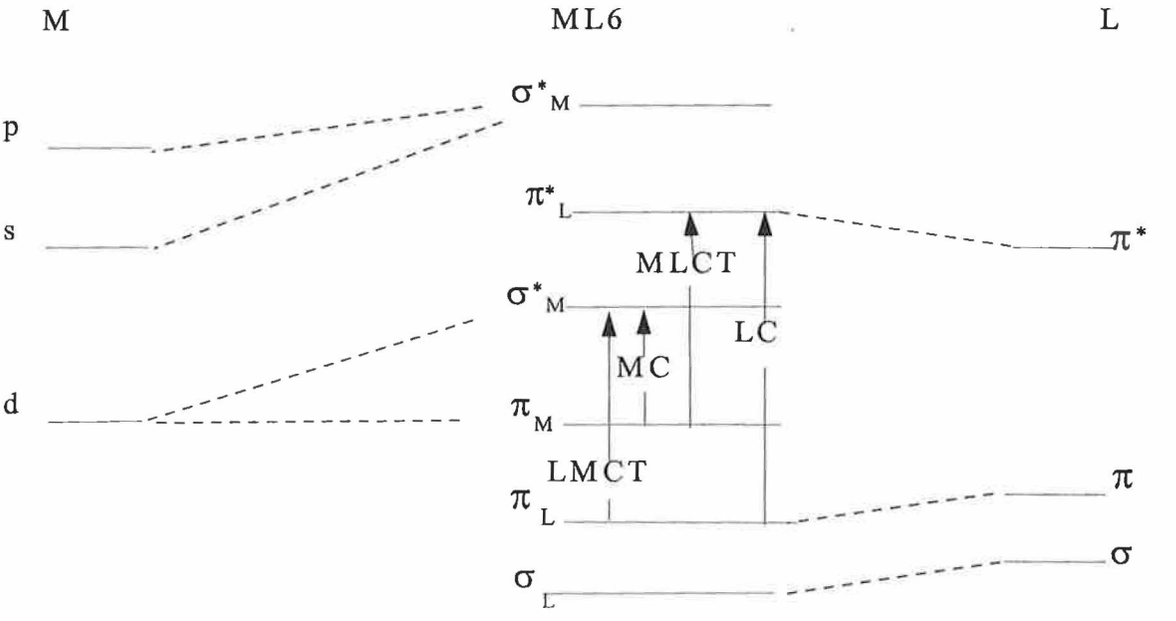

Figure 3.15 *MO diagram for a typical Ru(II) octahedral transition metal complex. The arrows indicate the four types of transitions based on localized MO configurations: metal centred (MC); ligand-to-metal charge transfer (LMCT); metal-to-ligand charge transfer (MLCT); Ligand centred (LC).*

Table 3.3 *Absorption and emission data for the complexes listed below*[A,B,C,D].

Complex	Absorbance λ_{max}, nm		Emission λ_{max}, nm				Lifetime (ns)
	Prot.	Deprot. (ε / $M^{-1}cm^{-1}$)	Prot. 300 K	Prot. 77 K	Deprot. 300 K	Deprot. 77K	at 300 K
bpyL1	435	482 (10159)	616	578	692	618	69
phenL1	420	427 (13512)	607	569	681	608	365
d_8-bpyL1	440	478 (10002)	620	582	689	617	88
d_8-phenL1	418	426 (13523)	607	570	680	606	496
dcbpyL1	478	490 (14725)	660	618	689	638	220

A: Protonation of the complexes was achieved by addition of perchloric acid and deprotonation by the addition of diethylamine.

B: All measurements at 300 K were performed in acetonitrile except for **dcbpyL1** which was performed in water.

C: All measurements at 77 K were performed in ethanol/methanol 4:1 v/v.

D: Samples for lifetime measurements were degassed using N_2 and the values stated above refer to the deprotonated complexes.

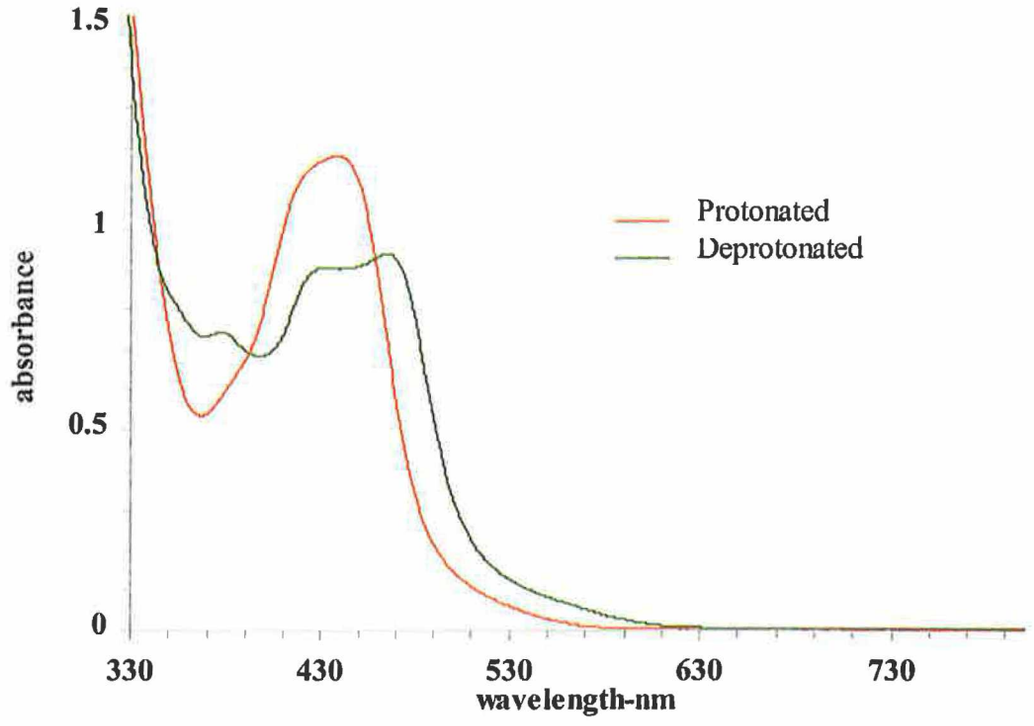

Figure 3.16 *Absorption spectra of $[Ru(bpy)_2(L1)]PF_6.H_2O$ protonated and deprotonated in acetonitrile (5×10^{-5} M).*

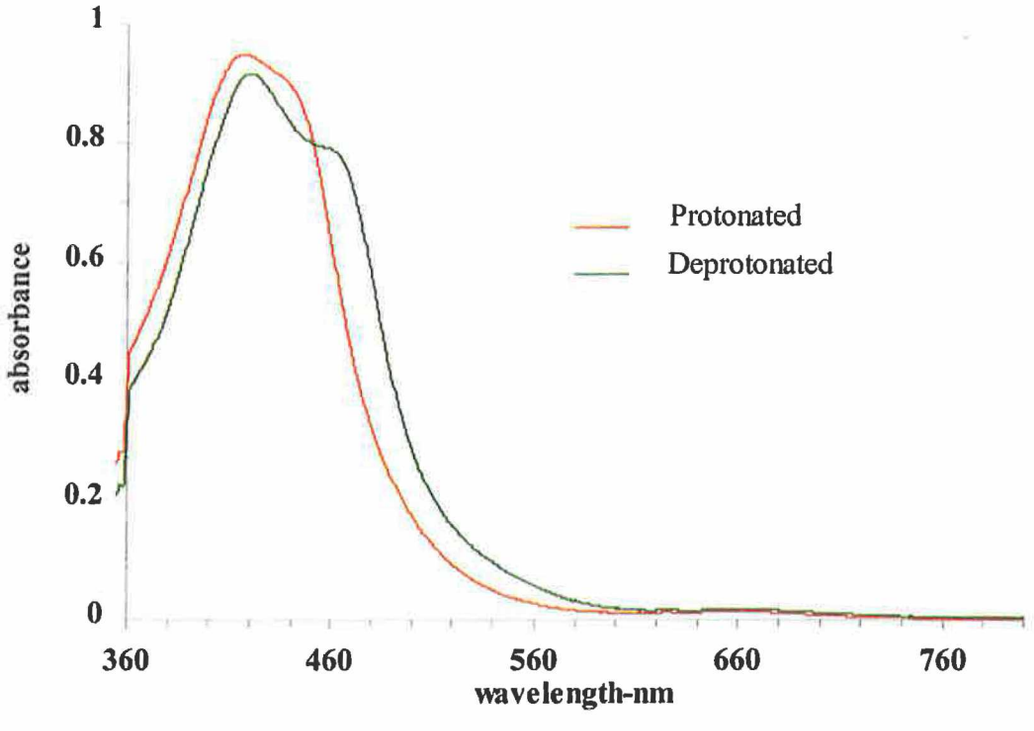

Figure 3.17 *Absorption spectra of $[Ru(phen)_2(L1)]PF_6.H_2O$ protonated and deprotonated in acetonitrile (5×10^{-5} M).*

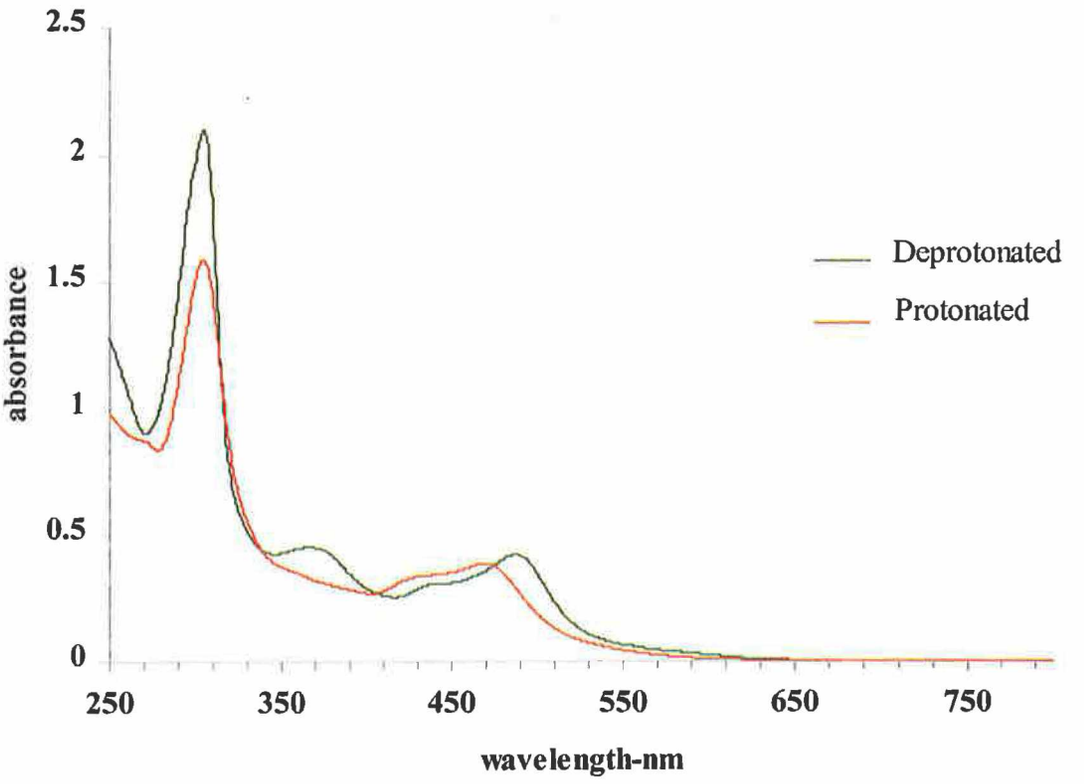

Figure 3.18 Absorption spectra of $[Ru(H_4dcbpy)_2(HL1)]Cl_2.5H_2O$ protonated and deprotonated in water($3 X 10^{-5} M$).

As stated earlier the triazole is in the deprotonated state after coordination to the $Ru(L)_2$ unit. The absorbances of the **dcbpyL1**, **bpyL1** and **d_8-bpyL1** complexes are red-shifted with respect to $[Ru(bpy)_3]^{2+}$ due to the strong σ-donation of the deprotonated triazole moiety and occur around 480 nm for the **bpyL1** and **d_8-bpyL1** complexes and 490 nm for the **dcbpyL1** complex. On protonation of the triazole ring the λ_{max} of the **bpyL1** and **d_8-bpyL1** complexes is blue shifted to approximately 435 nm (see Figure 3.16) while the **dcbpyL1** (see Figure 3.18) complex is blue-shifted to a less significant degree. This shift can be explained due to less electron density being present on the triazole ring. The Ru t_{2g} level is stabilised by increased π-acceptance by the ligand (weaker σ-donation) and the t_{2g}-MLCT gap is increased resulting in the observed blue-shifted

absorbance. The **phenL1** and **d_8-phenL1** complexes (see Figure 3.17) behave slightly different to the others in that the λ_{max} of the deprotonated complex is blue-shifted with respect to the **bpyL1**, **d_8-bpyL1** and **dcbpyL1** complexes. The λ_{max} of the deprotonated **phenL1** and **d_8-phen** complexes occurs around 427 nm and this may be due to the fact that phen is a poorer π acceptor than bpy. It drains less electron density from the pyridyltriazole ligand than bpy thus leaving a higher electron density on the triazole ring. In this instance the triazole ligand is a better π acceptor than in the case of the **bpyL1** and **d_8-bpyL1** complexes.

All the complexes exhibit room temperature emission when deprotonated and protonated associated with decay from the ^{3}MLCT state (see Figure 1.8 in chapter 1). The emission properties of the complexes were investigated in acetonitrile, with the exception of $[Ru(H_4dcbpy)_2(HL1)]Cl_2.5H_2O$ which was performed in water, by excitation at the λ_{max} (^{1}MLCT band). The emission maxima of the deprotonated complexes occurs at lower energy than that of $[Ru(bpy)_3]^{2+}$ (605 nm) [22]. This fact is due to the strong σ-donor properties of the anionic triazole ligand, resulting in increased electron density on the metal centre, a decrease in the t_{2g} - ^{3}MLCT energy gap and so a lowering of the emission energy. As with the absorption spectra, and for the same reasons, protonation of the complexes results in a blue shift of the emission maxima. The emission maxima for the **bpyL1** and **d_8-bpyL1** complexes (see Table 3.3) occurs in the 690 nm region for the deprotonated complexes and in the 620 nm region for the protonated complexes. As with the absorption spectra, the emission of the **phenL1** and **d_8-phenL1** complexes is blue-shifted with respect to the **bpyL1** complexes and for the similar reasons. The emission for the deprotonated **phenL1** and **d_8-phenL1** complexes occurs in the 680 nm region and for the protonated complexes in the 607 nm region. As

expected the lifetimes of the deuteriated complexes were longer than the undeuteriated ones and for the reasons discussed in the introduction (see Table 3.3). In the emission spectra of **dcbpyL1** a less considerable difference between the deprotonated and protonated complex was observed. However on protonation of the triazole, which may also include protonation of the dicarboxy units, there is a shift in the λ_{max} emission to 660 nm from 689 nm in the deprotonated state, which is not as significant a shift as the bpy complexes (see Table 3.3). This may be due to the fact that the energy difference between the metal t_{2g} and dcbpy π^* orbitals is smaller than that between the metal t_{2g} and bpy π^* orbitals. Thus the MLCT energy is lower and the emission λ_{max} is longer. The measurement was performed in water for solubility purposes.

At low temperature (77 K) the complexes exhibit a strong emission in an alcohol medium (see Table 3.3) with a distinct vibrational structure (see Figure 3.19-3.20). The emission λ_{max} is further blue shifted, in comparison to room temperature emission, for both protonated and deprotonated species. This is associated with a phenomenon termed as "rigidchromism" by Wrighton and coworkers who were one of the first to report on it[23]. In the alcoholic glasses formed at 77 K, the solvent dipoles are frozen in averaged orientations corresponding to the ground state electronic configuration of the complex. In the fluid state, at room temperature, the reorientation times for the solvent dipoles are short compared to the lifetime of the excited state. Whereas in frozen matrix solvent dipoles reorientate themselves very slowly with respect to the excited state. The result is an increase in the emission energy

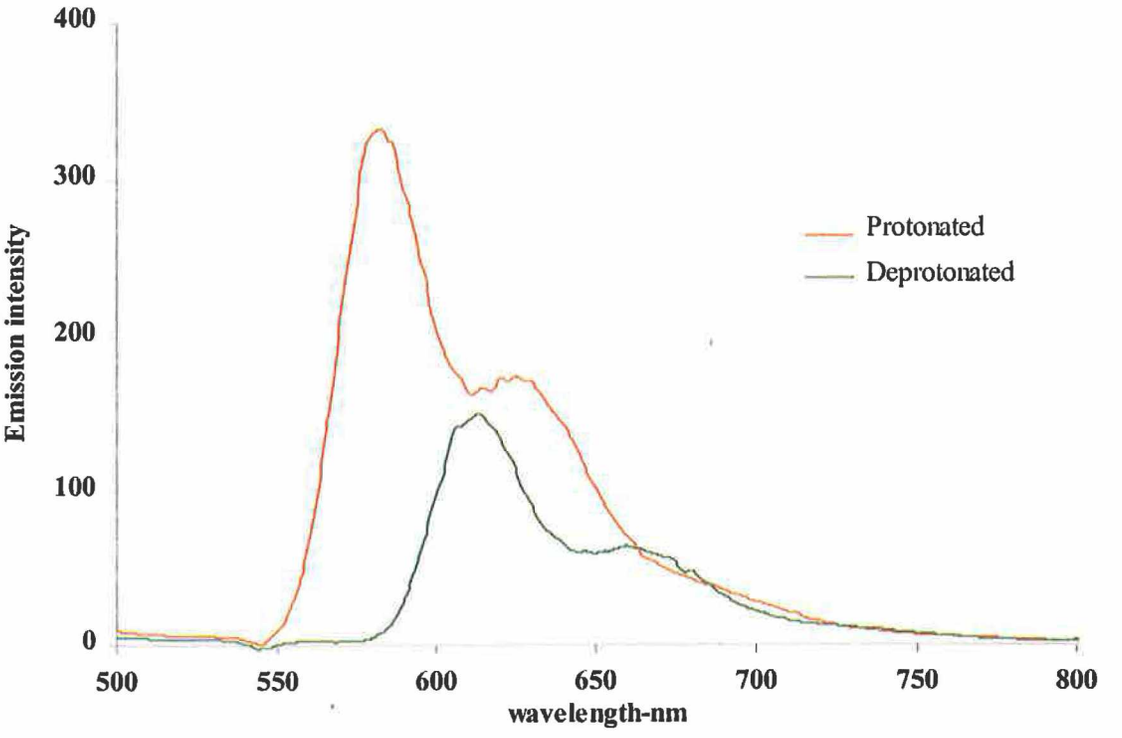

Figure 3.19 *Emission spectra of $[Ru(bpy)_2(L1)]PF_6.H_2O$ protonated and deprotonated* at 77 K in ethanol/methanol (4:1) (5 X 10^{-5} M).

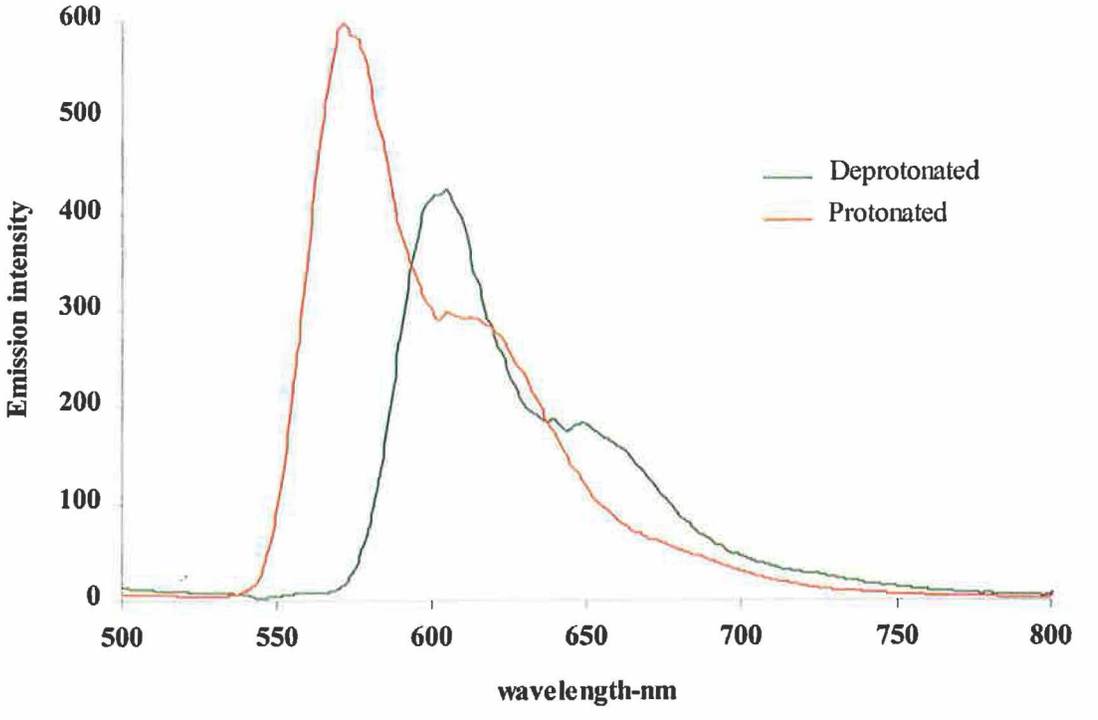

Figure 3.20 *Emission spectra of $[Ru(phen)_2(L1)]PF_6.H_2O$ protonated and deprotonated* at 77 K in ethanol/methanol (4:1) (5 X 10^{-5} M).

as confirmed by the blue shift in the emission spectra. Another influence of low temperature on the emission spectra of the complexes is to cause an increase in the intensity of the emission observed. This is related to two factors. Firstly, at low temperature the complex and its alcoholic medium are frozen making it less susceptible to vibronic coupling to low frequency, high amplitude Ru-N vibrations, which contribute to k_{nr}[21]. Solvent interactions which may contribute to k_{nr}, are also reduced considerably in the frozen matrix, as is oxygen quenching since diffusion of O_2 to the excited state is restricted. The second factor is related to the ^{3}MLCT-^{3}MC transition. Since this transition is thermally activated, at 77 K there will be insufficient thermal energy to populate the ^{3}MC, and as a result the intensity increases (see Figures 3.19-3.20).

3.2.5 Acid-base properties.

As was discussed earlier in the introduction the acid-base properties of pyridyltriazole complexes gives important information regarding the nature of the complexes and the location of excited states. The effect of protonation and deprotonation of the triazole ring on the λ_{max} of absorption and emission was discussed in the previous section 3.2.4. Protonation/deprotonation changes the σ-donor and π-acceptor properties of the HL1 ligand. In Ru-polypyridyl complexes the nature of the Ru-N bond is mainly σ but it is also stabilised by backbonding between the t_{2g} and π^* orbitals of the metal and ligand respectively[24,25,26]. By manipulation of the acid-base properties of the pyridyltriazole unit in the complexes, the ground state pKa can yield

information on the extent of backbonding from the metal and the σ-donor and π-acceptor properties of the ligand.

Table 3.4 *Ground and Excited state pKa values for the complexes of HL1.*

Complex	pKa ± 0.1	pKa* ± 0.1
bpyL1	4.1	1.7
phenL1	4.4	2.0
d_8-bpyL1	4.2	2.2
d_8-phenL1	4.0	1.8

Determination of the excited state pKa* gives important information regarding the properties of the ligand and the nature of the emitting state. For these reasons the acid-base behaviour of the complexes is presented in this section. In most ruthenium complexes the pKa value of the ligand decreases on coordination, which can be explained by strong σ-donation effects from the ligand to the metal centre. Less electron density is present on the triazole ring after coordination resulting in the increased acidity of the ligand[8]. Figures 3.21 and 3.22 are typical examples of the acid-base chemistry of the ruthenium(II) complexes containing the HL1 ligand. They are the absorption titration spectra for the complexes $[Ru(bpy)_2(L1)]PF_6.H_2O$ and $[Ru(phen)_2(L1)]PF_6.H_2O$ respectively. Clean and clear isobestic points are observed in the bpy complexes at 460, 390 and 345 nm and at 450 nm in the phen complexes indicating that there are no intermediates formed in the pH range examined. All the

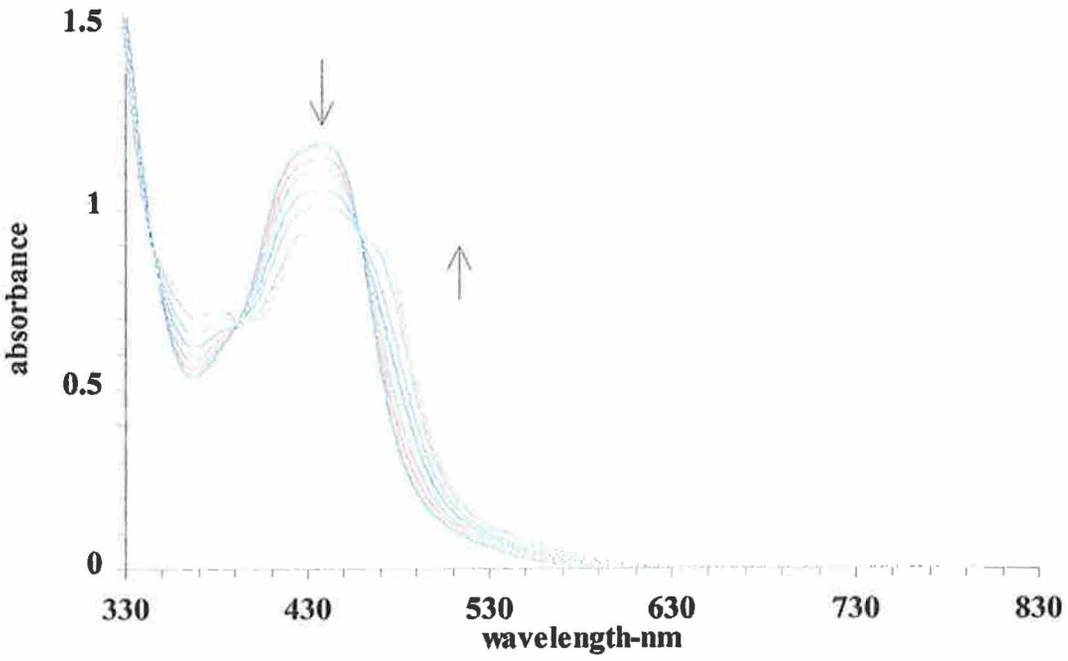

Figure 3.21 *pH dependence of the absorption spectra of $[Ru(bpy)_2(L1)]PF_6.H_2O$ (5×10^{-5} M) in an aqueous Britton-Robinson buffer at pH 1.20, 1.82, 2.50, 3.22, 3.69, 3.95, 4.65, 5.25, 5.98 and 7.06.*

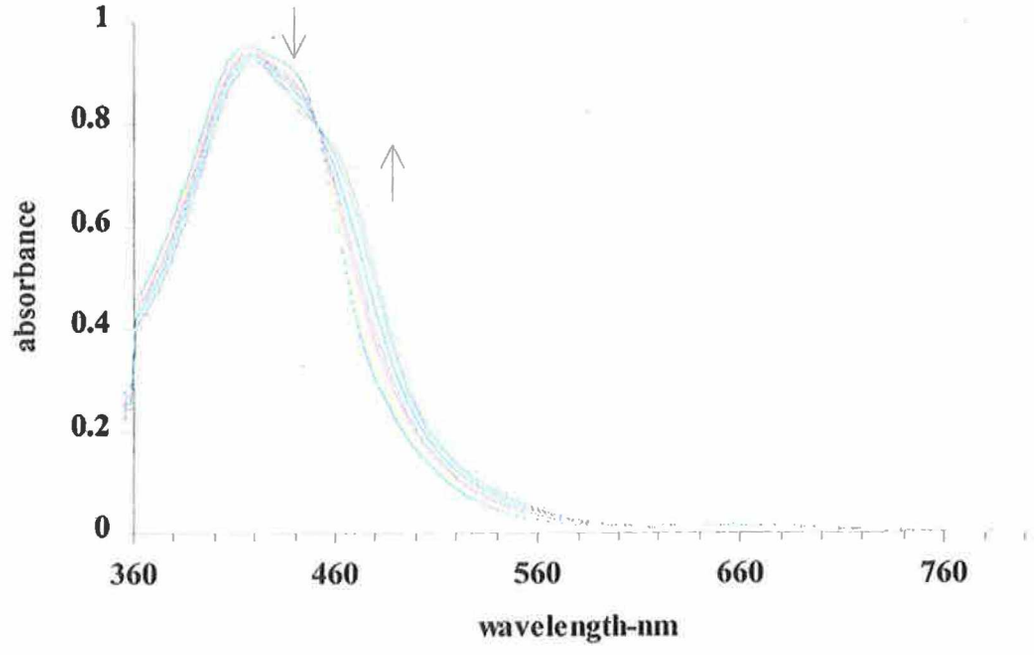

Figure 3.22 *pH dependence of the absorption spectra of $[Ru(phen)_2(L1)]PF_6.H_2O$ (5×10^{-5} M) in an aqueous Britton-Robinson buffer at pH 1.61, 2.49, 3.49, 4.12, 4.25, 4.55, 4.87, 5.07, 5.59 and 7.23.*

spectroscopic changes of the complexes are reversible in the pH range 1-9. The absorption titrations are performed by adjusting the pH of a 5 X 10^{-5} M solution of the complex in Britton Robinson buffer. Then by monitoring the spectral changes, at a wavelength where there is considerable change, as a function of pH graphical analysis was carried out by plotting percentage change in absorbance against pH. The pKa was determined from the point of inflection of the curve. The pKa represents the pKa of the triazole ring. In all titrations there is a blue shift of the MLCT band as the pH is lowered due to the stabilisation of the t_{2g} orbitals and the resultant increase in the ^{3}MLCT-t_{2g} energy gap.

The excited state pKa values (pKa*) can be evaluated in two different ways. The first method was one of the first and most important contributions to the excited state acid-base equilibria by Forster[27]. This thermodynamical treatment was based on the changes following protonation/deprotonation in the excited state of an organic species and it leads to the Forster cycle equation (3.1). Using this equation the excited state pKa* of a species can be calculated from its ground state properties.

$$pKa^* = pKa + (0.625/T)(\nu_{B^-} - \nu_{HB}) \qquad (3.1)$$

where ν_{B^-} and ν_{HB} are the $E_{0\text{-}0}$ values (in cm^{-1}) of the deprotonated and protonated complexes respectively. These values are taken from the λ_{max} of the emission spectra at 77 K as they are the most accurate means of obtaining an estimate for the energy difference involved in the 0-0 transition. An important point to remember in the use of the Forster equation (3.1) as a method for determining the pKa* is that small errors in the assessment of $E_{0\text{-}0}$ for ν_{B^-} and ν_{HB} produce considerable errors in pKa* [28]

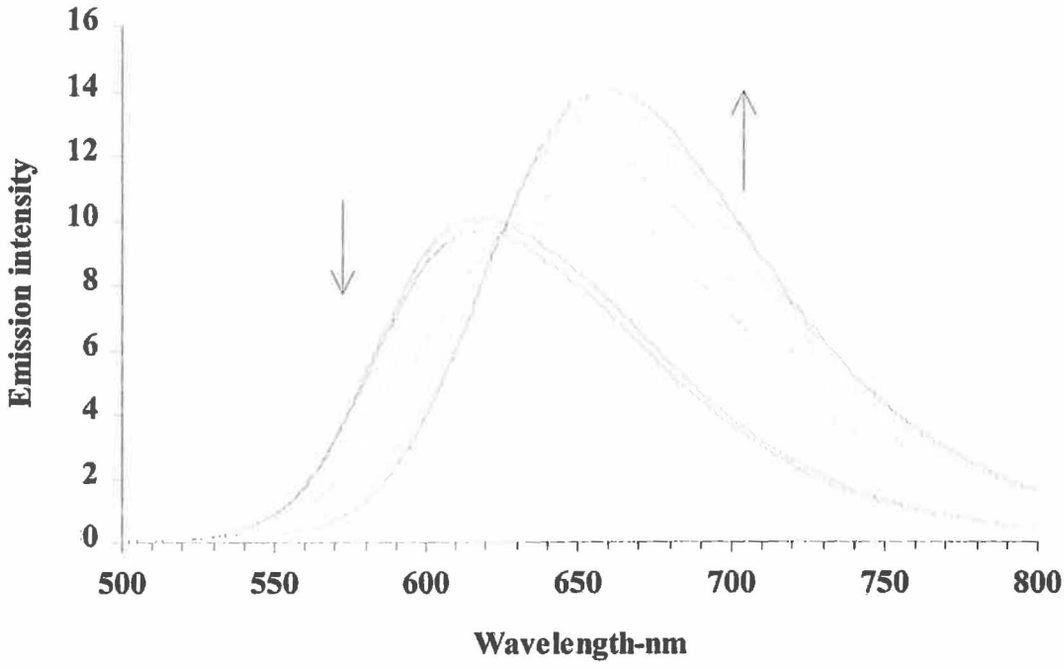

Figure 3.23 *pH dependence of the emission spectra of $[Ru(bpy)_2(L1)]PF_6.H_2O$ (5 X 10^{-5} M) in an aqueous Britton-Robinson buffer at pH 1.20, 1.82, 2.50, 3.22, 3.95, 4.65, 5.25, 5.98 and 7.06.*

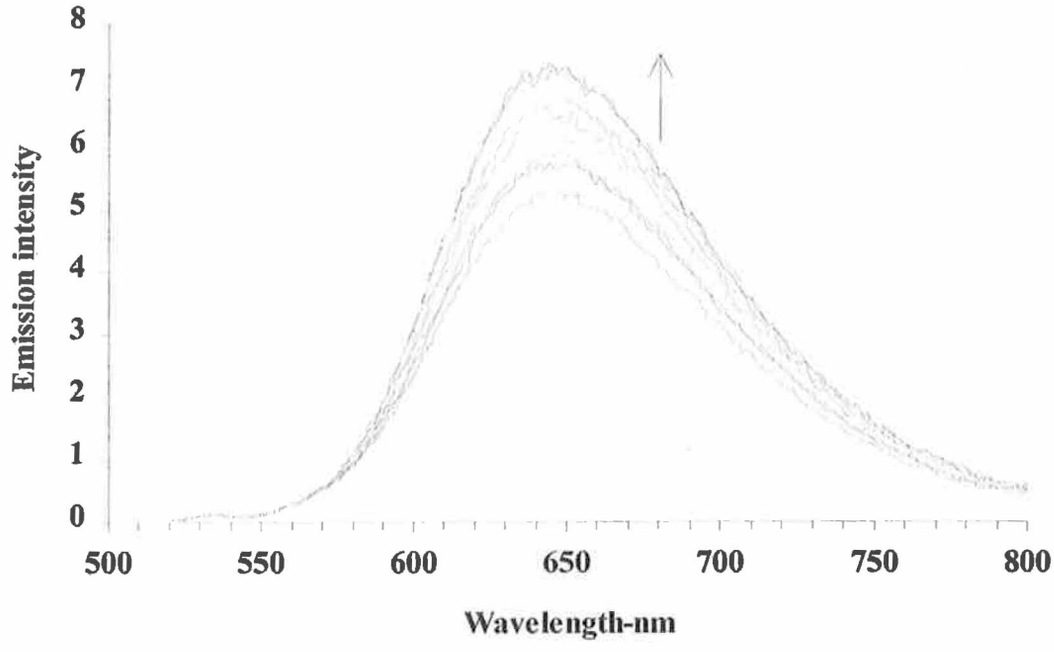

Figure 3.24 *pH dependence of the emission spectra of $[Ru(phen)_2(L1)]PF_6.H_2O$ (5 X 10^{-5} M) in an aqueous Britton-Robinson buffer between at pH 1.61, 2.49, 3.49, 4.12, 4.25, 4.55, 4.87, 5.07, 5.59 and 7.23.*

The second method employed for the determination of pKa^* is based on a kinetic model devised by Ireland and Wyatt[27] where the pKa^* may be measured from the emission lifetimes of the protonated (τ_{HB}) and deprotonated (τ_{B^-}) complexes and the point of inflection of the emission titration curve, pH_i . This pH_i value can be evaluated from emission titrations in Britton Robinson Buffer like those displayed in Figure 3.23 and 3.24. The point of inflection of the luminescence intensity against pH titration curve is pH_i . Equation 3.2 describes the model.

$$pKa^* = pH_i + \log (\tau_{HB} / \tau_{B^-}) \qquad (3.2)$$

Although this method would be the preferred choice for the evaluation of pKa^* it was not used due to the fact that it relies heavily on the establishment of the value via pHi and lifetimes. Thus the Forster cycle equation (3.1) was used for the evaluation of the pKa^* values shown in Table 3.4. The trend for all the pKa^* values is that they are more acidic than the ground-state pKa values. These results suggest that as expected the excited state is not based on the triazole ligand which can then be referred to as the spectator ligand. The triazole ligand does not become directly involved in the excited state confirming that the ^{3}MLCT is based on the bpy, d_8-bpy, phen or d_8-phen ligand of the respective complexes quoted in Table 3.4. These conclusions are in line with previous work on ruthenium(II) complexes of pyridyltriazole complexes[1,8,20]. It should be noted that the Forster equation assumes an accurate measurement of the $E_{0\text{-}0}$ values with small errors causing considerable errors in pKa^*. However from the values

calculated the direction of change in pKa when going from ground state to excited state can be asserted.

3.2.6 Electrochemical Properties.

It is known from previous work on ruthenium polypyridyl type complexes that oxidation and reduction processes are metal-centred and ligand-centred respectively[21]. The oxidation and reduction potentials of the ruthenium (II) complexes of the ligand HL1 are presented in Table 3.5. The anodic region of the cyclic voltammograms (Fig 3.25 and 3.27) feature reversible metal-centred oxidations when scanned not farther than 1.0 V. This is true for all the complexes examined in the deprotonated state. The oxidation potentials are lower than those of $[Ru(bpy)_3]^{2+}$ and $[Ru(phen)_3]^{2+}$ ($E_{1/2}$ = 1.27 V for both)[29] which again implies that the ligand L1 is a stronger σ-donor ligand than bpy or phen. The effect of protonation on the oxidation potential of the metal centre in the complex **bpyL1** is demonstrated in Figure 3.25. This figure shows an overlay of the cv of $[Ru(bpy)_2(L1)]PF_6.H_2O$ in the deprotonated and protonated state. There is an anodic shift of about 200 mV in the oxidation potential upon protonation. This is an expected feature of the protonation of the triazole ring since in its protonated form the coordinated ligand is a better π-acceptor and poorer σ-donor resulting in less electron density at the metal centre making it more difficult to oxidise. The loss of reversibility in the protonated state may be due to the fact that the oxidation potential of the metal centre is closer to the potential window of the methoxy groups which have an electrochemistry that induces an irreversible change in the chemical state of the complex.

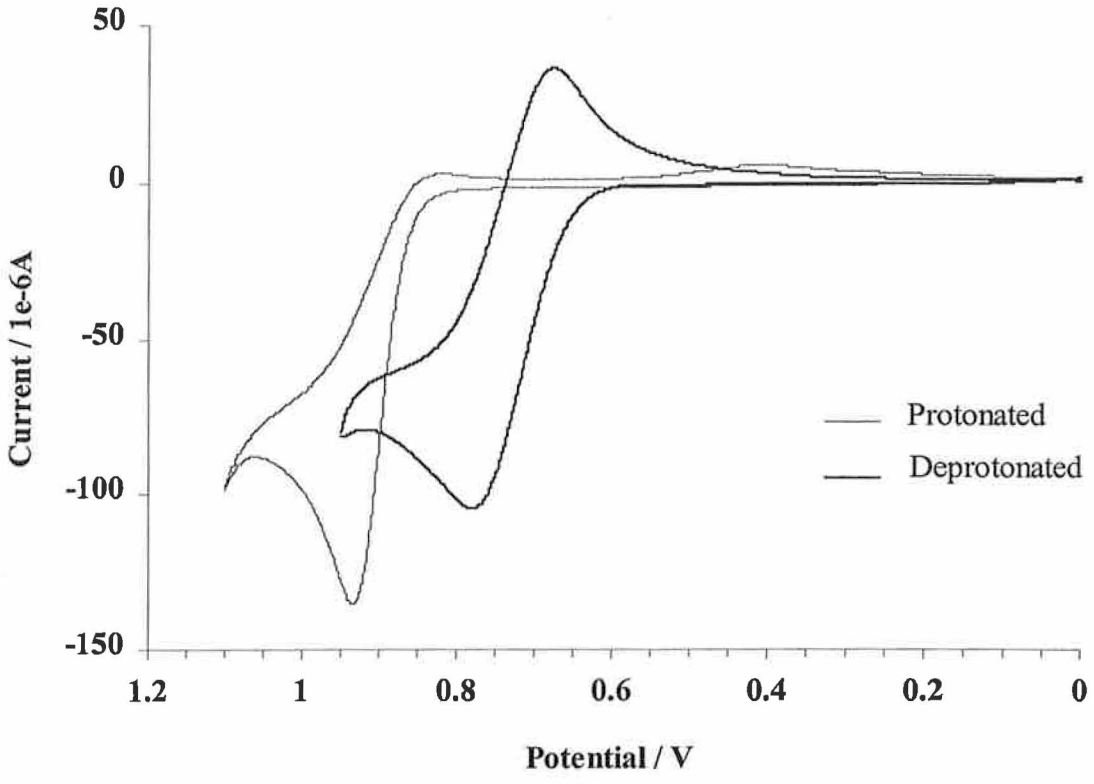

Figure 3.25 *Cyclic voltammogram of $[Ru(bpy)_2(L1)]PF_6.H_2O$ deprotonated and protonated in acetonitrile with 0.1 M TEAP (Scan rate : 100 mVS^{-1}).*

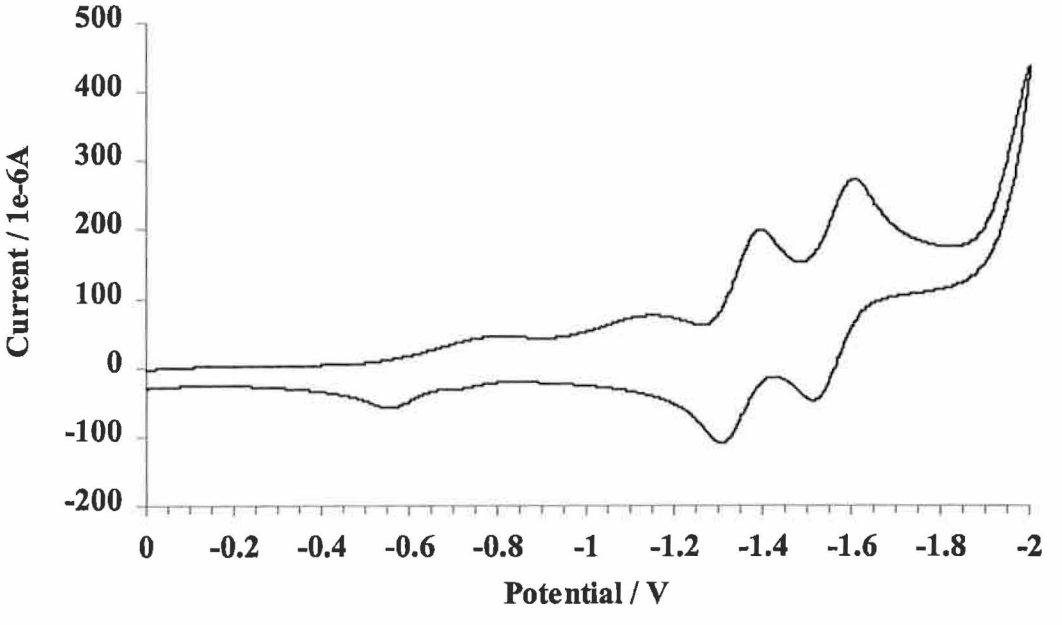

Figure 3.26 *Cyclic voltammogram of $[Ru(bpy)_2(L1)]PF_6.H_2O$ deprotonated in acetonitrile with 0.1 M TEAP at negative potentials(Scan rate : 100 mVS^{-1}).*

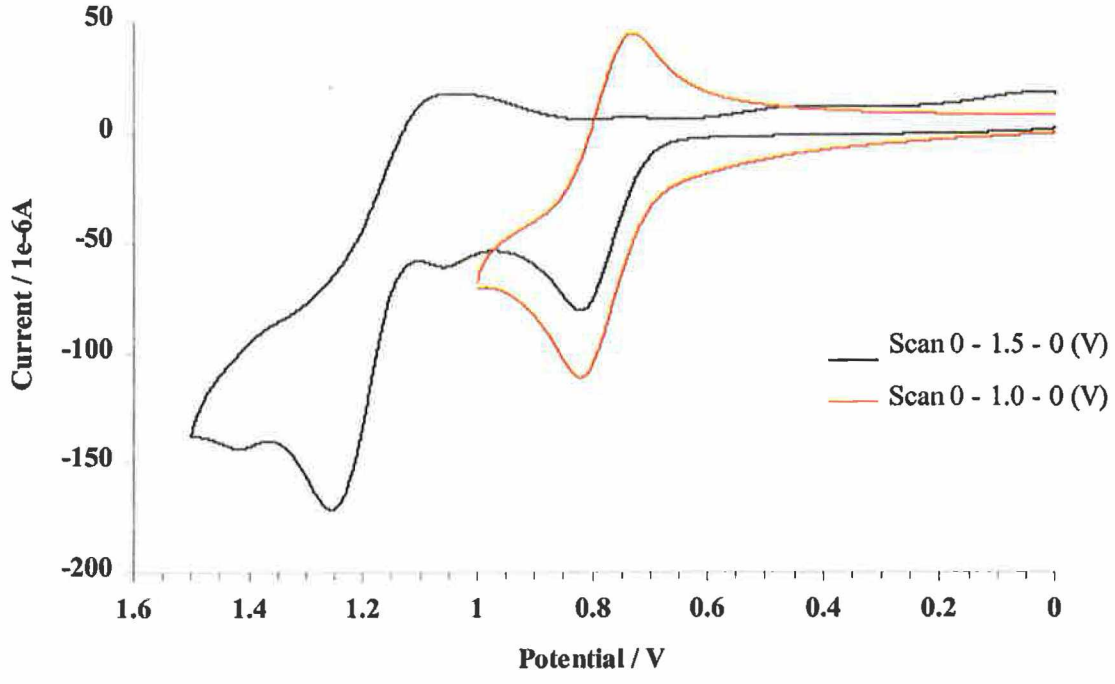

Figure 3.27 *Cyclic voltammogram of $[Ru(d_8\text{-phen})_2(L1)]PF_6.H_2O$ in acetonitrile with 0.1 M TEAP(Scan rate : 100 mVS^{-1}).*

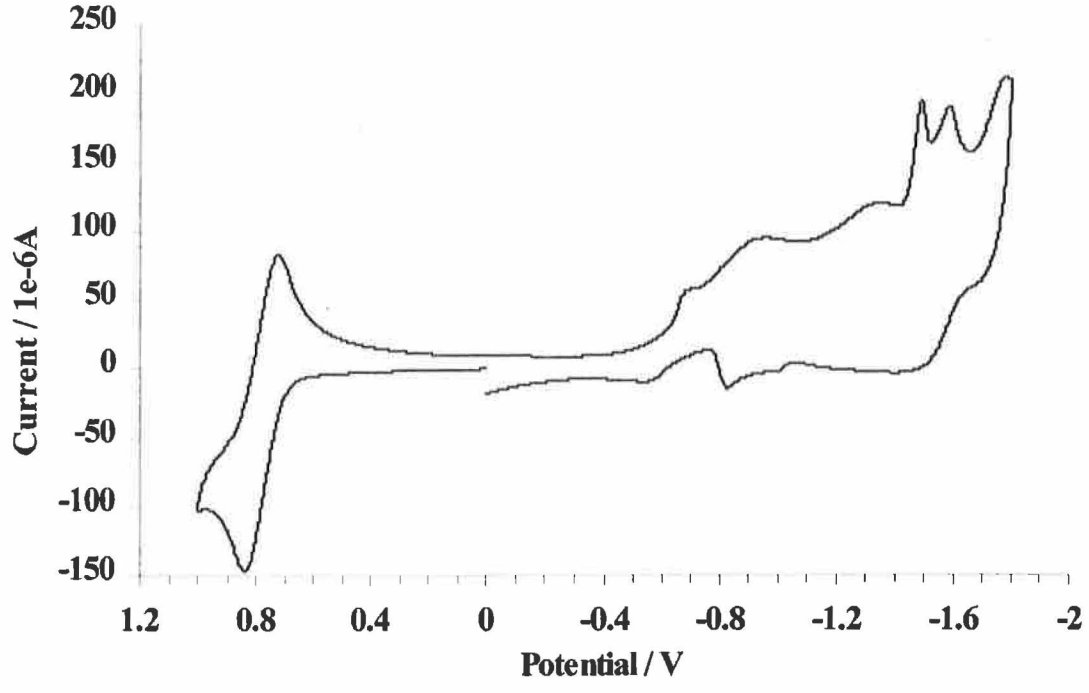

Figure 3.28 *Cyclic voltammogram of $[Ru(d_8\text{-phen})_2(L1)]PF_6.H_2O$ in acetonitrile with 0.1 M TEAP (Scan rate : 100 mVS^{-1}).*

Table 3.5 *Electrochemical data for the complexes of HL1 in V vs Ag/AgCl. All measurements were carried out on the deprotonated complexes in acetonitrile with 0.1 M TEAP (Scan rate : 100 mVS^{-1}).*

Complex	Oxidation Potentials / V Ru(II) / Ru(III)	Reduction Potentials / V
bpyL1	0.71	-1.35 ; -1.56
phenL1	0.76	-1.48(irr) ; -1.55(irr)
d_8-bpyL1	0.71	-1.35; -1.57
d_8-phenL1	0.78	-1.49(irr) ; -1.59(irr)

This effect is investigated by scanning further positive than 1.0 V and is demonstrated for the complex **d_8-phenL1** in the deprotonated state (see Figure 3.27). The system become irreversible and the complex appears irreversibly altered at higher potentials. The metal centre is no longer observed as a reversible couple and further irreversible oxidations can be observed at around 1.2 V. This can be assigned to oxidation of the dimethoxyphenyl group which is also observed and characterised in the complexes of the ligand L_x shown in Figure 3.29 from the work of Whittle et al[30]. In the CV of the complex $[Ru(terpy)(L_x)][PF_6]_2$ the metal oxidation when scanned alone occurs at 0.85 V and a second, irreversible oxidation is observed at around 1.2 V. It is also reported in this study by Whittle et al that electrochemical oxidation of 1,2-dimethoxybenzene is known to afford either soluble oligers or polymers bound to the electrode surface, via coupling of the initially generated radical cation.

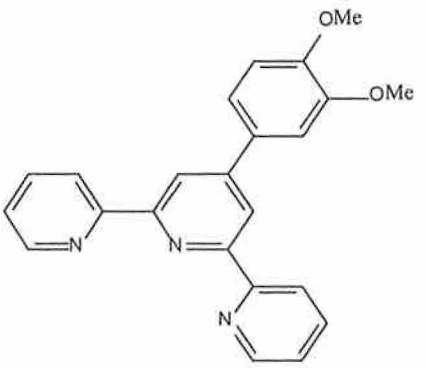

Figure 3.29 Structure of ligand 4′-(3,4-dimethoxyphenyl)-2,2′:6′,2″-terpyridine (L_x).

In the complexes studied in our work no further examination of the processes was examined. The reduction waves observed for the complexes are based on the ligands L′, where L′ is bpy, phen, d_8-bpy and d_8-phen respectively in the complexes examined of the type $[Ru(L')_2(L1)]^{1+}$. The ligand L1, being a weaker π-acceptor than the ligands L′, is consequently more difficult to reduce and the redox couples are expected to lie outside the potential window investigated. Surface effects appear to interfere with the reversibility and definition of the phenanthroline complexes but the region of reduction was stated in Table 3.5.

3.3 Concluding Comments

The synthesis and characterisation of several ruthenium (II) complexes of the ligand 3-(1′,2′-dimethoxyphenyl)-5-(pyridin-2-yl)-1,2,4-triazole (HL1) were presented in this chapter. The complexes **bpyL1**, **phenL1** and **dcbpyL1** were synthesised and the reactions followed by analytical HPLC. Synthesis of the **d_8-bpyL1** and **d_8-phenL1** complexes were performed to aid in the structural elucidation of **bpyL1** and **phenL1** and also to assess the effect of deuteriation on lifetimes when compared to the undeuteriated complexes. It was evident from the ^{1}H-NMR of the deuteriated complexes (see Figure 3.9 and 3.10) that there was slight residues of undeuteriated bipyridine and undeuteriated phenanthroline in the respective complexes. The complexes were estimated to be 94.06 % deuteriated for the **d_8-bpyL1** complex and 98.86 % deuteriated for the **d_8-phen** complex. Comparison between the deuteriated and undeuteriated complexes reveals no significant differences in their properties with the exception of the lifetimes. The lifetimes of the deuteriated complexes are longer due to the fact that, in all the complexes discussed in this work, the pyridyltriazole ligand is a spectator ligand and the excited state is based on the other ligands.

The coordination mode of the pyridyltrizole ligand (HL1) is confirmed by ^{1}H-NMR and X-Ray crystallography. The ligand coordinates via N1 of the pyridine nitrogen triazole ring and the pyridine nitrogen. The X-Ray data for the **d_8-bpyL1** complex and the **phenL1** complex is typical for pyridyltriazole complexes and was compared in this study to pyridyltriazole complexes studied by R. Hage[1] (see Figure 3.14). The bond angles (^{O}) and bond distances(Å) do not vary substantially between the two complexes and those of R. Hage. The only significant difference between the X-

Ray crystallography of the **d_8-bpyL1** and **phenL1** complexes is in the orientation of the phenyl ring. It appears from the projection of the structures of the complexes (see Figure 3.10 and 3.11) that the phenyl ring experiences greater steric hindrance in the **phenL1** complex than in the **d_8-bpyL1** complex due to the positioning of the methoxy units.

Investigation of the absorption, emission and acid-base properties of the complexes confirms the classification of the ligand HL1 as a weak π-acceptor and strong σ-donor (class b type ligand). Differences between the complexes can be explained by the varying π-acceptor abilities and hydrophobicity of the 2,2′-bipyridine, 1,10-phenanthroline and 4,4′-(dicarboxylicacid)-2,2′-bipyridine ligands of the respective complexes. The electrochemical properties of the complexes are metal centred (between 0.70 V and 0.78 V) and ligand centred. The ligand centred processes occur at negative potentials and are subject to surface effects which infringe on the reversibility of the processes. It was established that the methoxy units on the phenyl ring are non-innocent. When the cyclic voltammetry is allowed to scan higher than 1 V there is considerable irreversibility induced which causes the loss of the metal-centred redox couple.

The **bpyL1** and **phenL1** complexes discussed in this chapter are the precursors for the studies presented in the following chapters. The deprotection of the complexes produces catechol type complexes with appealing peripheral binding sites. The catechol complexes themselves are investigated along with the synthesis of O,O coordinated Ru-Ru dimers. Finally, the interaction of the catechol complexes with various transition metals is explored with the establishment of stability constants for the various complexes formed.

3.4 References.

1 R. Hage, Ph.D Thesis 1991, Leiden University.

2 T.E. Keyes, F. Weldon, E. Müller, P. Pechy, M. Grätzel, J.G. Vos, *J. Chem. Soc., Dalton Trans.*, 1995, 2705.

3 S. Chirayil, R. P. Thummel, *Inorg. Chem.*, 1989, 28, 813.

4 W. Siebrand, *J. Chem. Phys.*, 1967, 46, 440.

5 W. Siebrand, *J. Chem. Phys.*, 1971, 55, 5843.

6 V. Balzani and F. Scandola, *SupramolecularPhotochemistry*; Horwood: Chichester, UK 1991.

7 S. Rau, *Unpublished results.*

8 T.E. Keyes, Ph.D. Thesis, Dublin City University, 1995.

9 K.R. Seddon, E. Seddon, The Chemistry of Ruthenium, Elsevier, Amsterdam, 1984.

10 J. van Houten, R.J. Watts, *J. Am. Chem. Soc.*, 1976, 98, 4853.

11 J. van Houten, R.J. Watts, *Inorg. Chem.*, 1978, 17, 3381.

12 B. Durham, J.V. Casper, J.K. Nagle, T.J. Meyer, *J. Am. Chem. Soc.*, 1982, 104, 4803.

13 E.M. Ryan, R.Wang, J.G. Vos, R.Hage, J.G. Haasnoot, *Inorg. Chim. Acta.*, 1993, 208, 49.

14 A.C. Lees, B. Evrard, T.E. Keyes, J.G. Vos, C.J. Kleverlaan, M. Alebbi, C.A. Bignozzi, *Eur. J. Inorg. Chem*, 1999, 2309.

15 P. Belser, A.von Zelewsky, *Helv.Chim. Acta.*, 1980, 63, 1675.

16 E.C. Constable, J.Lewis, *Inorg. Chim. Acta.*, 1983, 70, 251.

[17] D.P. Rillema, D.G. Taghdiri, D.S. Jones, C.D. Keller, L.A. Worl, T.J. Meyer, H.A. Levy, *Inorg. Chem.*, 1987, 26, 578.

[18] D.P. Rillema, D.S. Jones, H.A. Levy, *J.Chem. Soc., Chem. Comm.*, 1979, 849.

[19] D.S. Eggleston, K.A. Goldsby, D.J. Hodgson, T.J. Meyer, *Inorg. Chem.*, 1985, 24, 4573.

[20] F. Weldon, Ph.D. Thesis, Dublin City University, 1998.

[21] A. Juris, V. Balzani, F. Barigelletti, S. Campagna, P. Belser, A. Von Zelewsky, *Coord. Chem. Rev.*, 1988, 84, 85.

[22] J.V. Caspar, T.J. Meyer, *J. Am. Chem. Soc.*, 1983, 100, 5583.

[23] M. Wrighton, D.L. Morse, *J. Am. Chem. Soc.*, 1974, 96, 996.

[24] D.E. Morris, Y. Ohsawa, D.P. Segers, M.K. DeArmond, K.W. Kanck, *Inorg. Chem.*, 1984, 23, 3010.

[25] P.J. Giordano, C.R. Bock, M.S. Wrighton, L.V. Interrante, R.F.X. Williams, *J. Am.Chem. Soc.*, 1977, 99, 3187.

[26] P.J. Giordano, C.R. Bock, M.S. Wrighton, *J. Am. Chem. Soc.*, 1978, 100, 6960.

[27] J. F. Ireland, P.A.H. Wyatt, *Ad. Phys.Org.Chem.*, 1976, 12, 32.

[28] J. G. Vos, *Polyhedron*, 1992, 11, 25.

[29] Y. Kawanishi, N. Kitamura, S. Tazuke, *Inorg. Chem.*, 1989, 28, 2968.

[30] B. Whittle, N. S. Everest, C. Howard, M. D. Ward, *Inorg. Chem.*, 1995, 34, 2025.

Chapter Four

Synthesis and Characterisation of Mononuclear Ruthenium Complexes Containing a Catechol Group

4.0 Introduction.

Hydroquinones and quinones play an essential role as electron mediators in the charge separation processes in photosynthesis[1]. Quinonoid species as a result of their redox properties have found frequent use as acceptors and donors in charge transfer complexes or as excited state quenching agents, free in solution. The involvement of quinones in electron donor-acceptor complex formation is a consequence of the fact that such molecules possess low lying unoccupied electronic energy levels and are therefore ready acceptors of electrons[2,3]. In this chapter the synthesis and characterisation of two ruthenium(II) complexes of a pyridyltriazole ligand containing a catechol ring are presented (see Figure 4.1). The catechol ring in these complexes is an appealing peripheral binding site, a fact which is exploited in further studies presented in chapter five and chapter six. The deprotection of the methoxy protected complexes $[Ru(bpy)_2(L1)]PF_6.5H_2O$ and $[Ru(phen)_2(L1)]PF_6.2H_2O$ to produce the catechol type complexes, is described. The structural elucidation was determined by ^{1}H-NMR and 2D COSY. The absorption, emission, photophysical and electrochemical properties of the complexes are also examined. The application of ruthenium(II) complexes for solar energy conversion systems was discussed in more detail in chapter one. A brief investigation of the attachment of the catechol complexes, introduced in this chapter, to dye sensitised titanium dioxide was also performed. The attachment to the surface is through the catechol moiety as opposed to the traditional mode of attachment in dicarboxy-bipyridyl complexes[4,5]. For this reason the results obtained for the catechol complexes are compared to a reference $[Ru(dcH_2bpy)_2](NCS)_2$, which is known to have the most efficient photon-to-current conversion[4]. The attachment of the catechol

complexes to TiO_2 is also compared with the attachment of the complex $[Ru(H_4dcbpy)_2(HL1)]Cl_2.5H_2O$ (**dcbpyL1**), which has the catechol site protected by methoxy groups. The synthesis and characterisation of **dcbpyL1** was described in chapter three.

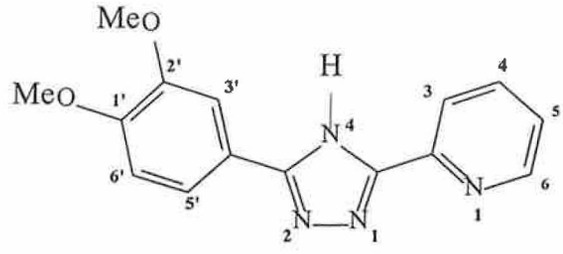

3-(1′,2′-dimethoxyphenyl)-5-(pyridin-2-yl)-1,2,4-triazole (HL1)

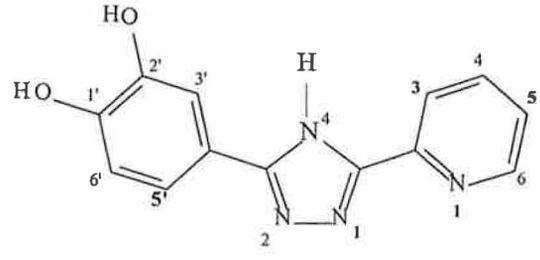

3-(1′,2′-dihydroxyphenyl)-5-(pyridin-2-yl)-1,2,4-triazole (H_3L2)

Figure 4.1 Structrures of ligands HL1 and H_3L2 cited in text.

4.1. Experimental

4.1.1. Deprotection of the protected mononuclear complexes of HL1.

$[Ru(bpy)_2(H_2L_2)]PF_6.5H_2O$ and $[Ru(phen)_2(H_2L_2)]PF_6.2H_2O$ were prepared by modifying a deprotection method using boron tribromide[6,7]. The conditions used in the reaction were developed after several modifications to the technique used and reaction conditions.

$[Ru(bpy)_2(H_2L_2)]PF_6.5H_2O$ **(bpyL2)**

$[Ru(bpy)_2(H_2L_2)]PF_6.5H_2O$ was prepared by demethylating the protected catechol complex $[Ru(bpy)_2(L_1)]PF_6.2H_2O$ with boron tribromide. 0.523 g (0.61 mmol) of $[Ru(bpy)_2(L1)]PF_6.H_2O$ was dissolved and stirred in 20 cm^3 dry dichloromethane (dried using lithium aluminium hydride) and in a moisture free atmosphere under a flow of N_2. The flask was placed in a toluene/liquid nitrogen bath (< -78 °C) and allowed to equilibrate for at least 20 minutes. 12 cm^3 (ten fold molar excess) of 1.0 M boron tribromide(BBr_3) in dichloromethane was syringed under an atmosphere of N_2 and slowly added to the reaction flask, fitted with a septum, maintaining the N_2 atmosphere. The temperature was maintained at - 78 °C for at least one hour and the reaction was left stirring under N_2 and warmed to room temperature overnight. The reaction was quenched by slowly adding iced water to the reaction flask. The product is quite soluble in the water layer and insoluble in dichloromethane, which was removed by extraction or simply by pipetting. The remaining solution was very acidic at this stage and was neutralised to pH 7.0-8.0 by adding an aqueous solution of concentrated sodium

carbonate. At this stage, after adding a few grains of ammonium hexafluorophosphate, the deep red deprotected ruthenium complex precipitated and was collected by vacuum filtration. The product was washed with diethyl ether and recrystallised in acetone/water (2:1 v/v). Successful demethylation was verified by TLC and by ^{1}H-NMR due to the absence of the singlet peaks between 3.7 and 3.9, which are present in the protected complex, indicative of the -OMe protons. Purity is established by ^{1}H NMR and analytical HPLC. Yield = 0.351 g (64 %). Calcd. for : $Ru_1C_{33}H_{35}N_8O_7P_1F_6$ C: 43.96; H: 3.91; N: 12.42 %. Anal. Found: C: 43.83; H: 4.00; N: 12.24 %.

$[Ru(phen)_2(H_2L2)]PF_6.2H_2O$ **(phenL2)**

The methylated complex $[Ru(phen)_2(L1)]PF_6.H_2O$ was deprotected to form the complex $[Ru(phen)_2(H_2L2)]PF_6.2H_2O$ using BBr_3 in a similar reaction to that described for the complex $[Ru(bpy)_2(H_2L2)]PF_6.5H_2O$. 0.650 g (0.718 mmol) of $[Ru(phen)_2(L1)]PF_6.H_2O$ was stirred in 20 cm^3 dry dichloromethane under N_2. After allowing the solution to cool to -78 °C 15 cm^3 of 1.0 M BBr_3 was syringed under an atmosphere of N_2 and slowly added to the reaction flask, fitted with a septum, maintaining the N_2 atmosphere. The reaction was worked up similarly to that described for $[Ru(bpy)_2(H_2L2)]PF_6.5H_2O$. The product obtained was recrystallised from acetone/water (2:1 v/v) and demethylation and purity were verified by ^{1}H-NMR and TLC. Yield = 0.535 g (83 %). Calcd. for : $Ru_1C_{37}H_{29}N_8O_4P_1F_6$ C: 49.62; H: 3.26; N: 12.51 %. Anal. Found: C: 49.86; H: 3.26; N: 12.17 %.

4.1.2. Attempted deprotection of the protected mononuclear complexes of HL1 using Iodotrimethylsilane.

The reaction was performed in dry acetonitrile under nitrogen using a 5 molar excess of Me_3SiI to $[Ru(bpy)_2(L_1)]PF_6.2H_2O$. The solution was placed under reflux at 60 °C for 26 hours and quenched by adding water. The volume was reduced under pressure and the product recrystallised from acetone/water, adding a few grains of NH_4PF_6 to aid crystallisation. Unsuccessful demethylation was verified by the presence of two sharp singlets around 3.7 ppm indicative of the -OMe protons.

4.2. Results and Discussion.

4.2.1. Synthetic Procedure.

The method applied in this section for the demethylation of the protected catechol complexes prepared in chapter three was modified from that published by McOmie et al in 1968[7]. It was implied in this work that aromatic ether cleavage at or below room temperature by boron tribromide could be improved by altering the reaction conditions. In the work of Whittle et al[8,9] the synthesis of protected catechol complexes of $[Ru(terpy)(L_x)][PF_6]_2$ and $[Ru(L_x)_2][PF_6]_2$ using boron triibromide was presented. It was reported in this work that 10 equivalents of boron tribromide was used and the reaction was performed at -78 °C and allowed warm to -10 °C at which point the reaction was quenched by addition of water.

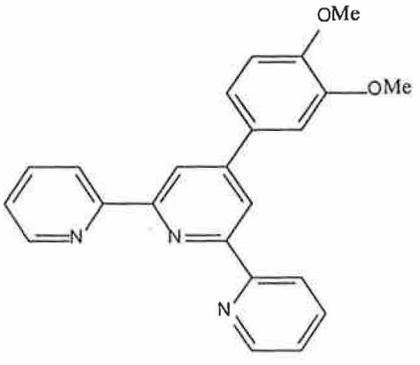

Figure 4.2 *Structure of ligand 4'-(3,4-dimethoxyphenyl)-2,2':6',2''-terpyridine (L_X) presented by Whittle et al[8].*

In the deprotection reaction of $[Ru(bpy)_2(H_2L_2)]PF_6.5H_2O$ and $[Ru(phen)_2(H_2L2)]PF_6.2H_2O$ (see Figure 4.3) the reaction conditions used were modified. A longer reaction time was allowed to ensure complete demethylation. After addition of boron tribromide to the protected complex, which was stirring in dry dichloromethane equilibrated at -78 °C for 20 minutes prior to reaction, the temperature

was maintained at -78 °C for one hour. It was then allowed to stir overnight under an atmosphere of N_2 and warm to room temperature. Boron tribromide is hydrolysed by moisture in the air thus making the proper handling of the air sensitive reagent essential. The reaction was carried out using dry glassware, dry solvent (dicloromethane) and under a constant atmosphere of N_2.

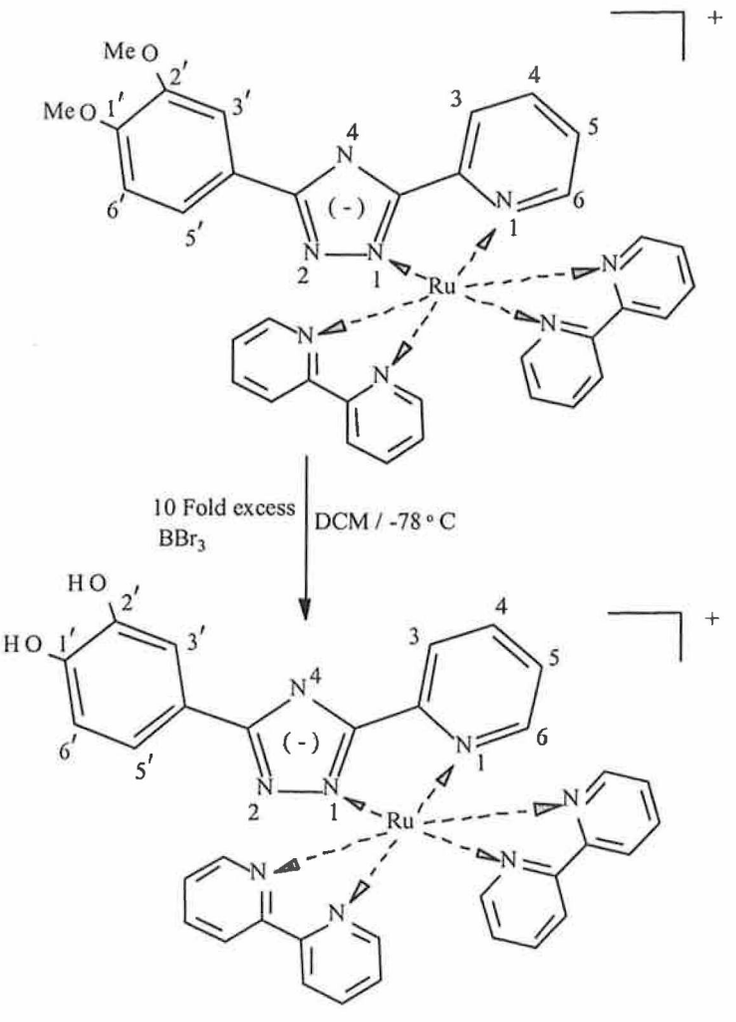

Figure 4.3 Deprotection reaction of $[Ru(bpy)_2(L_1)]PF_6.2H_2O$.

It is suggested that the demethylation of the aryl ethers by boron tribromide proceeds via a complex formed between the reagent and the ethereal oxygen atom[7] as depicted in the reaction scheme shown in figure 4.4. It is also suggested that one mole of BBr_3 be used per ether group together with an extra mole of reagent for each group containing a potentially basic N.

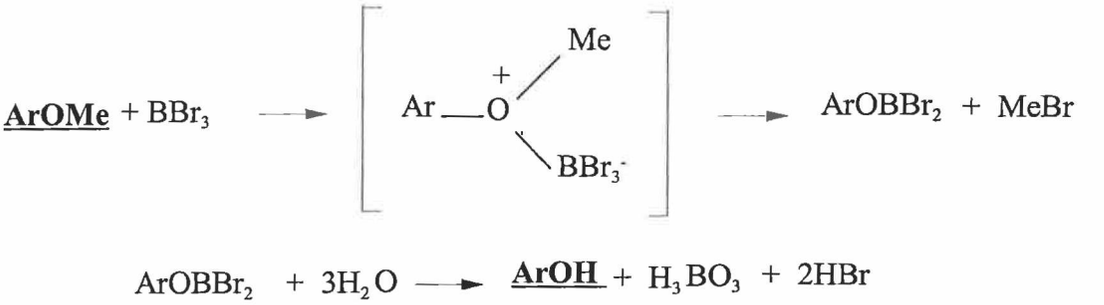

Figure 4.4 Scheme for demethylation by Boron tribromide.

For catechol dimethyl ethers, which is of particular interest to us, it is likely that demethylation can proceed stepwise and that one mole of reagent suffices for each catechol group since a cyclic borate can be formed as shown in figure 4.5.

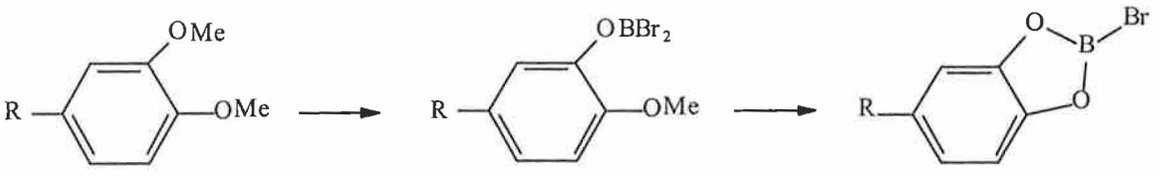

Figure 4.5 Cyclic borate formation in deprotection of catechol dimethyl ethers.

As can be seen in the scheme shown in Figure 4.4, the demethylation reaction with boron tribromide is quenched by slowly adding iced water to the reaction. At this stage it was clear that the deprotected complex was insoluble in the dichloromethane layer and was sparingly soluble in the water layer. After removal of the dichloromethane the remaining solution was quite acidic due to the production of HBr (as a result of the quenching with water) and was neutralised by adding concentrated sodium carbonate. It was also neutralised to remove any possible formation of a BBr_2 salt caused by attack of boron tribromide at the lone pair of electrons on the N4 of the triazole ring (see Figure 4.6).

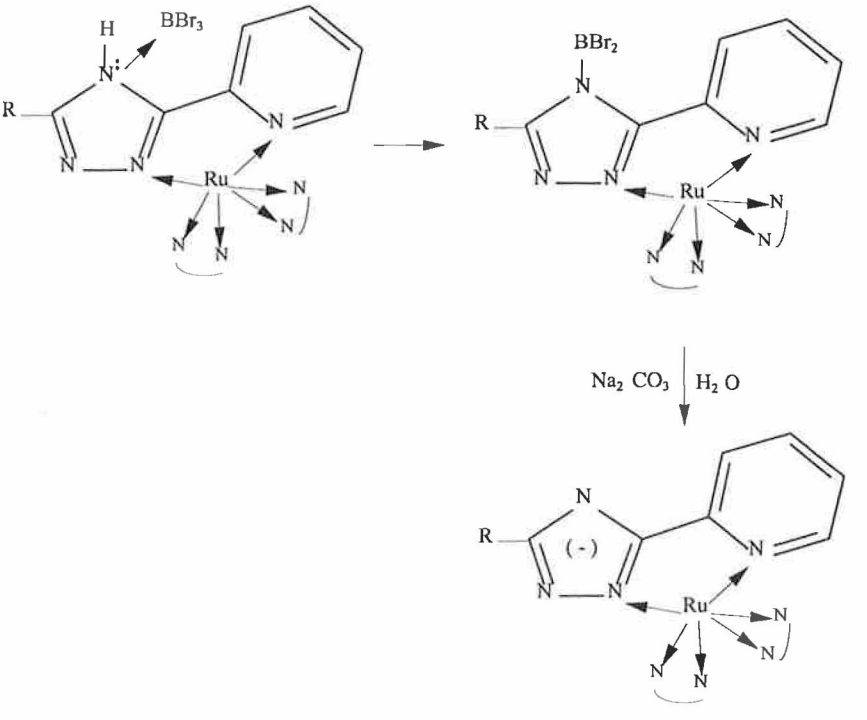

Figure 4.6 *Neutralisation by Na_2CO_3 to prevent isolation of BBr_3 complex where R is the catechol ring.*

It is important to carefully adjust the pH during neutralisation, by monitoring the addition of concentrated sodium carbonate using a pH meter, as irreversible semiquinone formation can occur at pH > 9. After neutralisation the complex was

isolated as the PF_6 salt and recrystallised from acetone/water (2:1). It is important to note that complete demethylation was achieved and the reaction gave the desired pure catechol complex in high yield. This was verified by the absence in the ^{1}H-NMR of the -OMe singlets around 3.8 ppm.

Another method for demethylation of the protected catechol complexes was attempted with iodotrimethylsilane. In a report by Jung and Lyster[10] the quantitative dealkylation of alkyl ethers via treatment with iodotrimethylsilane was reported. They suggest that simple and efficient dealkylation of methyl and other alkyl ethers in both aliphatic and aromatic systems was achieved in high yields. The reactions generally involved stirring with 1.3 equivalents of iodotrimethylsilane at 25 to 60 °C for 24 hours. The suggested mechanism for the dealkylation by iodotrimethylsilane of alkyl carboxylic ethers to carboxylic acids is shown below. In Figure 4.7 alkyl methyl ethers ((1) where R' = Me) react with iodotrimethylsilane (2) to afford mixtures of dealkylated products (3 and 4) and the alkyl iodides (5 and 6). Conversion of the trimetylsilyl ethers formed (3 and 4) can then be hydrolysed to the alcohols (7 and 8) by quenching the reaction with water or methanol. The components (5) and (6) are volatile and are removed at reduced pressure.

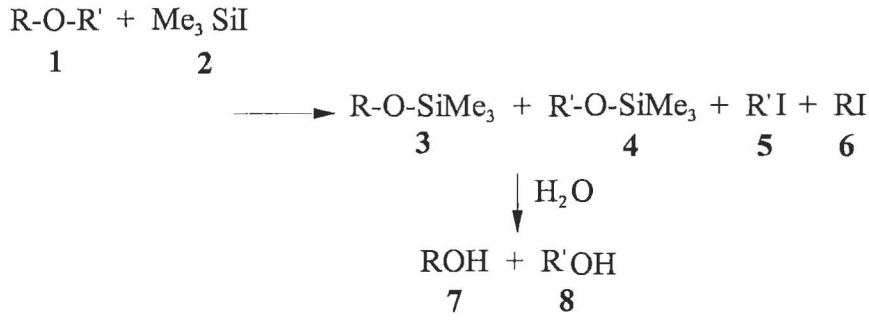

Figure 4.7 Scheme of dealkylation of alkyl ethers by Iodotrimethylsilane.

This method was also reported by Vickery et al[6] who compared iodotrimethylsilane and boron tribromide for the selective O-demethylation of catechol ethers. In general the demethylation of simple methyl aryl ethers was investigated with these reagents. The reaction times were faster for BBr_3 than Me_3SiI with Me_3SiI proving more selective for O-demethylation than BBr_3. However when this method of deprotection was applied to the methyl protected aromatic complex $[Ru(bpy)_2(L_1)]PF_6.2H_2O$ demethylation was not achieved. It is not known why the reaction was unsuccessful but it may be tentatively suggested that a stronger demethylating agent such as BBr_3 was required to demethylate the methyl protected catechol complex. Me_3SiI is a milder reagent than BBr_3 and may be more suitable and effective for simpler methyl ethers rather than Ru(II) polypyridyl complexes.

4.2.2 ^{1}H-NMR Spectroscopy.

^{1}H-NMR and 2D COSY spectra of the H_3L2 complexes are shown in Figures 4.8- 4.11. Table 4.1 presents the ^{1}H-NMR data for the complexes **bpyL2** and **phenL2** and the catechol ligand H_3L2 with the assignment of the H_3L2 ligand protons. The ^{1}H-NMR data for the catechol ligand H_3L2 is also included along with the assignment of the protons (see appendix 1 for ^{1}H-NMR spectrum of H_3L2). As with the ^{1}H-NMR spectra of the complexes **bpyL1** and **phenL1** discussed in section 3.2.2 it was only possible to assign ranges of proton resonances for the bpy and phen ligands respectively. This was due to their coincidental shifts whereby overlap of the bpy and phen proton signals respectively with each other and with those of the ligand H_3L2. In order to ensure the solubility of the complexes in d_3-acetonitrile a few drops of D_2O were required.

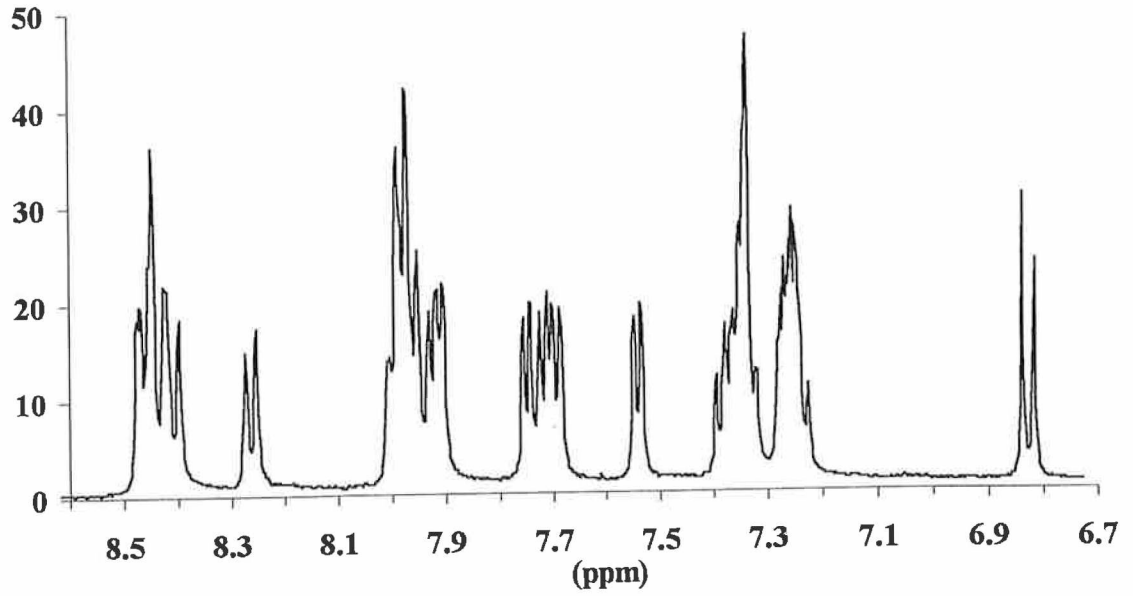

Figure 4.8 *^{1}H-NMR spectrum of $[Ru(bpy)_2(H_2L2)]PF_6.5H_2O$ d_3 -acetonitrile /D_2O*

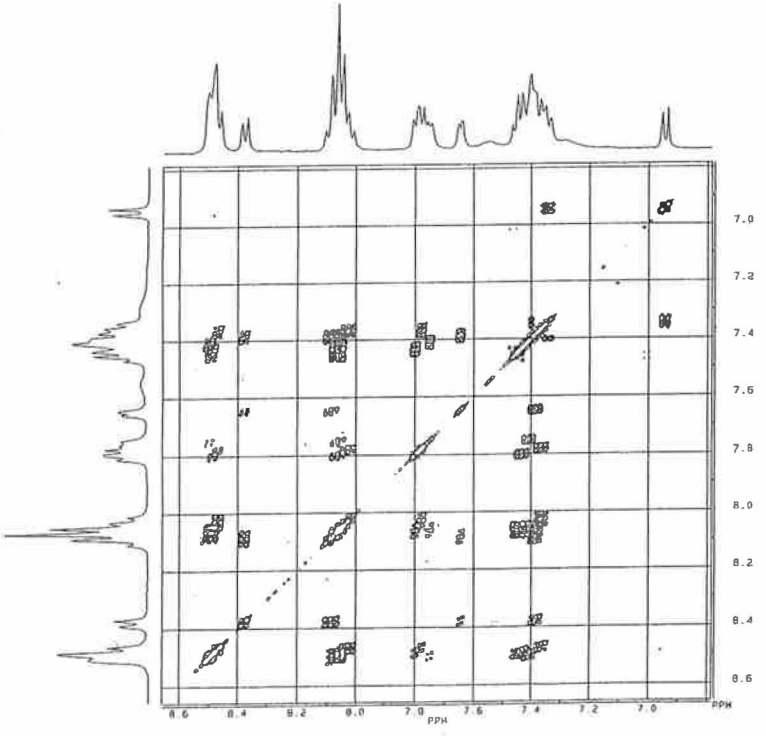

Figure 4.9 *COSY NMR spectrum of $[Ru(bpy)_2(H_2L2)]PF_6.5H_2O$ in d_3 -acetonitrile /D_2O*

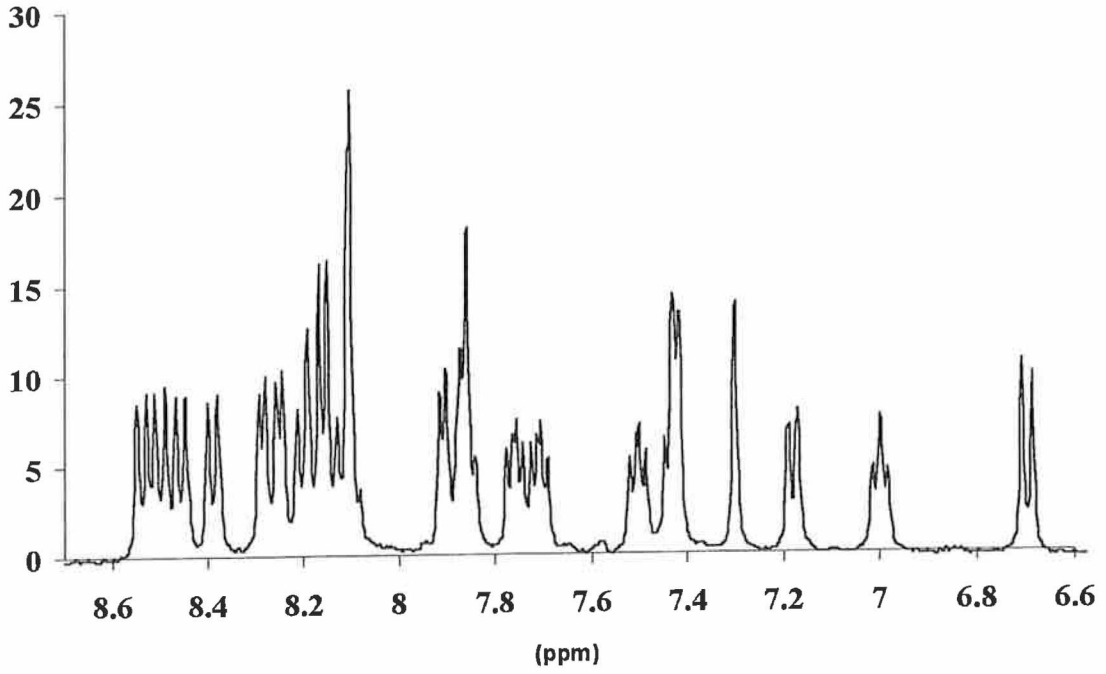

Figure 4.10 *^{1}H-NMR spectrum of $[Ru(phen)_2(H_2L2)]PF_6.2H_2O$ in d_3 -acetonitrile /D_2O.*

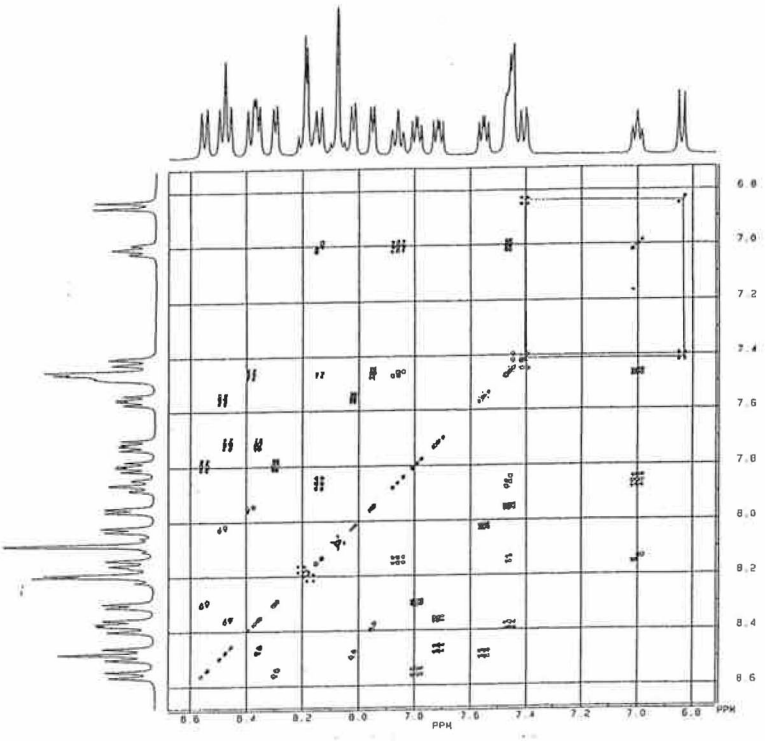

Figure 4.11 *COSY NMR spectrum of $[Ru(phen)_2(H_2L2)]PF_6.2H_2O$ in d_3 -acetonitrile /D_2O.*

Table 4.1 *^{1}H-NMR data for the ruthenium(II) complexes of H_3 L2^{A,B,C}.*

	H_3L2 Resonances (Chemical Shifts / ppm vs Me_4Si)						
Complex	**H^3**	**H^4**	**H^5**	**H^6**	**$H^{3'}$**	**$H^{5'}$**	**$H^{6'}$**
bpyL2	8.25(d)	7.96(dd)	7.28(dd)	7.54(d)	7.34(s)	7.26(d)	6.84(d)
phenL2	8.19(d)	7.87(dd)	7.01(dd)	7.42(d)	7.30(s)	7.18(d)	6.85(d)
H_3L2	8.05(d)	7.98(dd)	7.47(dd)	8.52(d)	7.30(s)	7.18(d)	6.65(d)

A: **bpyL2** and **phenL2** were measured in d_3-acetonitrile/D_2O and the ligand H_3L2 was measured in d_6-dimethyl sulphoxide.

B: bpy and phen resonances respectively were observed to occur in the following regions: **bpy** - 8.30-8.50 (H^3); 7.88-8.05 (H^4); 7.30-7.42 (H^5); 7.65-8.05 (H^6)

phen - 8.23-8.60; 7.84-8.18; 7.40-7.80

C: Water suppression ^{1}H-NMR was required for **bpyL2** and **phenL2** due to the presence of D_2O in the sample.

This caused some problems in the ^{1}H-NMR spectra with a large solvent signal for D_2O occurring around 4 ppm. The catechol complexes are synthesised (see section 4.1.1) by the demethylation of the protected catechol complexes discussed in chapter three. The quantitative demethylation of the parent complexes was verified by the absence of the -OMe singlets between 3.7 and 3.9 ppm. Thus the presence of a large broad solvent peak in this region of the ^{1}H-NMR spectra interferes with the verification of successful demethylation and often affects the resolution of the aromatic region. This problem was overcome by suppressing the D_2O signal in what is known as a solvent suppression NMR. This technique exploits the fact that the solvent usually relaxes more slowly than the resonances of interest. Another feature of note in the ^{1}H-NMR spectra of **bpyL2** (see Figure 4.8) and **phenL2** (see Figure 4.10) is the absence of signals for the catechol protons. This can be expected due to the fact that chemically labile protons such as O—H can exchange with labile deuterons from the solvent effectively removing them from the spectra. Assignment of the H_3L2 resonances of the complexes **bpyL2** and **phenL2** has been made using splitting patterns, by finding cross peaks in the 2D COSY spectra (see Figures 4.9 and 4.11) and by comparison with the complexes **bpyL1** and **phenL1** (though these spectra were run in the absence of D_2O). When the spectra of the complexes **bpyL2** and **phenL2** are compared to the free ligand H_3L2 (see appendix 1), an effect typical of coordinated pyridine rings was seen[11,12]. Similarly to the complexes discussed in chapter 3, coordination of $Ru(L)_2$ unit (where L is bpy or phen) to the ligand H_3L2 induces an upfield shift of the pyridyl H^6 proton (of the ligand H_3L2) of over 1 ppm which is observed in both complexes.

4.2.3 Electronic and Photophysical properties.

As expected the UV-Visible spectra of the catechol complexes (see Figure 4.12-4.13) are consistent with the complexes described earlier in 3.2.4. The spectra are dominated in the visible region (300-500 nm) by $d\pi$-π^* metal-to-ligand charge transfer (MLCT) transitions typical of complexes of this type[13]. The absorption spectra of the complexes are characterised in the UV region (250-300 nm) by intense π-π^* transitions associated with the pyridyltriazole ligand and bpy and phen ligands respectively. As stated earlier the triazole is in the deprotonated state when coordinated to the $Ru(L)_2$ unit (where L is bpy or phen). The absorbance of the **bpyL2** complex is red-shifted with respect to $[Ru(bpy)_3]^{2+}$ due to the strong σ-donation of the deprotonated triazole moiety and occurs at 476 nm. On protonation of the triazole ring the λ_{max} of **bpyL2** is blue shifted to approximately 440 nm (see Figure 4.12). This shift can be explained due to less electron density being present on the protonated triazole ring. The Ru t_{2g} level is stabilised by increased π-acceptance by the ligand (weaker σ-donation) and the t_{2g}-MLCT gap is increased resulting in the observed blue-shifted absorbance. The complex **phenL2** behaves slightly different in that the λ_{max} of the deprotonated complex is blue-shifted with respect to **bpyL2**. The λ_{max} of **phenL2** when the triazole is deprotonated occurs around 426 nm and this may be due to the fact that phen is a poorer π acceptor than bpy. It drains less electron density from the pyridyltriazole ligand than bpy thus leaving a higher electron density on the deprotonated triazole ring. In this instance the triazole ligand is a better π acceptor than in the case of **bpyL2**.

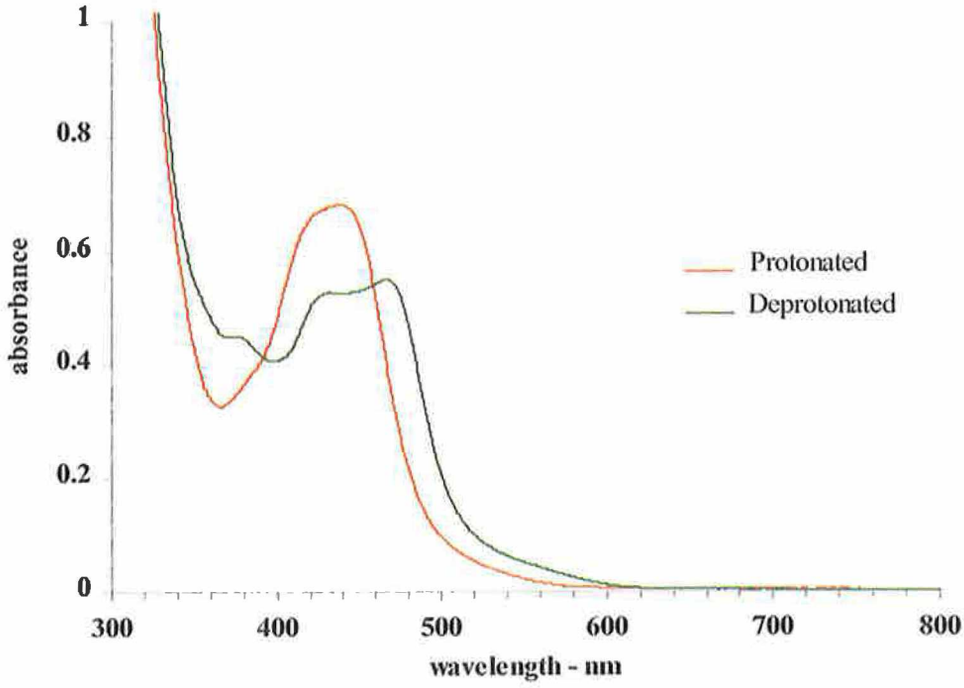

Figure 4.12 ***Absorption spectra of $[Ru(bpy)_2(H_2L2)]PF_6.5H_2O$ protonated and deprotonated in acetonitrile ($5 X 10^{-5} M$).***

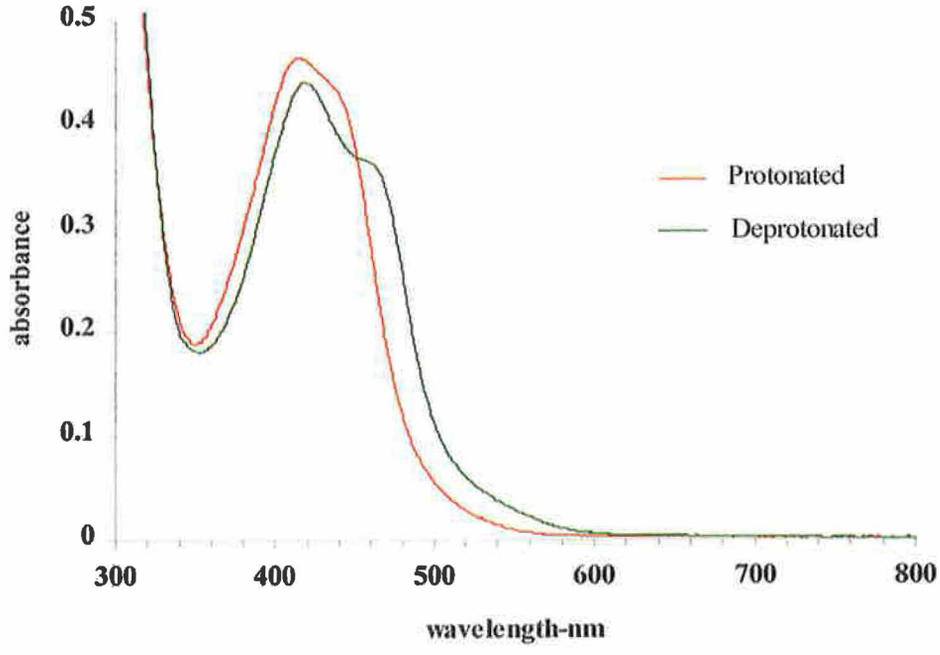

Figure 4.13 *Absorption spectra of $[Ru(phen)_2(H_2L2)]PF_6.2H_2O$ protonated and deprotonated in acetonitrile ($5 X 10^{-5} M$).*

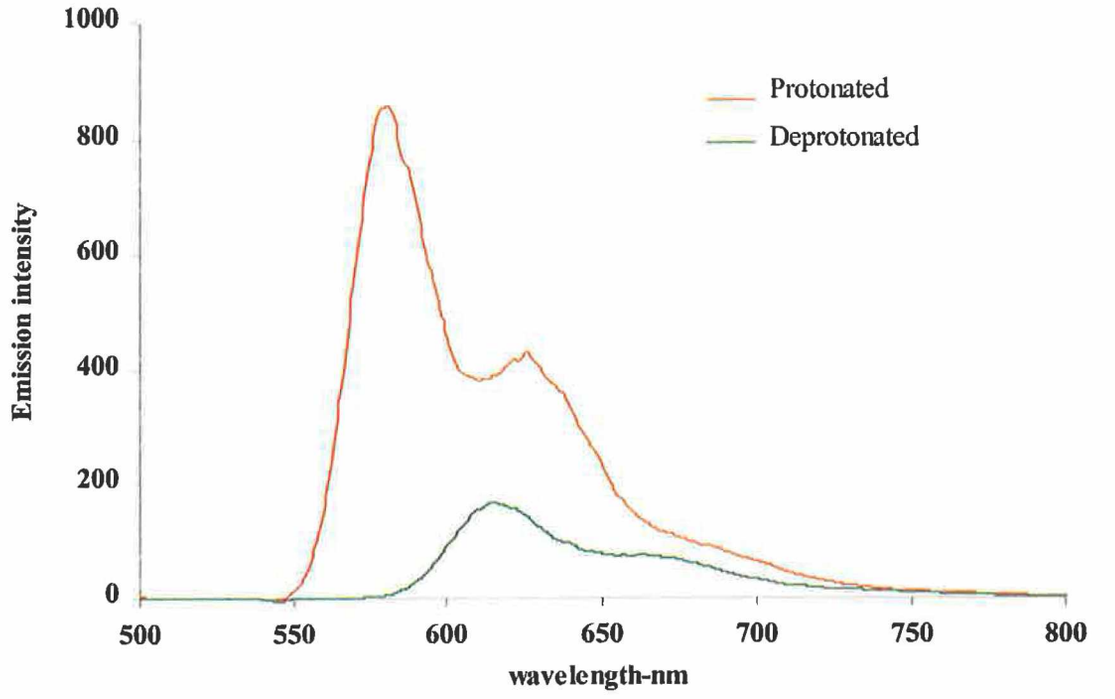

Figure 4.14 *Emission spectra of $[Ru(bpy)_2(H_2L2)]PF_6.5H_2O$ protonated and deprotonated* at 77 K *in ethanol/methanol (4:1) (5 X 10^{-5} M).*

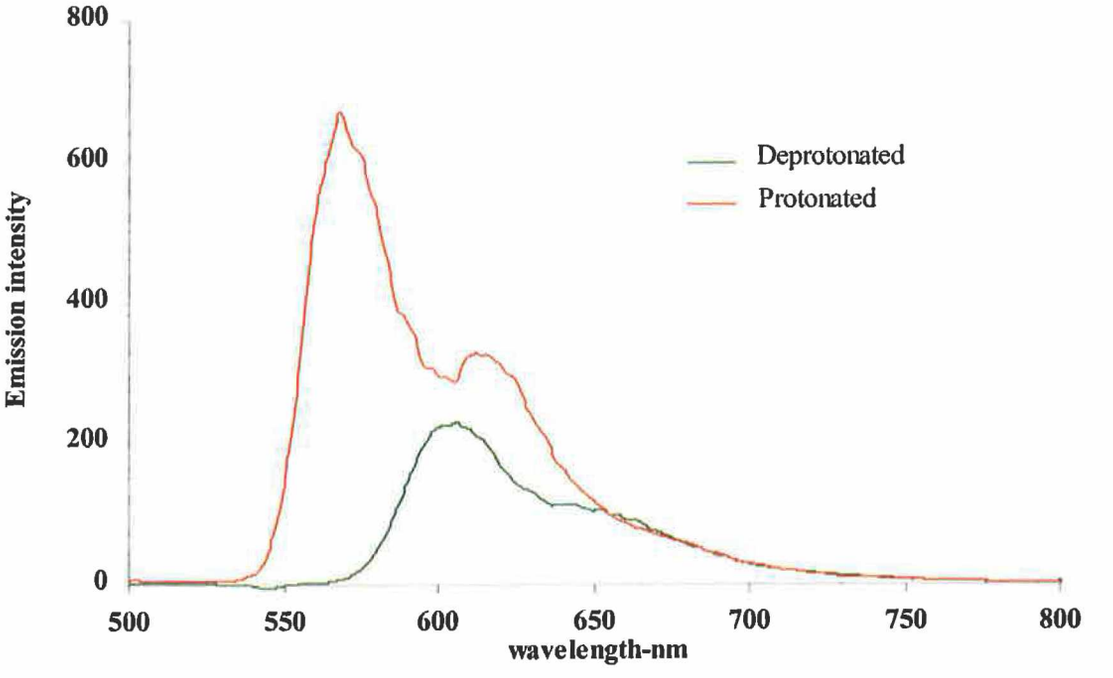

Figure 4.15 *Emission spectra of $[Ru(phen)_2(H_2L2)]PF_6.2H_2O$ protonated and deprotonated* at 77 K in ethanol/methanol (4:1) (5 X 10^{-5} M).

Table 4.2 UV-Vis *Absorption and emission data for the complexes listed below*[A-D].

Complex	Absorbance λ_{max}, nm		Emission λ_{max}, nm				Lifetime (ns)
	Prot.	Deprot. (ε / $M^{-1}cm^{-1}$)	Prot.		Deprot.		at 300 K
			300 K	77 K	300 K	77 K	
bpyL2	440	476 (10332)	622	577	689	625	64
phenL2	418	426 (13631)	607	568	663	609	224

A: Protonation of the complexes was achieved by addition of perchloric acid and deprotonation by the addition of diethylamine.

B: All measurements at 300 K were performed in acetonitrile.

C: All measurements at 77 K were performed in ethanol/methanol 4:1 v/v.

D: Samples for lifetime measurements were degassed using N_2. The lifetime values are for the complex in acetonitrile without any acid or base added.

There is a blue-shift upon protonation (see Figure 4.13) to around 418 nm for **phenL2** for the same reasons as those discussed above for **bpyL2**. Both of the catechol complexes **bpyL2** and **phenL2** exhibit room temperature emission when deprotonated and protonated associated with decay from the ^{3}MLCT state. The emission properties were investigated in acetonitrile and the emission maxima of the deprotonated complexes occurs at lower energy than that of $[Ru(bpy)_3]^{2+}$ (605 nm)[14]. Similar to the protected catechol complexes, this fact is due to the strong σ-donor properties of the

anionic triazole ligand, resulting in increased electron density on the metal centre, a decrease in the t_{2g} - ^{3}MLCT energy gap and so a lowering of the emission energy. As with the absorption spectra, and for the same reasons, protonation of the complexes results in a blue shift of the emission maxima. The emission maxima for the **bpyL2** occurs at 689 for the deprotonated complex and at 622 nm for the protonated complex. In a similar manner to the absorption spectra the emission of **phenL2** is blue-shifted with respect to **bpyL2** complexes and for similar reasons (see section 3.2.4). The emission for **phenL2** in the deprotonated state occurs at 663 nm and for the protonated complex at 607 nm.

At low temperature (77 K) the complexes exhibit a strong emission in an alcohol medium (see Table 4.2) with a distinct vibrational structure (see Figure 4.14 - 4.15). The emission λ_{max} is further blue shifted, in comparison to room temperature emission, for both protonated and deprotonated species. This is associated with a phenomenon termed as "rigidchromism" by Wrighton and co-workers who were one of the first to report on it[15] and its effects on the low temperature emission of the catechol complexes is similar to those experienced by the protected complexes (see section 3.2.4).

4.2.4 Acid-base properties.

The effect of protonation and deprotonation of the triazole ring on the λ_{max} of absorption and emission was discussed in the previous section 4.2.3. Protonation/deprotonation changes the σ-donor and π-acceptor properties of the H_3L2 ligand and determination of the excited state pK_a^* gives important information regarding the properties of the ligand and the nature of the emitting state[16,17,18]. For these reasons the acid-base behaviour of the complexes is presented in this section. Figures 4.16 and

4.17 are typical examples of the acid-base chemistry of the ruthenium(II) complexes containing the H_3L2 ligand. They are the absorption titration spectra for the complexes **bpyL2** and **phenL2** respectively. Clean and clear isobestic points are observed in the absorption spectra of **bpyL2** at 460 and 390 nm and in the absorption spectra of **phenL2** at 450 nm indicating that there are no intermediates formed in the pH range examined.

Table 4.3 *Ground and Excited state pKa values for the complexes of H_3L2.*

Complex	pKa ± 0.1	pKa^* ± 0.1
bpyL2	4.2	1.4
phenL2	4.0	1.5

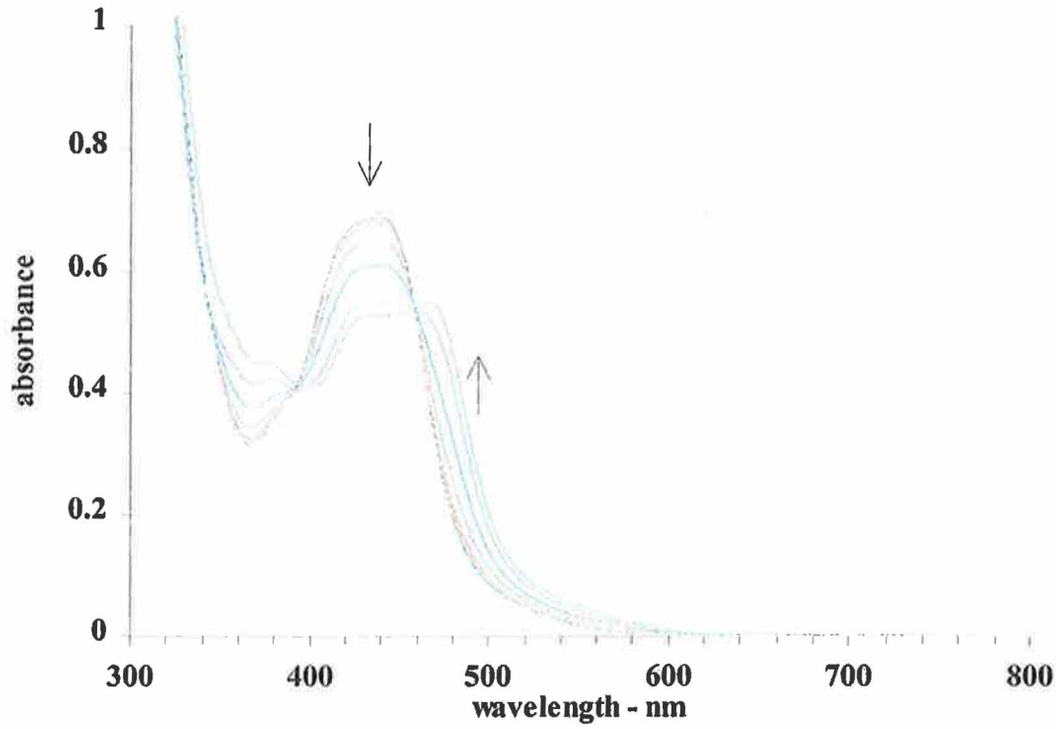

Figure 4.16 *pH dependence of the absorption spectra of $[Ru(bpy)_2(H_2L2)]PF_6.5H_2O$ (5×10^{-5} M) in an aqueous Britton-Robinson buffer at pH 1.44, 1.79, 2.09, 2.55, 2.95, 3.13, 3.70, 4.18, 4.92 and 6.66.*

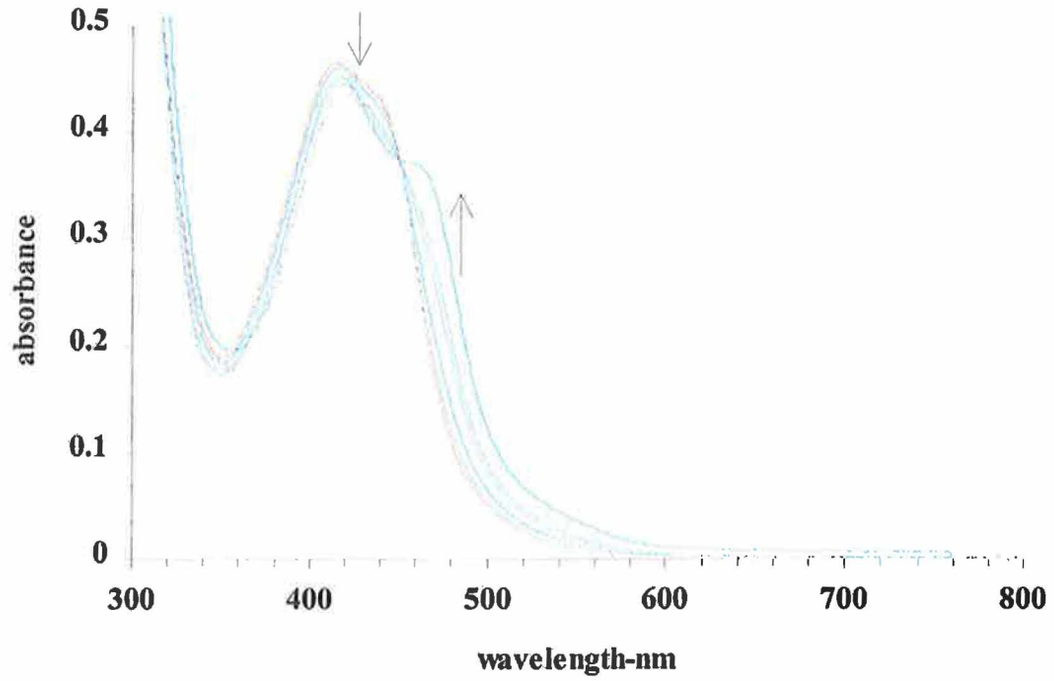

Figure 4.17 *pH dependence of the absorption spectra of $[Ru(phen)_2(H_2L2)]PF_6.2H_2O$ (5×10^{-5} M) in an aqueous Britton-Robinson buffer between pH 1.74, 2.32, 2.84, 3.22, 3.66, 4.23, 4.46, 5.28, 6.15 and 7.01.*

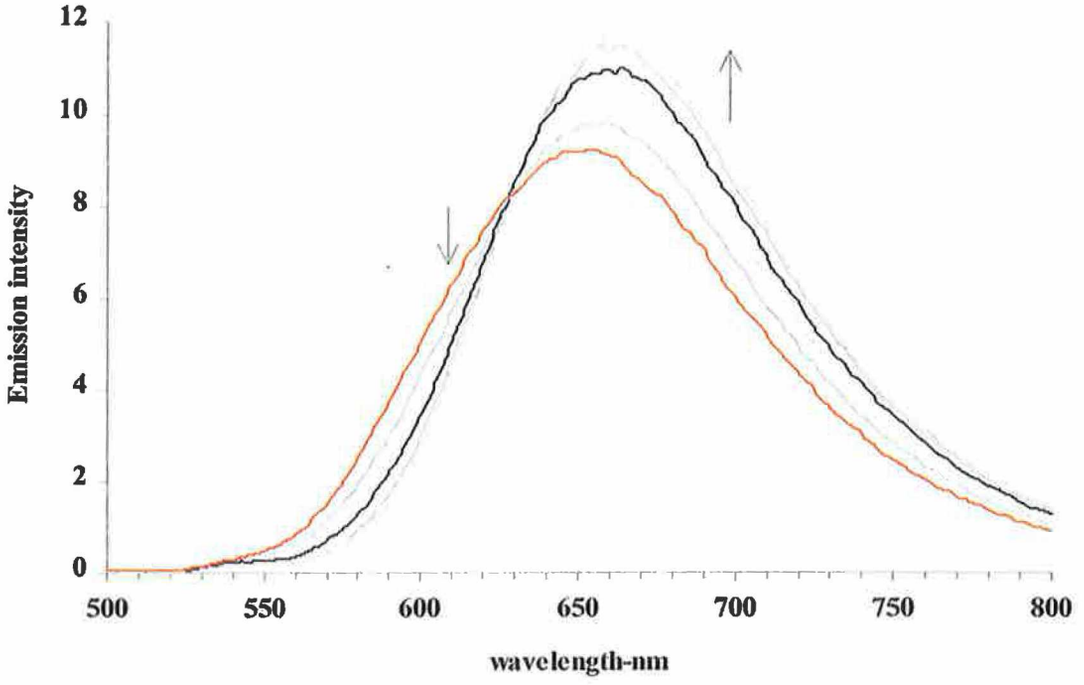

Figure 4.18 *pH dependence of the emission spectra of $[Ru(bpy)_2(H_2L2)]PF_6.5H_2O$ (5 X 10^{-5} M) in an aqueous Britton-Robinson buffer at pH 1.10, 1.58, 2.84, 3.26, 3.51, 4.41, 4.81, 5.72.*

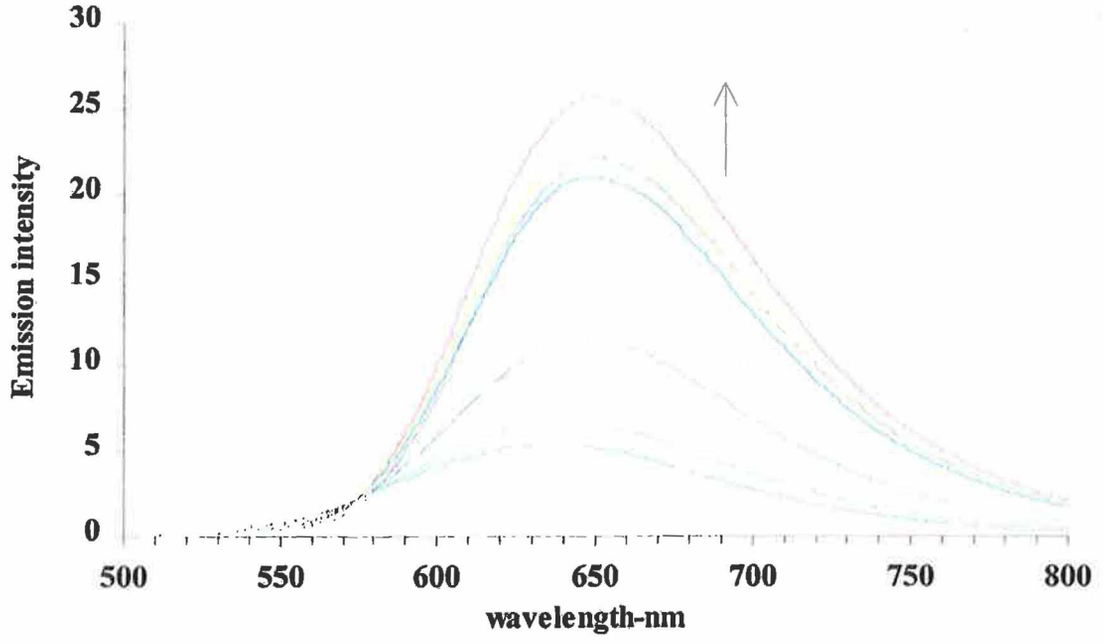

Figure 4.19 *pH dependence of the emission spectra of $[Ru(phen)_2(H_2L2)]PF_6.2H_2O$ (5 X 10^{-5} M) in an aqueous Britton-Robinson buffer at pH 1.72, 2.11, 2.32,2.84, 3.22, 3.53, 3.85, 4.11, 5.28 and 6.15.*

All the spectroscopic changes of the complexes are reversible in the pH range 1-8. However, the spectroscopic changes are not reversible in the pH range 8-12 and isobestic points are not maintained cleanly suggesting that there are intermediates forming over this pH range. This prevents any kind of accurate prediction of the catechol pK_a and pK_a^* values.

$$\underset{Q^{2-}}{L2^{3-}} \xleftrightarrow{pK_{a3}} \underset{QH^{-}}{HL2^{2-}} \xleftrightarrow{pK_{a2}} \underset{QH_2}{H_2L2^{-}} \xleftrightarrow{pK_{a1}} \underset{\text{triazole H}}{H_3L2} \qquad (4.1)$$

The scheme 4.1 shown above represents the acid-base behaviour that might be expected of the complexes **bpyL2** and **phenL2** if H_3L2 is taken to represent the case when the triazole and the catechol moieties are protonated. However the processes indicated as pK_{a2} and pK_{a3} are complex and do not appear to be reversible for the complexes studied here. This type of behaviour was also observed in the work of T.E. Keyes[19] in the study of the ruthenium (II) complex (bound by N1 of the triazole and N1 of the pyridine ring) of the hydroquinone ligand shown in Figure 4.20.

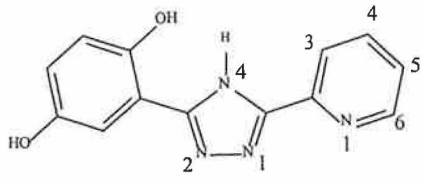

Figure 4.20 Hydroquinone ligand H_3L1 studied by T.E. Keyes.

It was reported in this work that the pH behaviour for the $Ru(bpy)_2$ complex of H_3L1 is most likely a function of the H_2Q/Q unit, which has very complex acid/base behaviour, which is further aggravated in aqueous solution. This latter fact is substantiated via

ESR studies that semiquinone radicals form spontaneously in aqueous solutions above pH 8[20]. This type of complexity is not evident in the protected catechol complexes (see section 3.2.5), however only one pK_a is expected in these complexes namely that of the triazole. The absorption titrations are performed by adjusting the pH of a 5 X 10^{-5} M solution of the complex in Britton Robinson buffer. Then by monitoring the spectral changes, at a wavelength where there is considerable change, as a function of pH graphical analysis was carried out by plotting percentage change in absorbance against pH. The pK_a was determined from the point of inflection of the curve.

The excited state pK_a values (pK_a^*) were evaluated using the Forster cycle equation (3.1) as described for the protected catechol complexes[21]. Using this equation the excited state pK_a^* of a species can be calculated from it's ground state properties. The trend for the pK_a^* values is that they are more acidic than the ground-state pK_a values. These results suggest that as expected the excited state is not based on the triazole ligand which can then be referred to as the spectator ligand. The triazole ligand does not become directly involved in the excited state confirming that the ^{3}MLCT is based on the bpy ligand of the respective complexes quoted in Table 4.3. These conclusions are in line with those made for the protected catechol complexes and compare with similar ruthenium(II) complexes based on pyridyltriazole ligands[19,22,23]. It should be noted that the Forster equation assumes an accurate measurement of the $E_{0\text{-}0}$ values with small errors causing considerable errors in pK_a^*. However from the values calculated the direction of change in pK_a when going from ground state to excited state can be asserted.

4.2.5 Electrochemical Properties.

The electrochemistry of the catechol complexes is quite complicated due to the intricate oxidation properties of the hydroquinone moeities. Referring back to the cyclic voltammetry of the protected complexes (see chapter three) reminds us that the methyl protected catechol moieties are 'non-innocent' and undergo irreversible oxidation. However the oxidation of the metal occurs before that of the ligand and this allows us to scan within an exclusive window to achieve reversibility of the Ru^{II}/Ru^{III} couple. In the case of the catechol complexes the true oxidation potential of the metal is difficult to determine since the hydroquinone moiety oxidation precedes the Ru^{II}/Ru^{III} process. This implies that what is observed is actually the oxidation of the metal in the semiquinone complex. The cyclic voltammetry was first performed using a polished glassy carbon electrode which leads to poor resolution with one wave for the hydroquinone processes and a poorly defined wave for the oxidation of the metal. This can be explained by adsorption of the oxidation products of the catechol complex onto the surface of the glassy carbon electrodes. A process for the resolution of such individual waves is described by Cabaniss et al[24]. The oxidative activation procedure involved oxidative sequences in 0.1 M H_2SO_4 for various time periods at an applied potential of +1.80 V. It was reported that oxidative activation (pretreatment) of glassy carbon electrodes resulted in noticeable increases in both alcoholic (phenolic) and ketonic (quinoidal) groups with the ratio of oxidised to graphitic carbon atom sites increasing to nearly one-half. The effective result of this type of pretreatment of glassy carbon electrodes on the cyclic voltammetry of catechol (1,2-dihydroxybenzene) was also described.

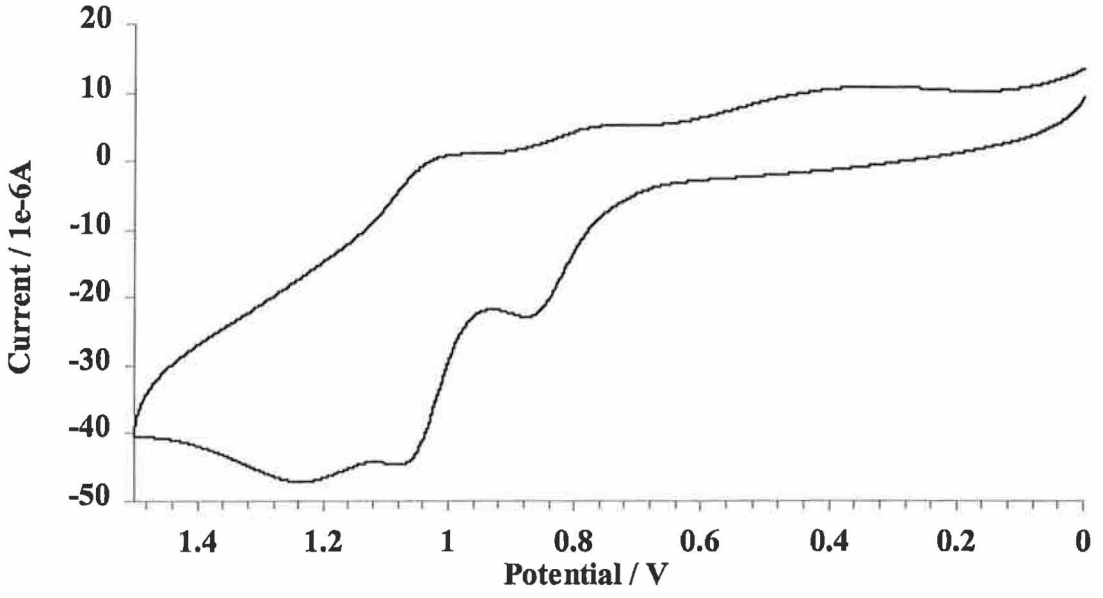

Figure 4.21 *Cyclic voltammogram of $[Ru(bpy)_2(H_2L2)]PF_6.5H_2O$ in acetonitrile with 0.1 M TEAP (Scan rate : 100 mVS^{-1}).*

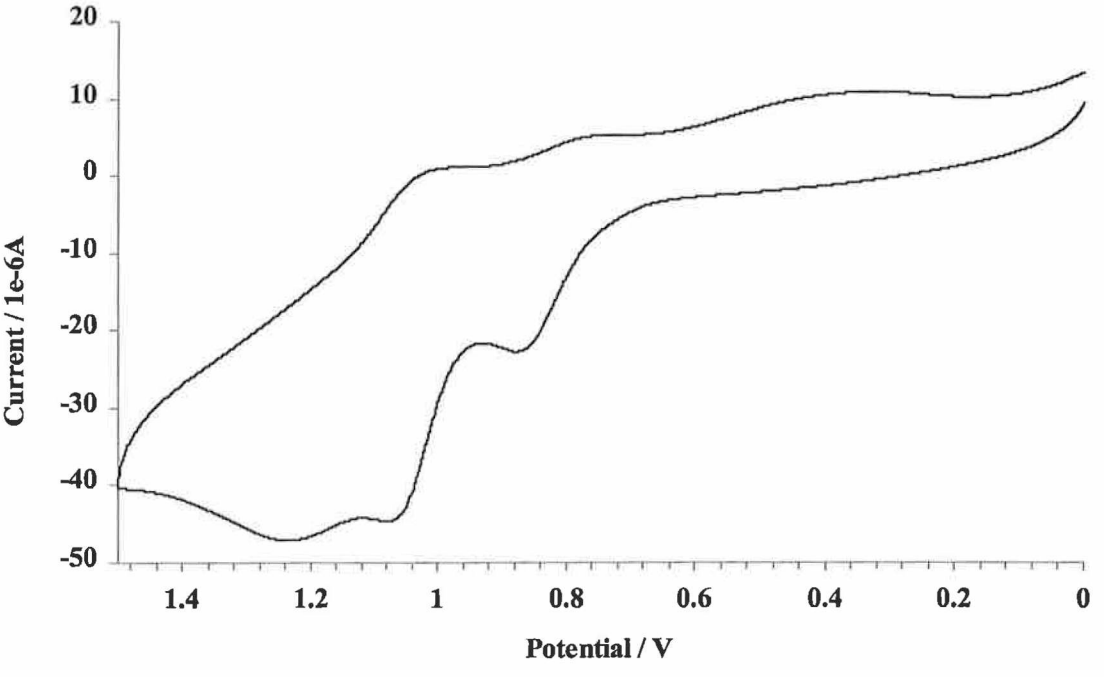

Figure 4.22 *Cyclic voltammogram of $[Ru(phen)_2(H_2L2)]PF_6.2H_2O$ in acetonitrile with 0.1 M TEAP(Scan rate : 100 mVS^{-1}).*

Table 4.4 *Electrochemical data for the complexes of H_3L2 in V vs Ag/AgCl. All measurements were carried out on the deprotonated complexes in acetonitrile with 0.1 M TEAP (Scan rate : 100 mVS^{-1})*[A].

Complex	Oxidation Potentials/V		Reduction Potentials/V
	Ru(II) / Ru(III)	E_{redox} (ligand)	
bpyL1	1.00	0.82, 1.22	
		0.50(red)	*
phenL1	1.05	0.86 , 1.24	
		0.77 , 0.42 (red)	*

A: The asterix symbol * denotes that surface effects hindered a study of the electrochemistry of the bpy and phen ligands respectively.

Before pretreatment, at a polished electrode an oxidation and its associated reduction appeared, but the two peak potentials were widely separated, the waves were broad, and the peak currents were unequal. After partial electrode activation, two distinct components appeared in both the oxidative and reductive waves which correspond to two, one-electron components of the overall two-electron process:

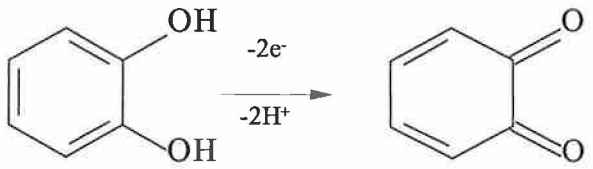

In the early stages of electrode activation, the wave for the initial oxidation step:

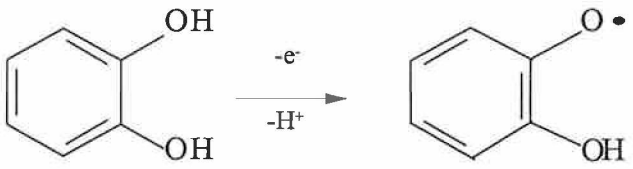

was selectively catalysed and approached the wave characteristics expected for a reversible, one-electron couple. However it was found that with further activation the second, one-electron oxidation:

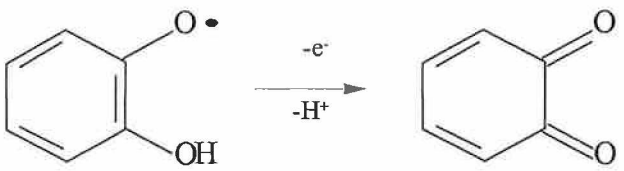

was catalysed further and eventually overtook the first wave. At the fully activated electrode, the wave shape approaches that expected for an overall two electron process where the intermediate state is unstable with respect to disproportionation. A similar type of pretreatment of the glassy carbon electrode was employed in the study of our compounds. This was performed by anodisation of the glassy carbon electrode by placing it in 0.1 M H_2SO_4 at a potential of 1.80 V for 1 minute[24]. This resulted in better resolution of the individual waves representative of the hydroquinone oxidations, similar to those described above. However it does not lead to the wave shape approaching that of a single wave for an overall two-electron process. The cyclic voltammogram for the complex **bpyL2** (see Figure 4.21) shows three oxidation waves of which only one appears to be reversible. We recall that the electrochemistry of the protected analogue **bpyL1** (see Figure 3.25) showed a reversible Ru^{II}/Ru^{III} at 0.71 V when the complex was swept within the 0-1.0 V potential window. When the potential window was extended beyond 1.0 V the irreversible oxidation of the pendant dimethoxyphenyl was observed at potentials close to 1.2 V. In relation to the deprotected analogue, **bpyL2**, examined in this chapter, the nature of the first oxidation potential at 0.82 V is shown to be associated with the catechol ring (see Figure 4.21). This was established by sweeping between 0 and 1.0 V. The oxidation wave at 0.82 V was quasi-reversible with an associated reduction peak around 0.5 V and is assigned to the oxidation of the catechol to semiquinone. The lack of reversibility may be due to extensive polymerisation of the -OH moieties onto the carbon electrode surface which is a fairly established phenomena for a redox active oxygen species[25]. The hydroxyls are oxidised before the metal and are polymerised at the electrode surface resulting in a non-observance of the bulk solution for the most part. The pretreatment of the electrode does improve the resolution of the

waves but does not appear to prevent the polymerisation at the electrode surface. Thus what is observed is the metal oxidation for the adsorbed species which may explain its unusual potential. Sweeping the potential from 0.95 to 1.2 V indicates a reversible one-electron process at 1.0 V which is assigned to the Ru^{II}/Ru^{III} couple. The final oxidation peak observed in the cv of **bpyL2** (see Figure 4.21) is assigned to the irreversible oxidation of the semiquinone to quinone, which involves the loss of protons and must, according to Shukla et al[26], necessarily be irreversible in an aprotic solvent such as acetonitrile. A similar type of explanation is offered for the cyclic voltammogram of **phenL2**. Assessment of the reduction potentials for the bpy and phen ligands in the respective catechol complexes was not clear once again due to adsorption at the electrode surface.

4.2.6 Attachment of complexes to TiO_2 surfaces.

The search for efficient solar energy conversion devices continues to be an important area of research (see chapter 1, section 1.1.2.1.)[27,28,29,30]. A solar cell harnesses light from the sun and converts it into electrical energy. The light can be thought to boost the electrons within certain regions of the solar cell to energetic regions and these electrons, which will be high in energy, can be subsequently withdrawn as electricity. Our interest here lies in the investigation of the attachment of ruthenium (II) type redox sensitisers to TiO_2 because of their light harvesting capacity which makes them important for solar energy conversion (see Chapter 2, section 2.11).

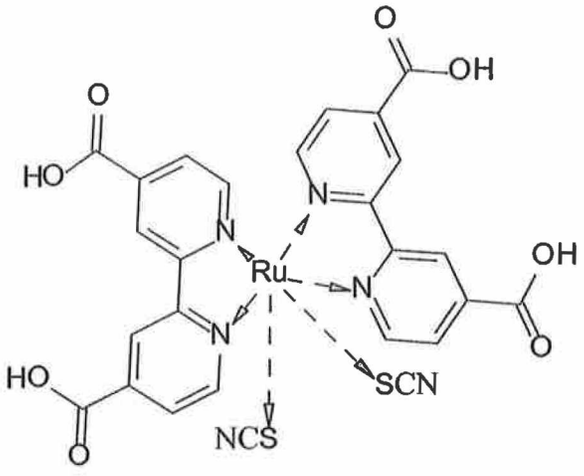

Figure 4.23 *Structure of the complex* $[Ru(dcH_2bpy)_2(NCS)_2]$.

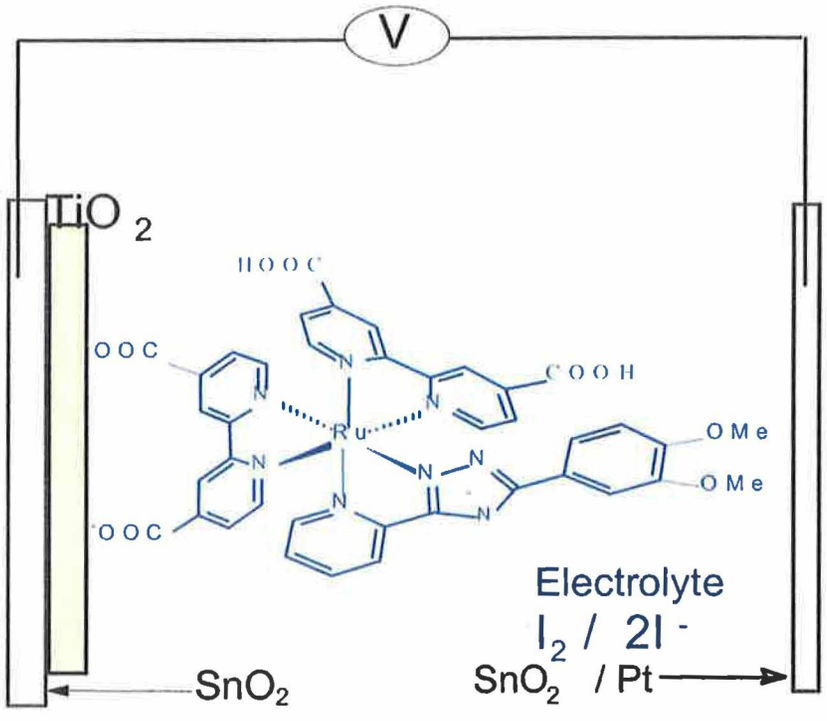

Figure 4.24 *Schematic representation of a dye-sensitised semiconductor cell showing the major components: A nanostructure semiconductor electrode* (TiO_2); *Sensitiser or dye* (Ru^{II} *dicarboxy complex); An electrolyte which acts as the redox couple* (I_2 / $2I^-$).

The mode of attachment of the catechol complexes **bpyL2** and **phenL2** (via the hydroquinone moieties) to nanocrystalline TiO_2 films is compared with that of the protected catechol complex **dcbpyL1** (via the dicarboxy moiety as depicted in Figure 4.24). The complexes were attached to TiO_2 and their photocurrent efficiency measured and compared with that of the complex $[Ru(dcH_2bpy)_2(NCS)_2]$ (See Figure 4.23) whose photocurrent efficiency is well known[31]. The schematic representation of a dye-sensitised semiconductor cell is presented in figure 4.24 and is comprised of three major components: a nanostructured semiconductor electrode, in this case TiO_2, the sensitiser or dye, and an electrolyte which acts as the redox couple. Light absorption is performed by a monolayer of the dye (complex) absorbed chemically at the semiconductor surface. After having been excited by a photon of light, the ruthenium(II) complex is able to transfer an electron to the semiconductor (TiO_2) (the process of injection). The electric field inside the bulk material allows extraction of the electron. Positive charge is transferred from the ruthenium(II) complex to a redox mediator (iodine/iodide electrolyte) present within the cell and then to the counter electrode. In this last electron transfer, the mediator is returned to its reduced state and the circuit is closed. The titanium dioxide serves as a high-surface-area support for the sensitiser, a pathway for the electrical current and a porous membrane for diffusion of the redox couple[32]. A colloidal suspension of the titanium dioxide is spread onto a glass substrate (transparent fluorine-doped tin dioxide) followed by a heating step at 444°. At this temperature the particles on the surface fuse together and a porous nanocrystalline semiconductor film is produced. The plate with the TiO_2 film is then soaked in a methanol solution of the ruthenium (II) complex at which stage the complex attaches to the surface of the TiO_2.

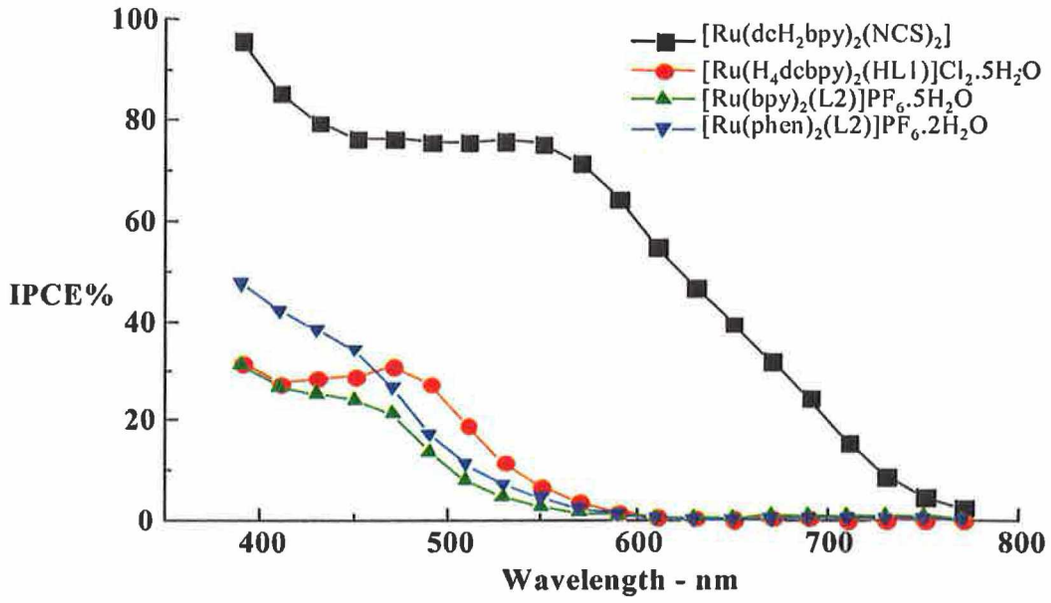

Figure 4.25 The incident photon-to-current efficiency (IPCE) as a function of wavelength (nm) for the complexes attached to TiO_2 electrodes.

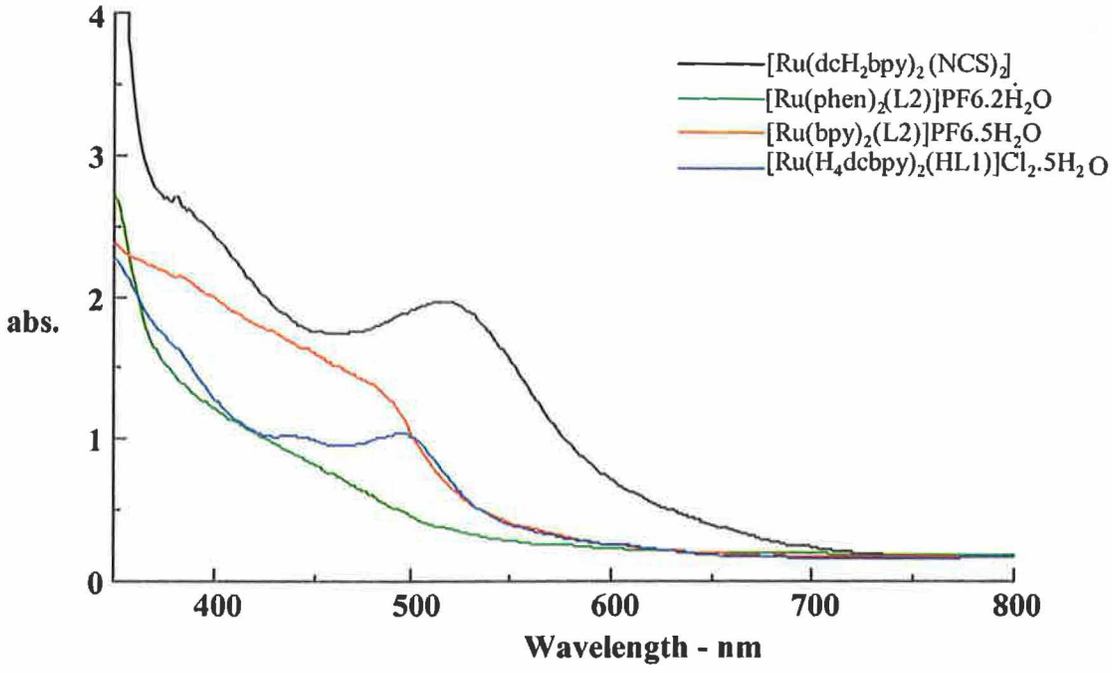

Figure 4.26 UV-Vis absorption spectra of complexes attached to TiO_2

In Figure 4.26 the UV-Vis spectra of the complexes attached to TiO_2 are presented. Each complex was absorbed as a layer onto an ~ 7 μM thick nanocrystalline TiO_2. The absorption spectrum represents a superposition of the complex and the TiO_2 but should closely resemble the absorption spectrum of the complex in solution but with a different intensity at the λ_{max}. The **dcbpyL1** complex spectrum on TiO_2 (see Figure 4.26) resembles that of the complex in solution (see Figure 3.18) however the spectra of **bpyL2** and **phenL2** appear different. This may be related to the mode of attachment of **bpyL2** and **phenL2** to TiO_2.

The redox mediator is a redox couple which ferries charge around the solar cell. It must not absorb solar energy and is utilised in the reduced form to regenerate the ruthenium (II) complex i.e. reduce it back to its ground state. A few drops of the redox mediator (iodine/iodide system) is used to sandwich the dye sensitised electrode with the counter platinum electrode. The cell can then be closed and sealed and the incident photon to current efficiency (IPCE) measurements performed. Illumination of the sandwich solar cell at open circuit produces a potential difference between the two electrodes. When the circuit is closed a photocurrent can be measured. The photocurrent production is reported as the incident photon-to-current efficiency, IPCE, which is the ratio of electrons measured in the external circuit to the photons incident on the solar cell. The spectra shown in Figure 4.25 represent the IPCE measured as a function of excitation wavelength and is called a photoaction spectrum. The complex $[Ru(dcH_2bpy)_2(NCS)_2]$ has emerged as the most efficient to date[29,30]. As a result of this observation it was used in this study to assess the performance of the **bpyL2, phenL2** and **dcbpyL1** as sensitisers. The photoaction spectra indicate that high monochromatic IPCE of $[Ru(dcH_2bpy)_2(NCS)_2]$ is only observed below ~ 700 nm and below ~ 600 nm

for the complexes **bpyL2**, **phenL2** and **dcbpyL1**. The IPCE % was slightly higher (~ 30 %) for **dcbpyL1** at 500 nm when compared to the catechol complexes (~ 10 - 15%). Between 400 - 450 nm the IPCE % was higher for **phenL2** than it was for either **bpyL2** or **dcbpyL1** by about 10 %. Another feature of interest is the fact that the catechol complexes compare well with **dcbpyL1** considering that the mode of attachment to TiO_2 is different. Carboxylate substituents on the bipyridyl ligand of **dcbpyL1** anchor the complex to the semiconductor surface (see Figure 4.24), presumably via Ti(IV) chelation[28], while the catechol complexes are anchored through the hydroxyl substituents of the catechol ring. This is an important distinction considering the fact that the excited

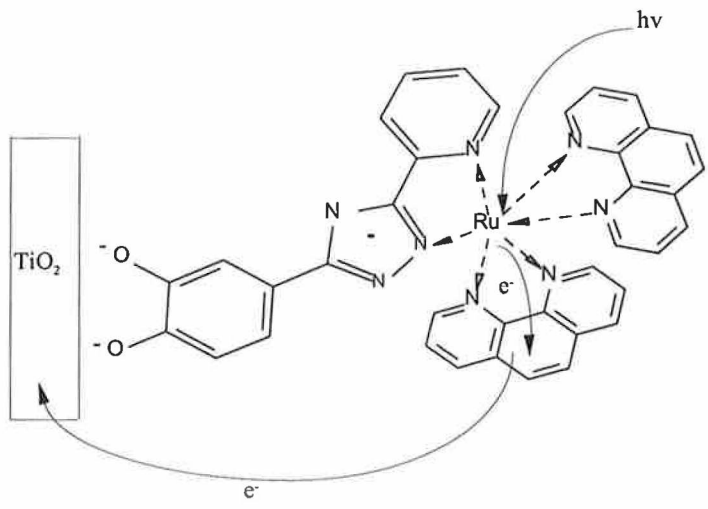

Figure 4.27 *Suggested schematic of the attachment of **phenL2** to TiO_2 and proposed through space electron transfer to the TiO_2 electrode.*

state of the catechol complexes lies on the ligands not directly attached to the surface of TiO_2. In the case of **dcbpyL1** the excited state of the complex is based on the dicarboxy ligands which is directly attached to the surface of TiO_2. Bimetallic coordination compounds based on rhenium and ruthenium where the facial geometry of the Re centre holds a Ru sensitiser proximate to the TiO_2 surface was a feature of work carried out by

Argazzi et al[27,33]. It is strongly implied as a result of this work that a direct chemical bond between the chromophoric ligand of Ru(II) sensitisers and the TiO_2 surface is not a requirement for efficient electron injection. It appears that efficient electron injection from MLCT excited states to TiO_2 can occur in the absence of any semiconductor-to-sensitiser link. An important implication from this conclusion is that sensitisers anchored to TiO_2 through nonchromophoric ligands or without a direct chemical bond may also be efficient for sensitisation of wide bandgap nanocrystalline semiconductors such as TiO_2. This conclusion is verified by the similar IPCE % obtained by the catechol complexes in comparison with **dcbpyL1**.

4.3 Concluding Comments

The synthesis and characterisation of two mononuclear ruthenium(II) pyridyltriazole complexes containing an external catechol moiety was described in this chapter. The complexes **bpyL2** and **phenL2** were prepared by demethylation of the protected complexes **bpyL1** and **phenL1** respectively. The demetylation reaction was performed by reaction of the protected complex with a ten fold molar excess of boron tribromide under a nitrogen atmosphere at low temperature. Verification of demethylation was ascertained by absence of the two -OMe singlet peaks around 4 ppm in the ^{1}H-NMR spectra.

The investigation of the absorption, emission and acid-base properties of the complexes confirms the classification of the ligand H_3L2 as a weak π-acceptor and strong σ-donor (class b type ligand). The features observed for the catechol complexes **bpyL2** and **phenL2** were quite similar to the protected complexes discussed in chapter 3. However the acid/base chemistry of the catechol complexes between pH 8-12 was very complex and pH dependent titrations in this region were irreversible.

The electrochemical studies of the complexes are complicated in comparison to their protected analogues. The oxidation of the catechol ligand (catechol/semiquinone) was quasi-reversible and precedes that of the metal centre (Ru^{II}/Ru^{III}). The final process occurred at a more positive potential than the metal centre and represents the irreversible oxidation process semiquinone/quinone. Pretreatment of the glassy carbon electrode was necessary to resolve the processes due to adsorption of oxidised species onto the surface of the electrode. Attachment of the catechol complexes to nanocrystalline TiO_2 films indicates incident photon-to-current efficiency (IPCE) of greater than 30%.

4.4 References

1 R.K. Clayton, Photosynthesis; Physical methods and chemical patterns, 1st ed., Cambridge University Press, 1980.

2 D. Gust, T.A. Moore, P.A. Liddell, G.A. Nemeth, L.R. Makings, A.L. Moore, D. Barrett, P.J. Pessiki, R.V. Benasson, M. Rougee, C. Chachaty, F.C. Deschryver, M. Van der Auweraep, A.R. Hotzwarth, J.S. Connolly, *J. Am. Chem. Soc*, 1987, 109, 846.

3 The Chemistry of Quinone compounds, Ed. Spatai, Chapter 6; R. Foster and M. I. Foreman, Wiley and Sons, 1988.

4 R. Argazzi, C.A. Bignozzi, T.A. Heimer, F.N. Castellano, G.J. Meyer, *Inorg. Chem.*, 1994, 33, 5741.

5 A.C. Lees, B. Evrard, T.E. Keyes, J.G. Vos, C.J. Kleverlaan, M. Alebbi, C.A. Bignozzi, *Eur. J. Inorg. Chem*, 1999, 2309.

6 E.H. Vickery, L.F. Pahler and E.J. Eisenbraun, *J. Org. Chem.*, 1979, Vol. 44, No. 24, 4444.

7 J.F.W. McOmie, M.L. Watts and D.E. West, *Tetrahedron*, 1968, Vol. 24, 2289.

8 B. Whittle, N.S. Everest, C.A. Howard, M.D. Ward, *Inorg. Chem.*, 1995, 34, 2025.

9 C.A. Howard, M.D. Ward, *Angew. Chem. Int. Ed. Engl.*, 1992, 31, No.8, 1028.

10 M.E. Jung, M.A. Lyster, *J. Org. Chem.*, 1977, Vol 42, No. 23, 3761.

11 P. Belser, A.von Zelewsky, *Helv.Chim. Acta.*, 1980, 63, 1675.

12 E.C. Constable, J.Lewis, *Inorg. Chim. Acta.*, 1983, 70, 251.

[13] A. Juris, V. Balzani, F. Barigelletti, S. Campagna, P. Belser, A. Von Zelewsky, *Coord. Chem. Rev.*, 1988, 84, 85.

[14] J.V. Caspar, T.J. Meyer, *J. Am. Chem. Soc.*, 1983, 100, 5583.

[15] M. Wrighton, D.L. Morse, *J. Am. Chem. Soc.*, 1974, 96, 996.

[16] D.E. Morris, Y. Ohsawa, D.P. Segers, M.K. DeArmond, K.W. Kanck, *Inorg. Chem.*, 1984, 23, 3010.

[17] P.J. Giordano, C.R. Bock, M.S. Wrighton, L.V. Interrante, R.F.X. Williams, *J. Am.Chem. Soc.*, 1977, 99, 3187.

[18] P.J. Giordano, C.R. Bock, M.S. Wrighton, *J. Am. Chem. Soc.*, 1978, 100, 6960.

[19] T.E. Keyes, Ph.D. Thesis, Dublin City University, 1995.

[20] H.H. Thorp, J.E. Surneski, G.W. Brudvig, R.H. Crabtree, *J. Am. Chem. Soc.*, 1989, 111, 9249.

[21] B.E. Buchanan, J.G. Vos, M. Kaneko, W.J.M van der Putten, J.M. Kelly, R. Hage, R.A.G. de Graaff, R. Prins, J.G. Haasnoot, J. Reedijk, *J. Chem Soc.,Dalton Trans.*, 1990, 2425.

[22] R. Hage, Ph.D Thesis 1991, Leiden University.

[23] F. Weldon, Ph.D. Thesis, Dublin City University, 1998.

[24] G.E. Cabaniss, A.A. Diamantis, W.R. Murphy Jnr., R.W. Linton, T.J. Meyer, *J. Am. Chem. Soc*, 1985, 107, 1845.

[25] A.J. Bard, L.R. Faulkner, *Electrochemical methods*, Wiley, N.Y, 1980.

[26] A.D. Shukla, B. Whittle, H.C. Bajaj, A. Das, M.D. Ward, *Inorg. Chim. Acta*, 1999, 285, 89.

[27] G.J. Meyer, *J. Chem. Ed.*, 1997, Vol. 74, No. 6, 652.

[28] S.G. Yan, L.A. Lyon, B.I. Lemon, J.S. Preiskorn, J.T. Hupp, *J. Chem. Ed.*, 1997, Vol. 74, No. 6, 657.

[29] R. Argazzi, C.A. Bignozzi, T.A. Heimer, F.N. Castellano, G.J. Meyer, *Inorg. Chem.*, 1994, 33, 5741.

[30] M.K. Nazeeruddin, A. Kay, I. Rodicio, R. Humphry-Baker, E. Müller, P. Liska, N. Vlachopoulos, M. Grätzel, *J. Am. Chem. Soc.*, 1993, 115, 6382.

[31] P. Liska, N. Vlachopoulos, M.K. Nazeeruddin, P. Comte, M. Grätzel, *J. Am. Chem. Soc.*, 1988, 110, 3686.

[32] B. O'Regan, M. Grätzel, *Nature*, 1991, 353, 737.

[33] R. Argazzi, C.A. Bignozzi, T.A. Heimer, G.J. Meyer, *Inorg. Chem.*, 1997, 36, 2.

Chapter Five

Synthesis and Characterisation of Ruthenium Dinuclear Complexes Containing a Catechol Binding Site

5.0 Introduction

Symmetric bridging ligands providing two equivalent binding sites are very prevalent[1,2,3,4,5]. Asymmetric bridges, with two inequivalent binding sites suitable for different metal fragments, are less abundant because of the obvious additional difficulties in their synthesis[6,7]. Recent attention has focused on the synthesis of large molecular assemblies, photochemical devices, which mimic biological photosynthesis by efficient intramolecular transfer of energy from the excited state 'antenna' to a reaction centre. The successful synthesis of multicomponent supramolecular assemblies of this type may be attained by the stepwise synthesis of heteropolynuclear complexes with a 'complexes as ligands' approach, in which a metal complex is prepared which contains a vacant, externally directed binding site[8]. A second complex fragment may then be attached to the vacant site, allowing the stepwise build-up of polynuclear species from individual building blocks whose properties are known.

O,O and O,N coordinated binuclear ruthenium complexes have been the topic of a number of recent studies [9,10]. Ernst et al reported on the formation and electronic structure of stable dinuclear ruthenium complexes based on *o*-semiquinone (phdo) and *p*-semiquinone ($bppq^{-}$) ligands shown (see Figure 5.1)[9]. The interest in preparing symmetrically binuclear complexes of semiquinones with the $Ru(bpy)_2$ fragment is based on the concept that two metal fragments induce a larger ligand perturbation than one, an additional bonus being the possibility of ligand mediated metal-metal interaction. Due to the electroactive nature of the bridging ligands investigated by Ernst et al, a high degree of delocalisation was observed in these compounds. The results

suggest that these dinuclear semiquinone complexes are situated at the borderline between anion radical complexes and metal-centred mixed valent dimers.

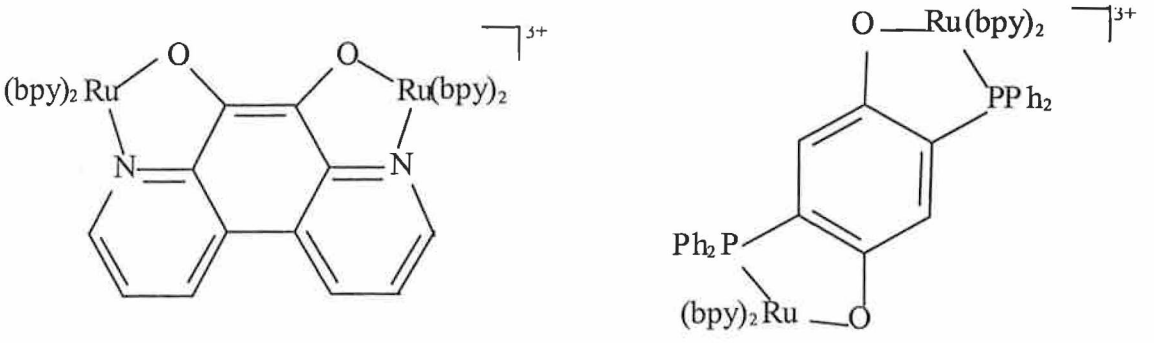

Figure 5.1 Dinuclear semiquinone complexes reported by S. Ernst et al[9].

Keyes et al investigated dioxolene-bridged ruthenium and osmium dinuclear complexes[10]. The extent of metal-ligand orbital mixing and the degree of electronic coupling between $[M(bpy)_2]^{2+}$ fragments linked through a redox active 1,4-dihydroxy-2,5-bis(pyrazol-1′-yl)benzene bridge is described, where M is Os or Ru and bpy is 2,2′-bipyridyl (see Figure 5.2). It is the first example of osmium and ruthenium/osmium metals linked across a 1,4-dioxolene bridge. The well behaved, mostly reversible, electrochemistry observed makes these dinuclear, dioxolene-based systems attractive models for investigating electronic coupling between metal centres and between metal centres and the bridge. Such redox active bridges create the possibility of modulating the degree of electronic coupling between the various molecular components since the electronic energy of both the bridge and its adjoining units will depend substantially on the redox state of the bridge. The focus on quinonoid or dioxolene bridges, by Keyes et al, is due to the preservation of redox activity after binding the metal centres. Therefore depending on the relative values of the formal potentials, the metal centres may be

linked by a quinone (Q), semiquinone (SQ), or hydroquinone (HQ), bridge. The investigation of the electronic properties of these different redox states was investigated by performing electrochemical and spectroelectrochemical measurements.

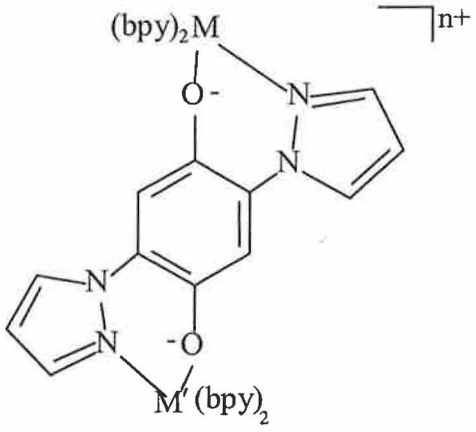

Figure 5.2 *O,N-coordinated dinuclear complexes (MHQM') of the ligand 1,4-dihydroxy-2,5-bis(pyrazol-1'-yl)benzene where M and M' is Ru or Os*[10].

UV-Vis spectroelectrochemistry, together with resonance Raman spectroscopy, of the dinuclear complexes suggest that the first two oxidation steps occur on the bridging ligand. In an earlier study of the Ru monomer of 1,4-dihydroxy-2,5 bis(pyrazol-1'-yl)benzene, an ill-defined quasi-reversible two-electron oxidation at 0.42 V was assigned to the hydroquinone-quinone oxidation and occurred before the metal-based Ru^{II}-Ru^{III} oxidation (1.30 V)[11]. In contrast oxidation of the dioxolene bridge for RuHQRu is reported to proceed in two well-resolved, reversible, one-electron steps at 0.13 V and 0.545 V. It was also established that a large degree of stabilisation was attained for the semiquinone state. Similar large stabilisation of semiquinone has been observed for mononuclear catechol (1,2-dioxolene) complexes,[12] where under neutral

conditions semiquinone is often the most stable species. Comparison of the spectroscopic properties of the dinuclear complexes of 1,4-dihydroxy-2,5-bis(pyrazol-1′-yl)benzene with each other, their mononuclear analogues, and other relevant species suggests that these systems possess a gradient of resonant mixing of metal and ligand orbitals across the oxidation range of the bridging ligand. Using the bipyridyl reductions as probes, minimal intermetal communication and metal bridge mixing was found in the hydroquinone state. There was moderate mixing of metal bridge states in the semiquinone state, with extensive mixing of metal and ligand orbitals for the quinone state. This work serves to illustrate how manipulation of metal sites and dioxolene oxidation states may be used to modulate the occurrence and extent of intercomponent interactions in a supramolecular system.

Evidence of dinuclear ruthenium complexes with 1,4-dioxolene ligands has been reported with the ligand 1,4,5,8-tetraoxonaphtalene (see Figure 5.3)[13]. The dinuclear complex was isolated as the hexafluorophosphate salt and the cation was formulated as $[Ru^{II}_2(bpy)_4(tetrox^{2-})]^{2+}$ with the tetraoxolene ligand acting as a bis-bidentate bridging ligand in its dinegative form. Due to the fact that the metal and ligand orbitals are of comparable energies, it was concluded in agreement with Lever et al[14], that the nature of the frontier orbitals for the $[Ru_2(bpy)_4(tetrox)]^{n+}$ cations depends on the relative stabilisation of the ruthenium and tetrox orbitals upon oxidation. For $[Ru^{II}_2(bpy)_4(tetrox^{2-})]^{2+}$ the metal orbitals are higher in energy than the ligand orbitals. Upon one-electron oxidation, the metal orbitals are more stabilised than the tetrox orbitals and even if the SOMO (Singly Occupied Molecular Orbital) of $[Ru_2(bpy)_4(tetrox)](PF_6)_3$ is essentially a metal orbital, a contribution from the

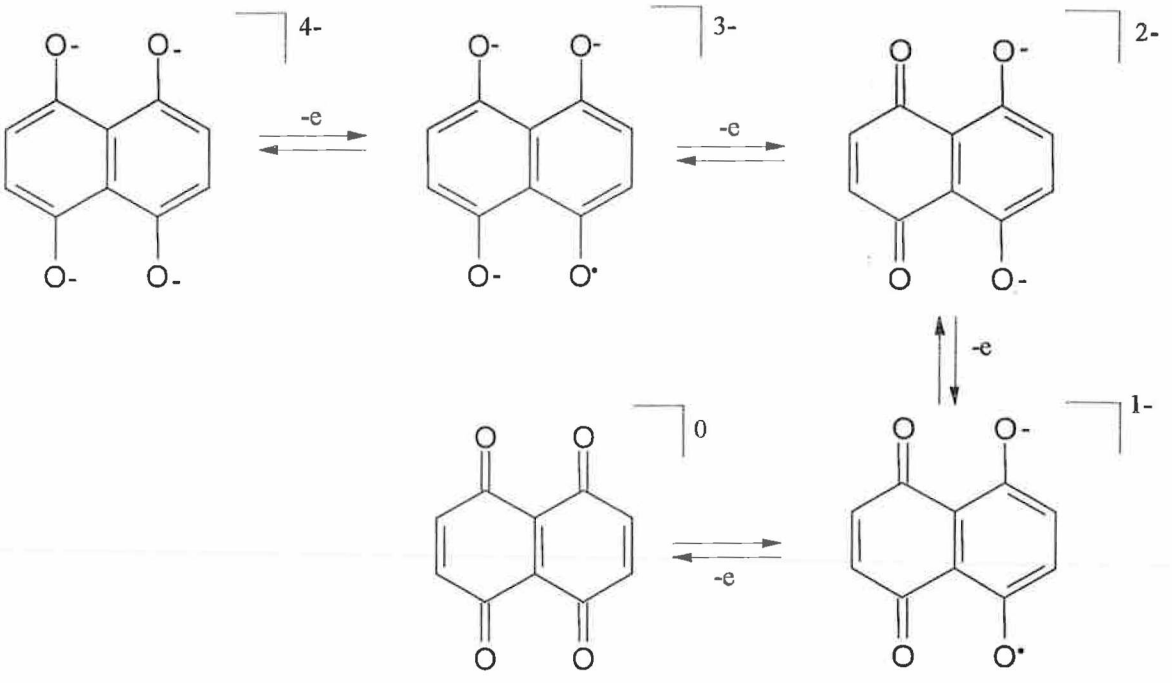

Figure 5.3 *Scheme for oxidation states of 1,4,5,8-tetraoxonaphtalene ligand (tetrox)*[13].

ligand orbital must not be neglected. Results suggest that this compound can be described as a Ru^{III}-Ru^{II} derivative, not neglecting the fact that there is partial delocalisation also onto the bridging ligand. Further, one-electron oxidation stabilises the metal orbitals more, to such an extent that in $[Ru_2(bpy)_4(tetrox)](PF_6)_4$ the orbital order is reversed and the frontier orbitals have more tetrox character, with the result that the complex can be labelled a ruthenium(II)-tetrox complex.

Catechol (benzene-1,2-diol) is perhaps the best-known and most studied dioxolene ligand and can coordinate to metal atoms in the dianionic catecholato mode, the monoanionic semiquinonate or the neutral quinone mode[14-17]. Such ligands are often referred to as non-innocent because there is an ambiguity as to how electrons will

be delocalised between them and the metal, and this will depend on the degree of mixing between appropriate metal and ligand orbitals.

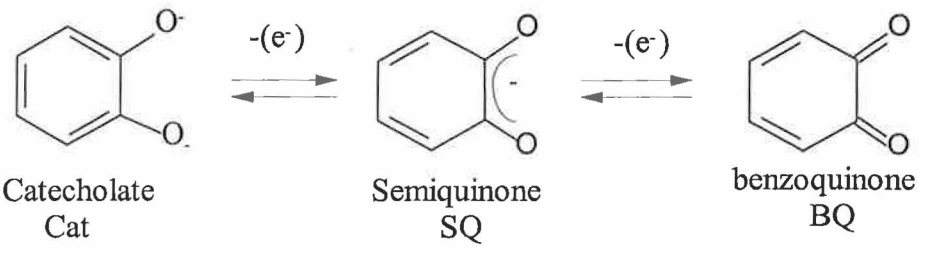

Figure 5.4 The three members of the dioxolene redox series.

It is this aspect which has led to interest in complexes of the dioxolene type. Reaction of simple catechols with $[Ru(bpy)_2Cl_2]$ in air affords $[Ru(bpy)_2(sq)]^+$, where sq denotes a 1,2-benzo-semiquinone arising from one-electron oxidation of the coordinated catecholate anion[15](see Figure 5.4). These are well known compounds, with many interesting characteristics: they are one-electron paramagnets; they have an intense $[Ru(d\pi)] \rightarrow$ sq MLCT band in the electronic spectrum; and they undergo reversible ligand-based oxidation and reduction to give coordinated quinone and catecholate, respectively[15].

There has been considerable interest recently in the synthesis and characterisation of dinuclear ruthenium complexes containing a 1,2-dioxolene (catechol) bridge[6,7,18,19,20]. The use of binucleating bridging ligands such as 3,3';4,4'-tetrahydroxybiphenyl(L1) or 3,3",4,4"-tetrahydroxy-*p*-terphenyl(L2) (see Figure 5.5) to produce dinuclear ruthenium complexes bound via 1,2-dioxolene fragments has been the focus of work by Joulié et al[18]. In each complex the co-ordinated catecholate (cat) fragment may be oxidised reversibly to the semiquinone (sq) and quinone (q) redox states, giving the five-membered redox series cat-cat, cat-sq, sq-sq, sq-q and q-q for the

bridging ligands. The manipulation of this redox series controls the conformation of the bridging ligand. For example in the sq-sq state the bridging ligands are planar due to the presence of double bonds between the aromatic rings; however in the cat-cat and q-q states there is formally

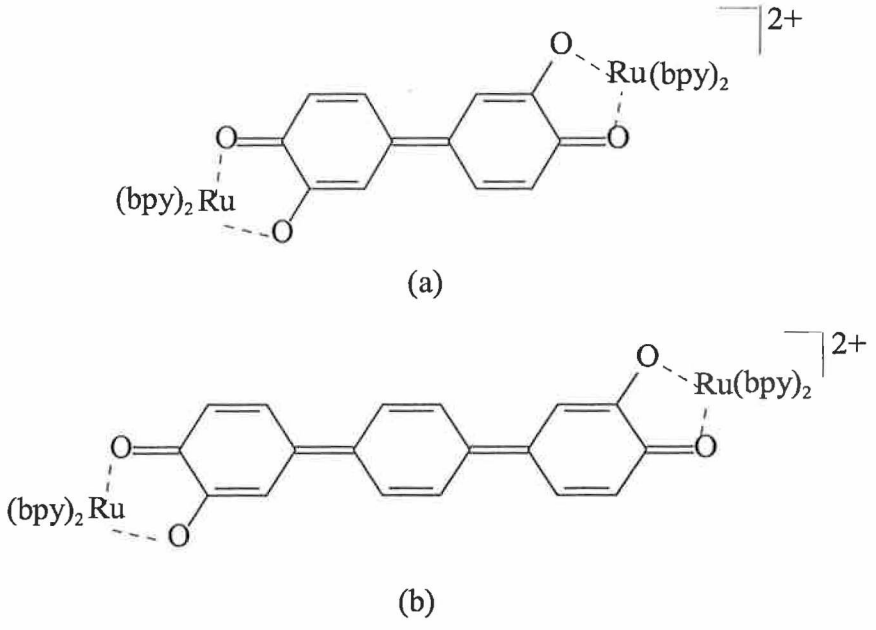

Figure 5.5 *Structures of bis-catechol complexes $[\{Ru(bpy)_2\}(\mu\text{-}L)\{Ru(bpy)_2\}]^{2+}$ where (a) L = 3,3';4,4'-tetrahydroxybiphenyl and (b) L = 3,3'',4,4''-tetrahydroxy-p-terphenyl presented by Joulié et al*[18].

no double bond between the aromatic rings and they are free to adopt a twisted conformation. This electrochemical control of bridging ligand conformation could provide a possible basis for a molecular switch since the conformational changes are known to affect rate of electron-transfer through molecular wires containing biphenyl groups[21,22]. It was reported that complex (a) (see Figure 5.5) displayed some of the essential features of a molecular switch but such conclusions for complex (b) were not

as forthcoming due to the fact that the mixed-valence states are not as electrochemically accessible.

Barthram et al also investigated dinuclear ruthenium complexes based on 1,2-dioxolene fragments (see Figure 5.6)[19]. As with the complexes reported by Joulié et al, these ligands possess two catechol fragments. They described the preparation of dinuclear complexes (a) and (b), shown in Figure 5.6, possessing ruthenium(II)-semiquinone fragments, in which a para-linked bridging ligand results in complete pairing of the semiquinone-based radicals to give a diamagnetic complex, whereas a meta-linked bridging ligand affords a diradical.

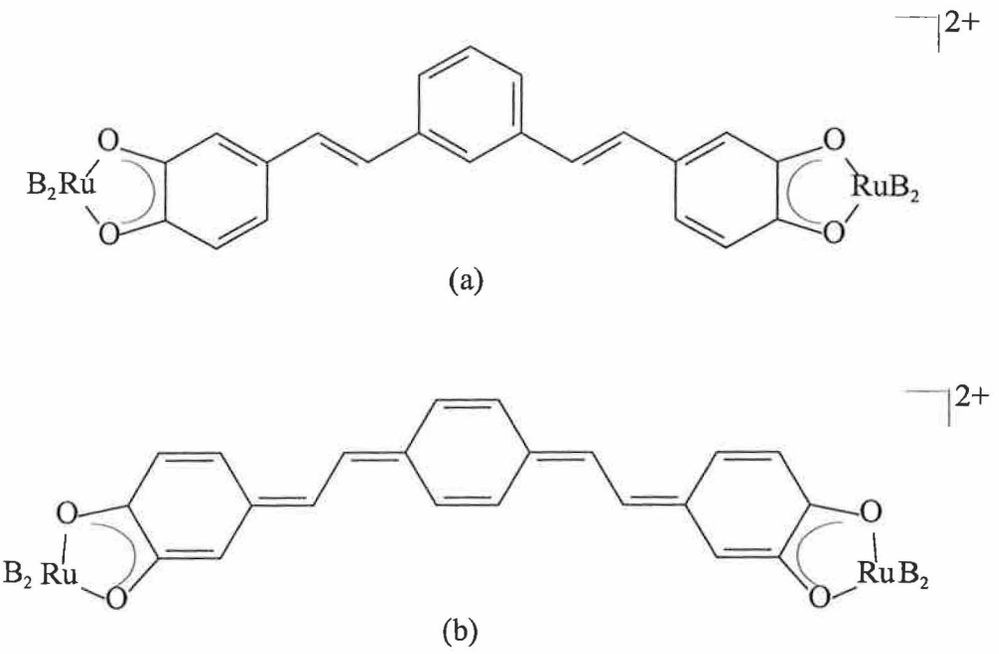

Figure 5.6 *Structures of bis-semiquinone complexes $[\{Ru(B)_2\}(\mu\text{-}L)\{Ru(B)_2\}]^{2+}$ where B = 4,4′-^{t}Bu$_2$-2,2′-bipyridine and (a) L = 1,3 substituted phenyl spacer and (b) L = 1,4 substituted phenyl spacer*[19].

In this instance aerial oxidation of the catecholate ligands to the semiquinone state has occurred. This was confirmed by electrospray mass spectroscopy which indicated that the overall charge on the complex was +2 and also by the electronic spectra which

displayed characteristic Ru(dπ) → semiquinone(π^*) MLCT transitions. In complex (b) shown in Figure 5.6 the two unpaired electrons that would be expected for two semiquinones can pair up to give a diamagnetic complex with a quinonoidal bridge, due to the 1,4 substitution pattern of the phenyl spacer. However in complex (a) this cannot occur due to the 1,3 substitution pattern and the complex is a diradical. The appeal of using these ruthenium (II) - semiquinone groups as the source of unpaired spins is twofold: the paramagnetic species are perfectly stable in air and moisture at room temperature, in contrast to most organic radicals; secondly, they undergo reversible interconversions between several oxidation states[15] which is of interest for the possible switching applications in magnetic materials.

This chapter will focus on the synthesis of the dinuclear ruthenium (II) complexes from the mononuclear catechol complexes $[Ru(bpy)_2(H_2L_2)]PF_6.5H_2O$ and $[Ru(phen)_2(H_2L_2)]PF_6.2H_2O$. The demethylation of the protected catechol complexes described in chapter four (see Figure 4.2) provides complexes with a peripheral catechol binding site which can be used to synthesise dinuclear metal complexes. The synthesis and purification of the complexes will be dealt with in detail. The issue of the charge on the complexes and the nature of the oxidation state of the coordinating complex will also be dealt with in detail. Electrospray ionisation mass spectrometry (ESI-MS), elemental analysis and cation exchange HPLC were used for complex identification and structure confirmation. The dinuclear complexes show electrochemical and UV-Vis spectroscopic properties and these will be discussed in detail. Comparison between the emission properties of the catechol precursors and the dinuclear complexes are also reported. The results obtained for our complexes will also be compared with those of similar dinuclear complexes containing a catechol binding site reported recently by

Ward and coworkers[6,7,20]. The structures of the complexes referred to in the text are presented in Figure 5.7.

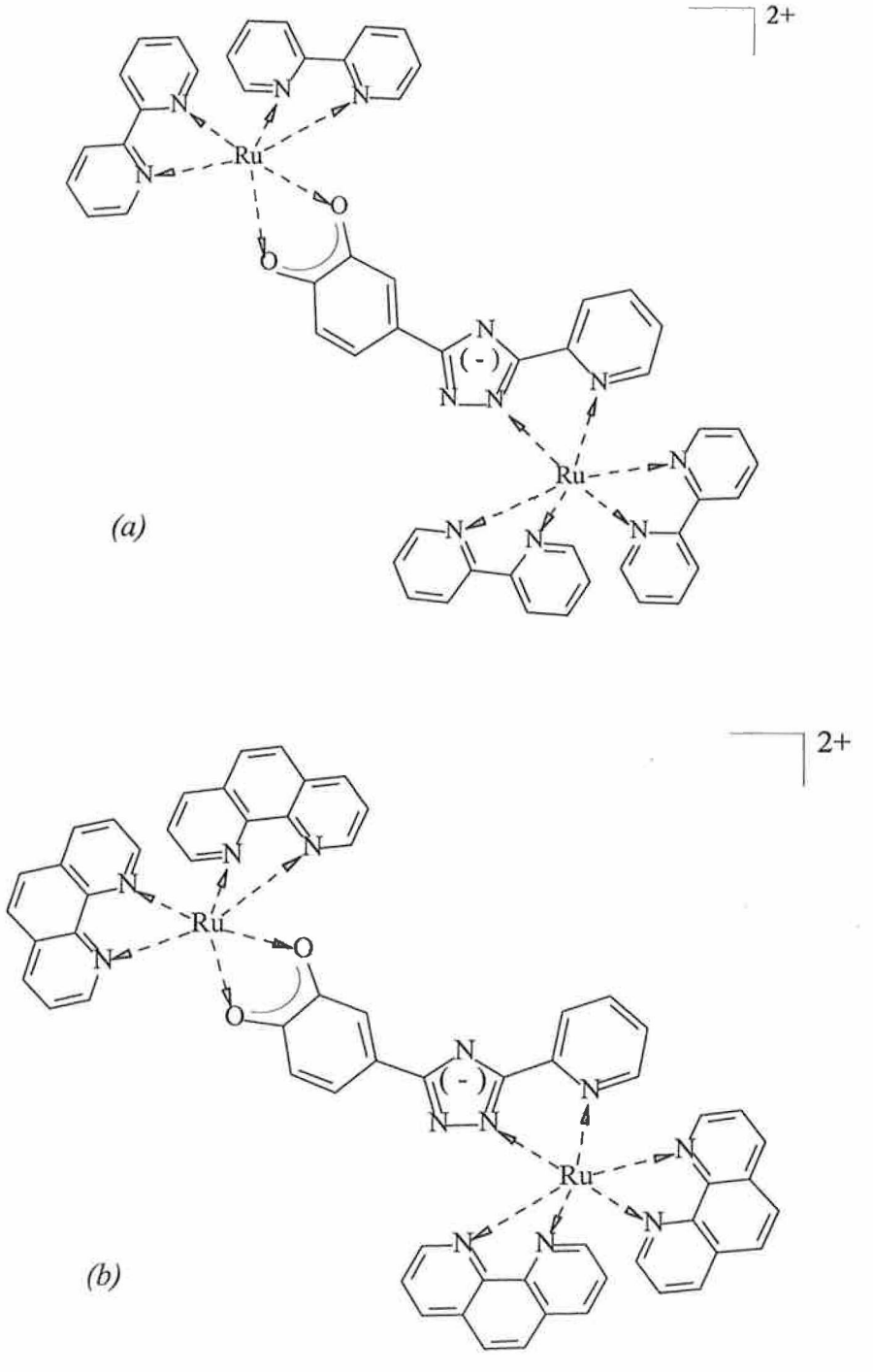

Figure 5.7 *Structure of the dinuclear complexes cited in the text*
(a) $[Ru(bpy)_2(L2)Ru(bpy)_2]^{2+}$ ***(bpybpy)***
(b) $[Ru(phen)_2(L2)Ru(phen)_2]^{2+}$ ***(phenphen)***

5.1 Experimental

5.1.1 Synthesis of dinuclear complexes

The synthesis of the dinuclear ruthenium complexes of the catechol ligand H_3L2 (see section 4.0 and Figure 4.1) are presented in this section. The complexes were prepared from the mononuclear catechol complexes, which were discussed in chapter four. The synthetic procedure and the difficulties associated with it are discussed in section 5.2.1 along with the purification techniques that were employed.

$[Ru(bpy)_2(L2)Ru(bpy)_2](PF_6)_2.KNO_3.2H_2O$ **(bpybpy)**

The reaction leading to the formation of $[Ru(bpy)_2(L2)Ru(bpy)_2](PF_6)_2.KNO_3.2H_2O$ was carried out under basic conditions and in an inert atmosphere. Structural elucidation is based mainly on C,H,N analysis and electrospray ionisation mass spectrometry (ESI-MS) (see section 2.13). 0.659 g (0.73 mmol) of $[Ru(bpy)_2(H_2L_2)]PF_6.5H_2O$ was dissolved in 50 cm^3 ethanol/water (1:1 v/v) and the solution was adjusted to pH 12 by addition of NaOH. To this solution 0.380 g (0.73 mmol) cis-$[Ru(bpy)_2Cl_2].2H_2O$ was added and the reaction heated to reflux under N_2 overnight. The progress of the reaction was monitored by analytical HPLC. After allowing the reaction to cool, the brown/black solution was reduced in volume. The complex was precipitated by addition of a concentrated aqueous solution of ammonium hexafluorophosphate. The precipitate was filtered and washed with a small volume of water and dried with diethyl ether. HPLC analysis of the product showed several peaks. Some unreacted catechol monomer present in the final product could be removed by column chromatography on neutral alumina with 90:10 acetonitrile/water containing 0.08 M $LiClO_4$ as eluent. The

catechol complex adheres to the alumina while the remainder of the product travels through the alumina without any degree of separation. However to isolate the pure dinuclear complex semi-preparative HPLC was used with a mobile phase of 80:20 acetonitrile/water containing 0.12 M KNO_3 and a flow rate of 2.0 cm^3/min. Yield = 0.22 g (20 %). Calcd. for : $Ru_2C_{53}H_{43}N_{13}O_7KP_2F_{12}$ C: 42.80; H: 2.72; N: 11.36 %. Anal. Found: C: 42.29; H: 2.88; N: 12.10 %. Mass Spectrum: m/z 539.4 (where z = 2).

$[Ru(phen)_2(L2)Ru(phen)_2](PF_6)_2.KNO_3.6H_2O$ **(phenphen)**

The synthesis and purification of $[Ru(phen)_2(L2)Ru(phen)_2](PF_6)_2.KNO_3.6H_2O$ is similar to that described above for **bpybpy**. 0.61 g (0.68 mmol) of $[Ru(phen)_2(H_2L2)]PF_6.2H_2O$ was dissolved in 50 cm^3 ethanol/water (1:1 v/v) and the solution was adjusted to pH 12 by addition of NaOH. To this solution 0.387 g (0.68 mmol) cis-$[Ru(phen)_2Cl_2].2H_2O$ was added and the reaction heated to reflux under N_2 overnight. The reaction was monitored by analytical HPLC and the product was extracted in a similar manner to that described for the synthesis of **bpybpy**. The pure dinuclear complex was isolated by semi-preparative HPLC using a mobile phase of 80:20 acetonitrile/water containing 0.12 M KNO_3 and a flow rate of 2.0 cm^3/min.

Yield = 0.25 g (22 %) Calcd. for: $Ru_2C_{61}H_{51}N_{13}O_{11}KP_2F_{12}$ C: 43.79; H: 3.07; N: 10.88 %. Anal. Found: C: 43.88; H: 2.60; N: 10.02 %. Mass Spectrum: m/z 587.5 (where z = 2).

5.2 Results and Discussion.

5.2.1. Synthetic Procedure.

The approach towards the synthesis of the dinuclear complexes discussed here was to first synthesise the mononuclear catechol complexes. The reasoning for adopting this policy was to avoid mixtures of monomer (O,O bound and N,N bound) and dimer complexes which would occur if synthesis of the dimer complexes was performed straight from the catechol ligand H_3L2. The dimer reactions were performed in ethanol/water (1:1) to ensure removal of both chlorides from the respective ruthenium dichlorides[23]. The presence of base ensures that the catechol monomer is deprotonated and reactive towards binding the second metal centre. The reactions were performed in an inert atmosphere in an effort to synthesise the dinuclear complex in which the coordinated dioxolene fragment would be in the catecholate state (see Figure 5.4). However, in the work-up of the complex it likely that aerial oxidation of the coordinated catecholate to semiquinone has occured. This assumption is made due to the inability to attain a ^{1}H-NMR spectrum of the crude product, suggesting the presence of the paramagnetic semiquinone dimer complex or indeed a Ru(III) bound complex. In the work of Whittle and co-workers, synthesis of a ruthenium dinuclear complex from a ruthenium monomer complex, possessing a pendant dioxolene fragment was performed in air[6]. When they analysed the reaction mixture, the presence of both the reduced catecholate complex and the oxidised semiquinone complex was detected. In order to simplify the workup of the reaction the crude mixture was treated with the mild oxidising agent $[Cp_2Fe][PF_6]$ (Cp = η^5-cyclopentadienyl), before chromatographic purification, resulting in conversion to the air-stable semiquinone complex.

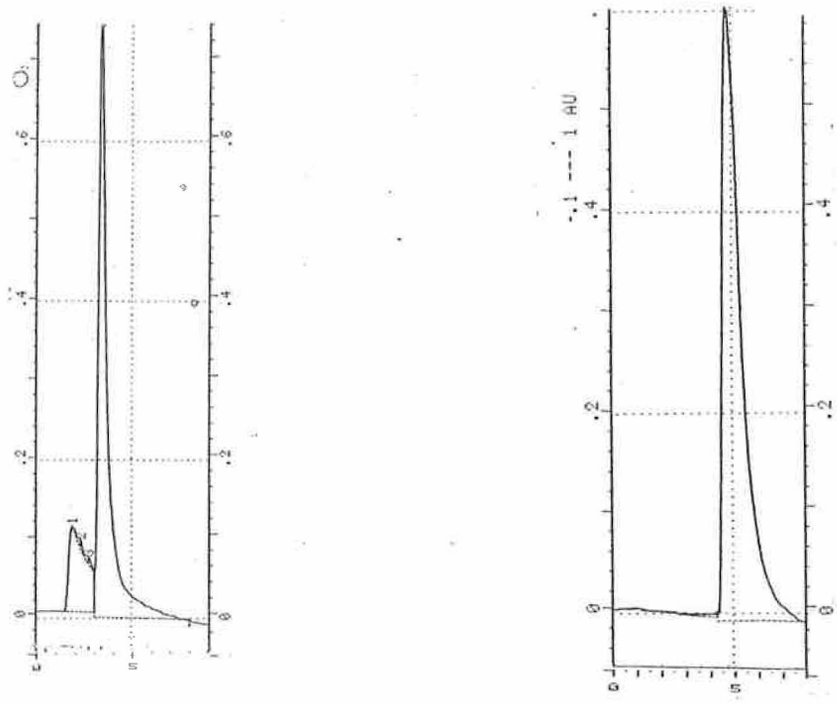

(a) *(b)*

Figure 5.8 *Chromatograpic trace of **bpybpy** with 0.08 M $LiCLO_4$ and flow rate 1.8 mls/min(a) before and (b) after semipreparative HPLC.*

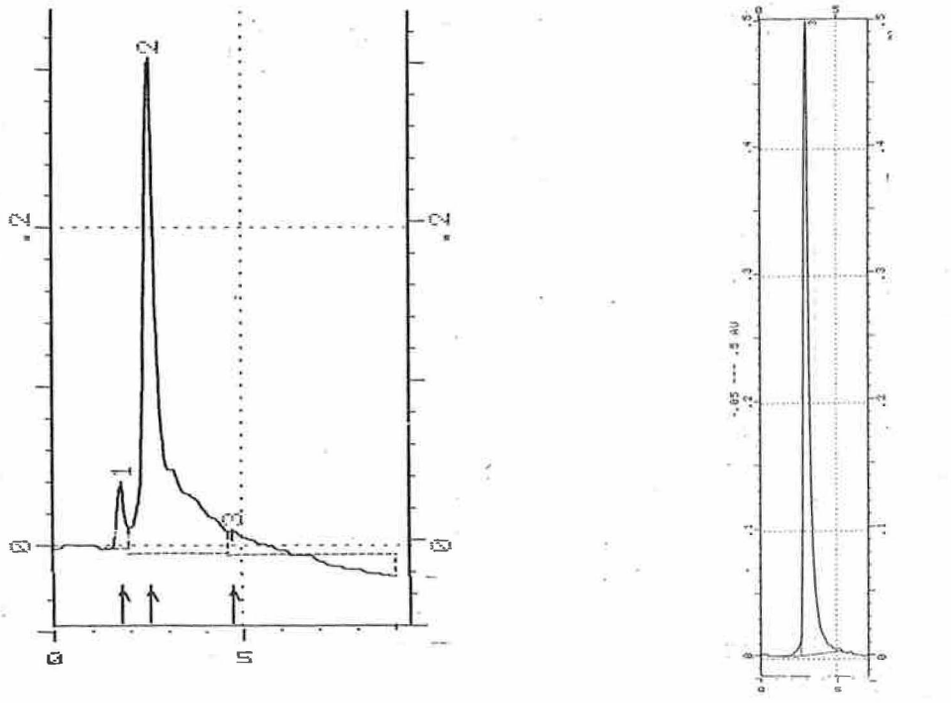

(a) *(b)*

Figure 5.9 *Chromatograpic trace of **phenphen** with 0.08 M $LiCLO_4$ and flow rate 1.8 mls/min (a) before and (b) after semipreparative HPLC.*

A similar approach was taken by Shulka et al who also found that the crude product of a reaction involving a ruthenium dioxolene monomeric complex with cis-$[Ru(bpy)_2Cl_2]$ resulted in a mixture of both oxidation states[20]. They also found that pre-oxidation of the crude product with $[Cp_2Fe][PF_6]$ simplified the purification procedure.

The reactions described in section 5.1.1 were monitored by cation exchange chromatography (see Figures 5.8 and 5.9). Periodic sampling of the reaction mixture confirmed the growing of a dimer peak at a longer retention time than that of the catechol monomer. The retention time of the dimer complex forming was longer by about two minutes than that of the monomer due to the increased bulk of the molecule and the increased charge (from +1 to +2). Analysis of the crude product suggested that the dimer complex was about 80 % pure. The shorter retention times of the impurities suggested that some unreacted dichloride and unreacted catechol monomer were present in the crude mixture as well as the possibility of a mixture of the dimer complex in the semiquinone and catecholate state. Successive recrystallisation of the complexes from acetone/water (2:1 v/v) did not purify the complexes significantly so it was decided to attempt column chromatography. A sample from the product of the **bpybpy** reaction gave four peaks on analysis by HPLC. This sample was separated on a silica column using 80/20 $MeCN/H_2O$ and 1% saturated solution of KNO_3. Two main bands were observed and the fractions were analysed using HPLC. However there was a big loss of compound on the silica and the elution time was quite long. From the HPLC analysis it appeared that the second band contained the pure dimer complex (comparing retention times), however when this band was collected and the solvent removed, the isolated product appeared to be a mixture once again. The only explanation that could be offered in this instance is that the dimer complex may have been isolated from the silica column

with the coordinated dioxolene fragment in the catecholate state which underwent aerial oxidation during the subsequent workup. Another effort at purifying the product from the **bpybpy** reaction was attempted using neutral alumina with 90:10 MeCN/H_2O containing 0.08 M $LiClO_4$ as eluent. Two bands were observed on the column with the second smaller band remaining unmoved by the eluent and indeed unmoved by 100 % methanol. This band is most likely the catechol monomer which adheres to neutral alumina. The first main band is collected as several fractions, which on analysis by HPLC confirms that some of the impurities have been removed, however full isolation of the complex was not achieved. Another column chromatographic method employed was the use of the size-exclusion material LH20. The solvent used to elute the product was acetonitrile. It was thought that the dimer would elute first from the column with the unreacted dichloride and catechol monomer being retained to a more significant degree. However no separation was achieved and the initial product was basically recovered.

Due to the fact that the purification of the dimer complexes **bpybpy** and **phenphen** proved unsuccessful with silica, alumina and LH20 it was decided use semi-preparative cation exchange HPLC. The separation pattern of the dimer complexes was first assessed on the analytical scale cation exchange HPLC before injection onto the semi-preparative scale system. Several fractions were collected in order to successfully isolate the pure dimer. The elution time on the semi-preparative system (10-15 minutes) was much longer than the corresponding analytical scale system (2-5 minutes) and required at least 30 minutes washing with mobile phase between injections. The mobile phase conditions were altered in an effort to optimise the retention time and separation of the complexes on the column. The most suitable conditions found were 0.12 M

KNO_3 in 80/20 acetonitrile/water. Any increase in the concentration of KNO_3 resulted in faster elution from the column, however the separation of the various components in the sample was much poorer with a greater overlap of peaks than with 0.12 M KNO_3. Any decrease in the concentration of KNO_3 from 0.12 M resulted in longer retention times and once again poorer resolution of peaks with increased overlapping and streaking. The fractions from the semi-preparative column were analysed by analytical HPLC and the pure dimer fractions were combined. At this stage the volume was reduced to near dryness under vacuum while avoiding full dryness due to the explosive nature of KNO_3. In order to remove the KNO_3 the product was dissolved in acetone in which KNO_3 is insoluble and subsequently filtered. However some traces of KNO_3 were still present as shown by IR and elemental analysis. The pure dimer was then recrystallised by adding water and a few drops of a concentrated aqueous solution of ammonium hexafluorophosphate to the acetone filtrate. The yield of the complexes after purification using semi-preparative HPLC was quite poor. This could be due to the fact that the components of the sample eluted quite close to each other and several fractions were required to successfully isolate the pure complex. It was not possible to record ^{1}H-NMR spectra of the dimer complexes suggesting that the coordinated dioxolene fragment was in the semiquinone state for both dimer complexes, **bpybpy** and **phenphen**. Such interpretation is further enhanced later by UV-Vis spectroscopy (see section 5.2.3) and electrochemistry (see section 5.2.4). Attempts to reduce the complexes to the catecholate state by addition of a few grains of sodium borohydride ($NaBH_4$) to the ^{1}H-NMR sample did not result in any clearer spectra.

5.2.2. Mass spectra.

The electrospray ionisation mass spectrometry (ESI-MS) analyses performed on the dimer complexes **bpybpy** and **phenphen** were a great asset in the elucidation of the structures[24]. The electrospray technique is a very mild way of obtaining the anions observed[25], and there is almost no fragmentation of the complexes. Until recently only low molecular weight, volatile compounds were amenable to analysis by conventional mass spectroscopic methods. Most larger species simply could not be promoted into the gas phase without substantial degradation and/or fragmentation. ESI-MS provides an inherently "gentle" ionisation that has been shown to produce intact ions from thermally labile biological molecules and inorganic transition metal complexes[25,26]. The ions detected are only those which form under the experimental conditions. The ESI-MS spectra for **bpybpy** are presented in Figure 5.10. The first spectrum in Figure 5.10 is a typical ESI-MS spectrum. The characteristic feature of ESI that distinguishes it from other ionisation techniques is that it generally imparts multiple charges to larger analyte molecules. The resulting highly charged molecular ions, which typically display little or no fragmentation, are thus within the m/z range where conventional mass spectrometers function quite well. Thus the first spectrum appears as relative intensity against m/z, where z is 2. The position of this peak, at half of the m/z value expected on the basis of the molecular mass, and the half-integral peak spacings in the isotopic pattern, both indicate that the charge on the cation was +2. This means that the coordinating catecholate ligand is at the semiquinone oxidation level, leaving a charge of -2 on the ligand (including the negative charge induced by the deprotonated triazole) and +2 charge on each $\{Ru(bpy)_2\}$ fragment.

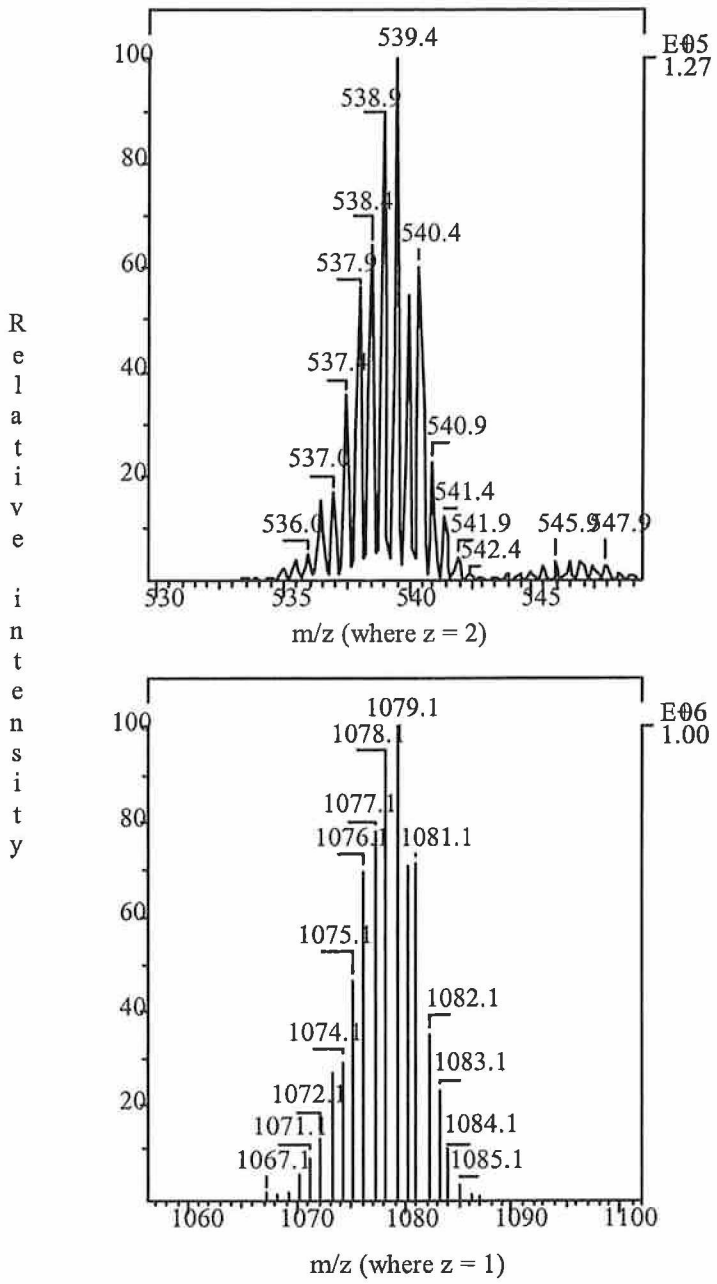

Figure 5.10 Electrospray ionisation mass spectra (ESI-MS) of ***bpybpy*** *complex in methanol.*

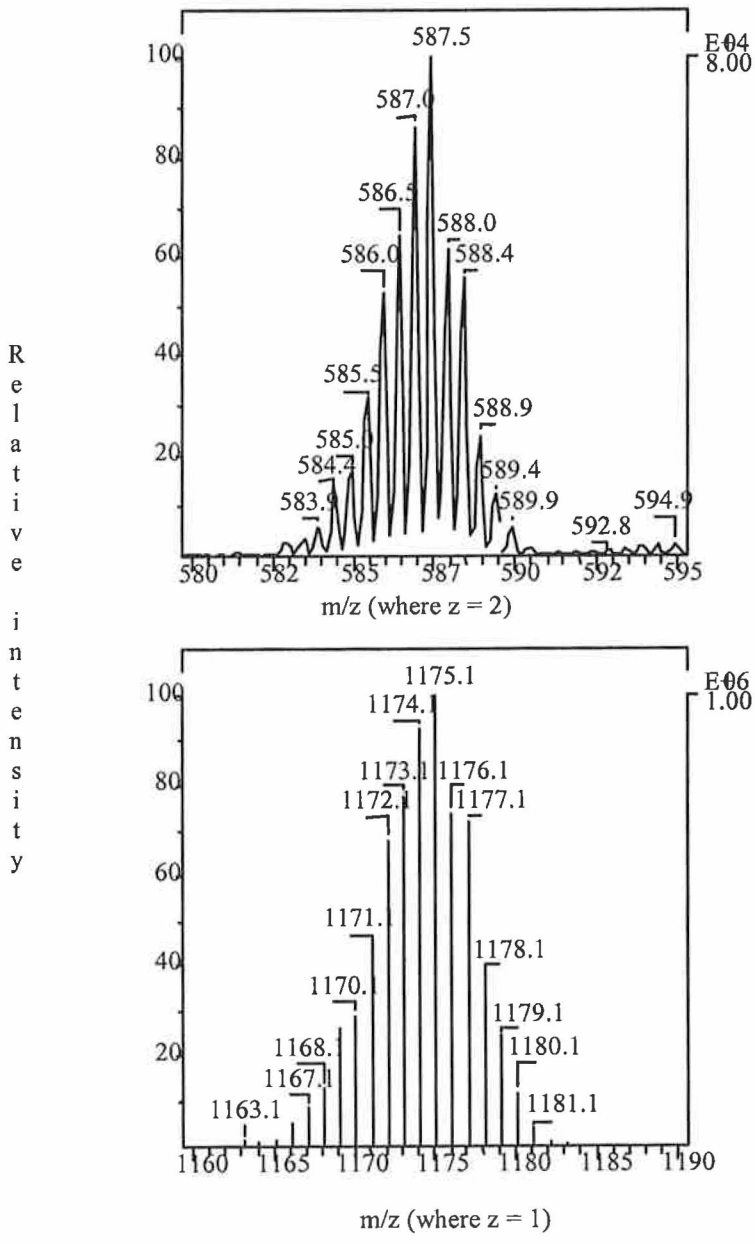

Figure 5.11 *Electrospray ionisation mass spectra (ESI-MS) of* ***phenphen*** *complex in methanol.*

All this leads us to the interpretation that the complex is a +2 cation enhancing the assumptions made from the elemental analysis and further credance to these assumptions will be added from the UV-Vis spectroscopy and electrochemistry studies. The strong molecular ion peak at 539.4 (highest relative intensity) is recognised as the molecular ion and represents a 2+ complex with a mass of 1078.8 g/mol. This compares favourably with the calculated molecular weight of the dimer complex (**bpybpy**) without the counterions (PF_6^-), $[Ru_2C_{53}H_{39}N_{12}O_2]^{2+}$, 1078.12 g/mol. It should also be noted that each peak differs from its neighbouring peak by only charge. In the first ESI-MS spectrum of Figure 5.10 and 5.11 the δm/z is 0.5 (1 as z=2) which implies that each peak differs by one proton. The second spectrum in Figure 5.10 was produced by trapment of the molecular ion (at m/z 539.4) and subsequent ionisation of this molecular species. The spectrum is consistent with that of the proposed dimer structure due to the large number of isotopes present in a Ru(II) complex, usually eleven or more peaks are detectable. These form a very easily recognisible pattern of the relative intensities of the isotopes. Similar interpretations can be offered for the ESI mass spectra shown in Figure 5.11 for the dimer complex **phenphen**. The molecular ion appears at m/z 587.5 representative of an ion of mass 1175 g/mol and again reflects the theory that the coordinating catecholate ligand is at the semiquinone oxidation level. This compares with the calculated molecular weight of the dimer cation $[Ru_2C_{61}H_{39}N_{12}O_2]^{2+}$ 1174.21 g/mol. A similar isotopic pattern is observed in the second ESI spectrum in Figure 5.11 to that observed for **bpybpy** shown in Figure 5.10.

5.2.3. Electronic and Photophysical properties.

One of the main questions which must be addressed with relation to the dimer complexes **bpybpy** and **phenphen** is the nature of the oxidation state of the catecholate fragment in the dinuclear complexes. The elemental analysis and the ESI-MS spectra support the notion that both complexes are 2+ charged. However this does not entirely imply that the catecholate fragment is in the semiquinone oxidation state as the overall charge could also be due to a Ru(III)-HQ coordination (where HQ refers to the catecholate ligand in the hydroquinone oxidation state). The electronic spectra of the complexes provides us with a useful tool towards solving this question and the conclusions derived are enhanced by electrochemistry (see section 5.2.4) and spectroelectrochemistry (see section 5.2.5) studies.

The UV-Vis spectra of the dimer complexes are presented in Figures 5.12 and 5.14 and the main features are summarised in Table 5.1. The spectra of the complexes are measured when the triazole is protonated and deprotonated. Also the complexes are measured in acetonitrile with no acid or base added, to confirm the natural state of the complex. The spectra of the complexes in pure acetonitrile and with some base added (deprotonated) are very similar indicating that as expected the dimer complexes are 2+ charged with the triazole deprotonated. The UV-Vis spectra are dominated by metal-to-ligand charge transfer (MLCT) transitions in the 400-500 nm region and intense transitions in the 890-980 nm region which are characteristic of the Ru($d\pi$) $\rightarrow$ semiquinone(π^*) MLCT transition of the secondary $\{Ru(L)_2(sq)\}^+$ fragment (where L = bpy or phen)[15,20].

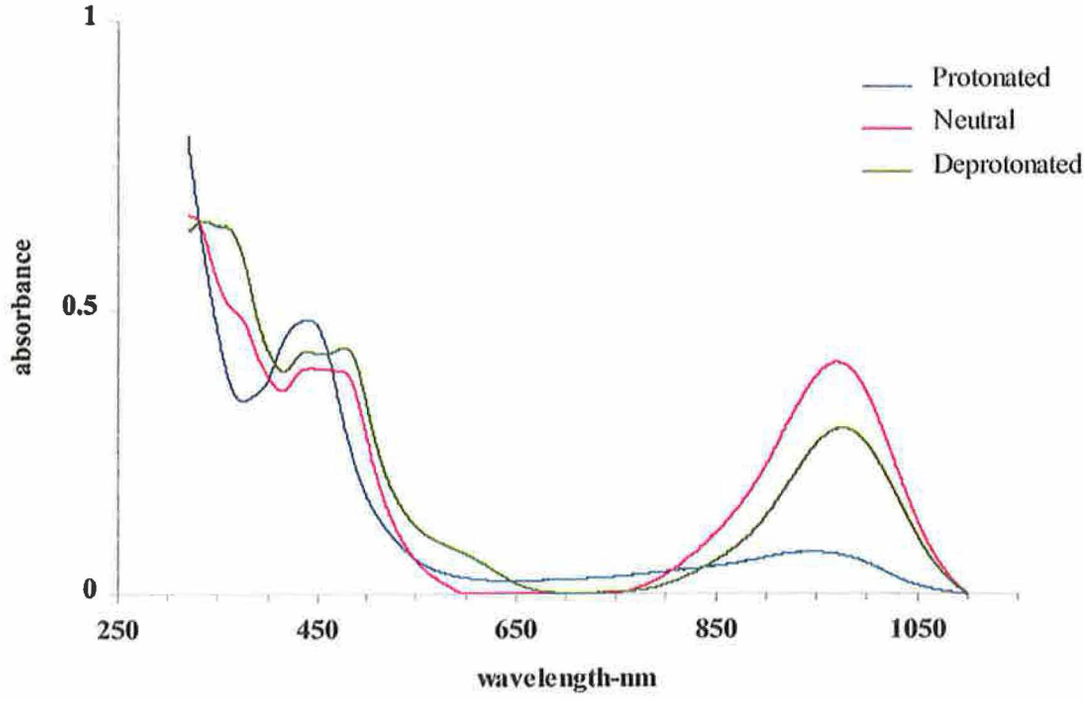

Figure 5.12 *Absorption spectra of **bpybpy** protonated, neutral and deprotonated in acetonitrile ($2.7 X 10^{-5} M$).*

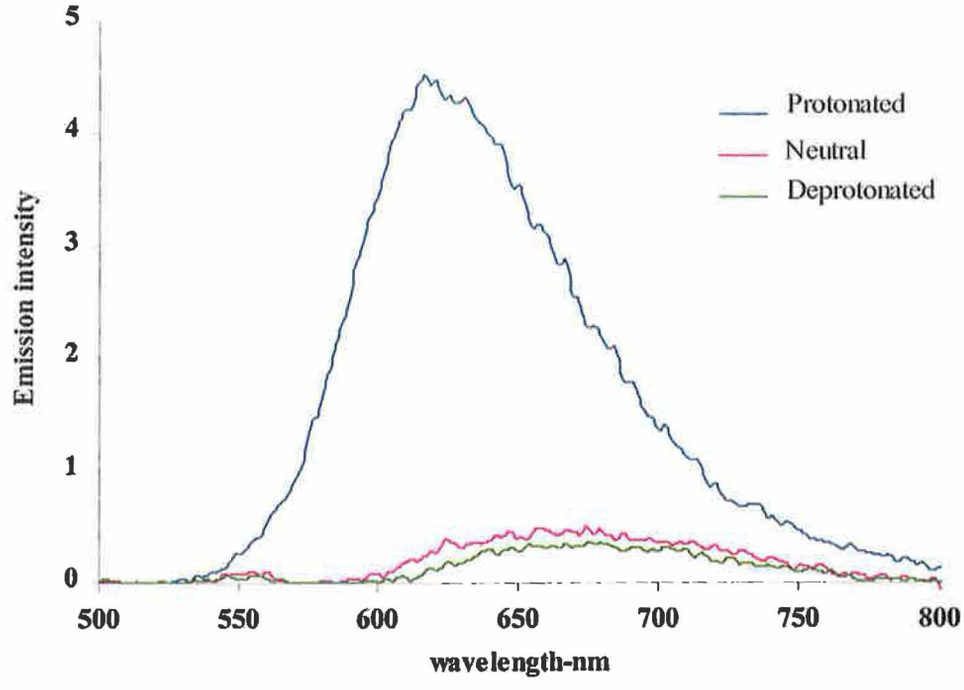

Figure 5.13 *Room temperature emission of **bpybpy** protonated, neutral and deprotonated in acetonitrile ($2.7 X 10^{-5} M$).*

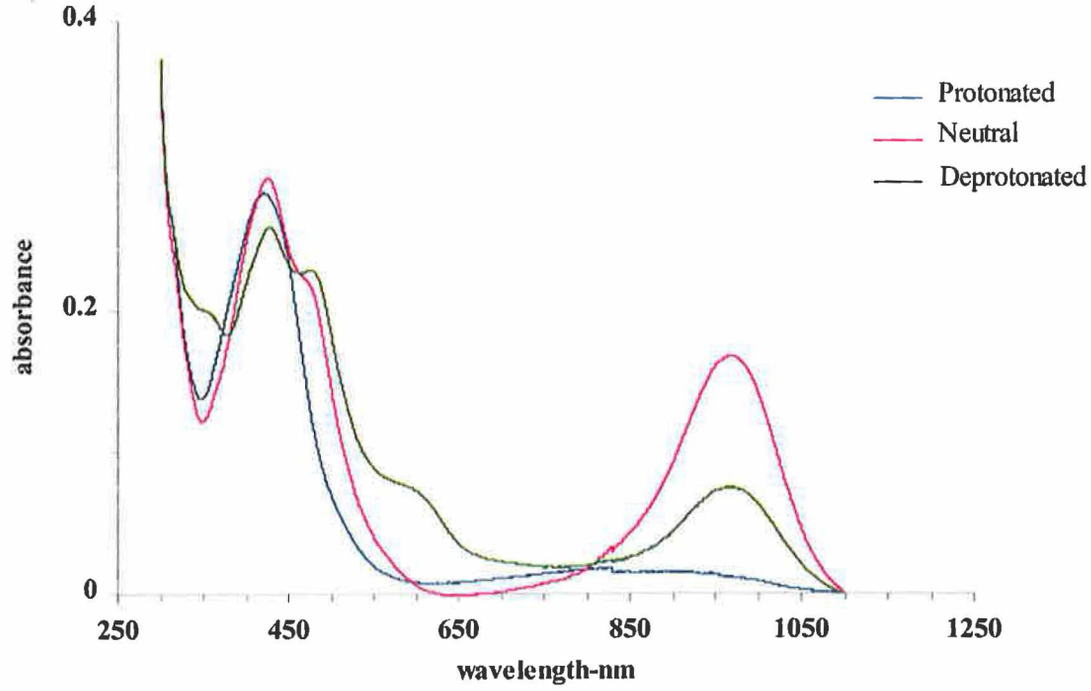

Figure 5.14 *Absorption spectra of **phenphen** protonated, neutral and deprotonated in acetonitrile (9.2×10^{-6} M).*

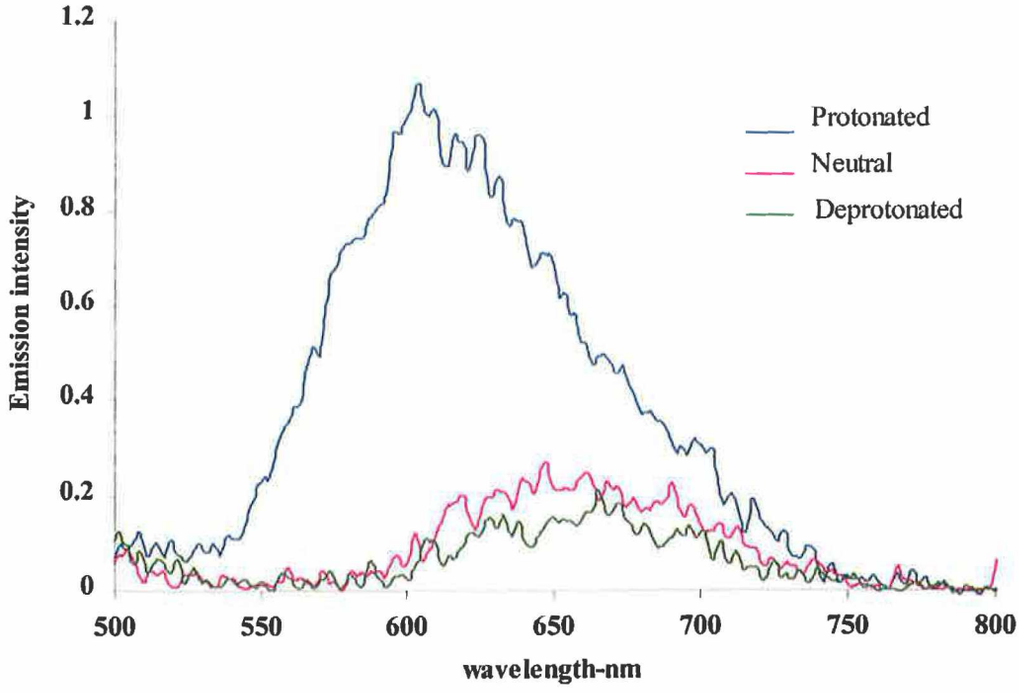

Figure 5.15 *Room temperature emission of **phenphen** protonated, neutral and deprotonated in acetonitrile (9.2×10^{-6} M).*

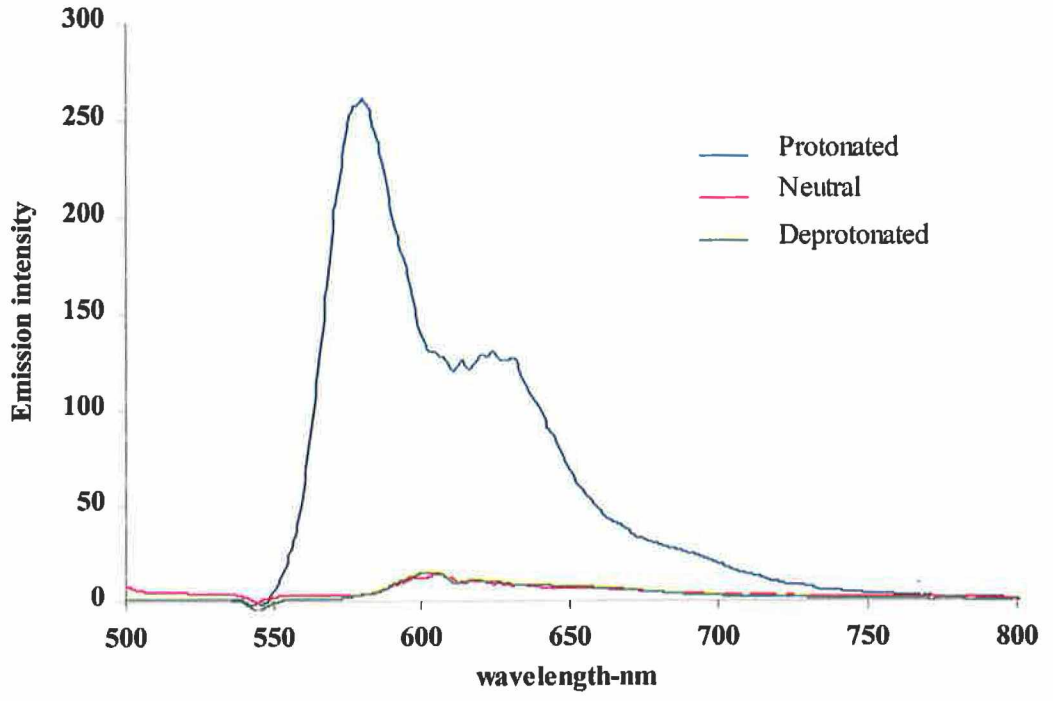

Figure 5.16 *Emission spectra of **bpybpy** protonated, neutral and deprotonated at 77 K in ethanol/methanol (4:1 v/v) (2.7 X 10^{-5} M).*

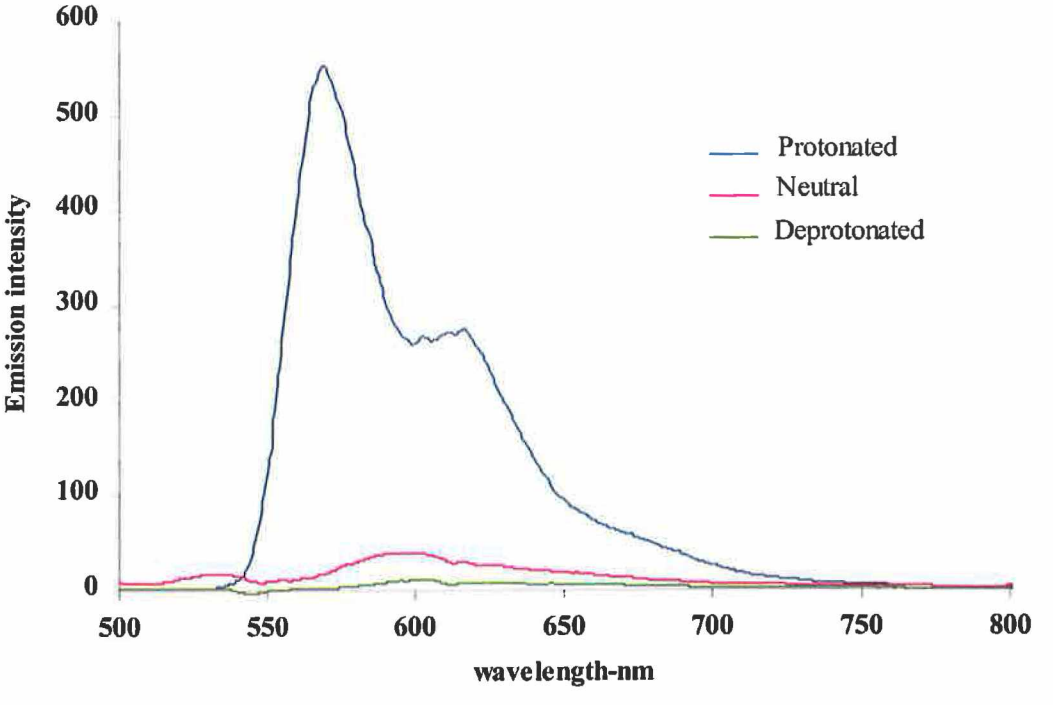

Figure 5.17 *Emission spectra of **phenphen** protonated, neutral and deprotonated at 77 K in ethanol/methanol (4:1 v/v) (9.2 X 10^{-6} M).*

Table 5.1 *UV-Vis spectral peaks for the complexes in acetonitrile*[A].

Complex	Absorption bands / nm (ε / $M^{-1}cm^{-1}$)		
	Neutral pH	**Deprotonated**	**Protonated**
bpybpy	971(15264), 477(14440), 444(13751), 370(sh)(18027), 330(sh)(23351), 290	975, 477, 441, 360(sh), 334(sh), 290	945, 441, 288
phenphen	969(19014), 426(31762), 265	969, 587(sh), 427, 360(sh), 265	895, 421, 264

Table 5.2 *Emission data for the complexes in acetonitrile*[A-D].

Complex	Emission λ_{max}, nm						Lifetime(ns) at 300 K
	Neutral pH		**Deprotonated**		**Protonated**		
	300 K	**77 K**	**300 K**	**77 K**	**300 K**	**77 K**	
bpybpy	675	605	675	606	617	580	*
phenphen	662	601	665	601	604	569	*

A: Protonation of the complexes was achieved by addition of a drop of perchloric acid and deprotonation by the addition of a drop of diethylamine. Neutral spectra refer to those performed in pure acetonitrile.

B: All the measurements at 300 K were performed in acetonitrile.

C: All the measurements at 77 K were performed in ethanol/methanol 4:1 v/v.

D: Lifetime measurements were performed in acetonitrile and degassed using N_2.

* Lifetimes was too short for the complexes in pure acetonitrile due to quenching.

In the UV-Vis spectrum of **bpybpy** in pure acetonitrile (referred to as neutral) the characteristic MLCT transition occurs at 477 nm and is similar in shape and λ_{max} to the mononuclear complex **bpyL2** (see Figure 4.12). The intense Ru(dπ) → semiquinone(π*) MLCT at 971 nm is red shifted in comparison to that observed in the mononuclear $[Ru(bpy)_2(sq)]^+$ (890 nm)[15] which may be due to the extended delocalisation of the semiquinone ligand of **bpybpy** compared to that of $[Ru(bpy)_2(sq)]^+$. In other words the semiquinone fragment in **bpybpy** is a better electron acceptor than that in $[Ru(bpy)_2(sq)]^+$ due to its attachment to the ruthenium bound pyridyltriazole fragment[6,7]. The shoulders at 334 and 360 nm may tentatively be assigned to internal semiquinone transitions which are observed in $[Ru(bpy)_2(sq)]^+$ at 344 and 377 nm. Protonation of the **bpybpy** results in a blue-shift of the MLCT transitions. The transition at 477 nm in the deprotonated and neutral spectra is shifted to 441 nm and this correlates with the shift observed in the mononuclear catechol complex **bpyL2** (see 4.2.3). The Ru(dπ) → semiquinone(π*) MLCT at 971 nm in pure acetonitrile is blue-shifted to 945 nm upon protonation of the triazole and shows a dramatic fall in intensity. There is less electron density present on the semiquinone ligand when the triazole is protonated resulting in a decrease in intensity and a shift to higher energy of this MLCT transition. Similar features are observed in the electronic spectra of **phenphen** and the interpretations are comparable to those made for **bpybpy**.

The room temperature and low temperature emission spectra of the dimer complexes are presented in Figures 5.13, 5.15, 5.16 and 5.17 and the main features are summarised in Table 5.2. One of the main features to note in both dimer complexes **bpybpy** and **phenphen** is that the emission is quenched. Both dinuclear complexes exhibit very weak emission at room temperature in neutral or basic acetonitrile, when

excited around the MLCT λ_{max} of the respective complexes, which may be due to weak trace residual emission characteristic of free mononuclear N,N bound complex. The fact that the emission was quenched in these dinuclear complexes is due to intramolecular quenching of the excited state by the semiquinone. This was also observed in the other similar semiquinone bound ruthenium dinuclear complexes reported by Ward et al[6,20]. Low temperature emission is observed at 77 K and is blue shifted and structured compared to emission at room temperature due to the phenomenon known as "rigidchromism", which was discussed in more detail in section 3.2.3. Keyes et al reported on the analogous mononuclear complex shown in Figure 5.18[27].

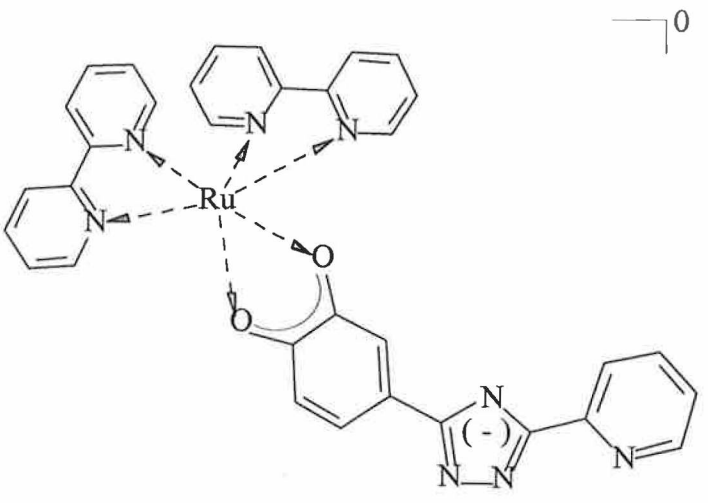

Figure 5.18 Structure of mononuclear O,O bound complex studied by Keyes et al[27].

This semiquinone bound complex (with an overall neutral charge) behaves similarly to the dimer complexes **bpybpy** and **phenphen** in neutral media. The emission was weak and unstructured at low temperature when the triazole was deprotonated, which is associated with intramolecular quenching of the excited state by the semiquinone. The most interesting observation reported was the almost complete extinction of emission

properties after protonation of the complex. Figures 5.13 and 5.15 display the effect of protonation on the analogous dimer complexes **bpybpy** and **phenphen**. The protonated spectra exhibit an increase in intensity and are blue shifted in comparison to the neutral and deprotonated spectra. The effect is even more substantial at low temperature (see Figure 5.16 and 5.17) whereby there is a huge increase in intensity upon protonation of the complexes. The more structured nature and λ_{max} of the emission spectra of the dimer complexes, when protonated, is very similar to the effects observed for the mononuclear catechol complexes in section 4.2.3 (compare Table 4.2 and 5.2). These factors would seem to indicate that protonation of the dimer complexes causes removal of the metal centre which is semiquinone bound. This could result in observation of emission properties similar to those of the mononuclear catechol complexes and would explain the increase in intensity and structure of the emission spectra in Figures 5.13-5.17. This phenomenon was further expored by HPLC analysis of the complexes in acetonitrile before and after the addition of a drop of perchloric acid. The samples were analysed using 80:20 acetonitrile/water containing 0.08 M $LiClO_4$ with a flow rate of 1.8 cm^3/min on a cation exchange HPLC column attached to a photodiode array detector. The HPLC trace of **bpybpy** in pure acetonitrile gave a single peak at a retention time, just over 10 minutes, representative of the pure dimer complex (the red trace in Figure 5.19). When a drop of perchloric acid ($HClO_4$) was added to the acetonitrile solution of **bpybpy** the colour changed from pale brown to light yellow/green and HPLC analysis showed showed two main peaks around 2 minutes and two further smaller peaks at 2.5 and 4 minutes respectively.

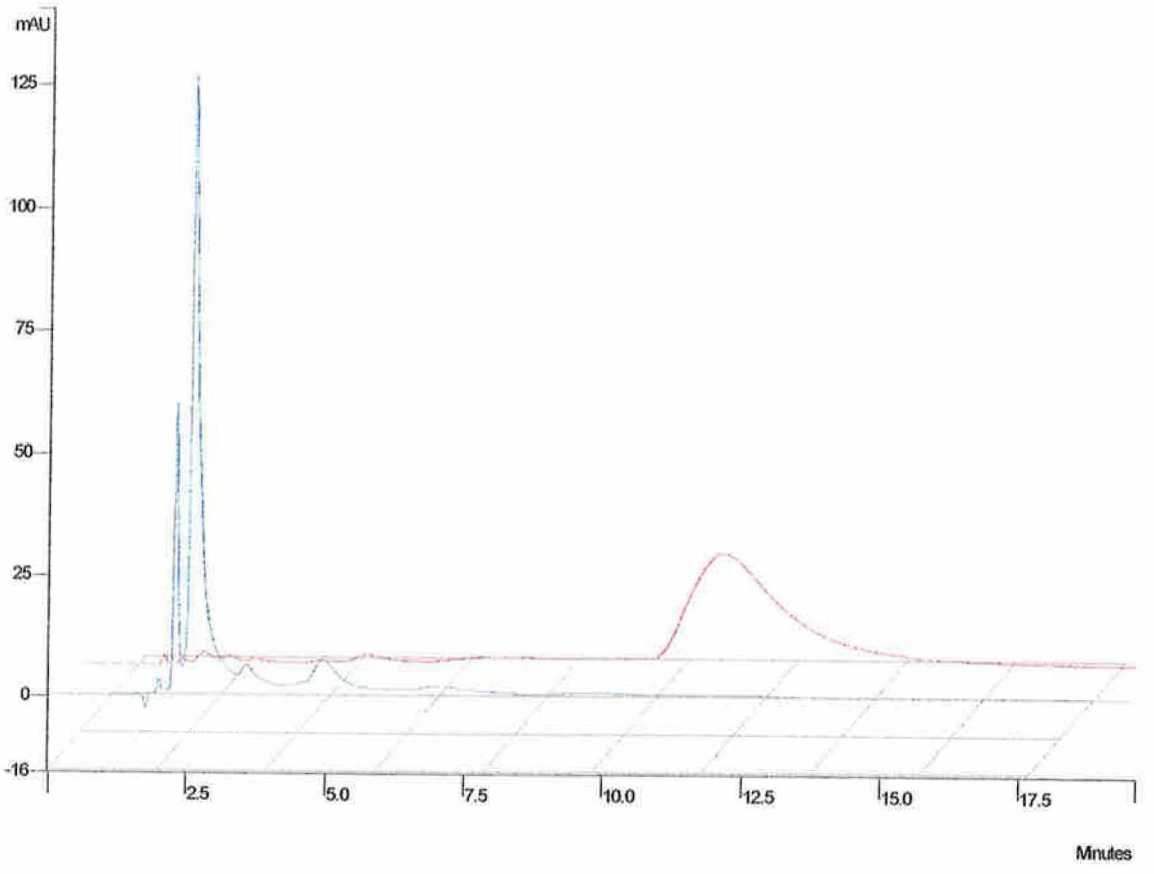

Figure 5.19 Overlay of HPLC trace before(red trace) and after (blue trace) the addition of a drop of perchloric acid to ***bpybpy*** *in acetonitrile.*

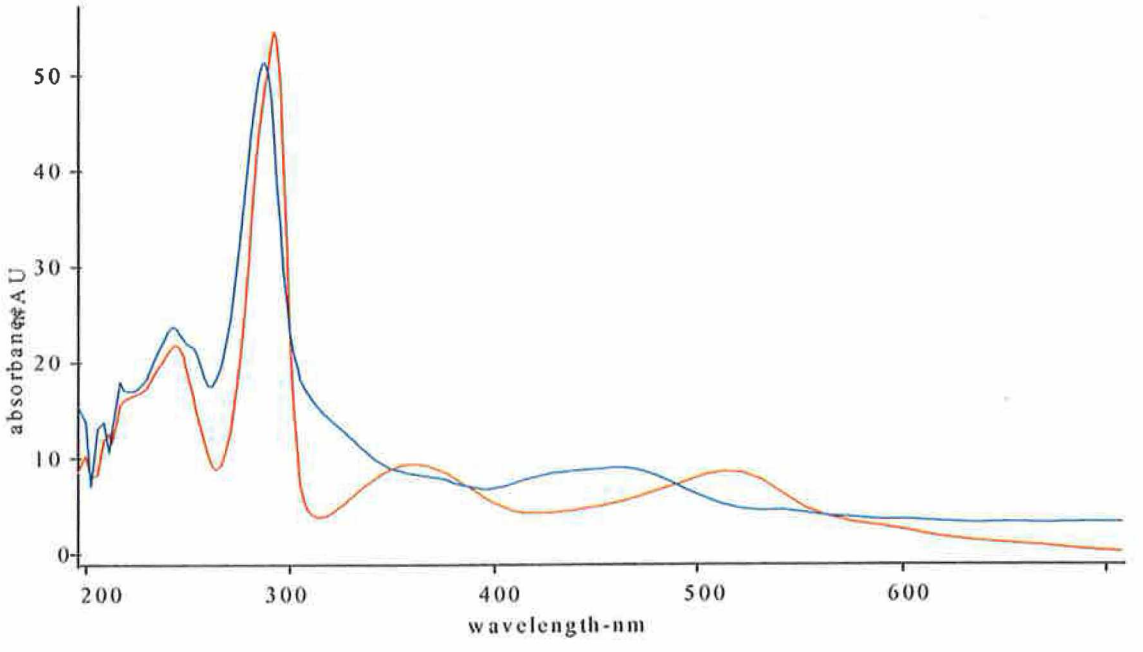

Figure 5.20 UV-Vis absortion spectra of the two main species observed in the HPLC analysis of a solution of ***bpybpy*** *in acetonitrile after the addition of a drop of perchloric acid (blue trace in Figure 5.19).*

The absorption spectrum of the first peak (red trace in Figure 5.20), in the region of 200-700 nm, resemles that of $[Ru(bpy)_2(X)_2]$ type complex where X in this case may be ClO_4^- or PF_6^-. The absorption spectrum of the second main peak (blue trace in Figure 5.20), in the region of 200-700 nm, resemles that of the mononuclear N,N bound catechol complex $[Ru(bpy)_2(H_3L2)]^{2+}$). Such similarities indicate that the dimer complex **bpybpy** breaks up in the presence of acid by removal of the $\{Ru(bpy)_2\}$ semiquinone bound fragment. This is not an uncommon phenomenon in dioxolene bound complexes and was reported by Keyes et al who found that O,N bound dioxolene mononuclear and dinuclear complexes were unstable at pH < 4 (see Figure 5.2)[11]. It was suggested in this report that the decomposition of the complexes may be due to protonation of the coordinated oxygen reducing its capacity to bond thus making the Ru(II)-O bond unstable. Such instability towards acid was also reported for ruthenium O,N bound complexes based on flavin ligands[28]. The confirmation of the break-up of **bpybpy** in acid by HPLC analysis confirms that the changes in absorption and emission properties of the dinuclear complex in the presence of acid are due to the instability of the complex in such a medium. In Figure 5.12 the absorption spectrum of **bpybpy** in an acidic medium (referred to as the protonated spectrum) confirms that the intense Ru($d\pi$) $\rightarrow$ semiquinone(π^*) MLCT at 971 nm is no longer present indicative of the fact that the $\{Ru(bpy)_2\}$ semiquinone bound fragment has broken off. The emission spectra of **bpybpy** at room temperature and at low teperature in the presence of acid (see Figure 5.13 and 5.16) reveal a significant increase in intensity. As stated earlier the λ_{max} of the emission, at both temperatures, in the presence of acid are coincident with those observed for the mononuclear analogue **bpyL2** in chapter four section 4.2.3. This indicates that the observed emission in **bpybpy** is due to the N,N bound mononuclear

catechol complex which is present from the break-up of the dinuclear complex in the presence of acid.

5.2.4. Electrochemical Properties.

The electrochemical properties of the dimer complexes **bpybpy** and **phenphen** were investigated using cyclic voltammetry (CV) and square-wave voltammetry (SWV). Square-wave voltammetry was used because of the improved resolution of the waves in both the oxidation and reduction scans. Whereas cyclic voltammetry consists of cycling the potential while continuously monitoring the current, square-wave voltammetry generates the entire current-potential response by a series of potential steps. In swv a rather large amplitude symmetrical square-wave perturbation is applied, each cycle of the square-wave coinciding with one cycle of an underlying staircase. The current is sampled twice during each square-wave cycle, once at the end of the forward pulse and again at the end of the reverse pulse. The output current on the resultant voltammogram is the difference between the current sampled at both these points. Swv discriminates against the charging current, as a result of this method of delaying the current measurement until close to the end of the pulse, so that the current remaining is purely Faradaic. This excellent suppression of the background signal enables low detection limits and, in the case of the dimer complexes studied in this section, greater resolution. The cyclic voltammograms for **bpybpy** and **phenphen** are represented in Figures 5.21 and 5.23 respectively, and the square-wave voltammograms for **bpybpy** and **phenphen** are represented in Figures 5.22 and 5.24 respectively.

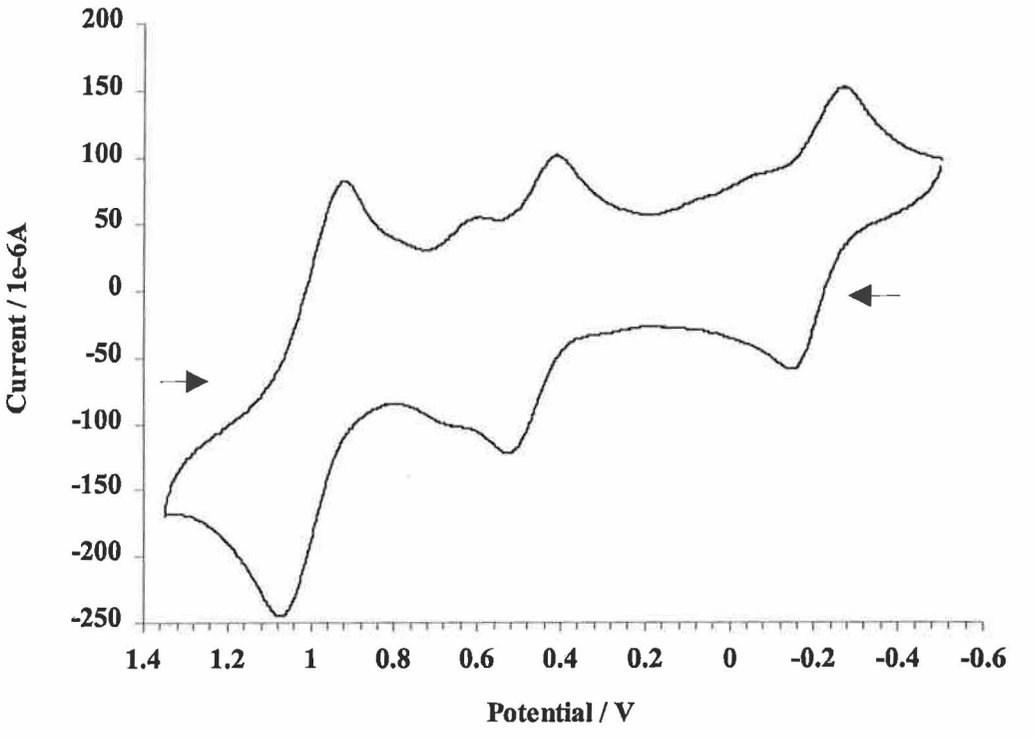

Figure 5.21 *Cyclic Voltammogram of **bpybpy** in acetonitrile with 0.1 M TEAP cycled in the direction shown starting from -0.6 V (scan rate : 500mVS^{-1}).*

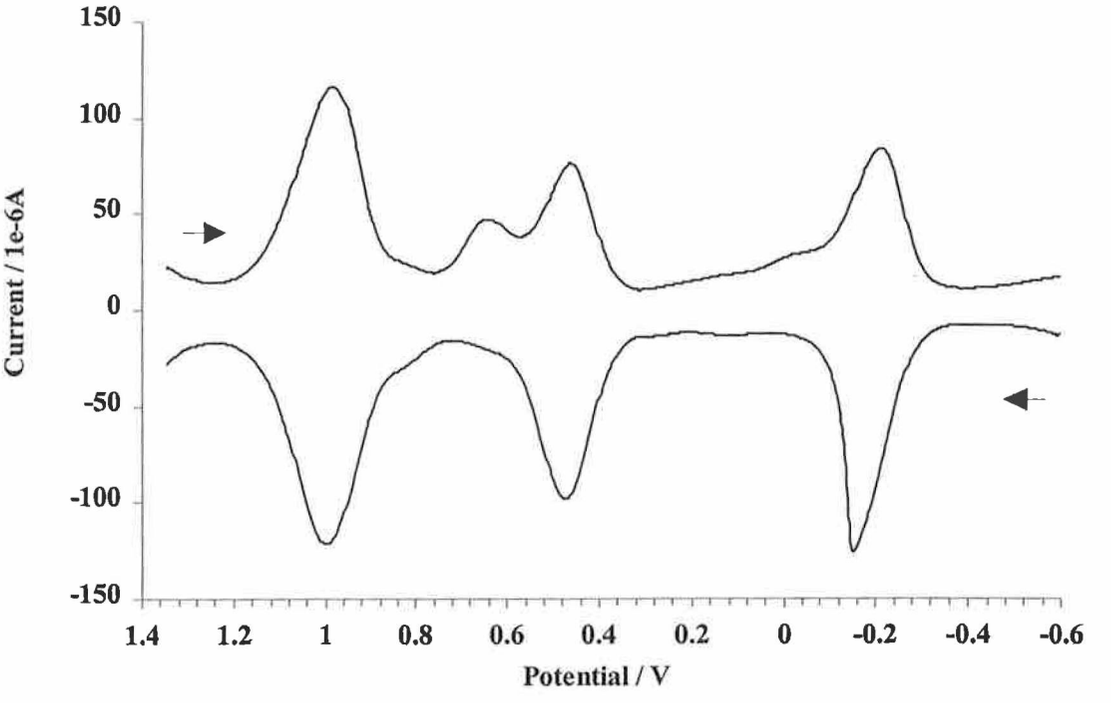

Figure 5.22 *Square-Wave Voltammogram of **bpybpy** in acetonitrile with 0.1 M TEAP swept in the directions shown (scan rate : 500mVS^{-1}).*

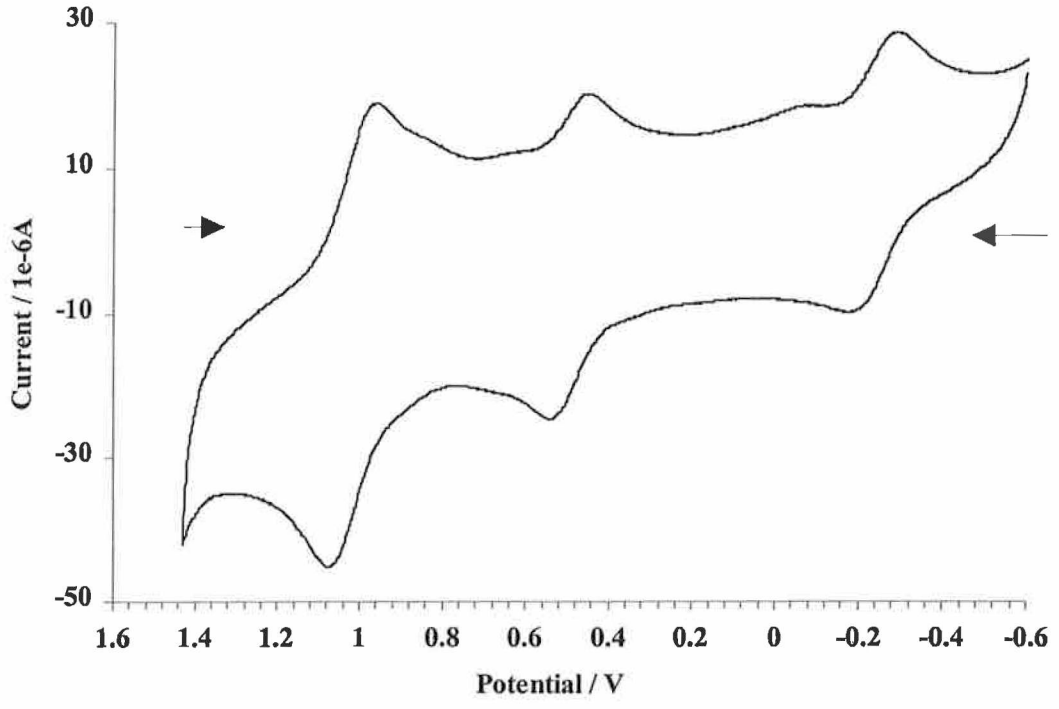

Figure 5.23 *Cyclic Voltammogram of **phenphen** in acetonitrile with 0.1 M TEAP cycled in the direction shown starting from -0.6 V (scan rate : 500mVS^{-1}).*

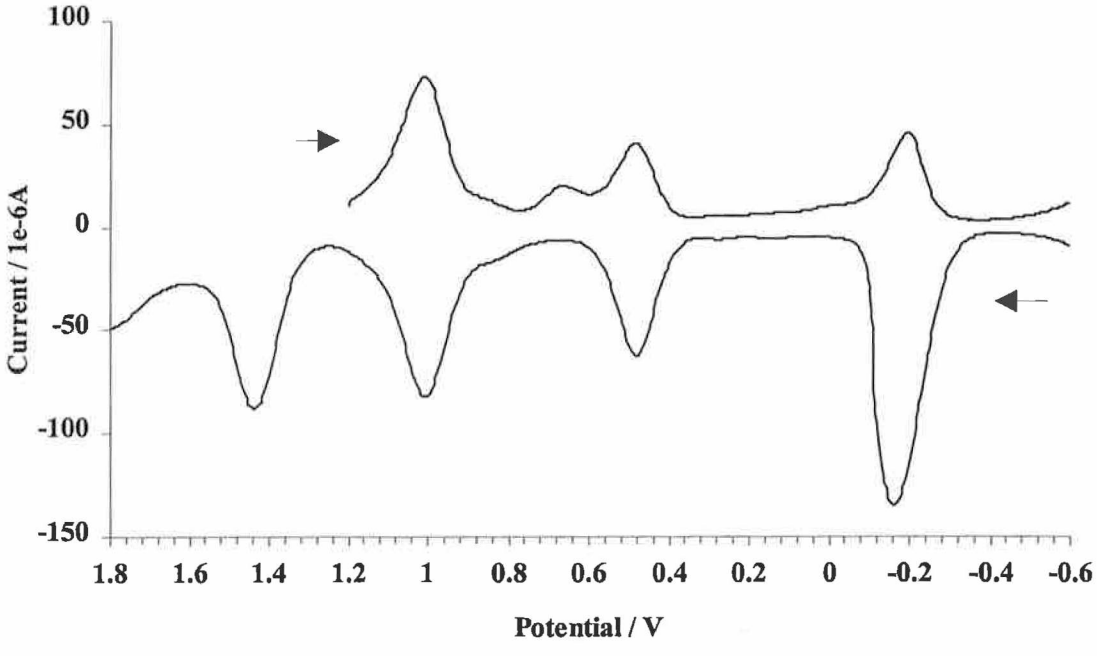

Figure 5.24 *Square-Wave Voltammogram of **phenphen** in acetonitrile with 0.1 M TEAP swept in the directions shown (scan rate : 500mVS^{-1}).*

Table 5.3 *Cyclic Voltammetry Electrochemical data for the dinuclear complexes of H_3L2 in V vs Ag/AgCl. All the measurements were carried out in neutral acetonitrile with 0.1 M TEAP (scan rate : 500mVS^{-1}).*

Complex	Oxidation Potentials/V		Reduction
	Ru(II) / Ru(III) (N,N bound)	E_{redox} (ligand)	Potentials/V
bpybpy	1.00	-0.20, 0.47	*
phenphen	1.02	-0.25, 0.49	*

Table 5.4 *Square Wave Voltammetry Electrochemical data for the dinuclear complexes of H_3L2 in V vs Ag/AgCl. All the measurements were carried out in neutral acetonitrile with 0.1 M TEAP. Note for negative potentials degassing was necessary.*

Complex	Oxidation Potentials/V		Reduction
	Ru(II) / Ru(III) N,N bound	E_{redox} (ligand)	Potentials/V
bpybpy	0.99	-0.18, 0.47	-1.47, -1.73, -1.98
phenphen	1.00 1.46 (O,O bound)	-0.18, 0.48	-1.40(irr), 1.71(irr) -1.99(irr)

The cyclic voltammetry electrochemical data of the dimer complexes are presented in Table 5.3 and the comparable square-wave voltammetry electrochemical data is presented in Table 5.4. There was no significant difference between the oxidation potentials achieved using both methods, however the square-wave voltammograms were better resolved and the reduction potentials for the bipyridine and phenanthroline ligands respectively, could be deduced. Since catechols, semiquinones and quinones are members of a redox series (see section 5.0 and Figure 5.4) a rich electrochemistry exists for dioxolene complexes. Electrochemical activity of dioxolene complexes may involve the dioxolene ligand, the metal, or both and it can often be difficult to disentangle these. Lever et al have performed extensive studies on semiquinone-quinone redox species involving bis(bipyridine)ruthenium (II) whereby the ruthenium is O,O bound[14,15,29]. Evidence was presented in these studies that oxidation of the dioxolene ligand to quinone occurs before oxidation of Ru(II) to Ru(III). Generally speaking four redox couples were observed corresponding to bpy/bpy$^-$, sq/cat, q/sq and Ru(III)/Ru(II). The Ru(III)/Ru(II) process does not occur until the dioxolene ligand was oxidised to the quinone level and is irreversible in acetonitrile, preventing preparation and study of a Ru(III)-quinone complex. Similar electrochemical behaviour was attained for dinuclear bis-dioxolene ruthenium (II) complexes, studied by Ward and coworkers[18,19] (see Figure 5.5 and 5.6), however the dinuclear ruthenium (II) complexes with one metal centre N,N bound and the other metal centre O,O bound through a 1,2 dioxolene ligand, provide the most similar system to that of our complexes[6,7,20].

The cv of the complex **bpybpy** (see Figure 5.21) shows three one-electron couples in the region (1.4 to -0.6 V) which are assigned as cat/sq (-0.2 V), sq/q (0.47 V) and Ru(II)/Ru(III) (1.0 V). This Ru(II)/Ru(III) oxidation wave is associated with the

N,N bound metal centre. There is also a noticable small oxidation wave at 0.67 V with an associated reduction wave at 0.61 V (only the reduction wave at 0.64 V is noticable in the SWV). This process may due to the second oxidation (sq/q) whose reversibility could be dependent on scan rate and the appearance of such a product wave suggests that the oxidised product undergoes a subsequent chemical reaction[10]. Similarly the cv of the complex **phenphen** (see Figure 5.23) can be interpreted as three one-electron couples, cat/sq (-0.25 V), sq/q (0.49 V) and Ru^{II}/Ru^{III}(1.00 V). As with **bpybpy** this Ru^{II}/Ru^{III} wave is associated with the N,N bound metal centre. In SWV of **phenphen** (see Figure 5.24) there is a product wave at 0.66 V in the reduction scan which, similarly to **bpybpy**, may be associated with the second oxidation process (sq/q). The effect of this process is also evident from the SWVs of the complexes indicate by the magnitude of the peaks in the reduction sweep (from 1.2 V to -0.6) compared with those The second metal-centre for both **bpybpy** and **phenphen** was irreversible and very anodic and their oxidation potentials could not be established. This is associated with the O,O bound metal centre from the $[Ru(L)_2(sq)]^+$ fragment[15,20] (where L= bpy or phen). However the square-wave voltammetry for **phenphen** (see Figure 5.24) indicates that the second Ru^{II}/Ru^{III} process occurs at 1.46 V. This could not be established as clearly for **bpybpy** as it is at the limit of the solvent window. Cycling beyond 1.4 V in the cyclic voltammetry of the complexes resulted in loss of resolution of the reduction peaks associated with the oxidation processes prior to 1.4 V.

The polypyridine-centred reductions occur at extreme negative potentials of -1.4 V and lower and were unresolved by cyclic voltammetry. This is probably due to surface effects at negative potentials where it is more likely to passivate the electrode due to small impurities in the electrolyte and solvent and due to interference by water.

Square-wave voltammetry proved much more successful in the resolution of the polypyridine-centred reductions although none of the reduction processes were fully reversible. The values quoted in Table 5.4 are the reduction potentials when swept from -0.6 V to -2.0 V. In the swv of **bpybpy** three waves appear representing the reduction of four phenanthroline ligands. The wave at -1.47 V probably represents a convolution of two waves. Likewise in the swv of **phenphen** three waves appear with the wave at -1.71 probably a convolution of waves. In both complexes the return square-wave voltammograms (-2.0 V to -0.6 V) do not have the same intensity, indicating that the polypyridine-centred reductions are not very reversible.

5.2.5. Spectroelectrochemical studies.

The spectroelectrochemical studies are performed on the dimer complexes in order to obtain further information about the nature of the redox changes and their effects on the electronic spectra of the complexes. The technique was described in chapter two (section 2.7) and the diagram of the OTTLE cell used in the experiment is shown in Figure 2.1. Similar effects are seen for both dimer complexes and the respective spectra are presented in Figures 5.25-5.28. The UV-Vis spectra are recorded at potentials approaching and after the first and second oxidation processes (assigned in section 5.2.4 as sq/q and Ru^{II}/Ru^{III} processes respectively) and the spectra shown are those when no further changes occur at those respective potentials. In Figure 5.25 the spectroelectrochemistry of $[Ru(bpy)_2(L2)Ru(bpy)_2]^{2+}$ in neutral acetonitrile containing 0.1 M TEAP at potentials of 0.1V, 0.7V and 1.2V is shown. At 0.1 V the complex is in

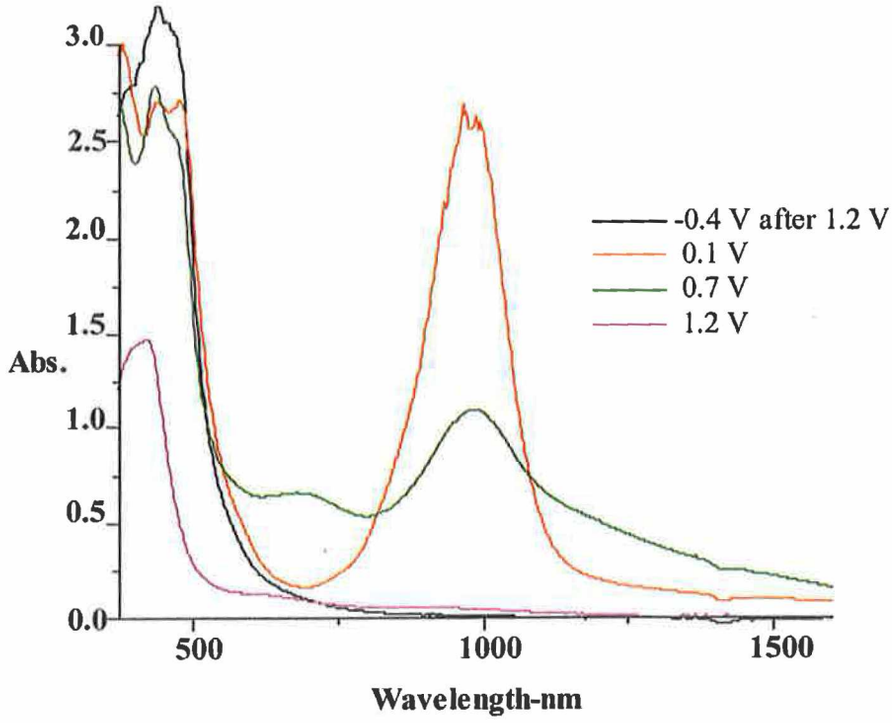

Figure 5.25 *Spectroelectrochemistry of $[Ru(bpy)_2(L2)Ru(bpy)_2]^{2+}$ in neutral acetonitrile containing 0.1 M TEAP, at potentials of 0.1V, 0.7V and 1.2V and returned to 0.2V .*

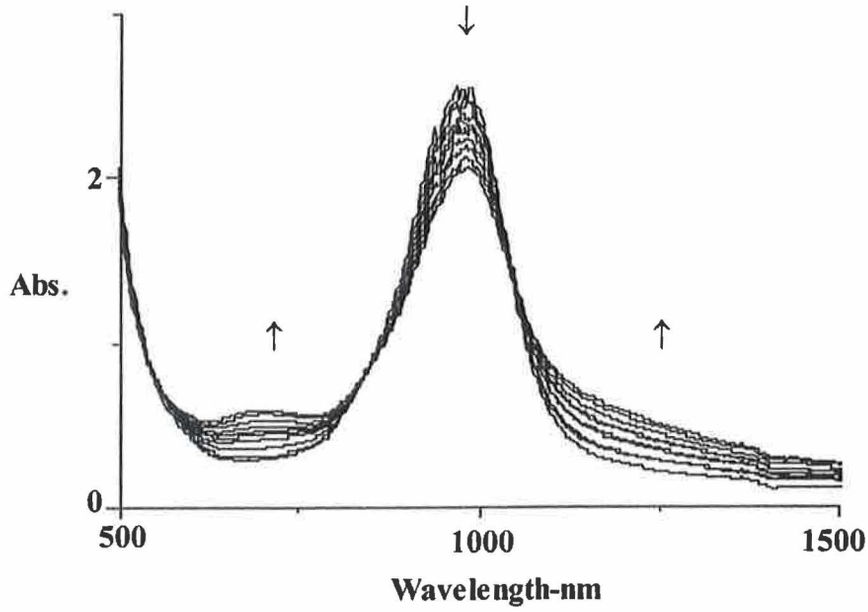

Figure 5.26 *Spectral changes of $[Ru(bpy)_2(L2)Ru(bpy)_2]^{2+}$ in neutral acetonitrile containing 0.1 M TEAP, for oxidative spectroelectrochemistry between 0.0V and 0.5V.*

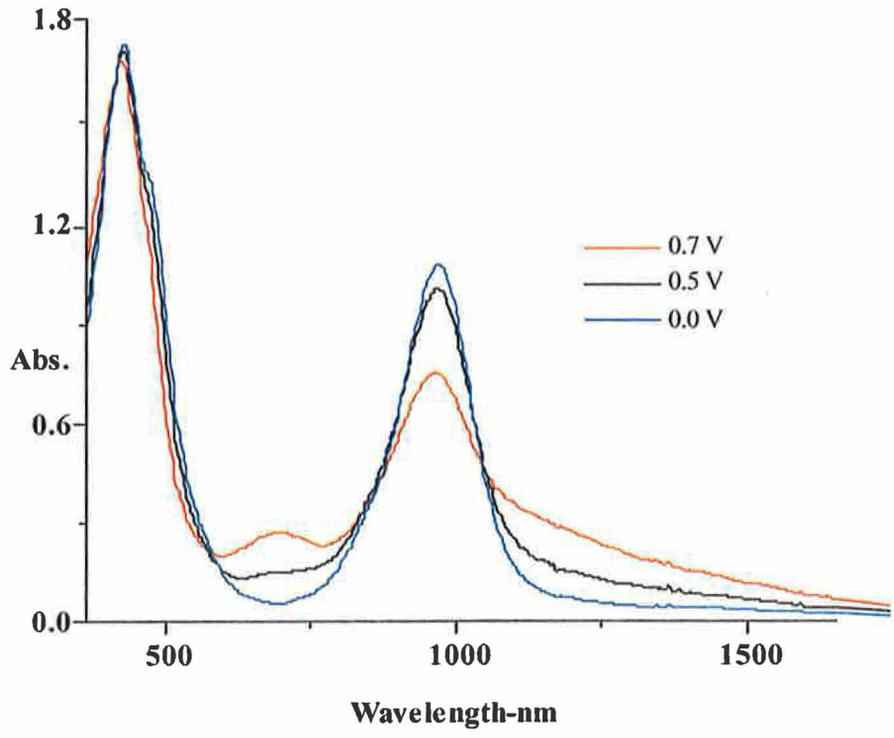

Figure 5.27 *Spectroelectrochemistry of $[Ru(phen)_2(L2)Ru(phen)_2]^{2+}$ in neutral acetonitrile containing 0.1 M TEAP, at potentials of 0.0V, 0.5V and 0.7V.*

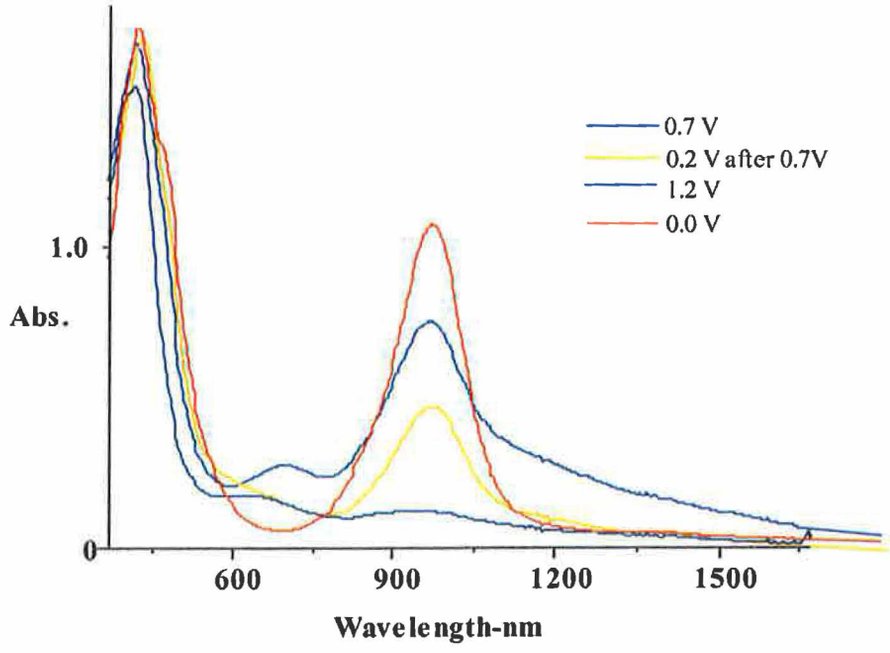

Figure 5.28 *Spectroelectrochemistry of $[Ru(phen)_2(L2)Ru(phen)_2]^{2+}$ in neutral acetonitrile containing 0.1 M TEAP, at potentials of 0.0V, 0.7V, 1.2V and returned to 0.2V.*

At 0.7 V the first oxidation process (sq/q) of the complex dramatically alters the UV-Vis spectrum. The λ_{max} of the Ru(II) $\rightarrow$ (bpy)π^* MLCT transition is blue shifted by about 30 nm and the Ru(dπ) $\rightarrow$ sq(π^*) transition at 975 nm (see Table 5.1) is reduced in intensity and two new features appear at 666 nm and around 1183 nm. The work of Lever and co-workers[15] on the catechol-quinone redox series involving bis(bipyridine) ruthenium (II) provides an important indicator of the nature of the transitions observed in the UV-Vis spectrum of **bpybpy** at 0.7 V. In the complex $[Ru^{II}(bpy)_2(q)]^{2+}$ (compared with $[Ru^{II}(bpy)_2(sq)]^{+}$) the Ru(II) $\rightarrow$ (bpy)π^* MLCT transition is shifted to higher energy and this is attributed to the fact that the dioxolene ligand in the quinone state is more electronegative than in the semiquinone state. Thus as a result of oxidation to the quinone, the Ru(II) $\rightarrow$ (bpy)π^* MLCT shifts to the blue due to the stabilisation of the t_2g level when the σ-donating capacity of the ligand is decreased. Also in $[Ru^{II}(bpy)_2(q)]^{2+}$ there is a strong band near 667 nm which is associated with the expected Ru(dπ) $\rightarrow$ q(π^*) MLCT transition[15]. The similarity between these features reported by Lever et al with those observed in Figure 5.27 for **bpybpy** is clear. As the dioxolene ligand is oxidised from semiquinone to quinone one would expect the reduction in the intensity of the Ru(dπ) $\rightarrow$ sq(π^*) transition and the growth of the Ru(dπ) $\rightarrow$ q(π^*) transition. The fact that the Ru(dπ) $\rightarrow$ sq(π^*) transition does not completely disappear may be attributed to the fact that the oxidation of the dioxolene may not be complete at 0.7 V. Joulié et al reported on the spectroelectrochemistry of binucleating bis catechol complexes (see Figure 5.5) which also showed similar changes in the UV-Vis spectra when the sq-sq complex was oxidised to the q-q complex[18]. The Ru(dπ) $\rightarrow$ sq(π^*) transition at 1225 nm disappears and is replaced by a Ru(dπ) $\rightarrow$ q band at 750 nm. In Figure 5.26 the Spectral changes of **bpybpy** for oxidative

spectroelectrochemistry between 0.0V and 0.5V is shown. This basically shows the growth of the band at 667 nm, the reduction in the intensity of the band at 975 and the increased tailing at around 1183 nm as the potential approaches that of the oxidation of **bpybpy** from semiquinone to quinone. The increased tailing around 1183 nm is in the region where $q(\pi) \rightarrow bpy(\pi^*)$ intra-ligand (ILCT) transitions may be expected to occur[10,15,18].

The effect on the spectral features of **bpybpy** after the oxidation of the metal from Ru(II) to Ru(III) is even more dramatic than the dioxolene oxidation. The transitions at 975 nm, 667 nm and the tailing at 1183 nm have virtually disappeared and the UV-Vis spectrum resembles that of the protonated mononuclear catechol complex while the intensity of the Ru(II) $\rightarrow$ (bpy)π^* MLCT (at 422 nm) is also reduced. There is no evidence of intervalence bands at lower energy. The oxidation of the metal is found to be irreversible considering the fact that none of the features observed at the beginning of the experiment at 0 V were present when the potential was returned to 0 V. In the cyclic voltammetry of **bpybpy** the redox couples cat/sq, sq/q and Ru^{II}/Ru^{III} appear quite reversible however this does not appear to be the case from the spectroelectrochemistry of the complex. This may be due to the fact that the timescale of the experiment is much less in the case of the cyclic voltammetry whereas in the spectroelectrochemical studies the complex is held at a particular potential until no further changes are evident in the UV-Vis spectra. This allows the process that occurs at a particular potential to go to completion whereas at a quick scan rate the cv may suggest that a fully reversible process occurs. It is not entirely sure what actually happens the complex at 1.2 V although it is tentatively suggested that after the first metal oxidation the complex breaks up resulting in the observed loss of reversibility. It is also possible that at 1.2 V

the second metal centre bound through the dioxolene bridge is being oxidised and from the evidence of the cyclic voltammetry and square-wave voltammetry this process is irreversible. Keyes et al reported on the spectroelectrochemistry of dinuclear O,N bound Ru(II) complexes (see Figure 5.2) with a similar redox series to that described for dioxolenes in Figure 5.4[10]. The spectral changes of the complex RuHQRu were reversible for the processes located on the bridge and first metal centre. However oxidising the solution around the second metal centre at 1.6 V gave irreversible responses and the formation of a product with a λ_{max} of 420 nm which was not further identified.

The spectroelectrochemistry of **phenphen** is shown in Figures 5.27 and 5.28. The spectral effects as the oxidation of the complex from semiquinone to quinone are shown in Figure 5.27 and can be explained in a similar fashion to the features observed for **bpybpy**. The fact that isobestic points are maintained in the spectroeclectrochemistry between 0 V and 0.7 V indicates that only one process is taking place. The intensity of the Ru(dπ) → sq(π*) transition at 969 nm is reduced and a new band grows at 696 nm, representative of a Ru(dπ) → q(π*) transition, while the tailing around 1179 nm may be due to intra-ligand (ILCT) transitions. After observing the spectral changes at 0.7 V the potential was returned to 0.2 V (see Figure 5.28) in order to ascertain the reversibility of the semiquinone to quinone oxidation. While the features at 696 nm and the tailing around 1179 nm are diminished, in comparison to the spectrum at 0.7 V, the intensity of the Ru(dπ) → sq(π*) transition at 969 nm is also less than that at either 0 V or 0.7 V. This would indicate that the oxidation from semiquinone to quinone was not fully reversible. At 1.2 V, after the first metal oxidation, the band at 969 nm has almost disappeared and the tailing around 1179 nm

has also disappeared. This may indicate the breakup of the complex by loss of the second metal centre as the q(π) $\rightarrow$ bpy(π^*) intra-ligand charge transfer (ILCT) around 1179 nm has disappeared and the Ru(dπ) $\rightarrow$ q(π*) band, at 696 nm in the UV-Vis spectrum at 0.7 V, has changed shape and is blue shifted to 638 nm. However the oxidised product was not identified but the process was found to be irreversible. As with the spectroelectrochemistry of **bpybpy** there was no evidence of intervalence bands at lower energy. The loss of isobestic points in Figure 5.28 indicates that more than one process is taking place over the potentials examined (0 V, 0.7 V, 1.2 V) and these processes are not in equilibrium.

5.3 Concluding Comments

Ru-Ru dinuclear complexes have been synthesised and characterised from the mononuclear catechol complexes discussed in chapter four. $[Ru(bpy)_2(L2)Ru(bpy)_2]^{2+}$ **(bpybpy)** and $[Ru(phen)_2(L2)Ru(phen)_2]^{2+}$ **(phenphen)** were prepared by reaction of the mononuclear catechol precursor with a stoichiometric molar equivalent of the respective dichloride and the reactions were followed by analytical HPLC and the complexes purified by semipreparative HPLC. The complexes were characterised by elemental analysis, HPLC and electrospray ionisation mass spectrometry (ESI-MS). Subsequently the electronic, electrochemical and spectroelectrochemical properties were examined.

The electronic features of the complexes **bpybpy** and **phenphen** are summarised in Table 5.1 and 5.2. In **bpybpy** the electronic spectrum of the deprotonated complex and neutral complex were similar with the most significant features the MLCT transition at 477 nm and the Ru(dπ) → semiquinone(π^*) MLCT transition at 971 nm. Their assignment was confirmed by spectroelectrochemistry. The similarity in the neutral and deprotonated spectra confirm that the complex is in the semiquinone state which was already established by elemental analysis and ESI-MS spectra. These MLCT transitions were blue shifted in the protonated spectra. Similar effects were seen in the electronic spectra of **phenphen**. **Bpybpy** and **phenphen** exhibited very weak emission at room temperature in neutral or basic acetonitrile which may be associated with quenching of the excited state by the $^3O_2$ of the semiquinone. The protonated spectra exhibited an increase in intensity, and were blue shifted in comparison to the neutral and deprotonated spectra, which was substantiated at 77 K. This may be indicative of

decomposition of the complex in acidic media with the more intense resultant emission comparable to the emission λ_{max} of the mononuclear catechol complexes.

The electrochemical properties of the complexes were typical of semiquinone bound dinuclear ruthenium complexes. **Bpybpy** showed three couples in the region (1.4 to -0.6 V) which were assigned as cat/sq (-0.2 V), sq/q (0.47 V) and Ru(II)/Ru(III) (1.0 V). Similarly the cv of the complex **phenphen** can be interpreted as cat/sq (-0.25 V), sq/q (0.49 V) and Ru(II)/Ru(III) (1.00 V). The second metal-centre for both **bpybpy** and **phenphen** were irreversible and very anodic. Spectroelectrochemical studies suggest an irreversible Ru(III)-quinone complex is formed at potentials greater than 1.2 V.

5.4 References

1 L. Sun, H. Berglund, R. Davydov, T. Norrby, L. Hammarström, P. Korall, A. Börje, C. Philouze, K. Berg, A. Tran, M. Andersson, G. Stenhagen, J. Mårtensson, M. Almgren, S. Styring, B. Åkermark, *J. Am. Chem Soc.*, 1997, 119, 6996.

2 S. Bodige, A.S. Torres, D.J. Maloney, D. Tate, G.R. Kinsel, A.K. Walker, F.M. MacDonnell, *J. Am. Chem Soc.*, 1997, 119, 10364.

3 M.D. Hossain, M. Haga, H. Monjushiro, B. Golamkhass, K. Nozaki, T. Ohno, *Chem. Lett.*, 1997, 573.

4 M. T. Indelli, F. Scandola, L. Flamigni, J.-P. Collins, J.-P. Sauvage, A. Sour, *Inorg. Chem.*, 1997, 36, 4247.

5 G.D. Storrier, S.B. Colbran, D.C. Craig, *J. Chem Soc.,Dalton Trans.*, 1997, 3011.

6 B. Whittle, N.S. Everest, C.A. Howard, M.D. Ward, *Inorg. Chem.*, 1995, 34, 2025-2032.

7 C.A. Howard, M.D. Ward, *Angew. Chem. Int. Ed. Engl.*, 1992, 31, No.8, 1028.

8 V. Balzani and F. Scandola, *SupramolecularPhotochemistry*; Horwood: Chichester, UK 1991.

9 S. Ernst, P. Hänel, J. Jordanov, W. Kaim, V. Kasack, E. Roth, *J. Am. Chem. Soc.*, 1989, 111, 1733.

10 T. E. Keyes, R.J. Forster, P.M. Jayaweera, C.G. Coates, J.J. McGarvey, J.G. Vos, *Inorg. Chem.*, 1998, 37, 5925.

[11] T.E. Keyes, P.M. Jayaweera, J.J. McGarvey, J.G. Vos, *J. Chem. Soc, Dalton Trans.*, 1997, 1627.

[12] W.P. Griffith, *Trans. Met. Chem.*, 1993, 18, 250.

[13] A. Dei, D. Gatteschi, L. Pardi, *Inorg. Chem.*, 1990, 29, 1442.

[14] A.B.P. Lever, P.R. Auburn, E.S. Dodsworth, M. Haga, W. Liu, M. Melnik, W.A. Nevin, *J. Am. Chem. Soc.*, 1988, 110, 8076.

[15] M. Haga, E.S. Dodsworth, A.B.P. Lever, *Inorg. Chem.*, 1986, 25, 447.

[16] R.S. da Silva, E. Tfouni, A.B.P. Lever, *Inorg. Chim. Acta*, 1995, 235, 427.

[17] R.B. Salmonsen, A. Abelleira, M.J. Clarke, *Inorg. Chem.*, 1986, 23, 447.

[18] L.F. Joulié, E. Schatz, M.D. Ward, F. Weber, L.J. Yellowlees, *J. Chem. Soc., Dalton Trans.*, 1994, 799.

[19] A.M. Barthram, R.L. Cleary, J.C. Jeffery, S.M. Couchman, M.D. Ward, *Inorg. Chim. Acta*, 1998, 267, 1.

[20] A.D. Shukla, B. Whittle, H.C. Bajaj, A. Das, M.D. Ward, *Inorg. Chim. Acta*, 1999, 285, 89.

[21] A. Helms, D. Heiler, G. McLendon, *J. Am. Chem. Soc.*, 1992, 114, 6227.

[22] A. Helms, D. Heiler, G. McLendon, *J. Am. Chem. Soc.*, 1991, 113, 4325.

[23] K.R. Seddon, E. Seddon, *The Chemistry of Ruthenium*, Elsevier, Amsterdam, 1984.

[24] ESI-MS samples were performed at the University of Jena, Germany with the co-operation of Sven Rau (see chapter two).

[25] S.A. Hoftstadler, R. Bakhtiar, R. D. Smith, *J. Chem. Educ.*, 1996, 73, A82-A88.

[26] V.K. Katta, S.K. Chowdhury, B.T. Chait, *J. Am.Chem. Soc.*, 1990, 112, 5348.

[27] T.E. Keyes, Ph.D. Thesis, Dublin City University, 1995.

[28] E.M. Kober, T.J. Meyer, Inorg. Chem., 1982, 21, 3967.

[29] D.J. Stufkens, TH.L. Snoeck, A.B.P. Lever, *Inorg. Chem.*, 1988, 27, 953.

Chapter Six

Investigation of the Complexation of Transition Metals by a Ruthenium Mononuclear Complex Containing a Catechol Binding Site

6.0 Introduction

The coordination chemistry of o-quinone ligands, primarily catechols, has been a subject of interest since the beginning of the last century. This has led to detailed studies on the composition and properties of quinone complexes many of which were summarised by W.P. Griffith in 1993 in an article entitled "Recent advances in dioxolene chemistry"[1]. In this article reviews are presented of the chelation of various 1,2-dioxolene ligands with several transition metals such as vanadium, molybdenum, tungsten, manganese, technetium, rhenium, iron, ruthenium, osmium, cobalt, nickel and copper. Catechol (benzene-1,2-diol), perhaps the best known and most studied dioxolene ligand, is often referred as a "non-innocent ligand" and can coordinate to metal atoms in the dianionic catecholato mode, the monoanionic semiquinonate or the neutral quinone mode. Electrochemical interconversion of these forms can occur by either one or two electron processes whereby complexes containing quinone ligands can undergo two electron transfer steps per quinone[2]. Dioxolene type ligands play a very important role in biological chemistry, with the siderophoric ligand chemistry in the body, as the neurotransmitting catecholamines and as 'phenolics' in plant tissues[3,4].

Siderophores are a class of low molecular weight chelating agents, which are manufactured by microorganisms, in response to an iron deficiency, and which facilitate uptake of iron into the organisms[5]. Iron is an essential nutrient for all pathogenic bacteria due to the fact that the availability of iron often limits the rate of bacterial growth. An important siderophore is enterobactin (see Figure 6.1), the siderophore for enteric bacteria, and the chelating moieties in enterobactin are catechol groups. The

interest in the coordination chemistry of enterobactin has led to the study of simpler catechol complexes as models for the more complicated biological molecules[5].

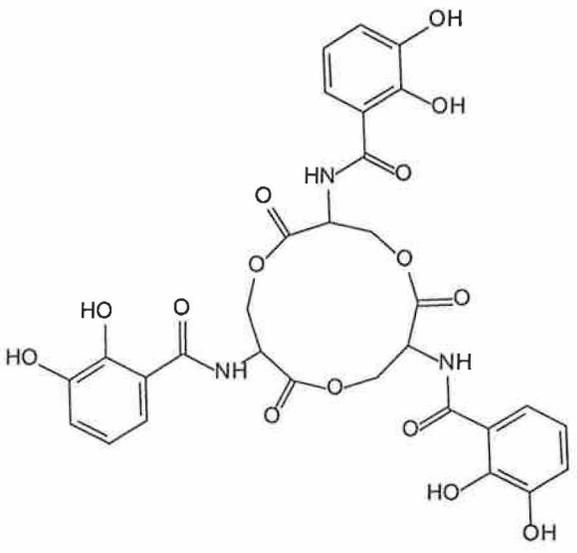

Figure 6.1 Structural diagram of enterobactin, the siderophore for enteric bacteria.

Enterobactin is a tricatechol and is estimated to have an overall formation constant (β) (see equation 6.1) with ferric ion which is greater than 10^{45}. Examination of the formation constants of ferric complexes with a variety of substituted catechol ligands show that the equilibrium constant for the reaction shown in 6.2, is in the range 10^{40} - 10^{45}.

$$\beta = [Fe(catechol)_3^{3-3q}]/ [Fe^{3+}][\ catechol^{q-}]^3 \qquad (6.1)$$

$$Fe^{3+} + 3\ catechol^{q-} \rightleftharpoons Fe(catechol)_3^{3-3q} \qquad (6.2)$$

This number is enormous by comparison with other oxygen-containing ligands. It predicts, for example, that catechol ligands should readily displace cyanide groups from

ferricyanide and that Fe_2O_3 (rust) should easily dissolve in basic solutions of catechol. This incredibly high affinity for Fe(III) has led to the incorporation of catechol moieties into compounds which can be used as 'Iron chelators' in the treatment of Iron overload in anaemic patients that accumulate toxic levels of iron in the body over time[6]. The method of choice when designing new selective iron chelators is to model compounds on the structures of natural siderophores thus including the highly selective and strong chelating properties of the catechol moieties. It was observed from these studies that catechol and the studied Fe(III) therapeutic chelators show incredibly selective high affinities for Fe(III) ($\beta = 10^{30}$-10^{50}) with much lower affinities for Cu(II) ($\beta = 10^{14}$-10^{25}) , Zn(II) ($\beta = 10^{11}$-10^{17}) , Mg(II) ($\beta = 10^{4}$-10^{7}) and Ca(II) ($\beta = 10^{2.5}$-$10^{4.5}$). Another example of iron chelation therapy by the synthesis of analogues of the enterobactin family was explored by Pecoraro et al[7]. They investigated the removal of iron from both ferritin and serum transferrin (proteins) by various synthetic derivatives of catecholate and the iron removal was monitored by measuring the iron content of the protein or ligand-Fe complex spectrophotometrically. Similarly, Lytton et al, presented work on the monitoring of Fe(III) removal from biological sources using a fluorescent siderophore[8]. Fluorescence was reported to be quenched upon binding of Fe(III) in solutions and Fe(III) mobilisation from cells and quantification was accomplished by dissociation of the siderophore-Fe complex by acidification.

As a result of its biological importance there has been considerable interest over the past several years in the coordination chemistry of various catechol ligands with Iron(III)[9-15]. Much of the work centres on the synthesis of tris(0-semiquinone) complexes and mixed-valence semiquinone-catecholate-iron complexes like those shown in Figure 6.2.

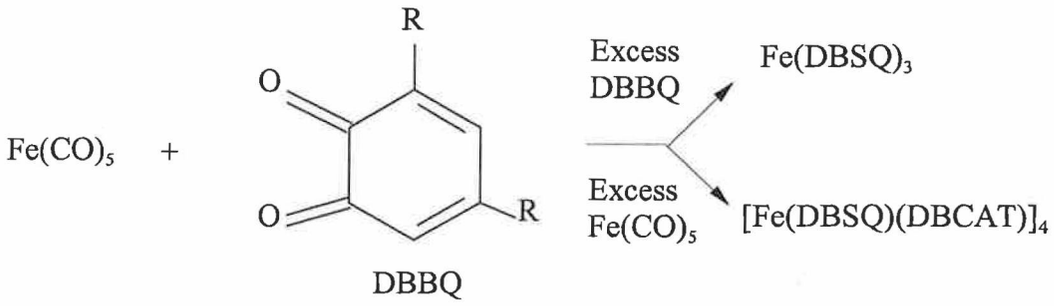

Figure 6.2 *Typical tris(o-semiquinone) and mixed-valence catechol-iron complexes of 3,5-di-tert-butyl benzoquinone (DBBQ)(where R = tertiary butyl)[9].*

When 3,5-di-tert-butyl benzoquinone (DBBQ) was used in excess, in the reaction with $Fe(CO)_5$, the product formed was the green semiquinone complex $Fe(DBSQ)_3$ and when $Fe(CO)_5$ was used in excess the blue mixed-valent semiquinone-catecholate iron complex, $Fe_4(DBSQ)_4(DBCat)_4$ was obtained.

Manipulation of the oxidation states of catecholate ligands can also lead to a variety of charged complexes and mixed-valence semiquinone-catecholate-iron complexes. The complex $[Fe(phenSQ)_3]$.phenQ, where phenQ and phenSQ are quinone and semiquinone forms respectively, of 9,10-phenanthrenequinone, reacts with either 2,2′-bipyridine (bpy), 1,10-phenanthroline (phen), or 5,5′-dimethyl-2,2′-bipyridine (dmbpy) to give complexes of the formulation Fe(phenSQ)(phenCAT)(bidentate nitrogen base)[10]. Magnetic exchange interactions between semiquinone radicals and high spin Fe(III) play an important part of the characterisation and investigation of Fe-catechol complex systems however it is beyond the scope of this thesis. Several studies focus on 1:3 Fe(III):catecholate complexes[9,10,14,15]. However there has also been evidence of 1:1 Fe(III):catecholate though these often form dimeric structures such as that reported by Zirong et al (i.e. $[FeCl_2(Cat)]_2^{2-}$)[11,12].

Studies on the coordination complexes of various catechol ligands with Cr(III)[15-18], Cu(II)[19-22], Zn(II)[23], Pt[24,25] and Mn[15] have also been reported. An interesting feature of these compounds is that they show a multielectron redox series based on the electrochemical activity of the ligands rather than the metal ion. The metal ion is kinetically stable and not directly involved in the redox activity, and not until the ligands are in a fully oxidised benzoquinone form does dissociation become a factor[17].

The powerful chelating ability of catecholate type ligands has also been utilised in the developing area of environmental inorganic chemistry[26,27]. It has led to the design of organic ligands, which contain catechol moieties, to selectively remove and recover metal ions from aqueous solution as a function of pH. The ligands are chemically bonded to modified cross-linked macroporous polystyrene-divinylbenzene beads and since diffusion of the metal ions into the hydrophobic polymer macropore phases is so important, it proved necessary to modify the catechol ligands with a hydrophilic group, such as a sulphonic acid substituent, to increase the kinetics and capacities of metal binding in aqueous solution, while also preventing the catechol ligand from being oxidised to the weaker metal binding o-quinone ligand[27].

In Figure 6.3 one of the polymer-supported catechol ligands used by Fish and co-workers is shown. Similar ligands are also investigated along with *PS-2-6-LICAMS* which show a remarkable selectivity for Fe(III) in competition with a similar concentration of Cu(II), Zn(II), Mn(II), Ni(II), Mg(II), Al(III), and Cr(III). The trivalent metal ions for all polymer pendant ligands studied were more readily removed from aqueous solution in comparison to the divalent metal series with the following order of selectivity: Fe(III) > Cr(III) > Al(III).

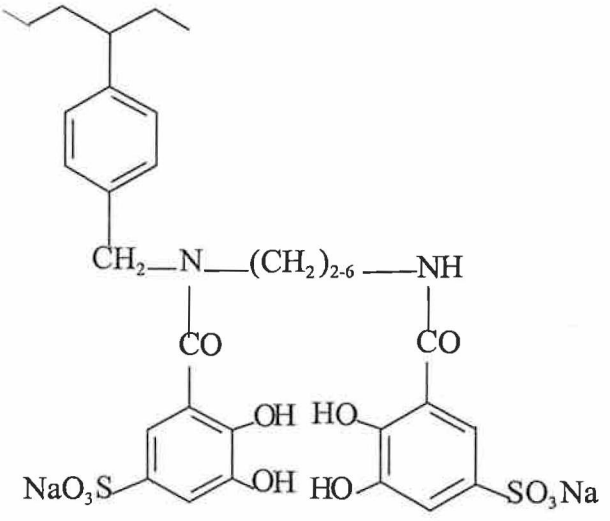

Figure 6.3 *Polymer-Supported Sulphonated bis(catechol) linear amide (Known as **PS-2-6-LICAMS**)*[27].

Manipulation of the pH of the solution (from 2.1 to 3.0) demonstrated that, in the absence of Fe(III) and in the presence of Hg(II), Mg(II), Al(III), Zn(II), Cu(II), Ni(II) and Pb(II) ions, the selectivity of the polymer-supported catechol ligands could be changed to Hg(II). This indicates the wide utility of these polymer pendant ligands for future environmental applications.

In this chapter we explore the chelating abilities of a pyridyltriazole bound ruthenium (II) complex containing a catechol ring (see Figure 6.4). The synthesis and characterisation of the N,N bound Ru(II) catechol complex, $[Ru(bpy)_2(H_2L_2)]PF_6.5H_2O$ **(bpyL2)**, was discussed in detail in Chapter Four. The coordinating power of the catechol moiety of **bpyL2** was demonstrated in Chapter Five where the synthesis and characterisation of **bpybpy,** from the starting complex **bpyL2**, was discussed in detail. This Chapter investigates the coordination of **bpyL2** with the transition metals Fe(III), Fe(II), Cu(II), Cr(III), Ni(II) and Zn(II). As such **bpyL2** becomes the ligand, by virtue of possessing the coordinating catechol moiety, and the formation of $\mathbf{M(bpyL2)_n}$ complexes is followed spectrophotometrically, by absorption and emission titrations.

The absorption and emission titrations were run in tandem. After each addition of a fractional molar equivalent of metal ion solution to a solution of the catechol complex (**bpyL2**), absorption and emission titrations were recorded. In the case of the absorption spectra the data files can be imported onto SIRKO. SIRKO is a program designed for the calculation of equilibrium constants and stability constants by the simultaneous processing of different sets of experimental results[28,29]. Stability constants are not directly measurable but must be calculated from an observed response function of a fixed, but experimentally adjustable, variable by the fitting of calculated values and experimental data. In the case of the emission titrations, the emission data files cannot be imported directly onto SIRKO and as a result the input of the intensity values must be carried out manually. A more detailed description of SIRKO and the method of calculation will be discussed in section 6.2. The stoichiometry of the reaction between the catechol complex (**bpyL2**) and the metal ion (M), the value of n in the complex formulation $\mathbf{M[bpyL2]_n}$, is predicted from the most suitable fit, with regard to errors and closeness of the fit to the measured values. Estimation of the stability constants from the absorption titrations is performed by selecting wavelengths where there appears to be the greatest degree of change in absorption units. Similarly stability constants are estimated from the emission titrations at a wavelength where the greatest change in intensity occurs (usually around the λ_{max} of intensity).

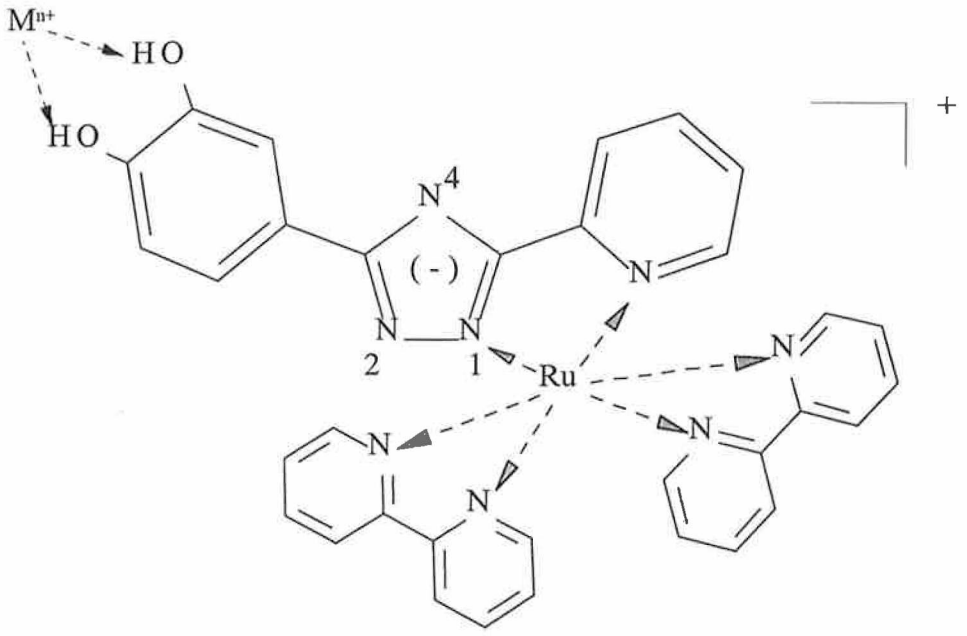

Figure 6.4 *Structure of $[Ru(bpy)_2(H_2L_2)]^+$ (**bpyL2**) cited in the text indicating the catechol coordinating site where the transition metals (M^{n+}) would be expected to bind (see chapter four for synthesis and characterisation of **bpyL2**).*

6.1 Experimental

6.1.1. Preparation of catechol and metal ion solutions.

HPLC-grade methanol was the solvent used in the preparation of all the catechol and metal ion solutions used in the spectrophotometric titrations.

bpyL1

0.0043g of $[Ru(bpy)_2(L1)]PF_6.H_2O$ was dissolved in 100 cm^3 of methanol to prepare a 5 X 10^{-5} M of **bpyL1**.

bpyL2

0.0045g of $[Ru(bpy)_2(H_2L_2)]PF_6.5H_2O$ was dissolved in 100 cm^3 of methanol to prepare a 5 X 10^{-5} M solution of catechol complex.

$[Ru(bpy)_3](PF_6)_2$

0.0038g of $[Ru(bpy)_3](PF_6)_2$ was dissolved in 100 cm^3 of methanol to prepare a 5 X 10^{-5} M solution of $[Ru(bpy)_3](PF_6)_2$.

Metals

Titrations were carried out by the addition of 10 μL (0.2 molar equivalents) of a 0.003 M solution of the metal ion, in HPLC-grade methanol, to 3 cm^3 of the catechol complex (5 X 10^{-5} M in methanol). The metal salts used were $FeCl_3$, $FeCl_2.4H_2O$, $Cu(NO_3)_2.3H_2O$, $CrCl_3.6H_2O$, $Ni(CH_3CO_2)_2.4H_2O$ and $Zn(CH_3CO_2)_2.2H_2O$.

6.1.2. Spectrophotometric titrations.

In order to ascertain the excitation wavelength required for each specific catechol : metal emission titration it was necessary initially to perform an absorption titration in isolation. The wavelength chosen for excitation should be close to the λ_{max} but at a point where there is no change in absorption units throughout the duration of the absorption titration in order to ensure that the changes during the emission titration reflect the reaction between the catechol and the metal. Once the excitation wavelength has been determined the absorption and emission titrations are performed at the same time. The following excitation wavelengths were used in the emission titrations of (a) **bpyL1**, (b) **bpyL2** and (c) **$[Ru(bpy)_3](PF_6)_2$** with the following transition metals.

Fe(III): (a) 462 nm, (b) 470 nm, (c) 475 nm;

Fe(II): (a) 490 nm, (b) 452 nm, (c) 475 nm;

Cu(II): (a) 490 nm, (b) 465nm;

Cr(III): (b) 460 nm; Ni(II): (b) 490 nm; Zn(II): (b) 490nm.

Titration Procedure:

3 cm^3 of **bpyL2, bpyL1** or **$[Ru(bpy)_3](PF_6)_2$** (5 X 10^{-5} M) in methanol was accurately measured into a clear-sided quartz cuvette containing a magnetic stirrer and sealed with a cuvette cover. Absorption and emission spectra of this solution provide us with the spectra of **bpyL2, bpyL1** or **$[Ru(bpy)_3](PF_6)_2$** before any metal ion solution was added. After the initial scan, a series of 0.2 molar equivalents of the metal ion in methanol (0.003 M) was added to the cuvette by micropipette (each 0.2 molar equivalent required 10 μL of the 0.003 M metal solution). The micropipette was calibrated by accurately

weighing 0.01g of water (density of water 1 g/cm^{-3}). The cuvette was covered and allowed to stir for one minute. Then the absorption spectrum was recorded followed by the emission spectrum (once the excitation wavelength has been established). This procedure was repeated several times to ensure that sufficient data points are available for subsequent analysis using SIRKO.

6.2 Results and Discussion.

6.2.1. Blank titrations.

Blank titrations were performed to assess the effect of dilution throughout the spectrophotometric titrations and to ensure that the changes observed in the absorption and emission titrations were due to complexation and not as a result of dilution. In this case 3 cm^3 of **bpyL2** (5 X 10^{-5} M) was titrated with several additions of 10 μL of pure methanol and the absorption and emission spectra were recorded after each addition. The absorption spectra are presented in Figure 6.5 and the emission spectra in Figure 6.6. The effect of dilution is clear from both with little change in the spectra. There is no shift in λ_{max} and no isobestic points. Figures 6.5 and 6.6 show that no significant changes occur in absorption or emission respectively.

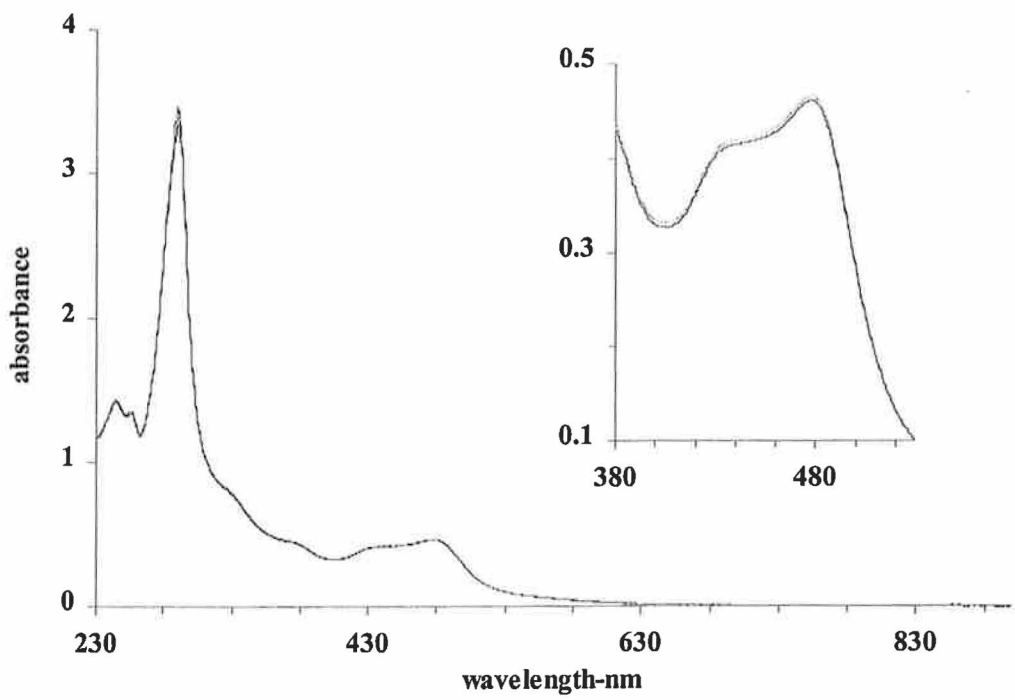

Figure 6.5 *Blank absorption Titration of a 3 cm^3 solution of 5 X 10^{-5} M* ***bpyL2*** *in methanol with 0,10,20,30,40 and 50 μL methanol.*

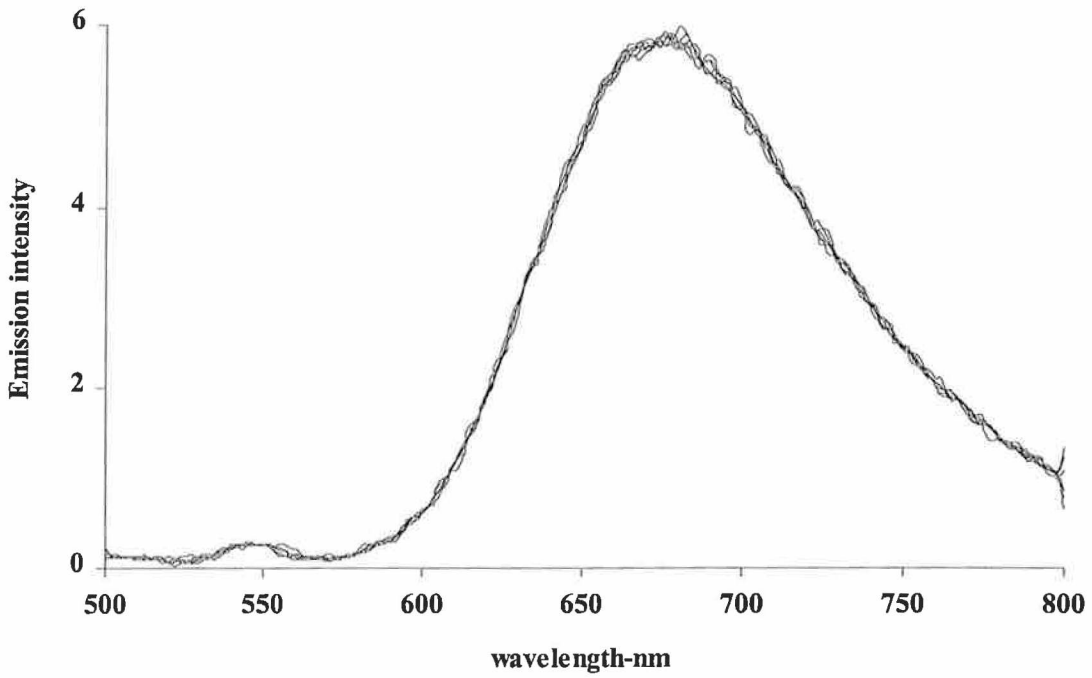

Figure 6.6 *Blank Titration of a 3 cm^3 solution of 5 X 10^{-5} M* ***bpyL2*** *in methanol with 0,10,20,30,40 and 50 μL methanol.*

6.2.2. Absorption and Emission titrations.

6.2.2.1. Use of SIRKO in the calculations.

Calculation of equilibrium constants / stability constants can be performed with various kinds of data. In our case a set of reagents was titrated and a property of the mixtures was measured at each titration point. The data obtained in this way are termed a *titration curve.* The most common methods employed are spectrophotometry, calorimetry and potentiometry. The data for the complexation titrations of **bpyL2** with various metal ions were obtained from absorption and emission spectra. The absorption spectra can be directly imported as a file directly into SIRKO, with prior selection of the wavelength at which the calculations can be performed. This wavelength was selected on the basis that it was in the area of greatest change, in absorption units, throughout the duration of the titration. In the case of the emission titrations, manual input of data

relating to the emission titration, such as emission intensity at a fixed wavelength, is required. The concentration of the catechol solution (5 X 10^{-5} M) and the metal ion solution (0.003 M) along with the initial volume of the catechol solution (3 cm^3) and the titrated volume of metal ion solution (10 μL) are all required for input.

Any experimentally measured property may be used in SIRKO, if it can be described by the general response function in equation 6.3.

$$F = Y_0 + Y_e \cdot \sum_{k=1}^{S} E_k \cdot [C_k] - Y_l \cdot \lg\left(\sum_{k=1}^{S} EH_k \cdot [C_k] \right) \qquad (6.3)$$

where F is the measured value,

S - number of components in solution

$[C_k]$ - equilibrium concentration of the k-th component

Y_0 - a constant value for a given method, often reflecting the solvent properties

Y_1 - scaling factor for potentiometric methods

Y_e - scaling factor for additive methods, such as spectrophotometry

E_k - physico-chemical parameter of the k-th component for additive methods

Eh_k - parameter of the k-th component for potentiometric methods.

So in equation 6.3 the term $Y_e \cdot \sum_{k=1}^{S} E_k \cdot [C_k]$ describes additive methods such as spectrophotometry while the term $Y_l \cdot \lg\left(\sum_{k=1}^{S} EH_k \cdot [C_k] \right)$ is the part which describes potentiometric methods. So, the response function used in SIRKO can be used to describe practically any type of experiment for measuring stability constants. Thus, for

spectrophotometry one can take Y_1 and EH_I to be zero and then F will represent the optical density of the solution, will reflect the molar indices of absorption (extinction coefficient, $\varepsilon(M^{-1}cm^{-1})$), Y_e is the scaling factor which is 1000 (thus the molar indices appear as 10^{-3}E), and Y_0 the optical density of the solvent. In the case of the emission titrations the value for E_i represents the intensity of the emission and is calculated from equation 6.4.

$$EI = ((\text{Intensity } \mathbf{bpyL2} \text{ at 0 eq})/[\mathbf{bpyL2}]))/1000 \qquad (6.4)$$

where [**bpyL2**] is the concentration of **bpyL2** at the beginning of the titration (5×10^{-5} M).

A significant characteristic of the program is that the variables involved in the general response function (such as Y_0 and E_k) may act both as model parameters and as independent variables. This can be defined by the user. It is rather simple for the user to change a variable between a parameter and an independent variable. Each parameter is defined with a key which can adopt the values 0 or 1. If the value is equal to 0, then the corresponding parameter will not be refined, and thus it acts as an independent variable. If the value is equal to 1, then the corresponding parameter will be refined. In the titrations performed in this study the parameters which can be refined or non-refined are the molar indices of absorption (extinction coefficient (ε / 10^{-3} $M^{-1}cm^{-1}$)) for the absorption titrations and *EI*, emission intensity (see equation 6.4), for the emission titrations. The value of the molar index for **bpyL2** at the selected wavelength of analysis is calculated by the program (from the data file containing the absorption

spectrum of **bpyL2** with no added metal ion solution) and thus is not refined. The molar indices of the metal ion solution can also be calculated by the program (from a data file containing the absorption spectrum of the metal ion solution) and is not refined. The molar index (extinction coefficient) of the newly formed metal-catechol complex, $[\mathbf{M(bpyL2)_n}]$, should be refined as this value is unknown to the user. This will be become clearer later in the discussion, with reference to SIRKO calculations for specific stoichiometric models for the complexation of **bpyL2**. Similar refinement or non-refinement refers of the *EI* values in the emission titrations. The *EI* value (emission intensity) for the metal was not refined and assumed to be zero while the *EI* value for the newly formed complex, $[\mathbf{M(bpyL2)_n}]$, should be refined. Refinement of parameters helps to eliminate systematic errors but they should be treated with caution, because this often makes the differences in models insignificant, and so the refined parameters should be carefully scrutinised. In any case, if some additional parameters correlate strongly with other ones, then its value can be refined experimentally and subsequently used as an independent variable. A stoichiometric model of the system employed in the titrations examined in this section can be represented as follows:

$$n\mathbf{bpyL2} + M = \mathbf{M(bpyL2)_n} \qquad \beta = [\mathbf{M(bpyL2)_n}] / [\mathbf{bpyL2}]^n[M] \quad (6.5)$$

where M is the metal Fe(III), Fe(II), Cu(II), Cr(III), Ni(II) or Zn(II) and β is the stability constant. In the program a value for log β is calculated based on the adaptation of a certain model, dependent on the value of n (see equations in 6.5). The determination of the model is best performed by comparing the calculated errors for different models. It is, therefore, important to try optimisation of constants for a variety of model systems

and to compare the results and errors. For determination of the stability constant and additional parameters (molar indices, initial analytical concentration, e.t.c) the least-squares method for which the best parameters are those which minimise the weighted summation of the squared deviation of the calculated values of the dependent variable from the measured ones. A satisfactory model is one in which the calculated and observed values agree within experimental error. The best model contains only those species whose presence has an appreciable effect on measured observations. A good test of the validity of a model is that the equilibrium constants should be chemically consistent, and have small errors.

6.2.2.2. Absorption spectra of metals and calculation of extinction coefficients.

The calculation of the extinction coefficients of the metals used in the absorption and emission titrations is important. The assessment of the observed changes in the absorption titrations would not be complete without allowing for the possibility of the additive effects from the absorption characteristics of the metal involved in the titration. The extinction coefficients ($\varepsilon \setminus M^{-1}cm^{-1}$) of the metal ions can be calculated both experimentally and by SIRKO and the values obtained from both methods are consistent. As discussed in the previous section 6.2.2.1., the predetermination of the extinction coefficient of the metal ion implies that E_i can be defined as a parameter while in other experiments this value would be used as an independent variable thus increasing the errors involved in the calculation. The experimentally calculated extinction coefficients of the metal ions are presented in table 6.1 and the absorption spectra of some of the metal ions are presented.

Table 6.1 *Extinction coefficients of the metal ions in methanol.*

Metal	ε ($M^{-1}cm^{-1}$)	Wavelength (nm)
$FeCl_3$	540	445
$FeCl_2.4H_2O$	43	472
$Cu(NO_3)_2.3H_2O$	0	450
$CrCl_3.6H_2O$	10	440
$Ni(CH_3CO_2)_2.4H_2O$	40	430
$Zn(CH_3CO_2)_2.2H_2O$	0	475

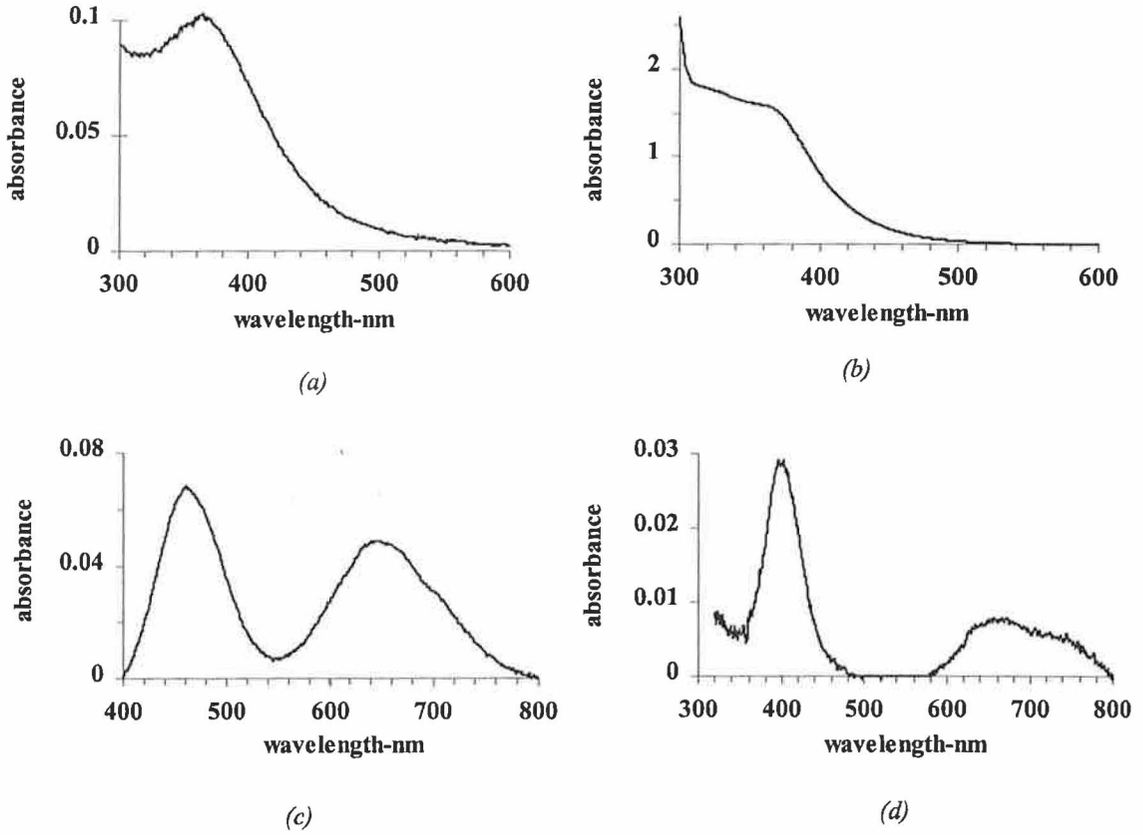

Figure 6.7 *Absorption spectra in methanol of (a) $FeCl_3$ ($9.7 X 10^{-5}$ M)(b) $FeCl_2.4H_2O$ (0.001 M) (c) $CrCl_3.6H_2O$ (0.003 M) (d) $Ni(CH_3CO_2)_2.4H_2O$ (0.003 M).*

$Cu(NO_3)_2.3H_2O$ and $Zn(CH_3CO_2)_2.2H_2O$ do not absorb in the visible and thus are assigned an extinction coefficient of zero at the wavelength at which the SIRKO calculations were performed.

6.2.2.3. Titration of $[Ru(bpy)_3]^{2+}$ with Fe(III) and Fe(II).

The titrations of $[Ru(bpy)_3]^{2+}$ with Fe(III) and Fe(II) respectively (see Figure 6.8 and 6.9), provide important information regarding the possible quenching of the emission of a ruthenium complex by Fe(III) or Fe(II) without actual binding of the metal. The titrations are carried out according to the method described in section 6.1.2. The absorption titrations of $[Ru(bpy)_3]^{2+}$ with Fe(III) and Fe(II) respectively demonstrate only the additive effects of the metal salts. The emission spectra are recorded by excitation at 475 nm where there was no change in the absorbance throughout the duration of the absorption titration between 0 and 5 molar equivalents of titrated Fe(III) or Fe(II). In Figure 6.8 the emission titration of $[Ru(bpy)_3]^{2+}$ with Fe(III) reflects about a 15 % quenching effect after 5 molar equivalents of Fe(III) had been titrated. Fe(III) is a good quencher without binding and quenching of the emission in this case may occur by energy transfer, $[Ru(bpy)_3]^{2+*} + Fe(III) \rightarrow [Ru(bpy)_3]^{2+} + Fe(III)^*$ [30]. The emission titration of $[Ru(bpy)_3]^{2+}$ with Fe(II) displays a similar quenching effect of around 13 %. The implications of the magnitude of the quenching experienced by $[Ru(bpy)_3]^{2+}$ by Fe(III) and Fe(II) without binding are important when assessing the emission titrations of **bpyL1** and **bpyL2** with Fe(III) and Fe(II), respectively. Any quenching effects displayed in these titrations will need to be compared with those experienced in the $[Ru(bpy)_3]^{2+}$ titrations where no binding occurs.

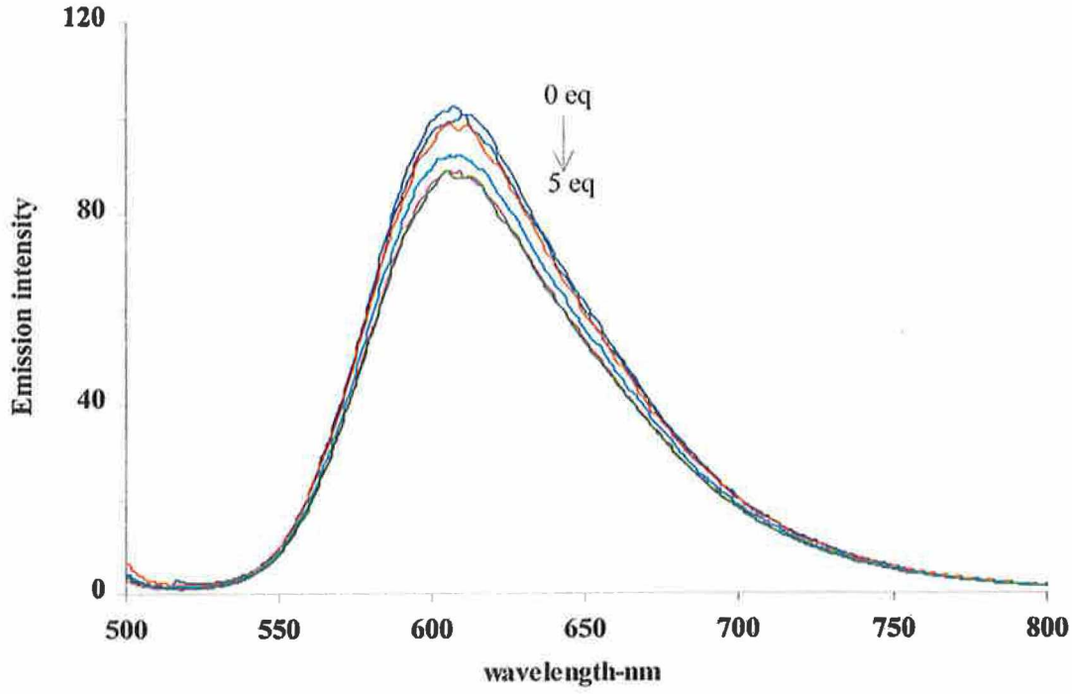

Figure 6.8 ***Emission titration in methanol of $[Ru(bpy)_3](PF_6)_2$ with 0,1,2,3,4,5 molar equivalents of Fe(III).***

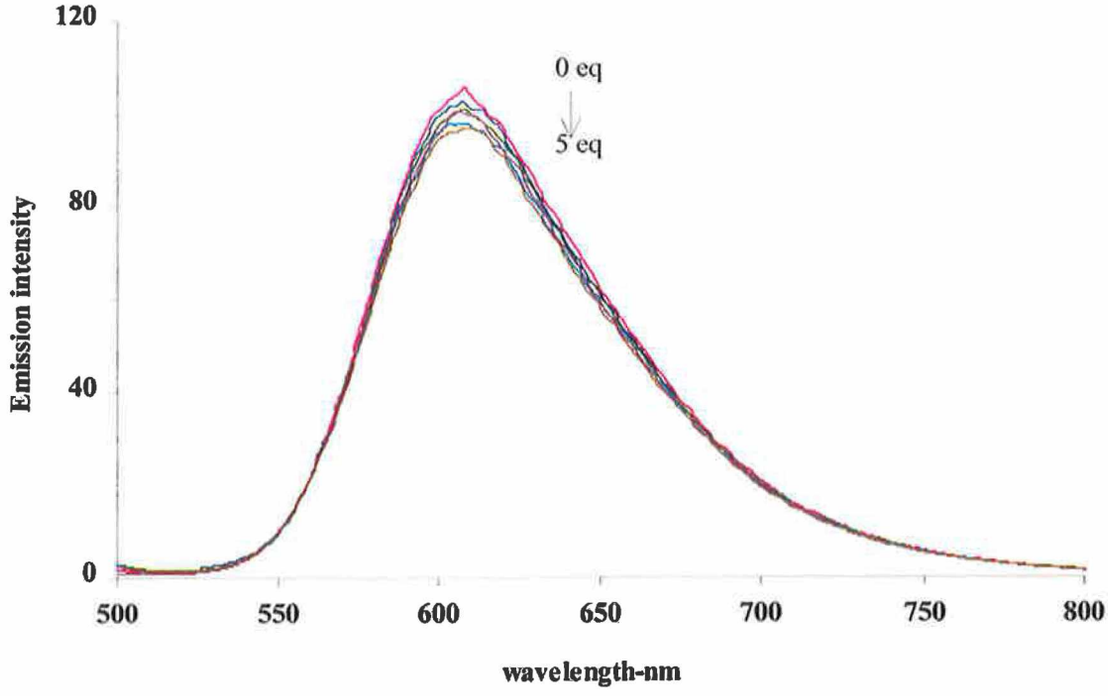

Figure 6.9 ***Emission titration in methanol of $[Ru(bpy)_3](PF_6)_2$ with 0,1,2,3,4,5 equivalents of Fe(II).***

6.2.2.4. Complexation titrations of Fe(III), Fe(II) and Cu(II) with the protected analogue (bpyL1) of the catechol complex bpyL2.

The absorption and emission titrations of the methyl protected catechol complex $[Ru(bpy)_2(L1)]PF_6.H_2O$ (**bpyL1**) (see Chapter 3, Figure 3.2 and Chapter 4, Figure 4.3) with Fe(III), Fe(II) and Cu(II) are presented in this section. These titrations were performed to assess the coordinating properties of the protected catechol complex and to compare the changes observed in the absorption and emission spectra here with those for the catechol complex titrations which will be discussed in sections 6.2.2.5 - 6.2.2.8. The changes observed in the absorption titrations of **bpyL1** with Fe(III) (see Figure 6.24) may have occurred for any of three reasons; protonation of the triazole, binding of Fe(III) through N4 of the triazole or binding of Fe(III) through the protected catechol moiety.

There was a blue shift in the MLCT band between 400-500 nm and an isobestic point at 462 nm, which was maintained for the duration of the titration, and these features are similar to those expected for protonation of the triazole (see Figure 3.21). However in the pH-dependent titration of **bpyL1** there is evidence of isobestic points at 345 nm and 390 nm which do not appear in the absorption titrations of **bpyL1** with Fe(III). The pK_a of **bpyL1** is 4.1 (see Table 3.4) and the titrations were performed in HPLC-grade methanol, which is very dry, suggesting that the possibility of protonating the triazole at these concentrations is less likely. The emission titration of **bpyL1** with Fe(III) (Figure 6.11) indicates that the emission was quenched as the titration proceeded. The issue of protonation of the triazole can be assessed by comparing Figure 6.11 with the pH-dependent emission titration of **bpyL1** shown in Figure 3.23.

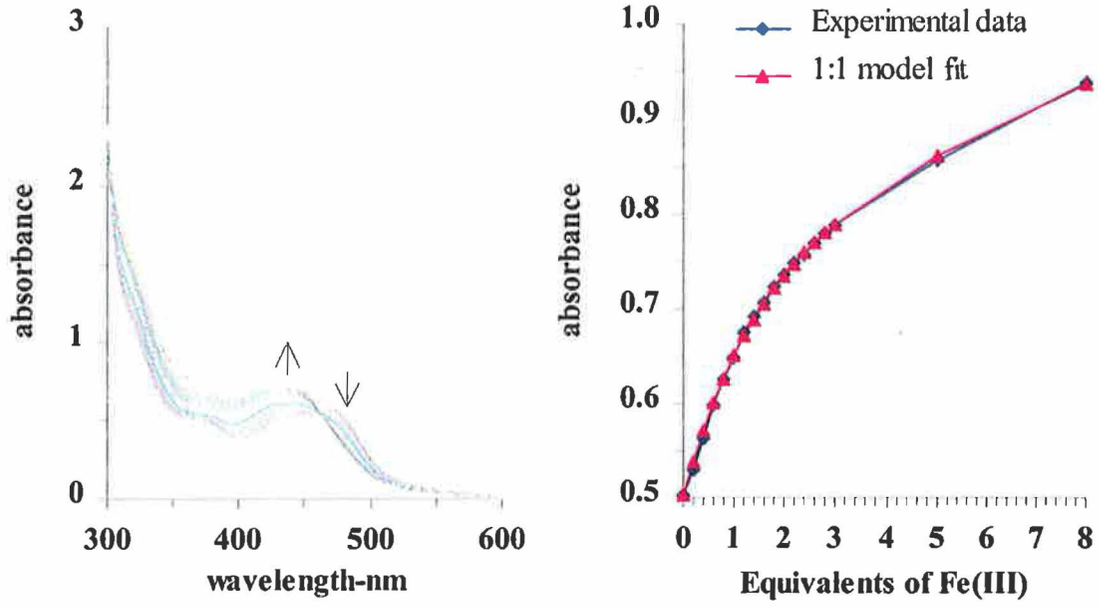

(a) (b)

Figure 6.10 *(a) Absorption Titration of **bpyL1** (5 X 10^{-5} M) with 0 - 2.0 molar equivalents of $FeCl_3$ in methanol (0.2 equivalent increments). (b) Absorption Titration plot of **bpyL1** with Fe(III) at 445nm: Experimental data and overlay of the most suitable stoichiometric model (1:1).*

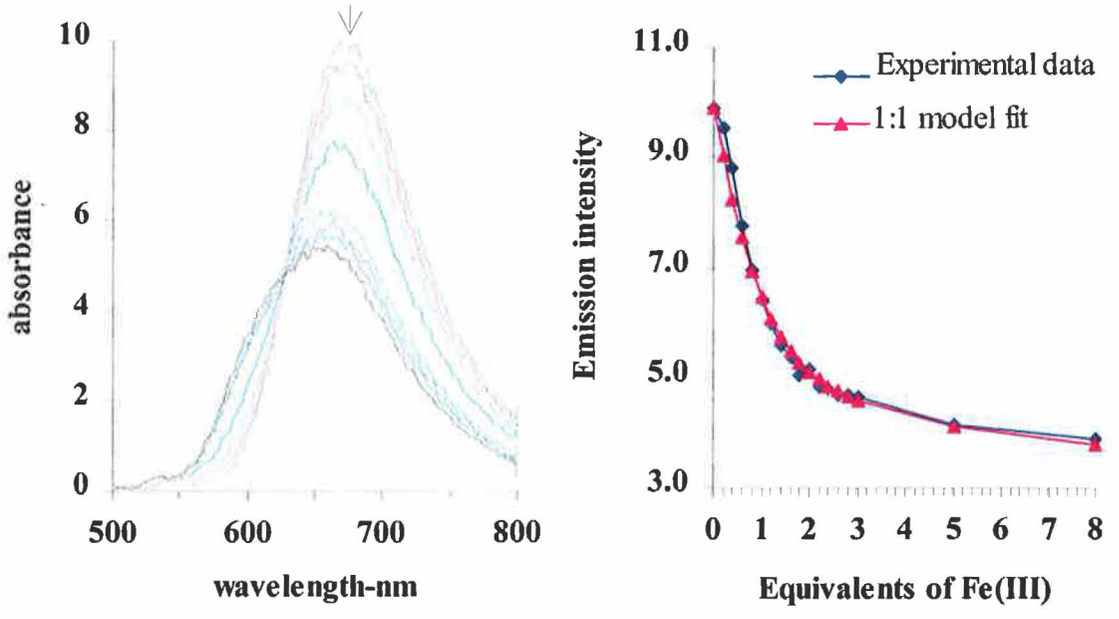

(a) (b)

Figure 6.11 *(a) Emission Titration (excited at 462 nm) of **bpyL1** (5 X 10^{-5} M) with 0-2.0 molar equivalents of $FeCl_3$ in methanol (0.2 molar equivalent increments). (b) Emission Titration plot of **bpyL1** with Fe(III) at 670 nm: Experimental data and overlay of the most suitable stoichiometric model (1:1).*

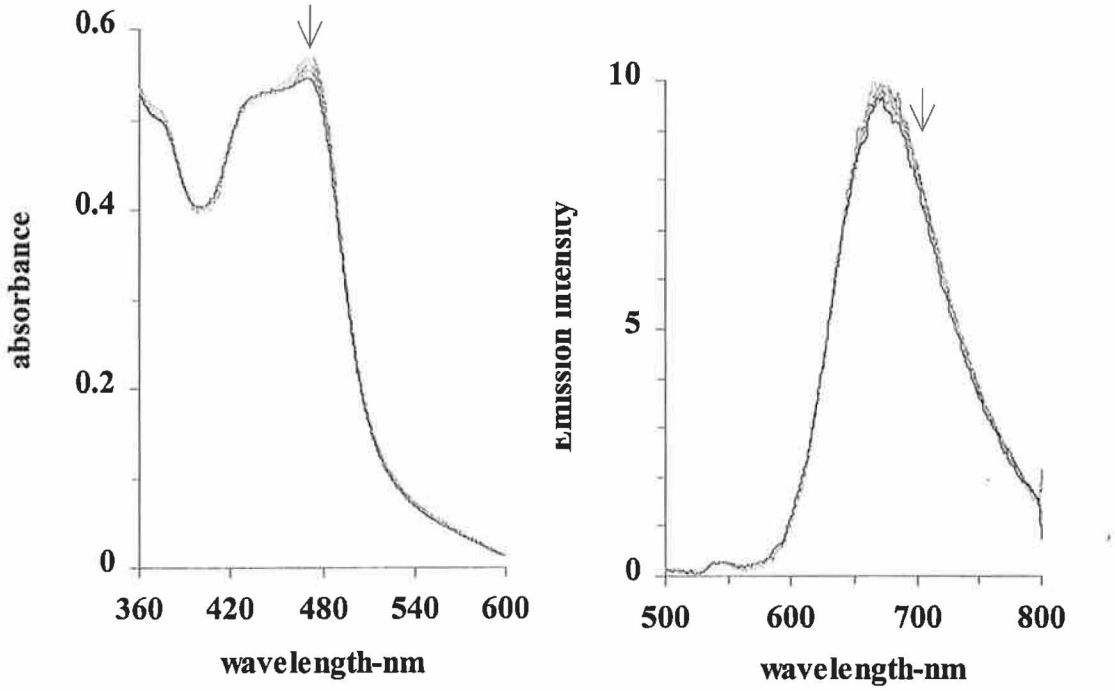

Figure 6.12 *(a) Absorption and (b) emission titrations (excited at 490 nm) of* ***bpyL1*** *(5 X 10^{-5} M) with 0 - 2 molar equivalents of $FeCl_2.4H_2O$ (0.2 molar equivalent increments).*

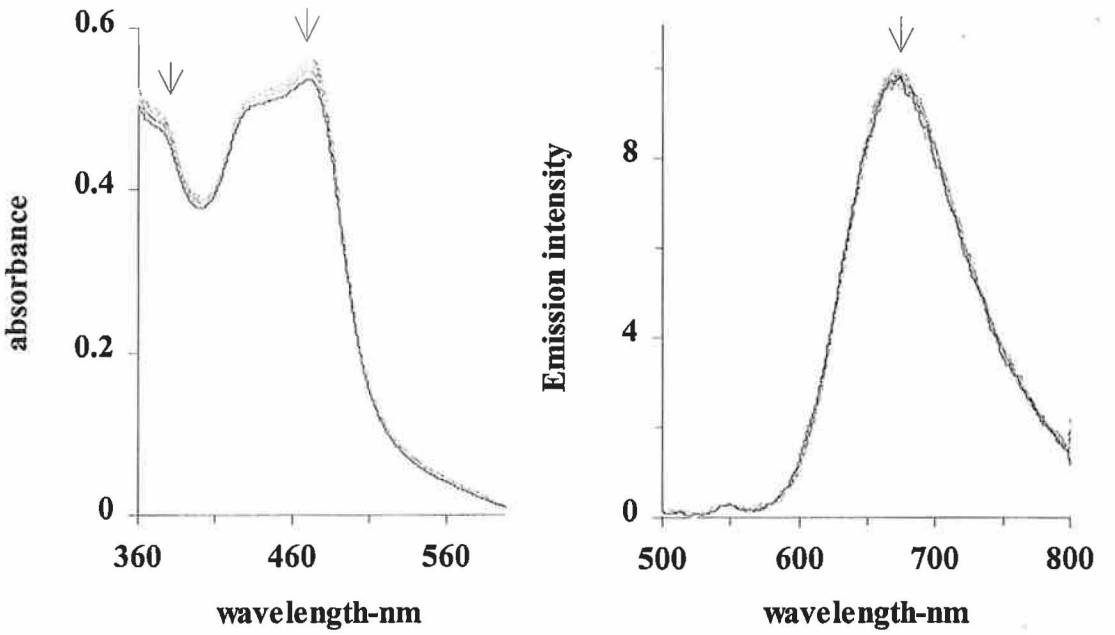

Figure 6.13 *(a) Absorption and (b) emission titrations(excited at 490 nm) of* ***bpyL1*** *(5 X 10^{-5} M) with 0 - 3 molar equivalents of $Cu(NO_3)_2.3H_2O$ (0.2 equivalent increments).*

While the quenching of the emission in Figure 6.11 may suggest protonation of the triazole it is more likely that the changes can be explained by a combination of energy transfer quenching by the Fe(III) (see section 6.2.2.3.) and binding of the Fe(III). The fact that the quenching is more significant than that experienced by $[Ru(bpy)_3]^{2+}$ when titrated with Fe(III) implies that some type of binding takes place between the **bpyL1** and Fe(III).

The affinity of Fe(III) for amine ligands is low[31] implying that the feasibility of the Fe(III) binding through the N4 of the triazole is unlikely. This leads to the conclusion that the Fe(III) was bound through the protected catechol moiety and the SIRKO calculations from the absorption titrations (at 445 nm) produce a very good model that indicates a 1:1 complex formation between **bpyL1** and Fe(III) with a stability constant of Log $\beta = 4.4 \pm 0.1$ (see Figure 6.10 (b)). The 1:1 model also fits the emission data (see Figure 6.11 (b)), with a comparable calculated stability constant of log $\beta = 4.7 \pm 0.2$. The calculations also suggest that 50 % of the 1:1 complex between **bpyL1** and Fe(III) was formed after 1.4 equivalents of titrated Fe(III) and by 8 equivalents almost 90 % of complex was formed. The suitability of the SIRKO models with the absorption and emission data suggests that the protected complex does indeed coordinate with Fe(III) with a stability constant (log $\beta = 4.54 \pm 0.11$).

The absorption and emission titrations of the protected catechol complex **bpyL1** with Fe(II) are presented in Figure 6.12 (a) and (b) respectively. In both titrations the changes in the spectra are not very significant and there is an absence of isobestic points. It was deduced that the changes may simply reflect dilution effects (compare with Figures 6.5 and 6.6) and the inability of the SIRKO calculations to determine a suitable fit for either the absorption or emission data was indicative of this assumption. Similar

conclusions can be derived from analysis of the absorption and emission titrations of **bpyL1** with Cu(II) (see Figure 6.13) where the changes in the spectra are again not very significant. The SIRKO calculations were unable to deliver a suitable stoichiometric model. The results from the titrations of **bpyL1** with Fe(II) and Cu(II) suggest that no complexation occurs between the protected complex and these metals.

6.2.2.5. Complexation titrations of bpyL2 with Fe(III).

The affinity of catechol complexes for Iron(III) and the abundance of Fe(III)-catechol complexes was detailed earlier in section 6.0[5-8]. The absorption titration between **bpyL2** and Fe(III) ($FeCl_3$) is shown in Figure 6.14. In the titration 8 equivalents of Fe(III) were added. Since the effects of dilution were more evident after 4 to 5 equivalents, the results obtained for the first 2 equivalents of Fe(III) added are shown in Figure 6.14. The data points between 4 and 8 equivalents are used in the SIRKO calculations because allowance is made in the program for volume changes in the course of the titration. The effect of the titration of **bpyL2** with Fe(III) is clear from the changes observed in the absorption spectra throughout the duration of the titration. The changes are significant when compared with the blank titrations shown in Figure 6.5. There is a clear increase in absorption around 445 nm and 560 nm and there is also a shift in the λ_{max} from 473 nm at 0 equivalents to 445 nm at 2.0 equivalents. The absorption spectrum of $FeCl_3$ shows two main transitions at 223.5 nm and 367 nm (see Figure 6.7(a)) and evidence of the growth of these absorption characteristics is also evident in Figure 6.14.

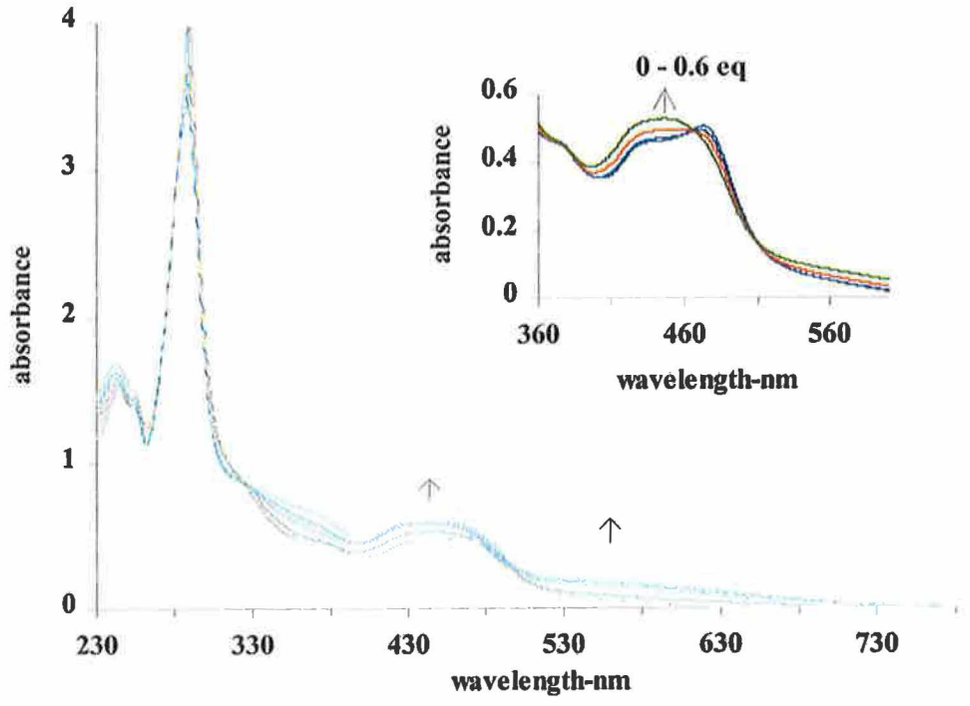

Figure 6.14 *Absorption titration of **bpyL2** (5 X 10^{-5} M) with 0, 0.2, 0.4, 0.6, 0.8, 1.0, 1.2, 1.4, 1.6, 1.8, 2.0 molar equivalents of $FeCl_3$ in methanol.*

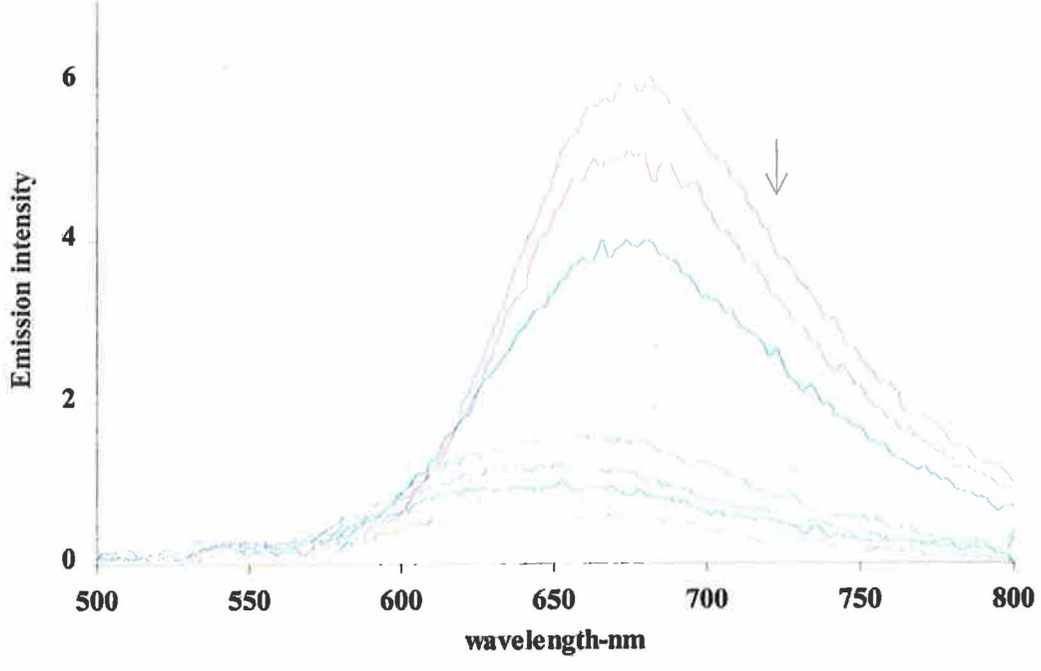

Figure 6.15 *Emission Titration of **bpyL2** (5 X 10^{-5} M),excited at 470 nm, with 0, 0.2, 0.4, 0.6, 0.8, 1.0, 1.2, 1.4, 1.6, 1.8, 2.0 molar equivalents of $FeCl_3$ in methanol.*

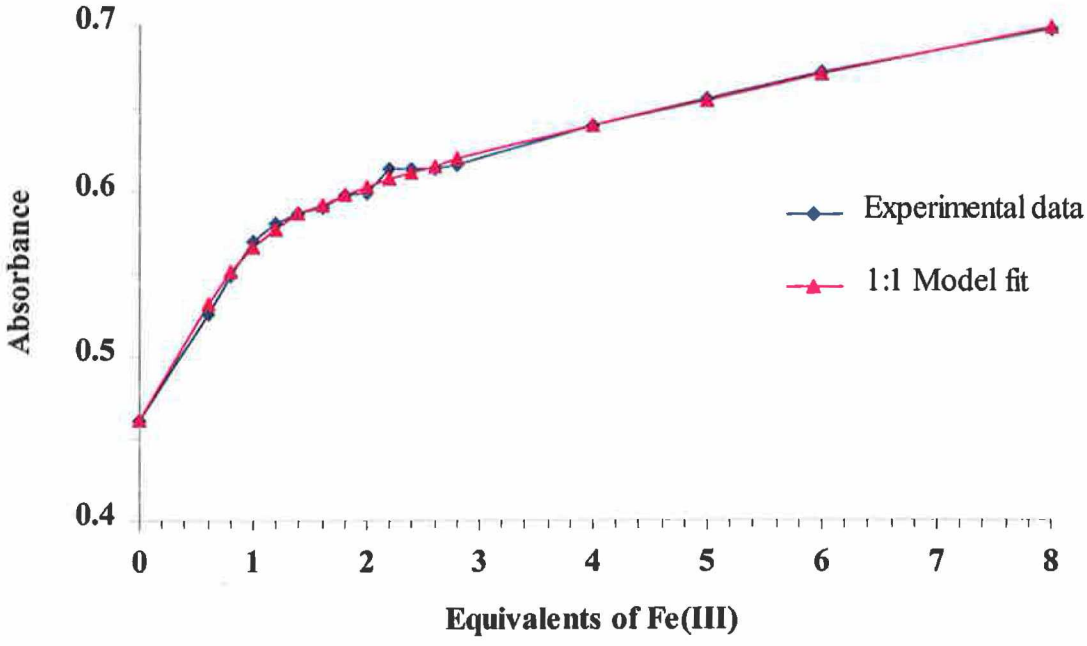

Figure 6.16 *Absorption titration plot of **bpyL2** with Fe(III) at 445nm : Experimental data and overlay of the most suitable stoichiometric model (1:1).*

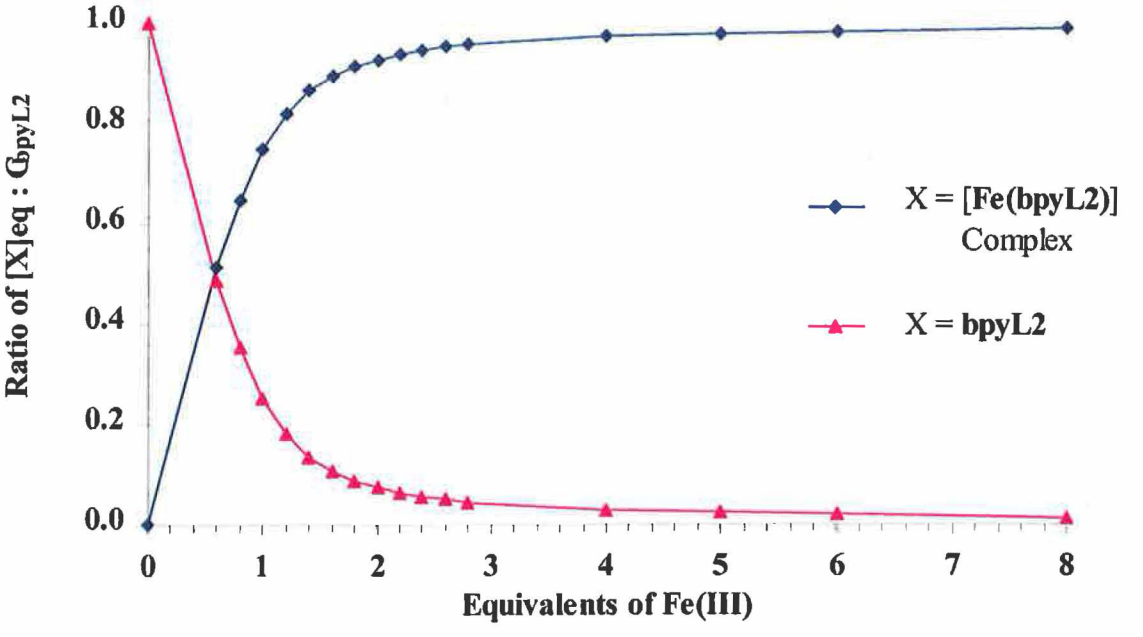

Figure 6.17 *Plot of the ratio of the equilibrium concentration of **[Fe(bpyL2)]** complex and **bpyL2** (respectively) to the analytical concentration of **bpyL2** (C_{bpyL2}) vs equivalents of Fe(III) (absorption titration SIRKO data).*

The inset of Figure 6.14 shows that clean isobestic points are only maintained in the region of 0 - 0.6 equivalents, indicative of only one equilibrium process, that is the complexation of Fe(III) by **bpyL2**. After 0.6 equivalents of Fe(III) has been titrated the isobestic points are lost possibly due to the fact that complexation is quite strong and almost 50 % of the complex is formed at 0.6 equivalents. This will be discussed in more detail later with reference to Figure 6.17. The isobestic points observed in the inset of Figure 6.14 occur at 383 nm, 466 nm and 510 nm. In the pH dependent absorption titration of **bpyL2** (see Figure 4.16) isobestic points are present at 390 nm and 460 nm. The fact that the isobestic point observed in the Fe(III) titration at 510 nm does not appear in the pH dependent absorption titration of **bpyL2**, is an indication that the changes observed in the Fe(III) absorption titration reflect the complexation of the catechol complex **bpyL2** with Fe(III) and not protonation of the triazole. The fact that the absorption maxima are shifted to higher energy as the titration proceeds is also an indication of binding of a second metal centre and may be explained by stabilisation of the metal-based ground state in the heteronuclear complex with respect to **bpyL2**[32].

The Fe(III) emission titration (see Figure 6.15) shows quite a dramatic effect between 0 and 2 equivalents of titrated Fe(III). There is a considerable quenching effect observed throughout the duration of the titration and at 2 equivalents of Fe(III) added the emission is almost quenched. Such a phenomenon is not unknown as Lytton et al demonstrated the use of a fluorescent siderophore for the monitoring of Fe(III) removal from biological sources[8]. Interestingly the fluorescence of the siderophore was also quenched upon binding of Fe(III) to the catechol moeities thus implying that the Fe(III)-siderophore was not fluorescent. The fact that the emission was quenched due to binding of the Fe(III) was further verified in the study by treatment of similar

fluorescent compounds, which were not expected to bind Fe(III), with iron salts resulting in no loss of fluorescence. The dramatic changes in the emission spectra provide further evidence of the formation of an [**Fe(bpyL2)$_n$**] complex. The quenching experienced by $[Ru(bpy)_3]^{2+}$ when titrated with Fe(III) (see Figure 6.8) was not as substantial as that displayed in the titration of **bpyL2** with Fe(III) indicating that the quenching was indicative of the formation of an [**Fe(bpyL2)$_n$**] complex. It should also be noted that the quenching displayed in the titration of **bpyL1** with Fe(III) was not as dramatic as that experienced in the titration of **bpyL2** with Fe(III) (compare Figure 6.11 (a) with Figure 6.15) and this indicates that the catechol complex (**bpyL2**) forms a stronger complex with Fe(III) than the protected catechol complex (**bpyL1**).

The operations and functions of SIRKO have been discussed in section 6.2.2.1. The determination of the stoichiometry of the complexation between Fe(III) and the catechol complex **bpyL2** and of the stability constant (β) for the chelation was carried out by combining the results obtained from both the absorption and emission titrations. The calculations for the absorption titrations are performed at 445 nm where there is a good degree of change in the absorption characteristics throughout the duration of the titration. The most suitable model obtained for the absorption titration was a stoichiometric ratio of 1:1 Fe/**bpyL2** and this was obtained with careful notice to the validity of the molar absorbance values calculated by SIRKO and the size of the errors and iteration factors. Figure 6.9 shows the experimental data for the titration at 445 nm with the most suitable fit as determined by SIRKO optimisation.

Table 6.2 *Stoichiometry and stability constants for the complexation of* ***bpyL2*** *with Fe(III) obtained using the SIRKO program.*

Model	Data	Comments
	Absorption titrations	
	(445 nm)	**ε units are $M^{-1}cm^{-1}$ (scaling factor is 1000)**
1:1	ε_{bpyL2} = 9.22 (not refined) ε_{FeCl3} = 0.54 (not refined) $\varepsilon_{Fe(bpyL2)}$ = 12.1 ± 0.1 **Log β = 5.4 ± 0.2**	This is the most suitable model obtained from the data and is presented in Figure 6.16. The value for ε_{FeCl3} is obtained from Table 6.1 and is refined. The $\varepsilon_{Fe(bpyL2)}$ value of 12.1 seems quite reasonable and the error values are acceptable.
2:1	ε_{bpyL2} = 9.22 (not refined) ε_{FeCl3} = 0.54 (not refined) $\varepsilon_{Fe(bpyL2)2}$ = 27.8 ± 1.3 **Log β = 8.5 ± 0.2**	This is not a bad fit but not as good as the 1:1 fit although the calculated value of $\varepsilon_{Fe(bpyL2)2}$ (27.8 ± 1.3) seems too high.
	Emission titrations	
	(673 nm)	(Excited at 470 nm)
1:1	EI_{bpyL2} = 121.10 EI_{FeCl3} = 0 (refined) $EI_{Fe(bpyL2)}$ = 7.4 ± 0.4 **Log β = 5.5 ± 0.1**	Very good fit for 1:1 with a considerable quenching of emission upon complexation. The value for log β agrees with the value obtained from the absorption titrations.
2:1, 3:1	*	No suitable fit

The calculated R-factor for the refinement (0.488 %) is less than the accuracy of the limit on degree of refinement (R_{lim} = 1.661 %) thus implying that the optimised values can be considered to be well-refined[29]. A summary of the best values obtained from the SIRKO program for the absorption and emission titrations is shown in Table 6.2. The results obtained from the SIRKO calculations using the data obtained from the absorption and emission titrations of **bpyL2** with Fe(III) are summarised in Table 6.2. The conclusions from both types of spectrophotometric titrations are that a 1:1 stoichiometric ratio is the most appropriate model for this complexation. This judgement is based on the closeness of the model 1:1 fit with that of the experimental data (see Figure 6.16). It is also important to note that the results obtained from the emission titrations suggest that only a 1:1 model fit is appropriate to describe the system. The values obtained for the logarithm of the stability constant (Log β) agree quite well within experimental error. The titrations are repeated in triplicate and suggest that a 1:1 complex was formed between **bpyL2** and Fe(III) with a Log β value of 5.5 ± 0.1. Figure 6.17 displays the plot of the ratio of the equilibrium concentration of **[Fe(bpyL2)]** complex and **bpyL2**, respectively, to the analytical concentration of **bpyL2** (C_{bpyL2}). This plot demonstrates that the complexation is quite strong and that after 0.6 molar equivalents of Fe(III) have been added, 50% of the **[Fe(bpyL2)]** has been formed. After 2 molar equivalents of Fe(III) has been added almost all the complex has formed and almost all of the **bpyL2** complex has been used up. This could explain the loss in isobestic points after 0.6 equivalents as the complex formation is almost complete at this stage and further addition of Fe(III) is manifested by the features of the absorption of $FeCl_3$ growing in the spectra.

While it is not possible to confirm the structure of **[Fe(bpyL2)]** without a crystal structure it is important to note that the majority of iron complexes are octahedral, but tetrahedral and square pyramidal ones also exist[31].

6.2.2.6. Complexation titrations of bpyL2 with Fe(II).

The titrations of **bpyL2** with Fe(II) resulted in significant changes in the absorption and emission spectra reflecting complex formation (see Figures 6.18 and 6.19). Unlike the Fe(III) titrations, in this case there is a clear isobestic point throughout the duration of the titration (at 452 nm), upto 10 equivalents of Fe(II) added. This is significantly different to the pH-dependent titration of **bpyL2** which has isobestic points at 390 nm and 460 nm (see Figure 4.16) indicating that the changes observed by the titration of Fe(II) are not due to protonation of the triazole. The λ_{max} of the spectra shifts from 473 nm at the beginning of the titration to 443.5 nm at the end of the titration which may be explained by stabilisation of the metal-based ground state upon binding a second metal centre. The SIRKO calculations for the absorption titrations are performed at 472 nm where there is a considerable drop in absorption in the course of the titration. Similarly to the Fe(III) titrations (see Figure 6.15) there is considerable quenching in the Fe(II) emission titrations (see Figure 6.19) although it is not as substantial. It is however much more significant than that displayed in the titration of $[Ru(bpy)_3]^{2+}$ with Fe(II) indicating that the quenching effect seen in titration of **bpyL2** with Fe(II) reflect binding of the Fe(II) by the catechol complex. In the Fe(III) titrations the emission is almost quenched when 2.0 molar equivalents of Fe(III) has been added while here, in the Fe(II) titrations, almost 10 molar equivalents of Fe(II) was required to cause substantial quenching.

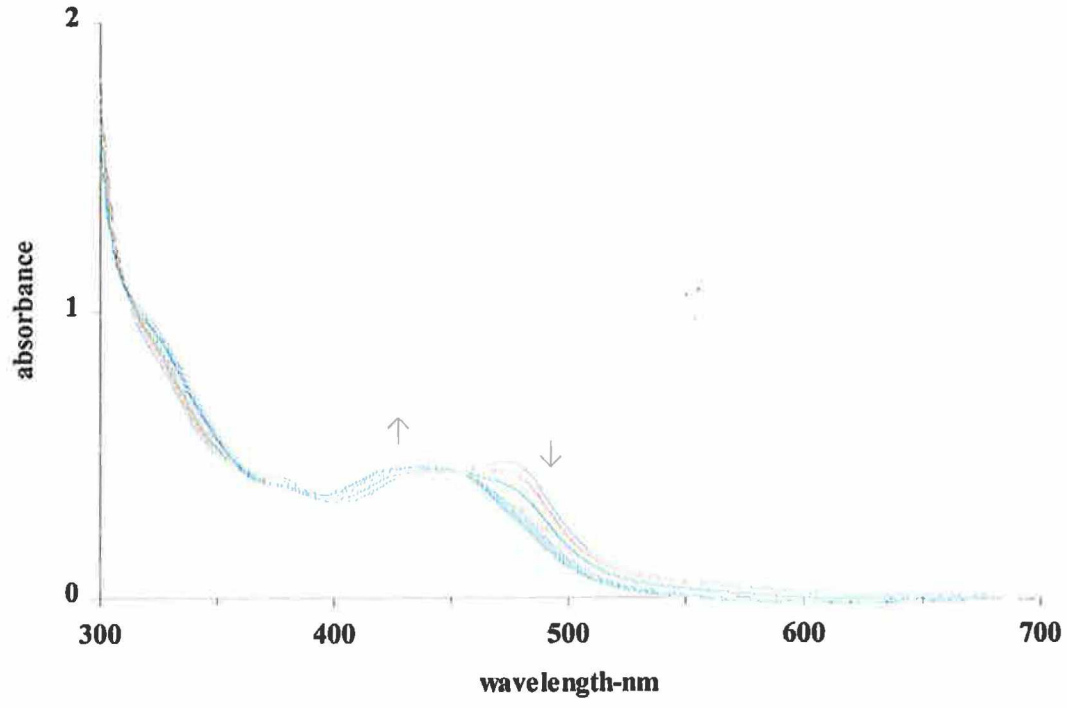

Figure 6.18 *Absorption titration of **bpyL2** (5 X 10^{-5} M) with 0, 1.0, 2.0, 3.0, 4.0, 5.0, 6.0, 7.0, 8.0, 9.0 molar equivalents of $FeCl_2$ in methanol.*

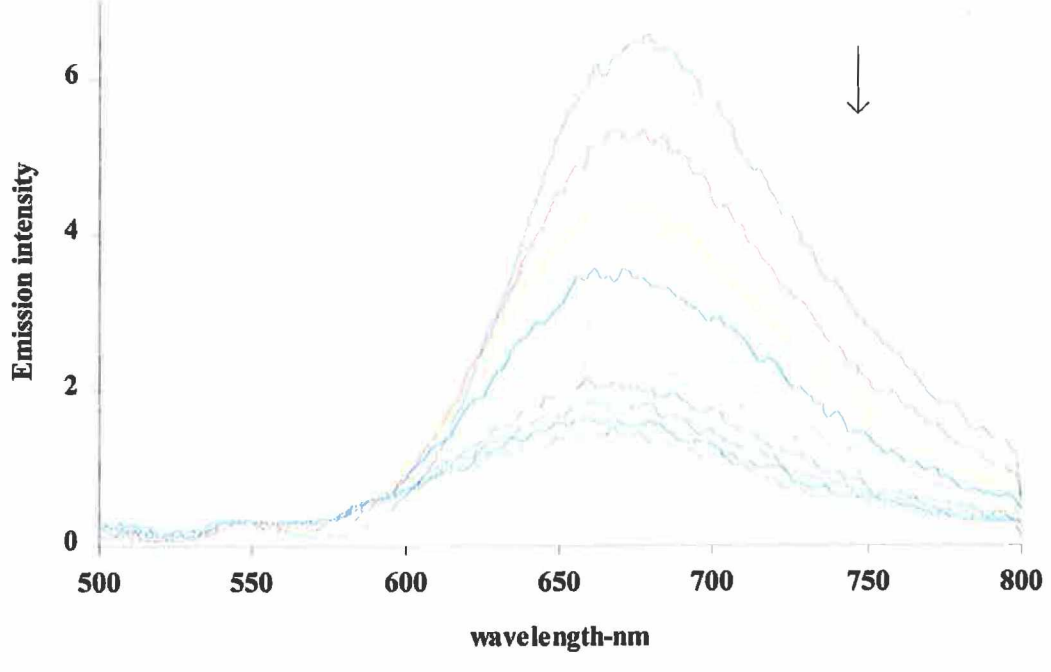

Figure 6.19 *Emission titration of **bpyL2** (5 X 10^{-5} M) with 0, 1.0, 2.0, 3.0, 4.0, 5.0, 6.0, 7.0, 8.0, 9.0 molar equivalents of $FeCl_2$ in methanol (excited at 452 nm).*

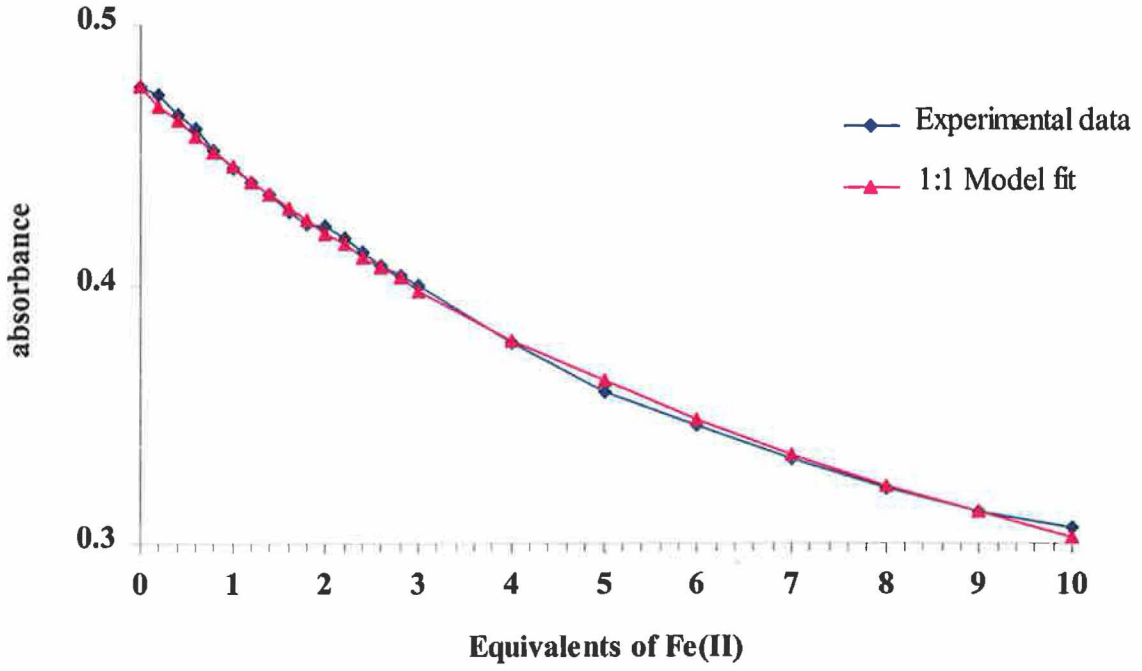

Figure 6.20 *Absorption titration plot of **bpyL2** with Fe(II) at 472 nm : Experimental data and overlay of the most suitable stoichiometric model (1:1).*

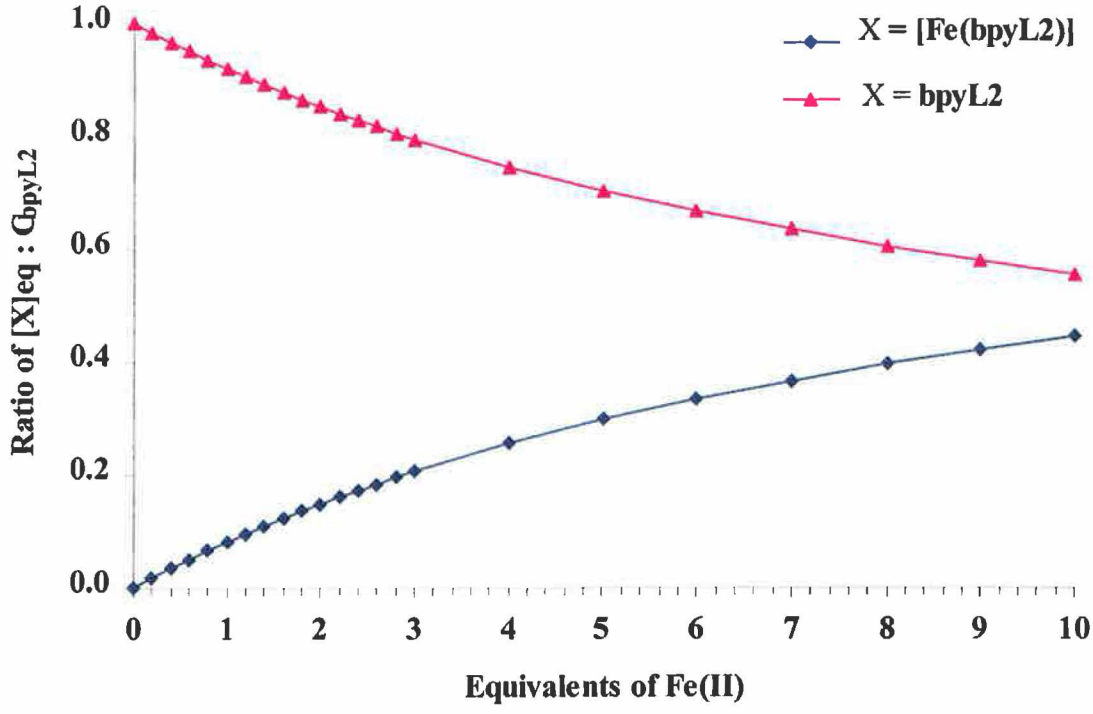

6.21 *Plot of the ratio of the equilibrium concentration of **[Fe(bpyL2)]** and **bpyL2** (respectively) to the analytical concentration of **bpyL2** (C_{bpyL2}) vs equivalents of Fe(II) (absorption titration SIRKO data).*

Table 6.3 *Stoichiometry and stability constants for the complexation of* ***bpyL2*** *with Fe(II) obtained using the SIRKO program.*

Model	Data	Comments
	Absorption titrations	
	(472 nm)	**ε units are $M^{-1}cm^{-1}$(scaling factor is 1000)**
1:1	ε_{bpyL2} = 9.52 (not refined) ε_{FeCl2} = 0.04 (not refined) $\varepsilon_{FebpyL2}$ = 3.9 ± 0.3 **Log β = 3.3 ± 0.1**	Good data set with an excellent fit for 1:1 model. The value for log β is lower than that obtained for the complexation of **bpyL2** with Fe(III) and the complexation is slower (see Figure 6.21).
2:1	ε_{bpyL2} = 9.52 (not refined) ε_{FeCl2} = 0.04 (not refined) $\varepsilon_{Fe(bpyL2)2}$ =1.74 ± 0.12 **Log β = 7.1 ± 0.1**	Good fit but the value for $\varepsilon_{Fe(bpyL2)2}$ is quite low especially for a 2:1 stoichiometric complex. The R-factor of 0.57% is higher than the value for the 1:1 fit. These factors suggest that the 1:1 model best describes the complexation.
	Emission titrations	
	(660 nm)	(excited at 452 nm)
1:1	EI_{bpyL2} = 130.9 (not refined) EI_{FeCl2} = 0 (not refined) $EI_{Fe(bpyL2)}$ =15 **Log β = 3.8 ± 0.1**	Good fit with an R-factor of 2.196% which is higher than the R_{lim} suggesting that though the fit is quite good the absorption titrations are more accurate.
2:1	*	No suitable fit

This may be indicative of slower [**Fe(bpyL2)$_n$**] complex formation with **bpyL2** having a lower affinity for Fe(II) than Fe(III). The SIRKO calculations for the absorption titrations postulate a 1:1 stoichiometry for the complexation between Fe(II) and **bpyL2** with a log β value of 3.3 ± 0.1. The 1:1 model fit is presented in Figure 6.20 and the R-factor for the refinement (0.51 %) is less than the accuracy of the limit on degree of refinement (R_{lim} = 2.41 %) verifying the suitability of the plot. The SIRKO plot of the ratio of the equilibrium concentration of **[Fe(bpyL2)]** complex and **bpyL2**, respectively, to the analytical concentration of **bpyL2** (C_{bpyL2}) (see Figure 6.21) substantiates the fact that the complexation is weaker, than that between Fe(III) and **bpyL2**, and indeed even after 10 equivalents of Fe(II) has been added less than 50% of the complex has been formed. The SIRKO calculations performed with the data from the emission titrations agree well with the conclusions derived from the calculations performed on the absorption titrations, indicating stoichiometry of 1:1 with a log β value of 3.8 ± 0.1. SIRKO calculations for the spectrophotometric titrations of Fe(II) with **bpyL2** are summarised in Table 6.3. Similarly to the complex formation between **bpyL2** and Fe(III) the structure of the **[Fe(bpyL2)]** complex formed between **bpyL2** and Fe(II) cannot be confirmed without a crystal structure. However Fe(II) is known to form a number of complexes most of them octahedral[31].

6.2.2.7. Complexation titrations of bpyL2 with Cu(II).

The absorption and emission titrations of **bpyL2** with Cu(II) show interesting features which were not present in the previous studies with Fe(III) and Fe(II). In the absorption titrations (see Figure 6.22) at 450 nm, the wavelength chosen for the SIRKO calculations, the absorption increases upto 0.6 equivalents of Cu(II) added. After this

the absorption levels off and gradually begins to decrease. While the changes in absorption are not very large (0.6 au to 0.52 au), they are significant in that similar changes were not observed in previous titrations and the effects are not the result of dilution (see section 6.2.1) or additive effects from the $Cu(NO_3)_2.3H_2O$ which does not absorb at wavelengths greater than 350 nm.

The **bpyL2** emission titrations with Cu(II) also display unusual characteristics. Initially, between 0 and 0.8 equivalents of Cu(II), the intensity of the emission spectra increases (see Figure 6.23 (a)) . However, further titration with Cu(II) results in a gradual decrease in the emission (see Figure 6.23 (b)), although it does not experience the same magnitude of quenching seen in the Fe(III) or Fe(II) titrations (see section 6.2.2.5 and 6.2.2.6). The changes observed in both the absorption and emission titrations imply that there may possibly be more than one process taking place. This was confirmed by the SIRKO analysis of the titration data. The results obtained from the SIRKO program are summarised in Table 6.4. Although both the 2:1 and the 2:1;1:1 models (see Figure 6.24 and scheme 6.6) are equally suitable models for the absorption titration data, SIRKO calculations on the emission titrations must also be taken into consideration. In the emission titrations the data can only be fitted with the 2:1; 1:1 model. The processes which create this model are shown below in scheme 6.6.

$$2\mathbf{bpyL2} + Cu(II) \rightarrow \mathbf{Cu(bpyL2)_2} \quad (2:1)$$

$$\mathbf{Cu(bpyL2)_2} + Cu(II) \rightarrow 2[\mathbf{Cu(bpyL2)}] \quad (1:1) \qquad (6.6)$$

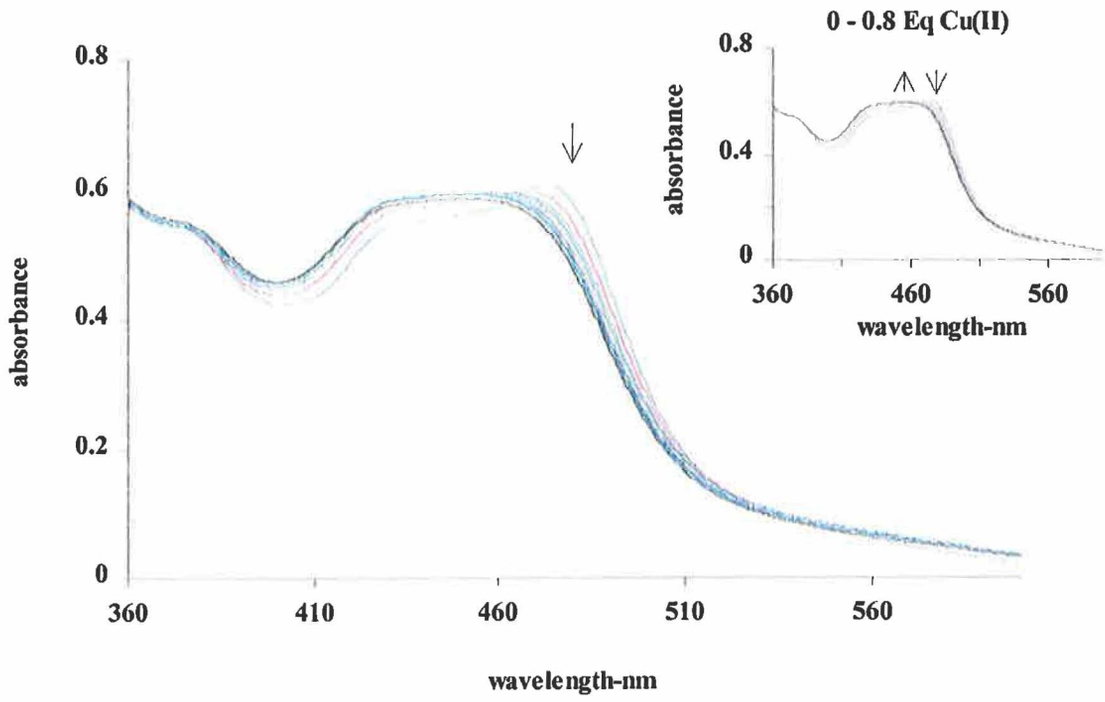

Figure 6.22 *Absorption Titration of **bpyL2** (5 X 10^{-5} M) with 0 - 3 molar equivalents of $Cu(NO_3)_2.3H_2O$ in methanol (0.2 molar equivalent increments).*

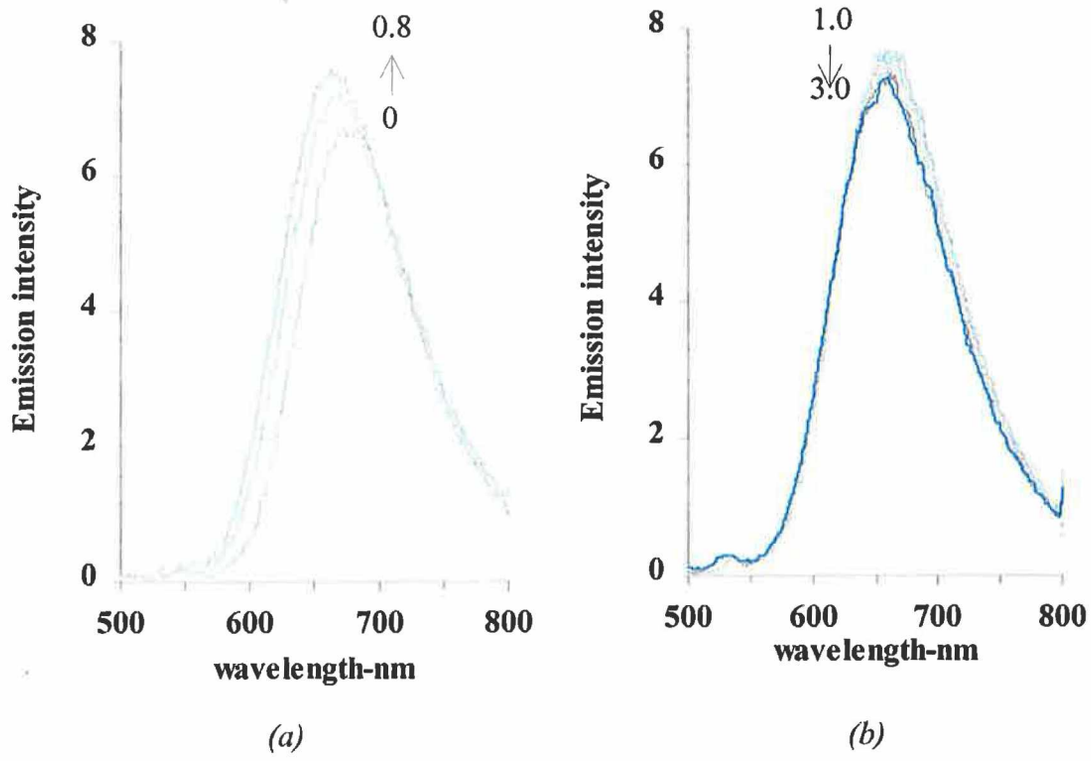

Figure 6.23 *Emission Titration of **bpyL2** (5 X 10^{-5} M) with $Cu(NO_3)_2.3H_2O$ in methanol (excited at 465 nm); (a) 0-0.8 equivalents (b) 1.0-3.0 equivalents. (0.2 molar equivalent increments in (a) and (b)).*

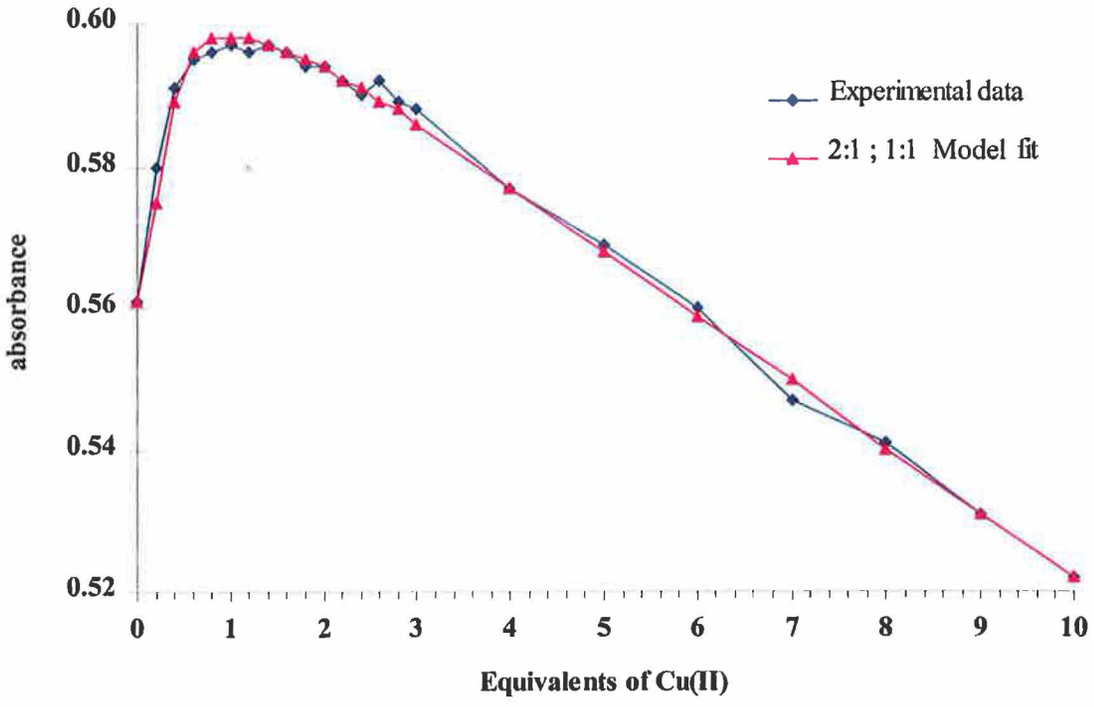

Figure 6.24 *Absorption titration plot of **bpyL2** with Cu(II) at 450 nm : Experimental data and overlay of the 2:1; 1:1 stoichiometric model*

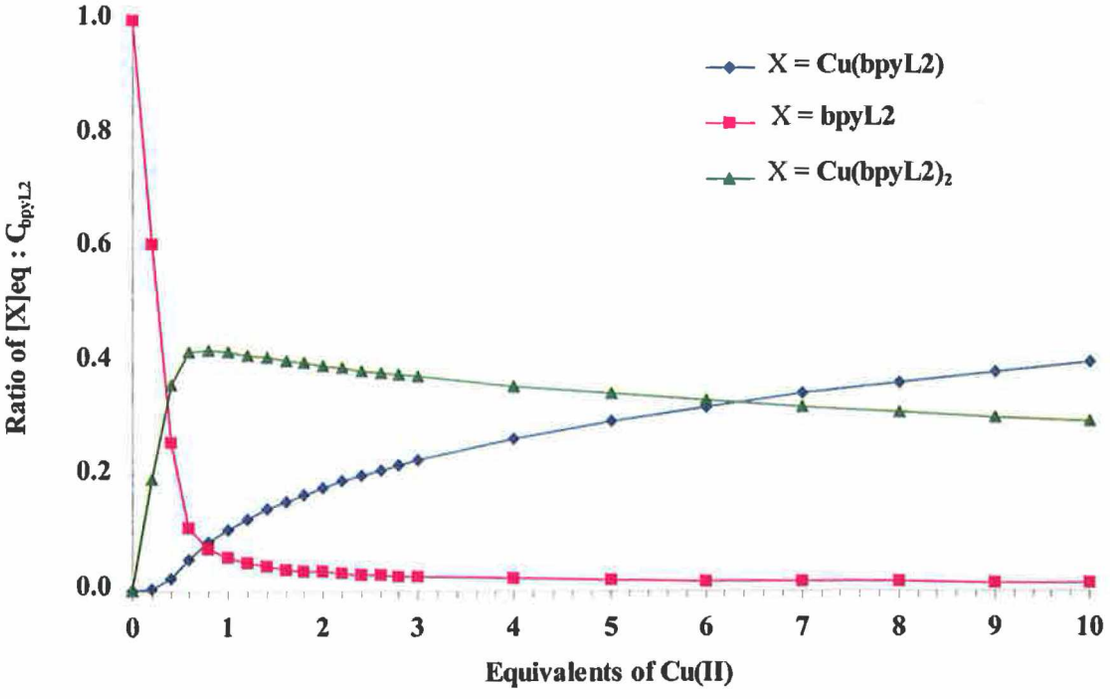

6.25 *Plot of the ratio of the equilibrium concentration of **Cu(bpyL2)**, **Cu(bpyL2)$_2$** and **bpyL2** (respectively) to the analytical concentration of **bpyL2** (C_{bpyL2}) vs equivalents of Cu(II) (absorption titration SIRKO data based on 2:1;1:1 model).*

Table 6.4 *Stoichiometry and stability constants for the complexation of* ***bpyL2*** *with Cu(II) obtained using the SIRKO program.*

Model	Data	Comments
	Absorption titrations	
	(450 nm)	**ε units are $M^{-1}cm^{-1}$(scaling factor is 1000)**
1:1	*	Poor fit for the first 1.0 equivalents of the titration but the fit was quite good for the remainder of the titration. However the model does not suitably describe the whole titration.
2:1	ε_{bpyL2} = 9.22 (not refined) $\varepsilon_{Cu(NO3)2.3H2O}$ = 0 (not refined) $\varepsilon_{Cu(bpyL2)2}$ =25.4 ± 0.12 **Log β = 9.2 ± 0.1**	This is quite a good fit with an R-factor of 0.418% which is lower than the R_{lim}. The value of $\varepsilon_{Cu(NO3)2.3H2O}$ can be assumed to be zero (see section 6.2.2.2) and is not refined.
2:1 1:1	ε_{bpyL2} = 9.22 (not refined) $\varepsilon_{Cu(NO3)2.3H2O}$ = 0 (not refined) $\varepsilon_{Cu(bpyL2)2}$ = 24.05 ± 0.12 $\varepsilon_{Cu(bpyL2)}$ = 14.09 ± 0.12 **Log $\beta_{2:1}$ = 11.1 ± 0.1** **Log $\beta_{1:1}$ = 4.9 ± 0.1**	This model (see Figure 6.24) fits the data quite well and has an R-factor of 0.28% which is lower than that for the 2:1 model (above). The formation of two complexes in the titration explains the changes seen in the absorption titrations and is reaffirmed by the suitability of this same model to the emission titrations.

	Emission titrations (660 nm)	(excited at 465 nm)
1:1	*	No suitable fit
2:1	*	No suitable fit
2:1 1:1	EI_{bpyL2} = 130.9 (not refined) $EI_{Cu(NO3)2.3H2O}$ = 0 (not refined) $EI_{Cu(bpyL2)2}$ = 313.2 ± 2.7 $EI_{Cu(bpyL2)}$ = 117.1 ± 4.2 **Log $\beta_{2:1}$ = 12.1 ± 0.1** **Log $\beta_{1:1}$ = 5.1 ± 0.1**	This is the only model which fits the data from the emission titrations. The R-factor is quite high at 1.62 % and is higher than the R_{lim} however this was a common trend with all the emission titrations due to the fact that the emission spectra were not as smooth as the absorption spectra.

The plot of the ratio of the equilibrium concentration of **Cu(bpyL2)**, **Cu(bpyL2)$_2$** and **bpyL2** to the analytical concentration of **bpyL2** (C_{bpyL2}) against the equivalents of titrated Cu(II) (see Figure 6.25) clarifies the processes suggested in scheme 6.6. After 0.8 molar equivalents of Cu(II) has been titrated about 40 % of the 2:1 complex **Cu(bpyL2)$_2$** has formed (log $\beta_{2:1}$ = 11.1 ± 0.1) and this process is reflected by the increase in absorption at 450 nm in the absorption titrations and by the increase in emission intensity in the emission titrations, over this titration range (see Figure 6.23 (a)). All but 10 % of the catechol complex **bpyL2** has been complexed at 1.0 molar equivalent of titrated Cu(II) and it was feasible, from the decrease in the absorption at 450 nm and the reduction in emission intensity, that another process was evolving. It is

suggested that the most likely description of this process was the formation of the 1:1 complex **Cu(bpyL2)** (log $\beta_{1:1}$ = 4.9 ± 0.1). In Figure 6.25 the formation of the 1:1 complex is depicted by the blue trace implying that the complexation is about 40 % complete at 10 equivalents of titrated Cu(II) while the reduction in the concentration of the 2:1 complex is represented by the green trace. The features of this plot (Figure 6.25) support the reactions suggested in scheme 6.6 and the SIRKO calculations (summarised in Table 6.4) confirm that the 2:1;1:1 model was the most suitable one to describe the changes observed in the spectrophotometric titrations. It is important to note that in all of the metal - **bpyL2** titrations performed in this study, the overall stoichiometry is established when the proposed model is the same for both the absorption and emission titrations. This was particularly important in this section whereby a 2:1 model was a good fit for the absorption titrations (see Figure 6.17) but not for the emission titrations. The only model that could accurately describe both of the spectrophotometric titrations was that shown in scheme 6.6 (2:1;1:1).

6.2.2.8. Complexation titrations of bpyL2 with Cr(III), Zn(II) and Ni(II).

The series of titrations of the catechol complex **bpyL2** with metals was completed by titrations with Cr(III), Zn(II) and Ni(II). The calculations from the SIRKO programme for both the absorption and emission titrations are summarised in Table 6.5. Figure 6.26 (a) is a typical example of an absorption titration of **bpyL2** with Cr(III). The changes in the spectra are quite distinct with a considerable drop in absorption at 475 nm and growth in the absorbance around 440 nm. The λ_{max} of the spectra shifts from 473

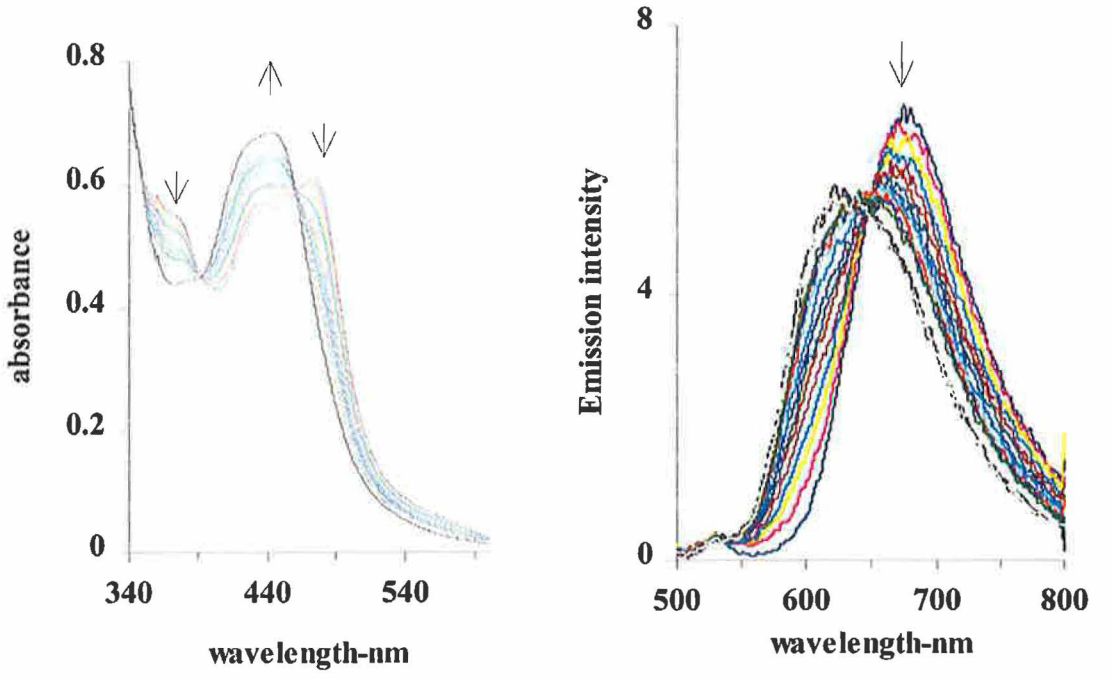

Figure 6.26 *(a) Absorption and (b) emission titrations (excited at 460 nm) of* ***bpyL2*** *(5×10^{-5} M) with 0 - 3 molar equivalents $CrCl_3.6H_2O$ in methanol (0.2 molar equivalent increments).*

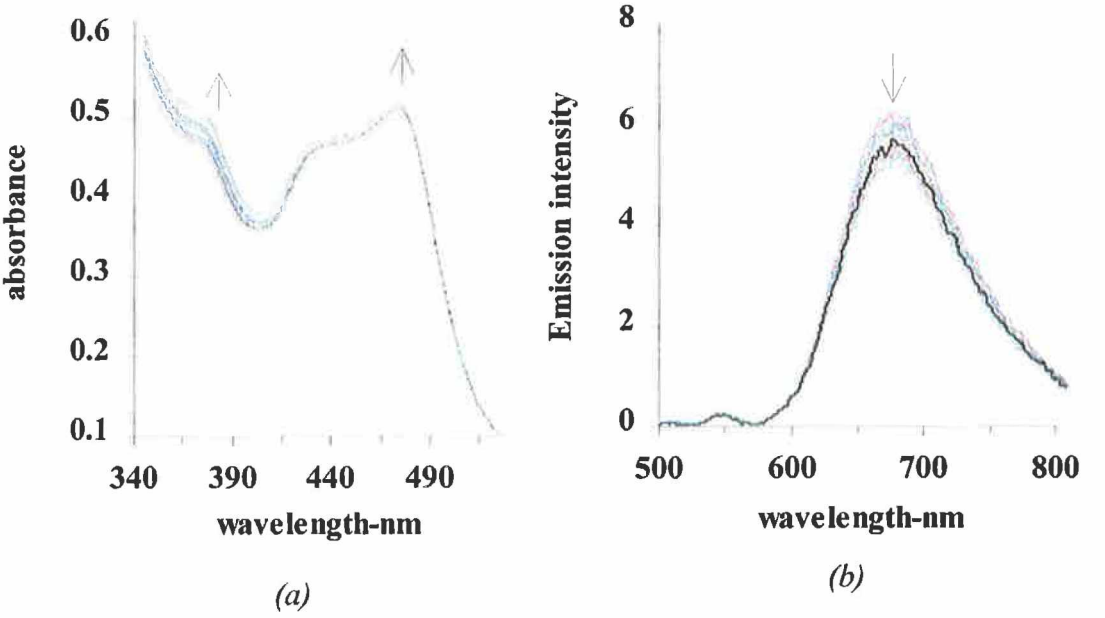

Figure 6.27 *(a) Absorption and (b) emission titrations (excited at 485 nm) of* ***bpyL2*** *(5×10^{-5} M) with 0 - 3 equivalents $Ni(CH_3CO_2)_2.4H_2O$ in methanol (0.2 molar equivalent increments).*

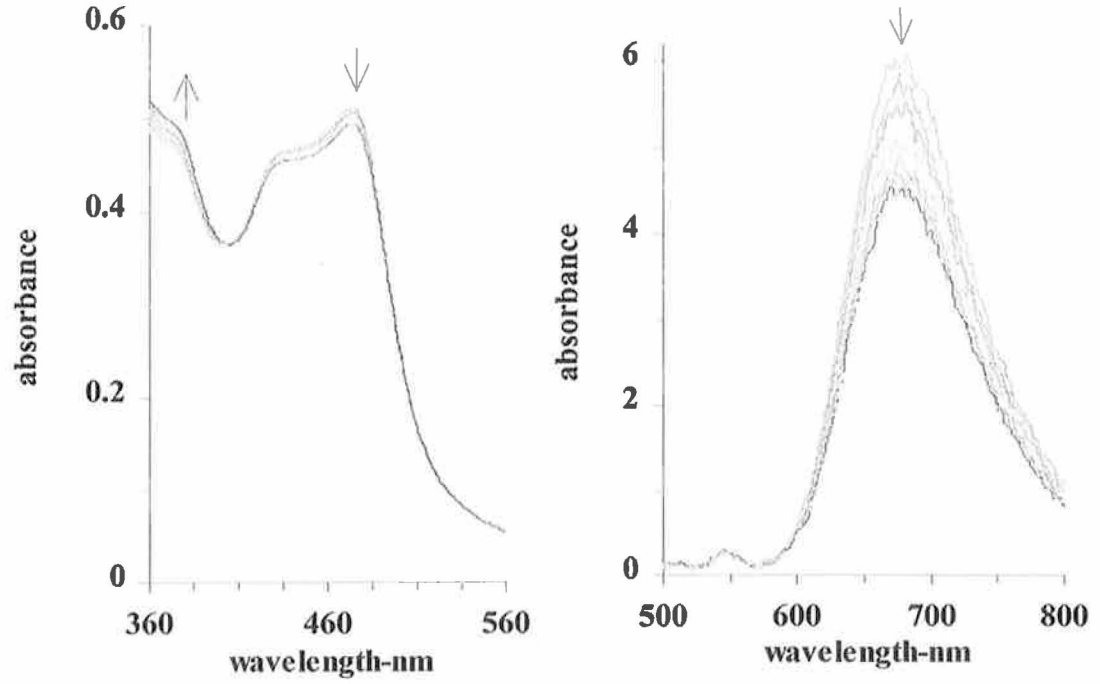

(a) *(b)*

Figure 6.28 *(a) Absorption and (b) emission titrations (excited at 485 nm) of* ***bpyL2*** *(5 X 10^{-5} M) with 0 - 3 molar equivalents of $Zn(CH_3COO)_2.2H_2O$ (0.2 equivalent increments).*

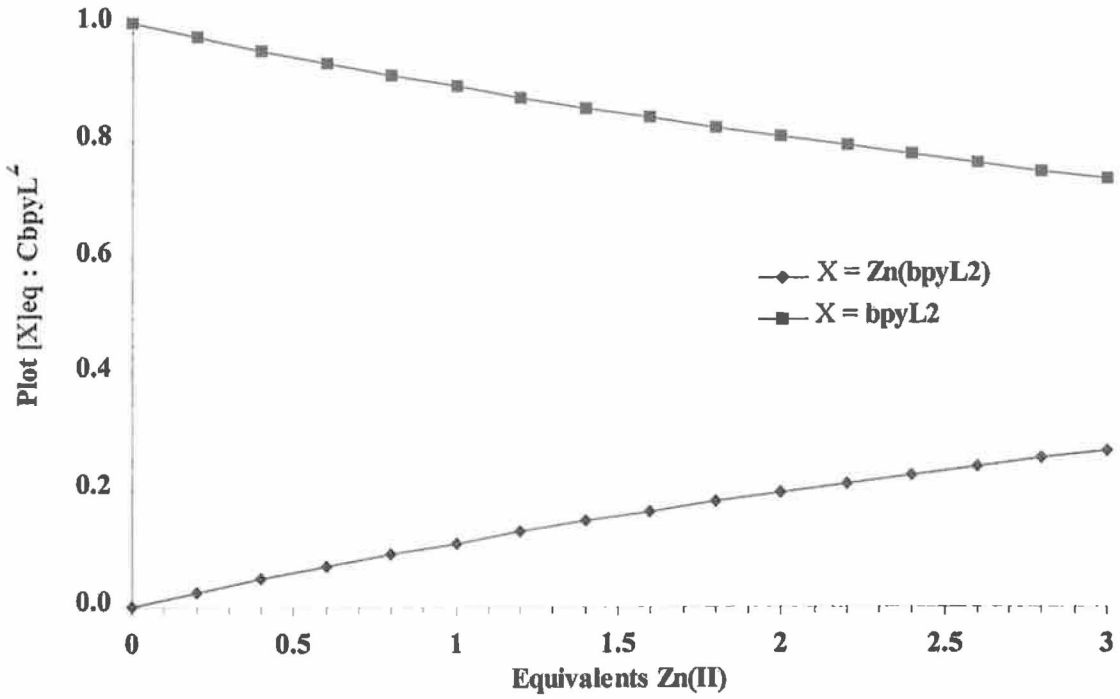

Figure 6.29 *Absorption plot of the ratio of the equilibrium concentration of* ***Zn(bpyL2)*** *and* ***bpyL2*** *to the analytical concentration of* ***bpyL2*** *(C_{bpyL2}) (1:1 model fit).*

Table 6.5 *Stoichiometry and stability constants for the complexation of* ***bpyL2*** *with Ni(II) and Zn(II) obtained using the SIRKO program.*

Model	Data	Comments
	Absorption titrations	
Ni(II)	**(430 nm)**	**ε units are $M^{-1}cm^{-1}$(scaling factor is 1000)**
1:1	$\varepsilon_{bpyL2} = 9.1$ (not refined) $\varepsilon_{Ni(II)} = 0.04$ (not refined) $\varepsilon_{Ni(bpyL2)} = 10.2 \pm 0.1$ Log $\beta = 4.0 \pm 0.1$	The calculations are performed at 430 nm although the changes in the absorbance are very small. The absorbance increases at this wavelength in the course of the titration. The fit is not very good as there is some scattering in the data probably due to the fact that the changes are quite small (R-factor = 0.33 %).
2:1	$\varepsilon_{bpyL2} = 9.1$ (not refined) $\varepsilon_{Ni(II)} = 0.04$ (not refined) $\varepsilon_{Ni(bpyL2)2} = 22.46 \pm 0.05$ Log $\beta = 7.6 \pm 0.1$	This fit is quite similar to the 1:1 fit. However the $\varepsilon_{Ni(bpyL2)2}$ is quite large considering the small changes in absorbance observed in the titration. Seems unlikely that Ni(II) would form a stronger complex than Fe(III) or Fe(II).
	Emission titrations	
Ni(II)	**(660 nm)**	(excited at 485 nm)
1:1	$EI_{bpyL2} = 130.9$ (not refined) $EI_{Ni(II)} = 0$ (not refined)	This fit is not bad and the calculated $EI_{Ni(bpyL2)}$ is a plausible value. The R-factor is quite good for an emission titration (R-factor 0.839).

	$EI_{Ni(bpyL2)} = 111.6 \pm 2.6$ **Log β = 4.5 ± 0.3**	However the changes observed appear more likely to be as a result of dilution rather than complex formation.
2:1	$EI_{bpyL2} = 130.9$ (not refined) $EI_{Ni(II)} = 0$ (not refined) $EI_{Ni(bpyL2)} = 202.2 \pm 11.1$ **Log β = 8.1 ± 0.2**	As with the absorption titrations for **bpyL2** with Ni(II) the 2:1 fit is an equally good fit for the data. The R-factor is slightly better for this fit (R-factor 0.813%).
	Absorption titrations	
Zn(II)	**(475 nm)**	
1:1	$\varepsilon_{bpyL2} = 9.52$ (not refined) $\varepsilon_{Zn(II)} = 0$ (not refined) $\varepsilon_{Zn(bpyL2)} = 10.81 \pm 0.02$ **Log β = 3.8 ± 0.2**	As with the Ni(II) titrations the change in absorbance at 475 nm throughout the course of the Zn(II) titrations is very small. This fit is quite good with an R-factor of 0.223 %.
2:1	$\varepsilon_{bpyL2} = 9.52$ (not refined) $\varepsilon_{Zn(II)} = 0$ (not refined) $\varepsilon_{Zn(bpyL2)2} = 21.66 \pm 0.04$ **Log β = 7.7 ± 0.2**	The 2:1 fit is quite good although the $\varepsilon_{Zn(bpyL2)2}$ value of 21.66 ± 0.04 is quite high considering that the changes in absorbance are so small.
	Emission titrations	
	(660 nm)	(excited at 485 nm)
1:1	$EI_{bpyL2} = 130.9$ (not refined) $EI_{Zn(II)} = 0$ (not refined)	This fit is quite good and after 10 equivalents of Zn(II) has been titrated the emission has quenched considerably which is indicated by

	$EI_{Zn(bpyL2)} = 46.21 \pm 4.60$	the small value for $EI_{Zn(bpyL2)}$ of 46.21 ± 4.60.
	Log β = 3.7 ± 0.1	
2:1	*	No suitable fit.

nm at the beginning of the titration to 442 nm at 3.0 equivalents of Cr(III) titrated. It is also important to note that clean isobestic points are maintained at 460 nm, 393 nm and 348 nm and are similar to the isobestic points of 390 nm and 460 nm observed in the pH-dependent absorption titration of **bpyL2** (see Figure 4.16). In the emission complexation titration of **bpyL2** with Cr(III) (see Figure 6.26 (b)) the emission shows a quenching effect at 660 nm and a blue shift in λ_{max}. These features are similar to those seen in the pH-dependent emission titration of **bpyL2** (see Figure 4.18). This similarity indicates that the changes seen in the Figure 6.26 (a) and (b) may reflect protonation of the triazole rather than complexation of Cr(III). This may be more likely to occur in this titration due to the fact that the chromium salt contains six water molecules.

The absorption titration of **bpyL2** with Ni(II) (see Figure 6.27 (a)) displays very small changes in the absorption spectra as the titration proceeds. There is no shift in the λ_{max} and no evidence of isobestic points. The fact that the absorption increases between 350 nm and 480 nm implies that the effects seen are the additive effects of the Ni(II) absorption (see Figure 6.7 (d)). In the emission titrations of **bpyL2** with Ni(II) (see Figure 6.27 (b)) there is a reduction in the emission intensity with titrated Ni(II) although the quenching is not as significant as that observed in the Fe(III) and Fe(II) titrations (see Figure 6.15 and Figure 6.19). The SIRKO calculations for the absorption titrations at 430 nm (see Table 6.5) reveal that the model fits (1:1 and 2:1) are not great with quite a lot of scattered points and a high R-factor of 0.53 %. The calculated

$\varepsilon_{Ni(bpyL2)2}$ of 29.95 ± 1.11 appears to be quite high considering the small changes in absorbance units during the titration and this may indicate that the 1:1 model fit best represents the complexation between **bpyL2** and Ni(II). The stability constants (log β) calculated from the absorption titrations are not reliable considering the scattering of the experimental data and the small changes in absorbance that were observed. The SIRKO calculations for the Ni(II) emission titrations (see Table 6.5) display moderate 1:1 and 2:1 model fits with R-factors in the region of 0.8 %, which was quite good for emission titrations. Another interesting factor from the SIRKO calculations indicated that after only 3 equivalents of Ni(II) have been titrated there was almost 70 % of complex formation. The results obtained from the Ni(II) absorption titrations do not readily imply that any complexation has taken place and the calculations reflect this uncertainty. However there is a more noticeable effect in the emission spectra during the titration and the SIRKO calculations reflect the changes with quite suitable 1:1 and 2:1 model fits.

The absorption and emission titrations of **bpyL2** with Zn(II) are presented in Figure 6.28 (a) and (b) respectively. As in the Ni(II) titrations, the changes in the absorption spectra in the Zn(II) titrations are quite small. There was no shift in the λ_{max} and no real evidence of isobestic points. There was a significant quenching effect observed in the emission titrations with about a 50 % reduction in the emission intensity after 10 equivalents of Zn(II) has been titrated. The SIRKO calculations indicate that the 1:1 model fit is the most suitable fit as the 2:1 model did not fit the emission data. It is important to note though that the plot shown in Figure 6.29 indicates that only 20 % of the **Zn(bpyL2)** complex has formed after only 3 molar equivalents of titrated Zn(II). With this fact in mind it would probably require a 20 fold excess of Zn(II) for 100 % complex formation.

6.3 Concluding Comments

In this chapter the ability of the catechol complex **bpyL2** to coordinate transition metals was demonstrated. In Chapter five the ruthenium dinuclear complex of **bpyL2**, bound via the catechol group, was synthesised, isolated and characterised. The complex formation between the catechol complex and a series of transition metals was followed by a series of spectrophotometric catechol-metal titrations. The absorption and emission data was manipulated by SIRKO, a program for calculating stability constants (β), and the validity of the complexation was ascertained by assessment of the output from SIRKO. The values for log β stated in this section represent the average value between the absorption and emission data.

Titration of the protected catechol complex, **bpyL1**, with Fe(III) showed significant changes in the absorption and emission titrations. The possibility of these changes occurring due to protonation of the triazole was considered unlikely due to the difference between the spectrophotometric complexation titrations and the spectrophotometric pH-dependent titrations. The possibility of the Fe(III) binding through the N4 of the triazole was also considered unlikely due to the low affinity of Fe(III) for amine type ligands indicating that the Fe(III) must have bound through the protected catechol moiety. The calculations estimated a 1:1 complex denoted as **Fe(bpyL1)** with **log B = 4.6 ± 0.2**. **BpyL1** was considered not to have complexed with either Fe(II) or Cu(II).

It was established that Fe(III) formed a 1:1 complex with **bpyL2 (log β = 5.5 ± 0.1)** with 50 % of the complex formation complete after 0.6 equivalents of titrated Fe(III) and 90 % complex formation after 2 equivalents of titrated Fe(III) (see Figure

6.10). In the Fe(III) emission titrations the emission was almost quenched after just 2 equivalents of titrated Fe(III) which was much more significant than the 15 % quenching effect displayed in the titration of $[Ru(bpy)_3]^{2+}$ with Fe(III). There was also a quenching effect observed in the **bpyL2** titrations with Fe(II), although in this case almost 9 equivalents of titrated Fe(II) was required to cause around 80 % reduction in the emission intensity. It was also established that only 40 % of the 1:1 complex formed between Fe(II) and **bpyL2**, [**Fe(bpyL2)**, was formed after 10 equivalents of titrated Fe(II) indicated by the lower stability constant, **log β = 3.4 ± 0.1,** than that estimated for the complexation with Fe(III).

The titration of **bpyL2** with Cu(II) produced the most interesting results in the spectrophotometric titrations. Analysis of the SIRKO calculations led to the assumption that two complexes were formed in the titration. Firstly between 0 and 0.8 equivalents of titrated Cu(II), a 2:1 complex was formed, **$Cu(bpyL2)_2$ (log β = 11.3 ± 0.1)**. When the titration proceeded further **$Cu(bpyL2)_2$** reacted with the titrated Cu(II) to produce the 1:1 complex **Cu(bpyL2) (log B = 4.8 ± 0.1)**. The complexation titrations of **bpyL2** with Cr(III), Ni(II) and Zn(II) produced less significant changes in the absorption and emission spectra than those previously studied. In the case of the Cr(III) the changes in the absorption and emission titrations are more similar to those expected for protonation of the triazole than complexation. The Ni(II) titrations also strongly indicate that no complexation takes place and the uncertainty in the values generated by SIRKO support this conclusion. Finally in the case of the Zn(II) titrations, the changes in the absorption spectra are quite small with more significant changes in the emission spectra. The SIRKO calculations indicate that complex formation is slow (**log β = 3.8 ± 0.1**) with only 20 % complex formation after 3 equivalents of titrated Zn(II).

6.4 References

1 W.P. Griffith, *Trans. Met. Chem.*, 1993, 18, 250.

2 H.H. Downs, R.M. Buchanan, C.G. Pierpont, *Inorg. Chem.*, 1979, 18, 1736.

3 T.D.P. Stack, T.B. Karpishin, K.N. Raymond, *J. Am. Chem. Soc.*, 1992, 114, 1512.

4 L. Sun, H. Berglund, R. Davydov, T. Norrby, L. Hammarstrom, P. Korall, A. Börje, C. Philouze, K. Berg, A. Tran, M. Andersson, G. Strenhagen, J. Mårtensson, M. Almgren, S. Styring, B. Åkermark, *J. Am. Chem. Soc.*, 1997, 119, 6996.

5 A. Avdeef, S.R. Sofen, T.L. Bregante, K.N. Raymond, *J. Am. Chem. Soc.*, 1978, 100, 5362.

6 P.S. Dobbin, R.C. Hider, *Chemistry in Britain*, 1990, 565.

7 V.L. Pecoraro, F.L. Weitl, K.N. Raymond, *J. Am. Chem. Soc.*, 1981, 103, 5133.

8 S.D. Lytton, B. Mester, J. Libman, A. Shanzer, Z.I. Cabantchik, *Analytical Biochemistry*, 1992, 205, 326.

9 S.R. Boone, G.H. Purser, H.R. Chang, M.D. Lowery, D.N. Hendrickson, C.G. Pierpont, *J. Am. Chem. Soc.*, 1989, 111, 2292.

10 M.W. Lynch, M. Valentine, D.N. Hendrickson, *J. Am. Chem. Soc.*, 1982, 104, 6982.

11 J-P. M. Tuchagues, D.N. Hendrickson, *Inorg. Chem.*, 1983, 22, 2545.

12 D. Zirong, R.C. Haltiwanger, S. Bhattacharya, C.G. Pierpont, *Inorg. Chem.*, 1991, 30, 4288.

[13] A.S. Attia, B.J. Conklin, C.W. Lange, C.G. Pierpont, *Inorg. Chem.*, 1996, 35, 1033.

[14] R.M. Buchanan, S.L. Kessel, H.H. Downs, C.G. Pierpont, D.N. Hendrickson, *J. Am. Chem. Soc.*, 1978, 100, 7894.

[15] S.R. Sofen, D.C. Ware, S.R. Cooper, K.N. Raymond, *Inorg. Chem.*, 1979, 18, 234.

[16] H.H. Downs, R.M. Buchanan, C.G. Pierpont, *Inorg. Chem.*, 1979, 18, 1736.

[17] R.M. Buchanan, J. Claflin, C.G. Pierpont, *Inorg. Chem.*, 1983, 22, 2552.

[18] D.E. Wheeler, J.K. McCusker, *Inorg. Chem.*, 1998, 37, 2296.

[19] S. Harmalker, S.E. Jones, D.T. Sawyer, *Inorg. Chem.*, 1983, 22, 2790.

[20] J.S. Thompson, J.C. Calabrese, *Inorg. Chem.*, 1985, 24, 3167.

[21] O. Kahn, R. Prins, J. Reedijk, J.S. Thompson, *Inorg. Chem.*, 1987, 26, 3557.

[22] G. Speier, S. Tisza, Z. Tyeklar, C.W. Lange, C.G. Pierpont, *Inorg. Chem.*, 1994, 33, 2041.

[23] M.E. Bodini, G. Copia, R. Robinson, D.T. Sawyer, *Inorg. Chem.*, 1983, 22, 126.

[24] W. Paw, R. Eisenberg, *Inorg. Chem.*, 1997, 36, 2287.

[25] W. Paw, W.B. Connick, R. Eisenberg, *Inorg. Chem.*, 1998, 37, 3919.

[26] R.H. Fish, R.S. Tannous, *Inorg. Chem.*, 1985, 24, 4456.

[27] S-P. Huang, W. Li, K.J. Franz, R.L. Albright, R.H. Fish, *Inorg. Chem.*, 1995, 34, 2813.

[28] A.V. Bogatsky, Phsico-Chemical Institute, Odessa. Laboratoire de Chemie Physique, ECPM, Strasbourg.
http://www.geocities.com/capecanaveral/Lab/9065.

[29] V.I. Vetrogon, N.G. Lukyanenko, M.-J. Schwing-Weill, F. Arnaud-Neu, *Talanta*, 1994, 41, 2105.

[30] P. Suppan, Principles of photochemistry, The Chemical Society, Bartholomew Press, Dorking, 1973.

[31] F.A. Cotton, G. Wilkinson, Advanced Inorganic Chemistry, Wiley, Chichester, 5th ed., 1988.

[32] S. Rau, T. Büttner, C. Temme, M. Ruben, H. Görls, D. Walther , M. Duati, S. Fanni, J.G. Vos, *Inorg. Chem.*, 2000, 39, 1621.

Chapter Seven

Final Remarks And Future Work

In this thesis the the synthesis and characterisation of several ruthenium (II) complexes of the ligand 3-(1′,2′-dimethoxyphenyl)-5-(pyridin-2-yl)-1,2,4-triazole (HL1), which was described in chapter 3, provides the groundwork for the rest of the research. Synthesis of the complexes from the protected ligand, HL1, ensures that the N,N bound mononuclear complexes can be more easily isolated than would be possible with synthesis of mononuclear complexes of the catechol ligand, H_3L2. The coordination mode of the pyridyl-trizole ligand (HL1) was confirmed by ^{1}H-NMR and X-Ray crystallography. The ligand coordinates via N1 of the pyridine nitrogen triazole ring and the pyridine nitrogen. The X-Ray data for the **d_8-bpyL1** complex and the **phenL1** complex is typical for pyridyltriazole complexes. Investigation of the absorption, emission and acid-base properties of the complexes of HL1 confirms the classification of the ligand HL1 as a weak π-acceptor and strong σ-donor (class b type ligand). In the electrochemical studies of these complexes it was established that the methoxy units on the phenyl ring are non-innocent. When the cyclic voltammetry was allowed to scan higher than 1 V there was considerable irreversibility induced which causes the loss of the metal-centred redox couple.

The demethylation of the complexes **bpyL1** and **phenL1** provided us with ruthenium(II) pyridyltriazole complexes containing a pendant catechol moiety. The advantages of a ruthenium(II) mononuclear complexes containing an appealing peripheral binding site was exploited in chapter 5 and 6. Attachment of the catechol complexes and the dicarboxy complex, **dcbpyL1**, to nanocrystalline TiO_2 films indicates incident photon-to-current efficiency (IPCE) of greater than 30%. In chapter 5 the synthesis of the semiquinone bound ru-ru dimers was discussed. The most

distinguishing factor in the electronic spectra of the dinuclear complexes was the Ru(dπ) → semiquinone(π^*) MLCT transition in the NIR region. The electrochemical properties of the complexes were typical of semiquinone bound dinuclear ruthenium complexes. **Bpybpy** showed three couples in the region (1.4 to -0.6 V) which were assigned as cat/sq (-0.2 V), sq/q (0.47 V) and Ru(II)/Ru(III) (1.0 V). Spectroelectrochemical studies suggest an irreversible Ru(III)-quinone complex is formed at potentials greater than 1.2 V. The square-wave voltammetry proved to be an important tool in the study of the electrochemical properties of the dinuclear complexes.

Chapter 6 examined the coordinating ability of the external catechol moiety of **bpyL2**. The most interesting results were obtained for the complexation titrations of **bpyL2** with Fe(III) (log $B_{1:1}$ = 4.6 ± 0.2) and Cu(II) (log $\beta_{2:1}$ = 11.3 ± 0.1 and log $\beta_{1:1}$ = 4.8 ± 0.1). In the case of Cu(II), initially a 2:1 complex was formed after 0.6 molar equivalents of Cu(II) had been titrated. Titration of further equivalents of Cu(II) resulted in the 2:1 complex breaking down to the 1:1 complex. The titration of the catechol complex with Cr(III), Ni(II) and Zn(II), respectively did not indicate any complexation while a weaker complex was formed between Fe(II) and **bpyL2** (log $\beta_{1:1}$ = 3.4 ± 0.1).

In future work the complexation titrations of **bpyL2** with Fe(III) and Cu(II) should be examined in more detail. It was established in chapter 6 that after 0.8 molar equivalents of Fe(III) had been titrated with **bpyL2**, almost 60 % of the 1:1 complex had formed. The titration of **bpyL2** with Cu(II) shows almost 40 % of the 2:1 complex formed after 0.8 molar equivalents of titrated Cu(II). Future studies should focuss on the region from 0 equivalent to 1.0 equivalent of titrated Fe(III) or Cu(II) with smaller

molar equivalents. It may also be possible to monitor complex formation by mass spectrometry.

In chapter three the deuteriated complexes, **d_8-bpyL1** and **d_8-phenL1** were synthesised and characterised aiding in the assignment of the ligand (L1) protons and probing the excited state of the complex by exhibiting a longer lifetime than the undeuteriated complexes. At present attempts at deuteriating the ligand itself is ongoing. This would provide further assistance in the structural elucidation although the lifetimes should not be affected.

Appendix 1

Section 1: ^{1}H-NMR spectrum of 3-(1′,2′-dimethoxyphenyl)-5-(pyridin-2-yl)-1,2,4-triazole (HL1) in d_6-dimethyl sulphoxide.

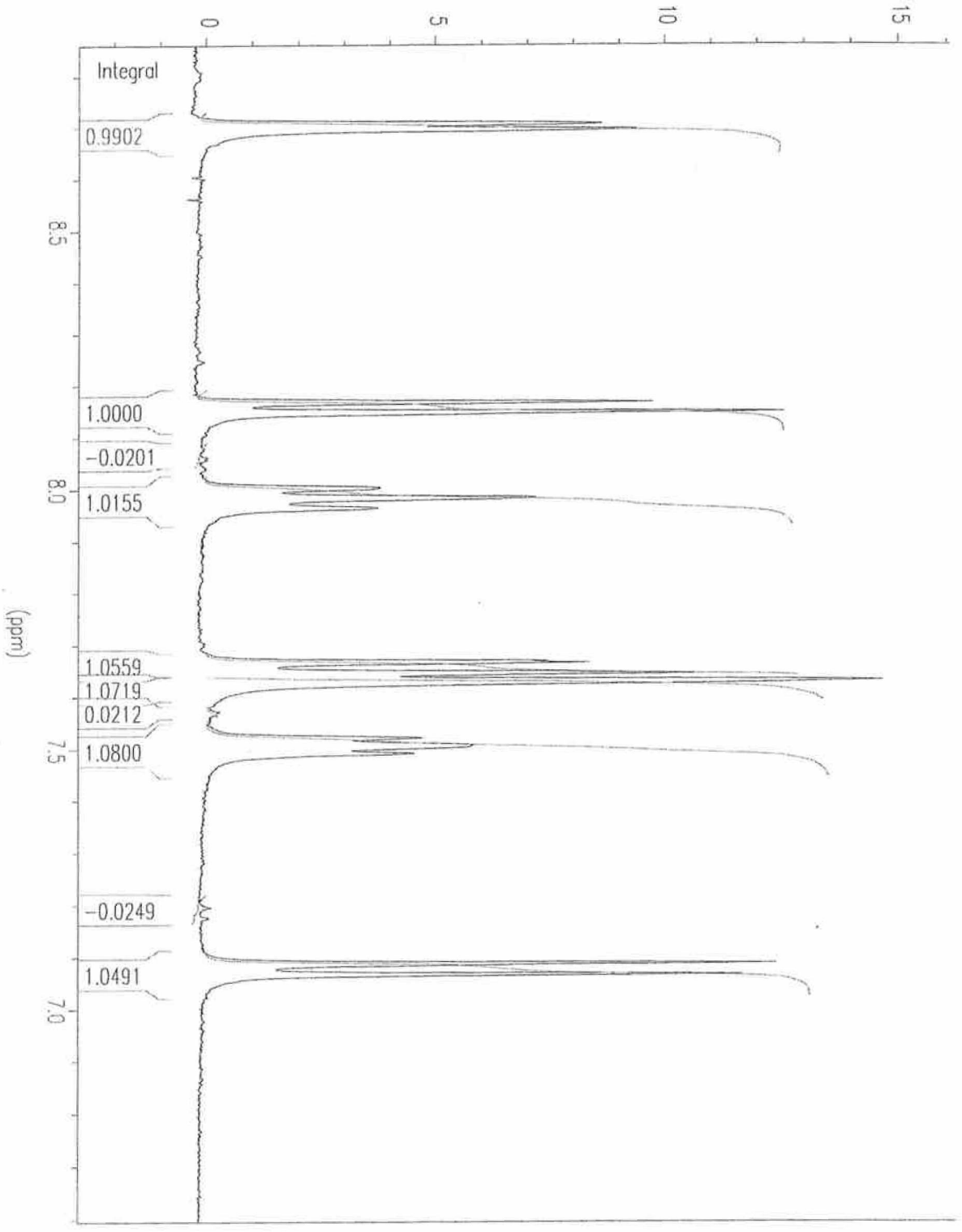

Section 2: ^{1}H-NMR spectrum of 3-(1′,2′-dihydroxyphenyl)-5-(pyridin-2-yl)-1,2,4-triazole (HL1) in d_6-dimethyl sulphoxide.

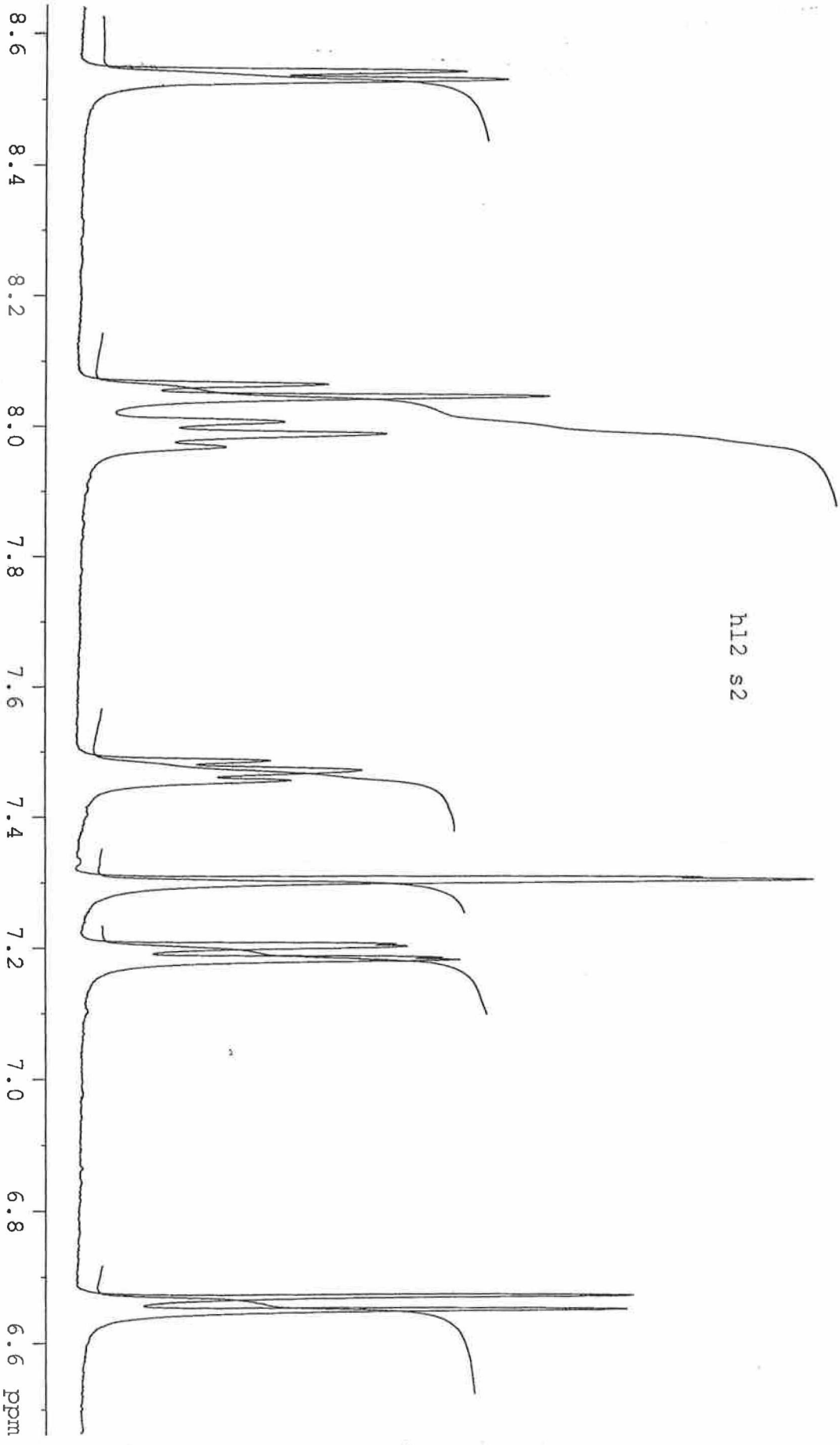

c

Section 3: **^{1}H-NMR spectrum of $[Ru(H_4dcbpy)_2(HL1)]Cl_2.5H_2O$ (dcbpyL1) in d_6-dimethyl sulphoxide.**

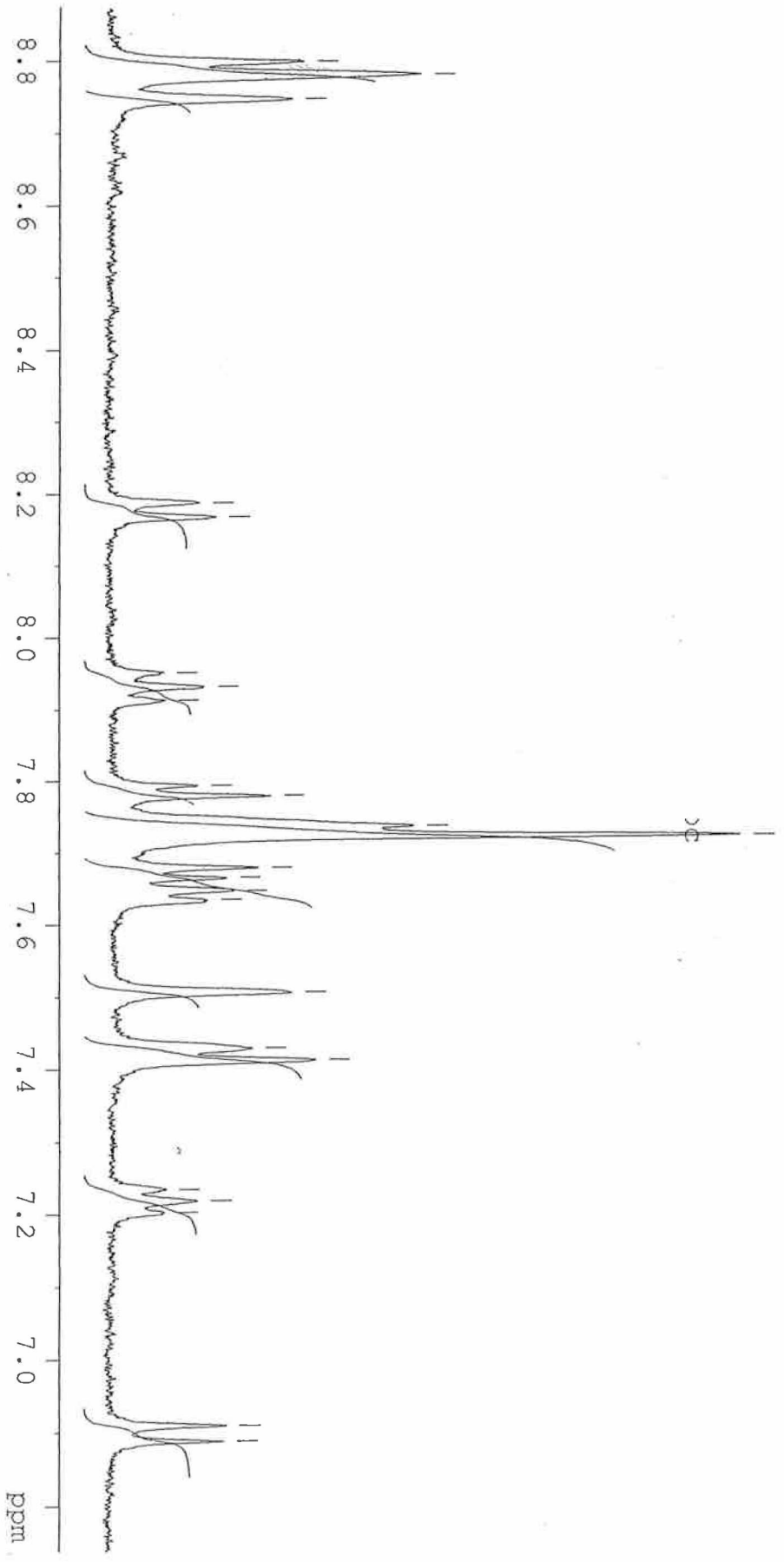

d

Appendix 2

Section 1. Crystal Structure Determination.

The intensity data for the compounds were collected on a Nonius KappaCCD diffractometer, using graphite-monochromated Mo-K_α radiation. Data were corrected for Lorentz and polarization effects, but not for absorption [1,2] .

The structures were solved by direct methods (SHELXS [3]) and refined by full-matrix least squares techniques against Fo^2 (SHELXL-97 [4]). The hydrogen atoms of the structures were included at calculated positions with fixed thermal parameters. All non-hydrogen atoms were refined anisotropically [4]. XP (SIEMENS Analytical X-ray Instruments, Inc.) was used for structure representations.

Crystal Data for $Ru(d_8\text{-}bpy)_2(L1)]PF_6.H_2O$: $Ru_1C_{35}H_{15}D_{16}N_8O_3P_1F_6$, Mr = 873.84 $gmol^{-1}$, red-brown prism, size 0.32 x 0.30 x 0.20 mm^3, monoclinic, space group $P2_1/n$, a = 9.1165(9), b = 18.068(1), c = 21.424(1) Å, β = 96.599(6) °, V = 3505.5(4) $Å^3$, T= -90 °C, Z = 4, $\rho_{calcd.}$ = 1.625 gcm^{-3}, μ (Mo-K_α) = 5.75 cm^{-1}, F(000) = 1736, 7296 reflections in h(-11/11), k(-22/0), l(0/26), measured in the range 2.34° ≤ Θ ≤ 26.31°, completeness Θ max = 99.8 %, 7106 independent reflections, R_{int} = 0.026, 4811 reflections with $F_o > 4\sigma(F_o)$, 482 parameters, 0 restraints, $R1_{obs}$ = 0.049, wR^2_{obs} = 0.139, $R1_{all}$ = 0.096, wR^2_{all} = 0.154, GOOF = 0.916, largest difference peak and hole: 1.183 / -0.658 e $Å^{-3}$.

Crystal Data for $[Ru(phen)_2(L1)]PF_6.H_2O$: $Ru_1C_{39}H_{31}N_8O_3P_1F_6$, Mr = 905.76 $gmol^{-1}$, red-brown prism, size 0.38 x 0.32 x 0.28 mm^3, monoclinic, space group $P2_1/c$, a = 11.6379(9), b = 19.473(2), c = 16.8790(10) Å, β = 102.944(7) °, V = 3728.0(5) $Å^3$, T= -90 °C, Z = 4, $\rho_{calcd.}$ = 1.582 gcm^{-3}, μ (Mo-K_α) = 5.42 cm^{-1}, F(000) = 1792, 7896 reflections in h(-14/14), k(-24/0), l(0/21), measured in the range 2.43° ≤ Θ ≤ 26.42°, completeness Θ

max = 99.4 %, 7631 independent reflections, R_{int} = 0.029, 4848 reflections with $F_o > 4\sigma(F_o)$, 508 parameters, 0 restraints, $R1_{obs}$ = 0.053, wR^2_{obs} = 0.142, $R1_{all}$ = 0.116, wR^2_{all} = 0.156 , GOOF = 0.997, largest difference peak and hole: 0.996 / -0.558 e $Å^{-3}$.

[1] COLLECT, Data Collection Software; Nonius B.V., Netherlands, **1998**

[2] Z. Otwinowski & W. Minor, "Processing of X-Ray Diffraction Data Collected in Oscillation Mode", in Methods in Enzymology, Vol. 276, Macromolecular Crystallography, Part A, edited by C.W. Carter & R.M. Sweet, pp. 307-326, Academic Press **1997**

[3] G.M. Sheldrick, *Acta Crystallogr. Sect. A* **1990**, *46*, 467-473

[4] G.M. Sheldrick, SHELXL-97, University of Göttingen, Germany, **1993**

Section 2. Crystal structure and data for $Ru(d_8\text{-bpy})_2(L1)]PF_6.H_2O$.

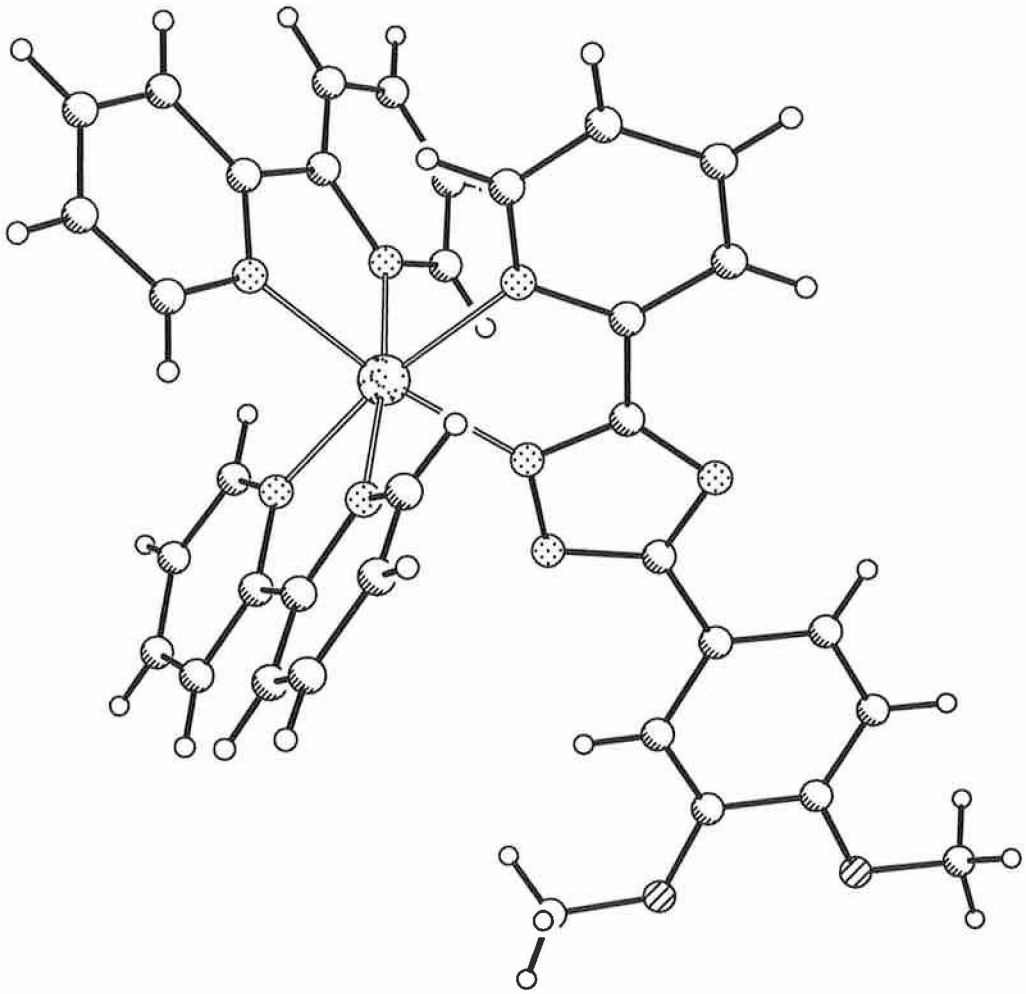

Figure 1. Schematic representation of $Ru(d_8\text{-bpy})_2(L1)]PF_6.H_2O$ crystal structure.

Table 1. **Bond distances (Å) and Bond angles (^{O}) for $[Ru(d_8bpy)_2(L1)]PF_6.H_2O$.**

Ru-N(4)	2.038(4)	N(4)-C(16)	1.337(6)
Ru-N(1B)	2.044(4)	N(4)-N(5)	1.369(5)
Ru-N(2A)	2.043(4)	N(5)-C(17)	1.342(6)
Ru-N(2B)	2.044(4)	N(6)-C(16)	1.336(6)
Ru-N(1A)	2.062(4)	N(6)-C(17)	1.358(6)
Ru-N(3)	2.109(4)	C(12)-C(13)	1.361(8)
N(1A)-C(1A)	1.327(6)	C(13)-C(14)	1.381(7)
N(1A)-C(5A)	1.371(6)	C(14)-C(15)	1.384(7)
N(2A)-C(6A)	1.352(7)	C(15)-C(16)	1.454(6)
N(2A)-C(10A)	1.351(7)	C(17)-C(18)	1.466(6)
C(1A)-C(2A)	1.388(8)	C(18)-C(19)	1.384(7)
C(2A)-C(3A)	1.353(9)	C(18)-C(23)	1.399(7)
C(3A)-C(4A)	1.356(9)	C(19)-C(20)	1.393(7)
C(4A)-C(5A)	1.372(8)	C(20)-C(21)	1.365(7)
C(5A)-C(6A)	1.480(7)	C(21)-O(2)	1.370(6)
C(6A)-C(7A)	1.389(7)	C(21)-C(22)	1.406(7)
C(7A)-C(8A)	1.376(9)	C(22)-O(1)	1.356(6)
C(8A)-C(9A)	1.351(9)	C(22)-C(23)	1.372(7)
C(9A)-C(10A)	1.369(7)	O(1)-C(24)	1.434(7)
N(1B)-C(1B)	1.350(6)	O(2)-C(25)	1.416(7)
N(1B)-C(5B)	1.357(7)	P-F(1A)	1.518(10)
N(2B)-C(10B)	1.334(7)	P-F(2A)	1.544(7)
N(2B)-C(6B)	1.351(7)	P-F(4)	1.55(3)
C(1B)-C(2B)	1.368(8)	P-F(3A)	1.563(9)
C(2B)-C(3B)	1.323(10)	P-F(6)	1.55(4)
C(3B)-C(4B)	1.421(10)	P-F(5A)	1.584(7)
C(4B)-C(5B)	1.394(8)	P-F(3)	1.61(2)
C(5B)-C(6B)	1.451(8)	P-F(6A)	1.608(8)
C(6B)-C(7B)	1.396(8)	P-F(4A)	1.640(8)
C(7B)-C(8B)	1.361(10)	P-F(2)	1.72(3)
C(8B)-C(9B)	1.345(10)	P-F(1)	1.71(3)
C(11)-N(3)	1.331(6)	P-F(5)	1.71(3)
C(11)-C(12)	1.374(7)	F(1)-F(6)	1.63(4)
N(3)-C(15)	1.355(6)	F(2)-F(6)	1.53(4)
C(9B)-C(10B)	1.357(9)	F(2)-F(5)	1.69(4)

N(4)-Ru-N(1B)	94.29(15)	C(1B)-N(1B)-C(5B)	119.5(5)
N(4)-Ru-N(2A)	171.43(16)	C(1B)-N(1B)-Ru	125.4(4)
N(1B)-Ru-N(2A)	93.29(15)	C(5B)-N(1B)-Ru	115.0(3)
N(4)-Ru-N(2B)	89.88(15)	C(10B)-N(2B)-C(6B)	118.3(5)
N(1B)-Ru-N(2B)	79.00(17)	C(10B)-N(2B)-Ru	126.4(4)
N(2A)-Ru-N(2B)	95.48(16)	C(6B)-N(2B)-Ru	115.2(3)

N(6)-C(16)-N(4)	112.8(4)	F(3)-P-F(6A)	80.3(8)
N(6)-C(16)-C(15)	130.1(4)	F(1A)-P-F(4A)	172.2(5)
N(4)-C(16)-C(15)	117.1(4)	F(2A)-P-F(4A)	90.2(4)
N(5)-C(17)-N(6)	114.1(4)	F(4)-P-F(4A)	37.7(11)
N(5)-C(17)-C(18)	121.8(4)	F(3A)-P-F(4A)	87.5(5)
N(6)-C(17)-C(18)	124.0(4)	F(6)-P-F(4A)	109.8(16)
C(19)-C(18)-C(23)	119.4(4)	F(5A)-P-F(4A)	84.1(4)
C(19)-C(18)-C(17)	120.4(4)	F(3)-P-F(4A)	63.1(8)
C(23)-C(18)-C(17)	120.2(4)	F(6A)-P-F(4A)	86.4(4)
C(18)-C(19)-C(20)	119.5(5)	F(1A)-P-F(2)	52.1(8)
C(21)-C(20)-C(19)	121.3(5)	F(2A)-P-F(2)	52.7(8)
C(20)-C(21)-O(2)	125.3(5)	F(4)-P-F(2)	96.9(15)
C(20)-C(21)-C(22)	119.3(4)	F(3A)-P-F(2)	132.8(9)
O(2)-C(21)-C(22)	115.4(5)	F(6)-P-F(2)	55.6(16)
O(1)-C(22)-C(23)	124.8(5)	F(5A)-P-F(2)	116.1(9)
O(1)-C(22)-C(21)	115.4(4)	F(3)-P-F(2)	145.9(11)

N(4)-Ru-N(1A)	96.11(15)	N(1B)-C(1B)-C(2B)	120.8(6)
N(1B)-Ru-N(1A)	99.22(16)	C(3B)-C(2B)-C(1B)	120.9(6)
N(2A)-Ru-N(1A)	78.73(16)	C(2B)-C(3B)-C(4B)	120.6(6)
N(2B)-Ru-N(1A)	173.89(15)	C(5B)-C(4B)-C(3B)	116.5(6)
N(4)-Ru-N(3)	77.86(15)	N(1B)-C(5B)-C(4B)	121.5(6)
N(1B)-Ru-N(3)	170.92(15)	N(1B)-C(5B)-C(6B)	114.7(5)
N(2A)-Ru-N(3)	94.88(15)	C(4B)-C(5B)-C(6B)	123.7(6)
N(2B)-Ru-N(3)	96.25(17)	N(2B)-C(6B)-C(7B)	119.4(6)
N(1A)-Ru-N(3)	86.28(15)	N(2B)-C(6B)-C(5B)	115.4(5)
C(1A)-N(1A)-C(5A)	118.2(4)	C(7B)-C(6B)-C(5B)	124.9(6)
C(1A)-N(1A)-Ru	127.0(3)	C(8B)-C(7B)-C(6B)	120.5(7)
C(5A)-N(1A)-Ru	114.5(3)	C(9B)-C(8B)-C(7B)	119.1(7)
C(6A)-N(2A)-C(10A)	117.9(4)	C(8B)-C(9B)-C(10B)	119.2(7)
C(6A)-N(2A)-Ru	115.9(3)	N(2B)-C(10B)-C(9B)	123.4(7)
C(10A)-N(2A)-Ru	126.2(4)	N(3)-C(11)-C(12)	122.9(5)
N(1A)-C(1A)-C(2A)	122.0(5)	C(11)-N(3)-C(15)	118.0(4)
C(3A)-C(2A)-C(1A)	119.2(6)	C(11)-N(3)-Ru	127.0(4)
C(2A)-C(3A)-C(4A)	119.9(6)	C(15)-N(3)-Ru	115.1(3)
C(3A)-C(4A)-C(5A)	119.8(6)	C(16)-N(4)-N(5)	107.4(4)
N(1A)-C(5A)-C(4A)	121.0(5)	C(16)-N(4)-Ru	116.3(3)
N(1A)-C(5A)-C(6A)	114.1(4)	N(5)-N(4)-Ru	136.1(3)
C(4A)-C(5A)-C(6A)	124.7(5)	C(17)-N(5)-N(4)	103.9(4)
N(2A)-C(6A)-C(7A)	121.1(5)	C(16)-N(6)-C(17)	101.8(4)
N(2A)-C(6A)-C(5A)	114.6(4)	C(13)-C(12)-C(11)	119.5(5)
C(7A)-C(6A)-C(5A)	124.3(5)	C(12)-C(13)-C(14)	118.8(5)
C(8A)-C(7A)-C(6A)	119.1(6)	C(13)-C(14)-C(15)	119.3(5)
C(9A)-C(8A)-C(7A)	119.9(5)	N(3)-C(15)-C(14)	121.5(4)
C(8A)-C(9A)-C(10A)	119.1(6)	N(3)-C(15)-C(16)	113.6(4)
N(2A)-C(10A)-C(9A)	122.8(6)	C(14)-C(15)-C(16)	124.8(4)

C(23)-C(22)-C(21)	119.7(5)	F(6A)-P-F(2)	73.6(9)
C(22)-C(23)-C(18)	120.7(4)	F(4A)-P-F(2)	134.6(9)
C(22)-O(1)-C(24)	116.7(4)	F(1A)-P-F(1)	40.8(8)
C(21)-O(2)-C(25)	117.9(5)	F(2A)-P-F(1)	134.0(10)
F(1A)-P-F(2A)	97.5(5)	F(4)-P-F(1)	146.3(13)
F(1A)-P-F(4)	148.9(13)	F(3A)-P-F(1)	51.3(9)
F(2A)-P-F(4)	57.4(11)	F(6)-P-F(1)	59.8(15)
F(1A)-P-F(3A)	84.8(6)	F(5A)-P-F(1)	109.6(9)
F(2A)-P-F(3A)	171.9(5)	F(3)-P-F(1)	70.4(12)
F(4)-P-F(3A)	122.7(12)	F(6A)-P-F(1)	74.2(9)
F(1A)-P-F(6)	69.9(16)	F(4A)-P-F(1)	132.0(10)
F(2A)-P-F(6)	92.6(15)	F(2)-P-F(1)	81.6(12)
F(4)-P-F(6)	91.4(18)	F(1A)-P-F(5)	31.7(11)
F(3A)-P-F(6)	95.5(15)	F(2A)-P-F(5)	82.7(12)
F(1A)-P-F(5A)	96.0(5)	F(4)-P-F(5)	139.4(16)
F(2A)-P-F(5A)	89.3(4)	F(3A)-P-F(5)	95.6(12)
F(4)-P-F(5A)	101.3(11)	F(6)-P-F(5)	98.4(19)
F(3A)-P-F(5A)	82.8(4)	F(5A)-P-F(5)	68.0(13)
F(1A)-P-F(3)	109.1(9)	F(3)-P-F(5)	122.5(14)
F(2A)-P-F(3)	153.0(9)	F(6A)-P-F(5)	121.9(13)
F(4)-P-F(3)	96.0(14)	F(4A)-P-F(5)	151.2(13)
F(3A)-P-F(3)	27.1(8)	F(2)-P-F(5)	59.1(14)
F(6)-P-F(3)	92.7(17)	F(1)-P-F(5)	67.7(14)
F(5A)-P-F(3)	91.9(8)	F(6)-F(1)-P	55.2(15)
F(1A)-P-F(6A)	92.8(5)	F(6)-F(2)-P	56.5(17)
F(2A)-P-F(6A)	94.7(4)	F(6)-F(2)-F(5)	100(2)
F(4)-P-F(6A)	73.2(10)	P-F(2)-F(5)	60.1(14)
F(3A)-P-F(6A)	93.0(4)	P-F(5)-F(2)	60.8(15)
F(6)-P-F(6A)	23.5(15)	F(2)-F(6)-P	68(2)
F(5A)-P-F(6A)	169.8(4)	F(2)-F(6)-F(1)	90(3)
F(6)-P-F(5A)	165.9(16)	P-F(6)-F(1)	65.0(18)

Table 2. **Atomic coordinates (x 10^4) and equivalent isotropic displacement parameters ($Å^2$x 10^3) for $Ru(d_8\text{-bpy})_2(L1)]PF_6.H_2O$. U(eq) is defined as one third of the trace of the orthogonalized U^{ij} tensor.**

	x	y	z	U(eq)
Ru	8510(1)	1839(1)	8127(1)	36(1)
N(1A)	8967(4)	2513(2)	8900(2)	41(1)
N(2A)	7407(4)	2784(2)	7829(2)	41(1)
C(1A)	9883(5)	2372(3)	9412(2)	47(1)
C(2A)	9976(6)	2826(3)	9938(3)	64(1)
C(3A)	9089(7)	3436(3)	9930(3)	68(2)
C(4A)	8154(6)	3594(3)	9404(3)	60(1)
C(5A)	8110(5)	3142(2)	8890(2)	47(1)
C(6A)	7258(5)	3295(2)	8272(2)	46(1)
C(7A)	6398(5)	3922(3)	8142(3)	56(1)
C(8A)	5765(6)	4046(3)	7540(3)	63(2)
C(9A)	5980(6)	3552(3)	7081(3)	60(1)
C(10A)	6788(5)	2924(3)	7238(3)	51(1)
N(1B)	10296(4)	2085(2)	7667(2)	42(1)
N(2B)	8009(4)	1271(2)	7306(2)	46(1)
C(1B)	11400(5)	2548(3)	7874(3)	50(1)
C(2B)	12591(6)	2638(3)	7552(3)	66(2)
C(3B)	12720(7)	2249(4)	7037(4)	80(2)
C(4B)	11600(7)	1763(4)	6799(3)	75(2)
C(5B)	10372(6)	1708(3)	7127(2)	52(1)
C(6B)	9045(6)	1282(3)	6913(2)	52(1)
C(7B)	8748(8)	957(3)	6314(3)	74(2)
C(8B)	7431(10)	633(3)	6138(3)	86(2)
C(9B)	6400(8)	621(3)	6540(3)	81(2)
C(10B)	6715(7)	930(3)	7118(3)	65(2)
C(11)	5422(5)	1693(3)	8584(3)	55(1)
N(3)	6779(4)	1407(2)	8588(2)	42(1)
N(4)	9439(4)	906(2)	8536(2)	36(1)
N(5)	10750(4)	540(2)	8536(2)	38(1)
N(6)	9247(4)	-114(2)	9102(2)	38(1)
C(12)	4349(5)	1364(3)	8895(3)	60(1)
C(13)	4679(5)	736(3)	9234(2)	52(1)
C(14)	6067(5)	431(3)	9247(2)	49(1)
C(15)	7094(4)	775(2)	8911(2)	37(1)
C(16)	8584(4)	503(2)	8871(2)	36(1)
C(17)	10581(4)	-63(2)	8886(2)	36(1)
C(18)	11739(4)	-632(2)	8991(2)	38(1)
C(19)	11718(5)	-1138(2)	9471(2)	44(1)
C(20)	12838(5)	-1669(3)	9569(2)	48(1)

C(21)	13962(5)	-1690(2)	9198(2)	47(1)
C(22)	13962(5)	-1186(2)	8700(2)	45(1)
C(23)	12860(5)	-670(2)	8598(2)	42(1)
O(1)	15110(4)	-1257(2)	8350(2)	64(1)
C(24)	15129(6)	-763(3)	7831(3)	68(2)
O(2)	15111(4)	-2183(2)	9263(2)	61(1)
C(25)	15201(8)	-2683(3)	9775(3)	79(2)
P	12794(2)	4446(1)	9046(1)	75(1)
F(1)	12120(20)	5221(12)	8649(12)	125(8)
F(2)	11630(20)	4763(12)	9562(10)	124(8)
F(3)	13120(20)	4266(15)	8334(11)	118(7)
F(4)	12590(30)	3664(16)	9348(13)	154(10)
F(5)	13450(40)	5232(18)	9453(16)	193(13)
F(6)	11130(50)	4530(20)	8870(20)	203(16)
F(1A)	12355(10)	5237(5)	9172(5)	139(3)
F(2A)	12590(7)	4169(4)	9713(3)	118(2)
F(3A)	13221(9)	4710(5)	8392(4)	132(3)
F(4A)	13327(7)	3617(4)	8872(3)	115(2)
F(5A)	14474(7)	4583(3)	9272(3)	106(2)
F(6A)	11175(8)	4193(4)	8740(3)	100(2)
O(3)	7862(5)	-1342(3)	9640(3)	127(2)

Table 3. Anisotropic displacement parameters ($Å^2 x\ 10^3$) for $Ru(d_8\text{-bpy})_2(L1)]PF_6.H_2O$. The anisotropic displacement factor exponent takes the form: $-2p^2[\ h^2\ a^{*2}U^{11} + ... + 2\ h\ k\ a^*\ b^*\ U^{12}\ ]$

	U^{11}	U^{22}	U^{33}	U^{23}	U^{13}	U^{12}
Ru	32(1)	33(1)	44(1)	6(1)	2(1)	1(1)
N(1A)	36(2)	40(2)	46(2)	6(2)	7(2)	-3(2)
N(2A)	34(2)	39(2)	50(2)	10(2)	3(2)	1(2)
C(1A)	44(2)	49(3)	46(3)	8(2)	3(2)	-2(2)
C(2A)	65(3)	66(3)	59(3)	3(3)	-5(3)	-7(3)
C(3A)	91(4)	58(3)	55(3)	-9(3)	12(3)	-5(3)
C(4A)	71(4)	46(3)	66(3)	-3(3)	25(3)	5(3)
C(5A)	44(2)	40(2)	57(3)	5(2)	12(2)	-2(2)
C(6A)	40(2)	41(2)	59(3)	10(2)	12(2)	0(2)
C(7A)	45(3)	43(3)	81(4)	7(2)	17(3)	8(2)
C(8A)	44(3)	49(3)	95(4)	23(3)	6(3)	11(2)
C(9A)	51(3)	56(3)	73(4)	23(3)	-2(3)	6(2)
C(10A)	44(3)	49(3)	60(3)	14(2)	2(2)	2(2)
N(1B)	38(2)	37(2)	53(2)	13(2)	7(2)	6(2)
N(2B)	53(2)	37(2)	45(2)	5(2)	-5(2)	-3(2)
C(1B)	36(2)	49(3)	65(3)	10(2)	3(2)	-2(2)
C(2B)	40(3)	72(4)	88(4)	15(3)	9(3)	-5(3)
C(3B)	50(3)	100(5)	95(5)	10(4)	36(3)	2(3)
C(4B)	70(4)	88(5)	71(4)	6(3)	32(3)	18(3)
C(5B)	55(3)	49(3)	52(3)	3(2)	11(2)	7(2)
C(6B)	67(3)	37(2)	54(3)	5(2)	10(2)	10(2)
C(7B)	111(5)	57(3)	57(3)	-7(3)	17(3)	-1(3)
C(8B)	139(7)	59(4)	55(4)	-8(3)	-10(4)	-11(4)
C(9B)	102(5)	58(4)	75(4)	4(3)	-19(4)	-22(3)
C(10B)	73(4)	47(3)	69(4)	7(3)	-15(3)	-13(3)
C(11)	33(2)	57(3)	75(4)	11(3)	7(2)	5(2)
N(3)	34(2)	43(2)	48(2)	2(2)	2(2)	-1(2)
N(4)	32(2)	36(2)	41(2)	-2(2)	3(2)	1(1)
N(5)	32(2)	35(2)	48(2)	2(2)	3(2)	1(1)
N(6)	38(2)	36(2)	41(2)	4(2)	4(2)	1(2)
C(12)	34(2)	68(3)	81(4)	10(3)	12(2)	1(2)
C(13)	39(2)	61(3)	58(3)	-5(2)	14(2)	-11(2)
C(14)	48(3)	47(3)	53(3)	-1(2)	12(2)	-4(2)
C(15)	36(2)	38(2)	37(2)	-1(2)	4(2)	1(2)
C(16)	35(2)	35(2)	39(2)	0(2)	7(2)	-3(2)
C(17)	36(2)	32(2)	40(2)	-2(2)	1(2)	-5(2)
C(18)	33(2)	35(2)	44(2)	-2(2)	-1(2)	3(2)
C(19)	39(2)	46(2)	48(3)	6(2)	5(2)	2(2)
C(20)	50(3)	42(3)	52(3)	9(2)	3(2)	8(2)

C(21)	40(2)	40(2)	57(3)	-4(2)	-4(2)	5(2)
C(22)	43(2)	43(2)	50(3)	-3(2)	7(2)	-1(2)
C(23)	40(2)	37(2)	47(3)	4(2)	3(2)	-3(2)
O(1)	51(2)	68(2)	79(3)	8(2)	29(2)	14(2)
C(24)	63(3)	75(4)	70(4)	5(3)	32(3)	4(3)
O(2)	53(2)	57(2)	73(2)	10(2)	3(2)	19(2)
C(25)	90(4)	60(4)	85(4)	13(3)	-1(4)	32(3)
P	78(1)	81(1)	68(1)	7(1)	10(1)	-9(1)
O(3)	76(3)	122(4)	176(6)	88(4)	-10(3)	-17(3)

Section 3. Crystal structure and data for $[Ru(phen)_2(L1)]PF_6.H_2O$.

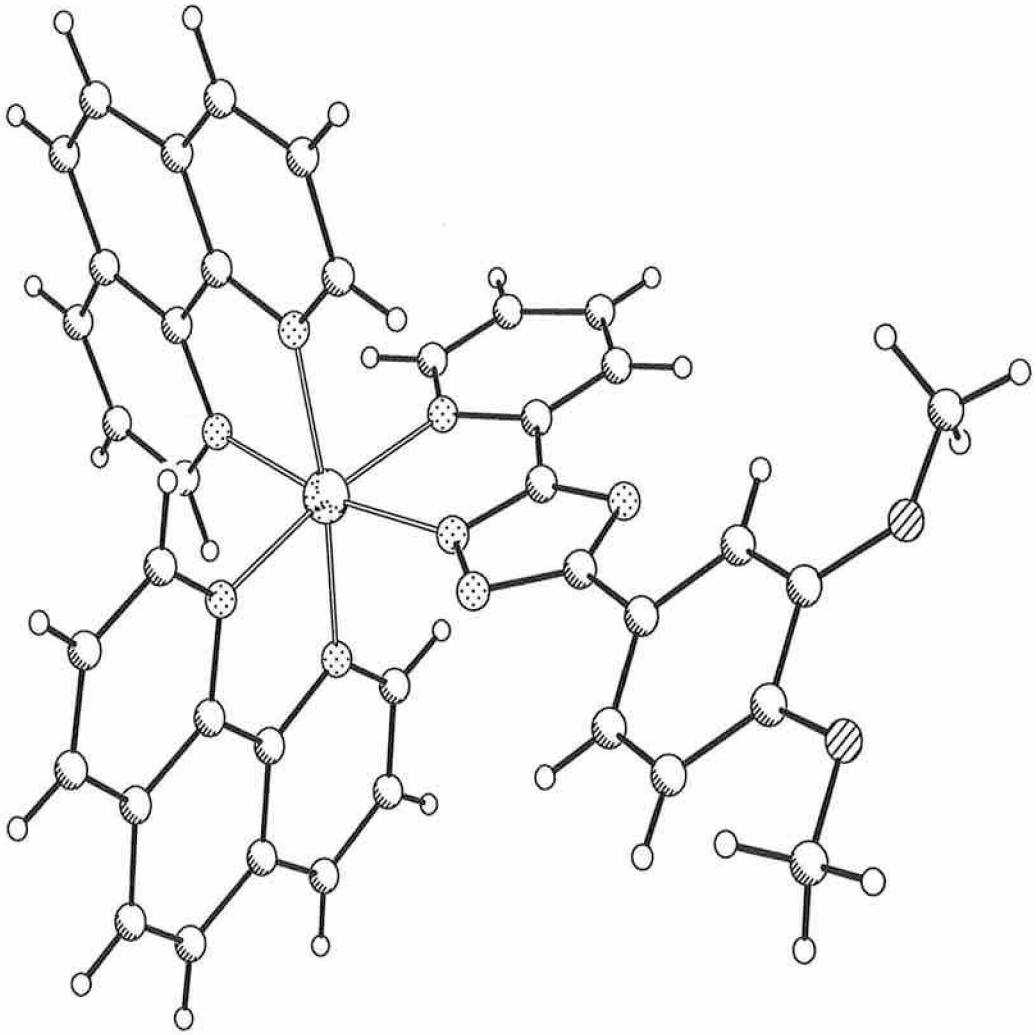

Figure 2. Schematic representation of $[Ru(phen)_2(L1)]PF_6.H_2O$ crystal structure.

Table 4. Bond distances (Å) and Bond angles (°) for $[Ru(phen)_2(L1)]PF_6.H_2O$.

Ru-N(4)	2.036(4)	C(11B)-C(12B)	1.382(7)
Ru-N(1A)	2.054(4)	N(3)-C(13)	1.335(6)
Ru-N(2B)	2.054(4)	N(3)-C(17)	1.363(5)
Ru-N(1B)	2.057(4)	N(4)-C(18)	1.328(6)
Ru-N(2A)	2.071(4)	N(4)-N(5)	1.367(5)
Ru-N(3)	2.089(4)	N(5)-C(19)	1.347(6)
N(1A)-C(1A)	1.330(6)	N(6)-C(18)	1.339(5)
N(1A)-C(12A)	1.365(6)	N(6)-C(19)	1.350(6)
N(2A)-C(10A)	1.336(6)	C(13)-C(14)	1.351(7)
N(2A)-C(11A)	1.353(6)	C(14)-C(15)	1.375(7)
C(1A)-C(2A)	1.388(9)	C(15)-C(16)	1.376(7)
C(2A)-C(3A)	1.349(10)	C(16)-C(17)	1.379(7)
C(3A)-C(4A)	1.377(9)	C(17)-C(18)	1.447(6)
C(4A)-C(12A)	1.395(8)	C(19)-C(20)	1.462(6)
C(4A)-C(5A)	1.448(9)	C(20)-C(25)	1.361(8)
C(5A)-C(6A)	1.326(10)	C(20)-C(21)	1.396(7)
C(6A)-C(7A)	1.423(9)	C(21)-C(22)	1.382(7)
C(7A)-C(11A)	1.394(7)	C(22)-O(1)	1.362(6)
C(7A)-C(8A)	1.420(8)	C(22)-C(23)	1.408(7)
C(8A)-C(9A)	1.337(9)	C(23)-C(24)	1.369(7)
C(9A)-C(10A)	1.400(7)	C(23)-O(2)	1.373(6)
C(11A)-C(12A)	1.425(7)	C(24)-C(25)	1.382(7)
N(1B)-C(1B)	1.327(6)	O(1)-C(26)	1.375(8)
N(1B)-C(12B)	1.378(6)	O(2)-C(27)	1.406(7)
N(2B)-C(10B)	1.312(7)	P-F(5)	1.524(13)
N(2B)-C(11B)	1.378(6)	P-F(6A)	1.530(14)
C(1B)-C(2B)	1.377(8)	P-F(3A)	1.536(16)
C(2B)-C(3B)	1.339(9)	P-F(4A)	1.545(14)
C(3B)-C(4B)	1.404(9)	P-F(3)	1.577(12)
C(4B)-C(12B)	1.411(7)	P-F(1)	1.591(14)
C(4B)-C(5B)	1.423(9)	P-F(4)	1.600(15)
C(5B)-C(6B)	1.324(11)	P-F(6)	1.601(10)
C(6B)-C(7B)	1.435(10)	P-F(2)	1.603(12)
C(7B)-C(11B)	1.391(7)	P-F(2A)	1.603(16)
C(7B)-C(8B)	1.418(10)	P-F(5A)	1.609(14)
C(8B)-C(9B)	1.353(11)	P-F(1A)	1.619(17)
C(9B)-C(10B)	1.379(9)		

N(4)-Ru-N(1A)	93.73(16)	N(1A)-C(12A)-C(11A)	116.9(5)
N(4)-Ru-N(2B)	92.47(15)	C(4A)-C(12A)-C(11A)	120.2(5)
N(1A)-Ru-N(2B)	172.10(15)	C(1B)-N(1B)-C(12B)	118.1(5)
N(4)-Ru-N(1B)	96.42(15)	C(1B)-N(1B)-Ru	129.1(4)

N(1A)-Ru-N(1B)	94.58(17)	C(12B)-N(1B)-Ru	112.7(3)
N(2B)-Ru-N(1B)	79.86(17)	C(10B)-N(2B)-C(11B)	118.2(5)
N(4)-Ru-N(2A)	170.42(15)	C(10B)-N(2B)-Ru	128.8(4)
N(1A)-Ru-N(2A)	79.83(15)	C(11B)-N(2B)-Ru	113.0(3)
N(2B)-Ru-N(2A)	94.59(16)	N(1B)-C(1B)-C(2B)	122.3(6)
N(1B)-Ru-N(2A)	91.19(15)	C(3B)-C(2B)-C(1B)	121.4(6)
N(4)-Ru-N(3)	78.16(15)	C(2B)-C(3B)-C(4B)	119.0(6)
N(1A)-Ru-N(3)	90.17(16)	C(3B)-C(4B)-C(12B)	117.9(6)
N(2B)-Ru-N(3)	95.88(17)	C(3B)-C(4B)-C(5B)	124.9(6)
N(1B)-Ru-N(3)	173.03(15)	C(12B)-C(4B)-C(5B)	117.2(6)
N(2A)-Ru-N(3)	94.66(15)	C(6B)-C(5B)-C(4B)	121.5(6)
C(1A)-N(1A)-C(12A)	118.2(5)	C(5B)-C(6B)-C(7B)	121.6(6)
C(1A)-N(1A)-Ru	128.5(4)	C(11B)-C(7B)-C(8B)	116.8(6)
C(12A)-N(1A)-Ru	113.3(3)	C(11B)-C(7B)-C(6B)	118.0(6)
C(10A)-N(2A)-C(11A)	117.3(4)	C(8B)-C(7B)-C(6B)	125.2(6)
C(10A)-N(2A)-Ru	129.3(4)	C(9B)-C(8B)-C(7B)	118.7(6)
C(11A)-N(2A)-Ru	113.4(3)	C(8B)-C(9B)-C(10B)	121.4(7)
N(1A)-C(1A)-C(2A)	121.0(6)	N(2B)-C(10B)-C(9B)	122.0(6)
C(3A)-C(2A)-C(1A)	120.6(6)	N(2B)-C(11B)-C(12B)	116.9(4)
C(2A)-C(3A)-C(4A)	120.3(7)	N(2B)-C(11B)-C(7B)	122.8(5)
C(3A)-C(4A)-C(12A)	116.9(6)	C(12B)-C(11B)-C(7B)	120.3(5)
C(3A)-C(4A)-C(5A)	125.3(7)	N(1B)-C(12B)-C(11B)	117.3(5)
C(12A)-C(4A)-C(5A)	117.8(6)	N(1B)-C(12B)-C(4B)	121.3(5)
C(6A)-C(5A)-C(4A)	121.8(7)	C(11B)-C(12B)-C(4B)	121.4(5)
C(5A)-C(6A)-C(7A)	120.8(6)	C(13)-N(3)-C(17)	118.6(4)
C(11A)-C(7A)-C(8A)	116.6(5)	C(13)-N(3)-Ru	126.5(3)
C(11A)-C(7A)-C(6A)	119.5(6)	C(17)-N(3)-Ru	114.9(3)
C(8A)-C(7A)-C(6A)	124.0(6)	C(18)-N(4)-N(5)	107.1(4)
C(9A)-C(8A)-C(7A)	120.0(5)	C(18)-N(4)-Ru	115.9(3)
C(8A)-C(9A)-C(10A)	119.7(5)	N(5)-N(4)-Ru	136.4(3)
N(2A)-C(10A)-C(9A)	122.6(5)	C(19)-N(5)-N(4)	104.1(4)
N(2A)-C(11A)-C(7A)	123.7(5)	C(18)-N(6)-C(19)	101.7(4)
N(2A)-C(11A)-C(12A)	116.5(4)	N(3)-C(13)-C(14)	122.2(5)
C(7A)-C(11A)-C(12A)	119.7(5)	C(13)-C(14)-C(15)	120.3(5)
N(1A)-C(12A)-C(4A)	122.9(5)		

C(14)-C(15)-C(16)	118.5(5)	F(3)-P-F(1)	94.7(7)
C(15)-C(16)-C(17)	119.3(5)	F(5)-P-F(4)	84.1(7)
N(3)-C(17)-C(16)	121.1(4)	F(6A)-P-F(4)	83.0(7)
N(3)-C(17)-C(18)	113.5(4)	F(3A)-P-F(4)	104.8(8)
C(16)-C(17)-C(18)	125.4(4)	F(4A)-P-F(4)	20.4(7)
N(4)-C(18)-N(6)	113.3(4)	F(3)-P-F(4)	85.9(7)
N(4)-C(18)-C(17)	117.3(4)	F(1)-P-F(4)	178.7(8)
N(6)-C(18)-C(17)	129.3(4)	F(5)-P-F(6)	87.6(6)
N(5)-C(19)-N(6)	113.9(4)	F(6A)-P-F(6)	37.9(6)
N(5)-C(19)-C(20)	122.2(5)	F(3A)-P-F(6)	144.4(8)

F(2)-P-F(5A)	141.1(8)	F(1)-P-F(1A)	20.2(7)
F(2A)-P-F(5A)	176.9(8)	F(4)-P-F(1A)	160.9(8)
F(5)-P-F(1A)	76.9(7)	F(6)-P-F(1A)	86.6(7)
F(6A)-P-F(1A)	85.6(8)	F(2)-P-F(1A)	101.4(7)
F(3A)-P-F(1A)	85.5(8)	F(2A)-P-F(1A)	99.3(8)
F(4A)-P-F(1A)	178.4(8)	F(5A)-P-F(1A)	83.0(7)
F(3)-P-F(1A)	92.9(7)		

N(6)-C(19)-C(20)	123.9(4)	F(4A)-P-F(6)	94.3(6)
C(25)-C(20)-C(21)	119.0(5)	F(3)-P-F(6)	177.0(7)
C(25)-C(20)-C(19)	122.3(5)	F(1)-P-F(6)	85.8(6)
C(21)-C(20)-C(19)	118.6(5)	F(4)-P-F(6)	93.6(6)
C(22)-C(21)-C(20)	120.2(5)	F(5)-P-F(2)	177.7(7)
O(1)-C(22)-C(21)	125.0(5)	F(6A)-P-F(2)	128.2(8)
O(1)-C(22)-C(23)	115.6(4)	F(3A)-P-F(2)	57.1(7)
C(21)-C(22)-C(23)	119.4(5)	F(4A)-P-F(2)	77.3(7)
C(24)-C(23)-O(2)	125.6(5)	F(3)-P-F(2)	92.1(7)
C(24)-C(23)-C(22)	119.9(5)	F(1)-P-F(2)	81.2(7)
O(2)-C(23)-C(22)	114.5(5)	F(4)-P-F(2)	97.7(7)
C(23)-C(24)-C(25)	119.6(5)	F(6)-P-F(2)	90.8(6)
C(20)-C(25)-C(24)	121.9(5)	F(5)-P-F(2A)	137.8(9)
C(22)-O(1)-C(26)	118.8(5)	F(6A)-P-F(2A)	87.6(8)
C(23)-O(2)-C(27)	117.1(5)	F(3A)-P-F(2A)	97.1(9)
F(5)-P-F(6A)	50.4(6)	F(4A)-P-F(2A)	80.3(7)
F(5)-P-F(3A)	123.9(8)	F(3)-P-F(2A)	132.6(9)
F(6A)-P-F(3A)	170.5(8)	F(1)-P-F(2A)	83.3(7)
F(5)-P-F(4A)	104.5(7)	F(4)-P-F(2A)	95.4(8)
F(6A)-P-F(4A)	95.9(7)	F(6)-P-F(2A)	50.3(6)
F(3A)-P-F(4A)	93.1(8)	F(2)-P-F(2A)	40.7(6)
F(5)-P-F(3)	89.5(7)	F(5)-P-F(5A)	40.5(6)
F(6A)-P-F(3)	139.2(8)	F(6A)-P-F(5A)	90.5(8)
F(3A)-P-F(3)	38.3(6)	F(3A)-P-F(5A)	85.2(8)
F(4A)-P-F(3)	86.3(7)	F(4A)-P-F(5A)	97.5(7)
F(5)-P-F(1)	97.0(7)	F(3)-P-F(5A)	49.0(6)
F(6A)-P-F(1)	97.2(7)	F(1)-P-F(5A)	99.4(7)
F(3A)-P-F(1)	75.2(8)	F(4)-P-F(5A)	81.9(7)
F(4A)-P-F(1)	158.5(8)	F(6)-P-F(5A)	128.1(7)

Table 5. Atomic coordinates (x 10^4) and equivalent isotropic displacement parameters ($Å^2$x 10^3) for $Ru(phen)_2(L1)]PF_6.H_2O$. U(eq) is defined as one third of the trace of the orthogonalized U^{ij} tensor.

	x	y	z	U(eq)
Ru	9076(1)	7689(1)	327(1)	34(1)
N(1A)	10076(3)	6856(2)	157(2)	42(1)
N(2A)	8022(3)	7280(2)	-720(2)	39(1)
C(1A)	11103(5)	6650(3)	612(4)	61(2)
C(2A)	11687(6)	6085(4)	391(5)	89(2)
C(3A)	11248(7)	5748(4)	-310(5)	100(3)
C(4A)	10172(6)	5931(3)	-788(4)	73(2)
C(5A)	9594(8)	5595(4)	-1537(5)	99(3)
C(6A)	8538(7)	5788(4)	-1952(5)	90(2)
C(7A)	7955(6)	6363(3)	-1699(3)	59(2)
C(8A)	6810(6)	6587(4)	-2097(4)	67(2)
C(9A)	6332(5)	7136(3)	-1820(3)	59(2)
C(10A)	6961(5)	7484(3)	-1134(3)	49(1)
C(11A)	8501(4)	6724(3)	-1003(3)	45(1)
C(12A)	9610(5)	6497(3)	-535(3)	48(1)
N(1B)	9861(3)	8348(2)	-345(2)	41(1)
N(2B)	8049(4)	8547(2)	328(2)	42(1)
C(1B)	10790(5)	8243(3)	-665(3)	50(1)
C(2B)	11199(6)	8734(4)	-1121(4)	67(2)
C(3B)	10666(6)	9345(4)	-1273(4)	67(2)
C(4B)	9675(6)	9485(3)	-954(3)	59(2)
C(5B)	9033(7)	10112(3)	-1062(4)	71(2)
C(6B)	8108(8)	10209(3)	-740(4)	79(2)
C(7B)	7721(5)	9692(3)	-253(3)	59(2)
C(8B)	6760(7)	9761(4)	131(4)	83(2)
C(9B)	6519(6)	9237(4)	595(4)	80(2)
C(10B)	7177(5)	8641(3)	691(3)	60(2)
C(11B)	8333(5)	9073(3)	-140(3)	44(1)
C(12B)	9295(4)	8972(2)	-480(3)	42(1)
N(3)	8306(3)	7114(2)	1116(2)	41(1)
N(4)	10125(3)	7928(2)	1428(2)	39(1)
N(5)	11142(3)	8290(2)	1703(2)	43(1)
N(6)	10682(4)	7719(2)	2757(2)	47(1)
C(13)	7350(4)	6718(3)	909(3)	49(1)
C(14)	6930(5)	6353(3)	1464(3)	60(2)
C(15)	7497(5)	6373(3)	2272(3)	64(2)
C(16)	8487(4)	6776(3)	2498(3)	52(1)
C(17)	8877(4)	7147(3)	1914(3)	39(1)

C(18)	9894(4)	7596(3)	2063(3)	40(1)
C(19)	11434(4)	8153(3)	2506(3)	45(1)
C(20)	12487(4)	8440(3)	3041(3)	47(1)
C(21)	13017(4)	8078(3)	3741(3)	50(1)
C(22)	14026(4)	8328(3)	4254(3)	53(1)
C(23)	14524(5)	8946(3)	4056(3)	51(1)
C(24)	14000(5)	9296(3)	3366(4)	63(2)
C(25)	12977(5)	9043(3)	2874(3)	63(2)
O(1)	14620(4)	8012(3)	4944(3)	87(2)
C(26)	14171(7)	7414(4)	5186(5)	111(4)
O(2)	15539(4)	9139(2)	4596(3)	75(1)
C(27)	16109(6)	9735(4)	4409(5)	88(2)
P	4187(2)	9090(1)	-2112(1)	74(1)
F(1)	4027(12)	9220(8)	-1212(8)	113(5)
F(2)	4385(13)	9905(6)	-2070(7)	130(4)
F(3)	2836(10)	9173(7)	-2520(7)	123(4)
F(4)	4367(13)	8974(8)	-3014(9)	126(5)
F(5)	4027(13)	8313(6)	-2117(7)	131(4)
F(6)	5549(9)	8964(6)	-1700(6)	104(3)
F(1A)	3929(14)	8936(8)	-1225(10)	140(6)
F(2A)	5240(15)	9634(9)	-1855(9)	174(6)
F(3A)	3167(15)	9606(9)	-2208(10)	172(6)
F(4A)	4415(12)	9257(8)	-2958(8)	116(5)
F(5A)	3170(13)	8526(8)	-2401(8)	149(4)
F(6A)	5114(14)	8523(8)	-1906(8)	153(5)

Table 6. Anisotropic displacement parameters ($Å^2 x\ 10^3$) for $Ru(phen)_2(L1)]PF_6.H_2O$. The anisotropic displacement factor exponent takes the form: $-2p^2[\ h^2\ a^{*2}U^{11} + ... + 2\ h\ k\ a^*\ b^*\ U^{12}\ ]$

	U^{11}	U^{22}	U^{33}	U^{23}	U^{13}	U^{12}
Ru	32(1)	40(1)	27(1)	2(1)	-1(1)	-1(1)
N(1A)	38(2)	45(2)	39(2)	4(2)	0(2)	7(2)
N(2A)	39(2)	45(2)	29(2)	3(2)	-1(2)	-4(2)
C(1A)	56(3)	61(4)	59(3)	5(3)	-3(3)	16(3)
C(2A)	74(5)	86(5)	93(5)	3(4)	-10(4)	40(4)
C(3A)	96(6)	77(5)	111(6)	-23(5)	-9(5)	46(4)
C(4A)	73(4)	66(4)	72(4)	-17(3)	1(3)	21(3)
C(5A)	115(7)	68(5)	105(6)	-40(5)	3(5)	23(5)
C(6A)	92(5)	88(5)	78(5)	-43(4)	-4(4)	8(4)
C(7A)	70(4)	62(4)	41(3)	-9(3)	1(3)	-2(3)
C(8A)	68(4)	83(5)	42(3)	-14(3)	-8(3)	-14(4)
C(9A)	54(3)	79(4)	34(3)	3(3)	-7(2)	0(3)
C(10A)	41(3)	62(4)	38(3)	0(2)	-1(2)	6(2)
C(11A)	47(3)	49(3)	40(3)	-1(2)	7(2)	-3(2)
C(12A)	52(3)	43(3)	46(3)	-3(2)	6(2)	2(2)
N(1B)	43(2)	51(3)	26(2)	2(2)	0(2)	-5(2)
N(2B)	43(2)	44(2)	36(2)	-4(2)	-2(2)	4(2)
C(1B)	47(3)	59(3)	43(3)	3(3)	7(2)	-4(3)
C(2B)	60(4)	89(5)	52(3)	0(3)	16(3)	-17(4)
C(3B)	71(4)	77(5)	51(3)	11(3)	10(3)	-24(4)
C(4B)	75(4)	53(3)	37(3)	10(2)	-11(3)	-18(3)
C(5B)	107(6)	46(4)	50(3)	9(3)	-7(4)	-4(4)
C(6B)	113(6)	41(3)	60(4)	2(3)	-28(4)	17(4)
C(7B)	64(4)	56(4)	47(3)	-5(3)	-9(3)	15(3)
C(8B)	91(5)	71(5)	70(4)	-13(4)	-16(4)	31(4)
C(9B)	73(5)	101(6)	68(4)	-9(4)	22(4)	30(4)
C(10B)	55(3)	80(4)	47(3)	4(3)	13(3)	15(3)
C(11B)	52(3)	44(3)	28(2)	-1(2)	-8(2)	4(2)
C(12B)	48(3)	37(3)	33(2)	2(2)	-7(2)	-3(2)
N(3)	38(2)	48(2)	31(2)	3(2)	-3(2)	-2(2)
N(4)	34(2)	43(2)	36(2)	5(2)	-2(2)	-7(2)
N(5)	38(2)	45(2)	42(2)	5(2)	-4(2)	-10(2)
N(6)	40(2)	60(3)	33(2)	6(2)	-8(2)	-11(2)
C(13)	43(3)	59(3)	38(3)	3(2)	-9(2)	-15(3)
C(14)	44(3)	79(4)	51(3)	6(3)	-1(2)	-29(3)
C(15)	56(3)	86(5)	47(3)	17(3)	7(3)	-21(3)
C(16)	42(3)	73(4)	38(3)	6(3)	1(2)	-12(3)
C(17)	29(2)	54(3)	32(2)	4(2)	-1(2)	-4(2)

C(18)	37(2)	51(3)	29(2)	5(2)	0(2)	-7(2)
C(19)	42(3)	47(3)	39(3)	7(2)	-3(2)	-5(2)
C(20)	43(3)	55(3)	37(3)	2(2)	-7(2)	-13(2)
C(21)	44(3)	56(3)	45(3)	10(3)	-4(2)	-11(3)
C(22)	40(3)	62(4)	48(3)	12(3)	-8(2)	-8(3)
C(23)	42(3)	47(3)	53(3)	1(2)	-10(2)	-7(2)
C(24)	53(3)	55(3)	66(4)	14(3)	-15(3)	-24(3)
C(25)	66(4)	61(4)	48(3)	14(3)	-17(3)	-15(3)
O(1)	64(3)	100(3)	73(3)	43(3)	-37(2)	-26(3)
C(26)	87(5)	116(6)	101(6)	76(5)	-41(5)	-31(5)
O(2)	54(2)	74(3)	74(3)	13(2)	-34(2)	-24(2)
C(27)	70(4)	81(5)	93(5)	10(4)	-24(4)	-40(4)
P	66(1)	86(1)	80(1)	16(1)	34(1)	23(1)

Appendix 3

Poster presentations:

Attended the following conferences at which my work was presented in poster formation;

1: European Research Conference : "Chemistry and Physics of Multifunctional Materials", San Feliu de Guixiols, Spain 21 - 26 September 1999.

2: EPA (European Photochemistry Association) Summer School 1998 in Noordwijk, The Netherlands -June 16-20 1998.

3: The Forty-ninth Irish Universities Chemistry Research Colloquium in Dublin City University - 25-27 June 1997.

4: TMR (Training, Mobility and Research) European Research Network workshop in St. Remy-Les Chevreuse - Paris 1-4 April 1997.